INFORMATION TO USERS

This material was produced from a microfilm copy of the original document. While the most advanced technological means to photograph and reproduce this document have been used, the quality is heavily dependent upon the quality of the original submitted.

The following explanation of techniques is provided to help you understand markings or patterns which may appear on this reproduction.

1. The sign or "target" for pages apparently lacking from the document photographed is "Missing Page(s)". If it was possible to obtain the missing page(s) or section, they are spliced into the film along with adjacent pages. This may have necessitated cutting thru an image and duplicating adjacent pages to insure you complete continuity.

2. When an image on the film is obliterated with a large round black mark, it is an indication that the photographer suspected that the copy may have moved during exposure and thus cause a blurred image. You will find a good image of the page in the adjacent frame.

3. When a map, drawing or chart, etc., was part of the material being photographed the photographer followed a definite method in "sectioning" the material. It is customary to begin photoing at the upper left hand corner of a large sheet and to continue photoing from left to right in equal sections with a small overlap. If necessary, sectioning is continued again — beginning below the first row and continuing on until complete.

4. The majority of users indicate that the textual content is of greatest value, however, a somewhat higher quality reproduction could be made from "photographs" if essential to the understanding of the dissertation. Silver prints of "photographs" may be ordered at additional charge by writing the Order Department, giving the catalog number, title, author and specific pages you wish reproduced.

5. PLEASE NOTE: Some pages may have indistinct print. Filmed as received.

Xerox University Microfilms

300 North Zeeb Road
Ann Arbor, Michigan 48106

74-25,132

ALEM, Nabih Mohammed, 1940-
A DISCRETE-PARAMETER HEAD INJURY MODEL.

The University of Michigan, Ph.D., 1974
Engineering, mechanical

University Microfilms, A XEROX Company, Ann Arbor, Michigan

THIS DISSERTATION HAS BEEN MICROFILMED EXACTLY AS RECEIVED.

A DISCRETE-PARAMETER HEAD INJURY MODEL

by
Nabih Mohammed Alem

A dissertation submitted in partial fulfillment
of the requirements for the degree of
Doctor of Philosophy
(Mechanical Engineering)
in The University of Michigan
1974

Doctoral Committee:

Associate Professor James H. McElhaney, Chairman
Professor Ivor K. McIvor
Professor Wen-J. Yang
Doctor Verne L. Roberts

ACKNOWLEDGEMENTS

I am deeply grateful to Professor James H. McElhaney for his continuous moral, academic and financial support. Without his assistance, guidance and encouragement, this study could not have been completed.

I would like to thank Professors Ivor K. McIvor and Wen J. Yang, and Doctor Verne L. Roberts for their helpful suggestions during this investigation, and for their critical reviews of this manuscript.

I wish to express my appreciation to members of the Biosciences Division of the Highway Safety Research Institute at The University of Michigan. In particular:

Doctor Robert L. Ness for his financial support of the final year of the investigation.

Doctors Bruce M. Bowman, John W. Melvin and Han Chou Wang for the many stimulating discussions, their practical suggestions and their assistance in acquiring experimental data.

Doctor Richard L. Stalnaker, whose work in experimental head injury provided much of the basis for this investigation.

Mr. Robert O. Bennett for his helpful hints on the computational problems.

Finally, Mrs. Kay Saucier for typing the final manuscript.

TABLE OF CONTENTS

		Page
ACKNOWLEDGEMENTS		ii
LIST OF TABLES		v
LIST OF FIGURES		vi
LIST OF APPENDICES		ix
Chapter		
1	INTRODUCTION	1
	1.1 FOREWORD	1
	1.2 HEAD INJURY PREDICTION	3
	1.3 MECHANICS OF HEAD INJURY	4
	1.4 MODELING FOR HEAD INJURY	8
	1.4.1 Structural Head Models	9
	1.4.2 Functional Head Injury Criteria	10
	1.4.3 Functional Head Injury Models	14
2	A PROPOSED HEAD INJURY MODEL	23
	2.1 INJURY MECHANISMS TO BE SIMULATED	23
	2.2 PHYSICAL PARAMETERS OF MODEL	24
	2.3 THE ASSEMBLED HEAD-NECK INJURY MODEL	27
	2.4 ALLOWED TYPES OF IMPACTS	30
	2.5 METHODS OF FORMULATION AND SOLUTION	31
	2.5.1 Formulation of Lagrange's Equations of Motion	32
	2.5.2 Methods of Solution	34
	2.6 THE "HEAD" SIMULATION PROGRAM	35
3	DETERMINATION OF MODEL CONSTANTS	37
	3.1 VALIDITY OF OBSERVED PROPERTIES AND SELECTED CONSTANTS	37
	3.2 AVAILABLE EXPERIMENTAL DATA	39

Chapter		Page
	3.3 LUMPING OF PARAMETERS	47
	3.3.1 Neck Properties	47
	3.3.2 Skull Properties	50
	3.3.3 Brain Properties	60
	3.4 CONCLUDING REMARKS	67
4	RESPONSES OF THE MODEL	68
	4.1 IMPEDANCE PARAMETRIC STUDY	68
	4.1.1 General Observations	69
	4.1.2 Effects of Some Springs and Dashpots	70
	4.2 TWO TYPICAL IMPACT SIMULATIONS	80
	4.2.1 Side Impact to Rhesus Head	80
	4.2.2 Whiplash Simulation of Human Head	103
	4.3 COMPARATIVE SIMULATIONS	126
	4.3.1 Whiplash Simulations of Two Heads	126
	4.3.2 Five Direct Impacts to One Head	128
5	CONCLUSIONS AND RECOMMENDATIONS	131
	5.1 CONCLUSIONS	131
	5.2 RECOMMENDATIONS	132
REFERENCES		134
APPENDICES		137

LIST OF TABLES

Table		Page
1.	Some Available Anatomical Data of the Head.....	41
2.	Nonlinear Characteristics of Various Springs.....	59
3.	Brain-Skull Couplings.....	66
4.	Comparison of Peak Responses of Two Whiplash Simulations.....	127
5.	Comparison of Peak Responses of Five Direct Impact Simulations.....	130
B.1	Correspondance Between Program Arrays and Problem Coordinates.....	175

LIST OF FIGURES

Figure		Page
1.	Mid-Sagittal View of Human Head	6
2.	Wayne-State Tolerance Curve	12
3.	One-Mass Head Injury Model	15
4.	Two-Mass Head Injury Model	16
5.	Impedance Curves for Model and Cadaver Head	21
6.	Maximum Strain Ctriterion Tolerance Curves	22
7.	Sub-Models of Neck, Skull and Brain	28
8.	Proposed Head Injury Model	29
9.	Moment (about Occ. Condyles) versus Head-Torso Angle	42
10.	Static Load-Deflection Curve for Human Skull	43
11.	Mechanical Impedance of a Cadaver Head	44
12.	Free Standing Compression of Human Brain Tissue	45
13.	Rotation of Rhesus Brain Relative to Skull	46
14.	General Load-Deflection (spring) Characteristics	49
15.	Adjusting D1 and D2 to Match Skull Moment of Inertia	52
16.	Estimation of Torso-Neck and Skull-Neck Angles	56
17.	Impedance of Human A-P Model Compared with Two Actual Cadavers' Impedances	72
18.	Effects of K1S (M1-M2 Spring)	73
19.	Effects of K3S (M1-M3 Spring)	74
20.	Effects of K1B (M1-MB Spring)	75
21.	Effects of C1S (M1-M2 Damping)	76
22.	Effects of C3S (M1-M3 Damping)	77

Figure		Page
23.	Effects of C1B (M1-MB Damping)	78
24.	Effects of C4B (MB-M2 Damping)	79
25.	Input Data to Side Impact Simulation	86
26.	Resultant Absolute Velocity of Skull	87
27.	Brain Absolute Velocity	88
28.	Skull Absolute Angular Velocity	89
29.	Brain Absolute Angular Velocity	90
30.	Resultant Absolute Acceleration of Skull	91
31.	Brain Absolute Acceleration	92
32.	Skull Absolute Angular Acceleration	93
33.	Brain Absolute Angular Acceleration	94
34.	Distance of Brain Relative to Skull	95
35.	Brain-Skull Angle	96
35(A).	Brain-Skull Angle (Free Head)	97
36.	Skull Horizontal (L-R) Deflection	98
37.	Skull Vertical (S-I) Deflection	99
38.	Moment at Neck-Skull Joint	100
39.	Axial (S-I) force at Neck-Skull Joint	101
40.	Shear (L-R) Force at Neck-Skull Joint	102
41.	Input Data to Whiplash Simulation	107
42.	Input Acceleration at Neck-Torso Joint	108
43.	Neck Axial Deformation	109
44.	Orientation of Neck (relative to torso)	110
45.	Angle of Skull Relative to Torso	111
46.	Horizontal (A-P) Skull Deformation	112

Figure Page

47. Vertical (S-I) Skull Deformation 113
48. Motion (distance) of Brain Relative to Skull 114
49. Motion (angle) of Brain Relative to Skull 115
49(A). Brain-Skull Angle (10-g, less accuracy) 116
50. Absolute Angular Velocity of Skull 117
50(A). Skull Angular Velocity (10-g, less accuracy) 118
51. Brain Absolut Angular Velocity 119
52. Skull Absolute Angular Acceleration 120
53. Brain Absolute Angular Acceleration 121
54. Constraint Force on XO 122
54(A). Constraint Force on XO (10-g, less accuracy) 123
55. Constraint Force on YO 124
56. Constraint Moment at (XO,YO) 125

A.1. Formulation Diagram of the Problem 138
A.2. Coordinates Used in the Formulation 140
A.3. External Inputs to the Model 151
B.1. Symbolic Form of the Matrix of Problem's Equations 158
B.2. Phases of the Simulation 167
B.3. Symbolic Matrix for Type II Input Solution 177
C.1. Mechanical Network of Skull-Brain Sub-system 183
C.2. Transformations of Basic Elements and Networks 186
C.3. Vertical-Direction Impedance 188
C.4. Horizontal-Direction Impedance 189

LIST OF APPENDICES

Appendix		Page
A	FORMULATION OF THE PROBLEM	137
	A.1 Generalized Coordinates	137
	A.2 Kinetic and Potential Energies, Dissipation	141
	A.3 Constraint Equations	143
	A.4 Constraint Forces	147
	A.5 Generalized Applied Forces	150
	A.6 Lagrange Equations of Motion	153
B	SOLUTION OF THE PROBLEM	156
	B.1 Examination of Equations and Unknowns	156
	B.2 Preparation and Outline of Solution	159
	B.3 Input Data	161
	B.4 Phases of the Simulation	165
	B.5 Solution of the Equations	168
C	IMPEDANCE REDUCTION TECHNIQUE OF A MECHANICAL NETWORK	182
	C.1 Method	182
	C.2 Basic Elements	185
	C.3 Basic Combinations	185
	C.4 Applications	187
	C.5 Conclusions	195

CHAPTER 1

INTRODUCTION

1.1 FOREWORD

Accidents are the fourth leading cause of deaths in the United States, following heart disease, cancer and stroke. The National Safety Council has recently published statistics [1], stating that in 1971 there were over 50 million accidents resulting in about 85,000 fatalities and two million disabling injuries. The design of safety equipments, particularly for head protection, has been a challenge to engineers; and their implementation, a legislative issue to law-makers.

Much of the design is often based on the designer's intuition and on the little available information about the tolerance of the human head to the violent environment to which it is exposed. The problem of head injury has long been recognized as a serious one. The first major conference devoted exclusively to head injury was held in 1965 [2]. By 1969, the various aspects of this subject gained the attention of wide segments of the medical and the engineering communities. Today the problems associated with head injury remain subject to continuing intensive research.

This has resulted in a voluminous literature dealing with various aspects of head injury, with the ultimate goal of preventing or reducing head injury, and its rehabilitation. By understanding its mechanisms, physicians would successfully rehabilitate the injured, and engineers would have a better basis for the design of effective protective devices.

To help put the present study into perspective, one should have an idea about the violent environment to which the head is subjected, as well as the internal physical processes incurred inside the head as a result of this hostile environment.

The mechanical causes of head injuries may be classified into three broad categories [3]:

(a) an impact, defined as the collision of the head with a solid object at an appreciable speed,

(b) an impulsive load which produces sudden motion of the head without significant effects traceable to physical contact,

(c) a static or quasi-static loading where the consequences of speed may be neglected.

The human head is usually exposed to one or a combination of these causes, resulting in damages of one or more of the following types:

(a) an external, soft tissue injury such as scalp or facial skin lacerations,

(b) a hard tissue injury, e.g., bone fracture of the skull or the facial bones,

(c) an internal injury of the intracranial contents such as dural clots, brain hemorrhage or concussion.

Head injuries may occur, and usually do, in a combination of the types of injuries mentioned above. Once the causes of head injury are defined, and its mechanisms understood, work may proceed to the final phases of injury prevention, prediction, protection and/or rehabilitation. The present study concerns one of these final phases, namely the prediction of head injury under certain loading conditions.

1.2 HEAD INJURY PREDICTION

The purpose of predicting head injury is to develop a protective system which reduces injury. To this end one must understand the mechanisms of injury, isolate significant "indicators" or parameters associated with injury, then establish human tolerance levels for these parameters. Protection of the head becomes then a matter of designing safety equipments which keep those parameters below the established tolerance levels.

The variety of causes and mechanisms of head injuries necessitates that effort be concentrated on a spectrum of injury mechanisms, under general sets of loading conditions. It was felt in this study that, in terms of the seriousness of the injury, the intracranial contents are the most vulnerable parts of the head, while scalp tissue injuries and bone fractures are less important, unless they contribute directly or indirectly to brain injury. It was also concluded that short duration forces to the skull and impulsive loads at the cervical-thoracic articulation are the most frequently encountered loading conditions in injurious accidents.

There have been two basic approaches to head injury prediction. One approach is experimental in which human volunteers, cadavers, and sub-human primates are subjected to loading conditions in a controlled laboratory environment, and their responses, reactions and injuries are carefully observed and recorded, then analyzed. The other approach is theoretical, whereby the head is represented by a physical or a mathematical model, which is subjected to loading conditions similar to those producing injury in the actual head. The response of the model is either observed or computed, and hopefully,

indication of a simulated injury is obtained.

These two approaches, along with data from actual accidental injury, complement one another. A mathematical model must rely on experimental results for its validation, and the experiments must observe and record responses suggested by theoretical considerations.

The theoretical approach is taken in the present work. Thus, a mathematical model for head injury prediction will be developed and compared to actual responses. Mathematical modeling is merely a technique of physical research in which simplified idealizations are substituted for the actual systems. Models are not intended to duplicate the systems they represent; rather, they tend to approximate those characteristics which are critical to the understanding of the responses and behavior of the actual systems.

1.3 MECHANICS OF HEAD INJURY

Injuries to the head may be of one of the following varieties [4]: (a) scalp injuries, (b) skull fractures, (c) intracranial clots and (d) brain injuries. As a result of a serious accident, usually a combination of these injuries occurs. The severity of head injury is very difficult to define, but is usually described by simple key-words, phrases and examples of typical injuries. Many scales of severity have been suggested to assign a single number to the injury as an indication of its severity. A typical scale assigns the number 1 for minor injuries, the number 4 for fatal injury, with 2 and 3 for moderate and dangerous injuries respectively. The points on this scale may be described as follows [5]:

(1) A minor injury such as contusions, abrasions, loosened teeth, fracture of nose.

(2) Moderate injury, which is one that is non-dangerous to survival. This class includes deep lacerations, extensive lacerations without dangerous hemmorhage, skull fracture without concussion, loss of an eye.

(3) When survival of the injured is not assured, the injury is termed dangerous such as depressed skull fractures, evidence or intracranial damage and loss of consciousness up to two hours, with or without skull fracture.

(4) The most severe injury is one which would be fatal within 24 hours of its occurrence.

The injuries of concern in the present study are those which are at the thresholds of survival and recovery, i.e. the moderate and dangerous ones. The author is aware of the importance of the other injuries. The fact that minor injuries are not included in this presentation expresses the relative importance of, and need for protection from severe head injuries. The term "head injury" will henceforth generally imply serious damages to the skull and to its contents.

In order to understand the mechanics of head injury, particularly when it has no local external evidence, a hypothesis about the physical processes and mechanisms must be formulated based on careful autopsies. There are several hypotheses for head injury mechanics [6]:

(1) The pressure gradient hypothesis suggesting that impacts to the head set up shear stresses along the brain stem axis leading to concussion. This theory points out that the flow of the brain and brain stem, from the cranial cavity through the tentorial incisura and foramen magnum (see figure 1), induces a pressure gradient which easily causes the shear stresses to develop along the brain stem axis.

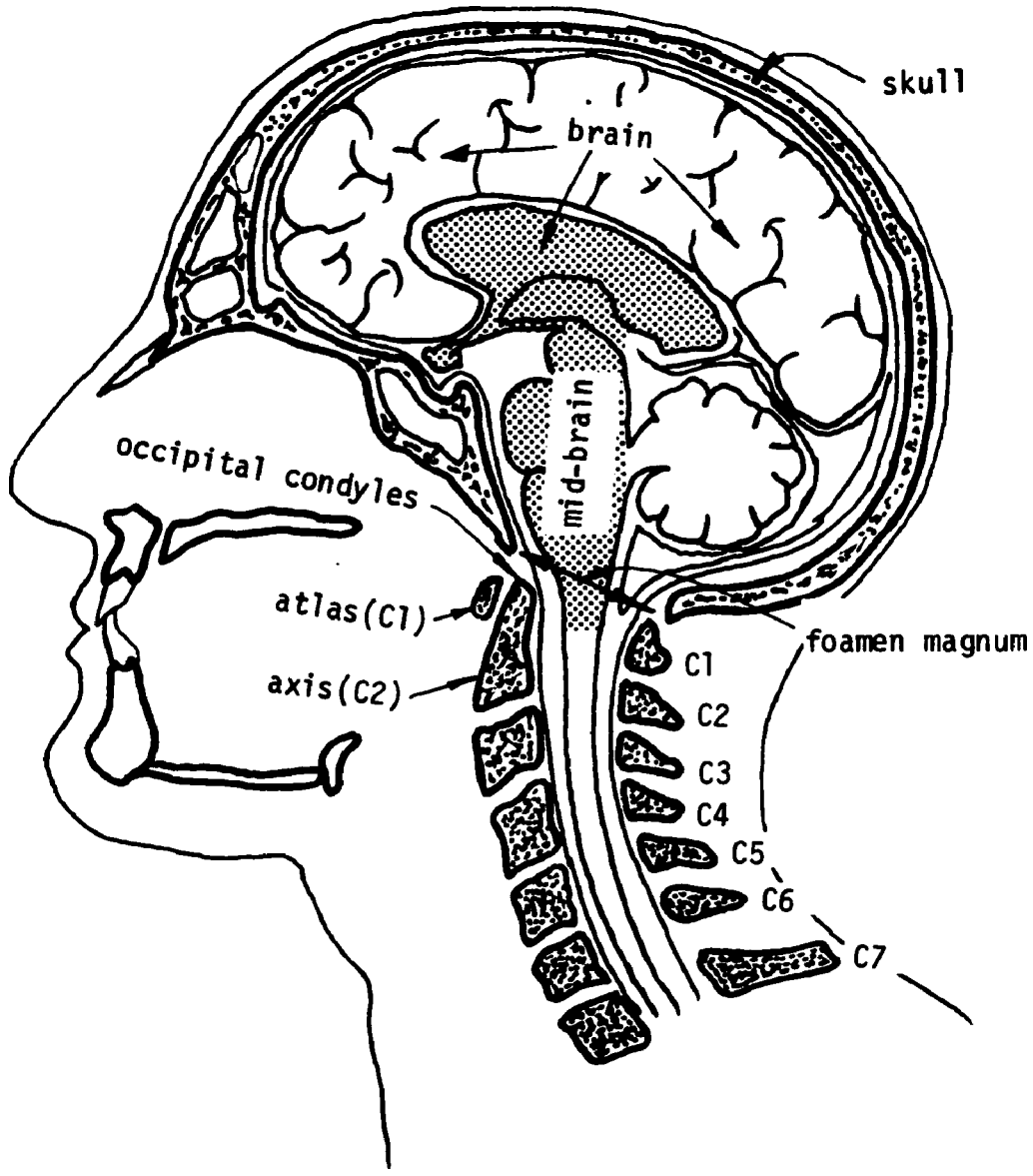


Figure 1. Mid-Sagittal View of the Human Head

Negative pressure may also exist at the antipole of the point of impact causing cavitation lesions.

(2) This hypothesis attributes injury primarily to the bending and/or stretching of the upper cervical cord. This occurs during head and neck motions, causing the brain and brain stem to move relative to the skull and the cervical cord.

(3) The third hypothesis is more general than the previous ones, insofar as it states several possible mechanisms as causes of injury. This hypothesis attributes brain injury to two main causes: (a) deformation of the skull with or without fracture and (b) sudden rotation of the head causing shear stresses within its contents.

All three theories agree that, in order for brain injury to occur, the brain and brain stem must move inside the skull. They differ in theorizing what type of motion is occurring, and what effects this motion has on the physical structure of the intracranial contents. Each one of these hypotheses has been tested and is backed up by experimental and actual injury cases as well as physical models. But because of the variations in the types of injuries encountered, none of these theories has been successful in explaining each and every type of injury. Parallel to this inadequacy, no single mathematical or physical model has been conceived which could simulate, once and for all, head injury.

The inadequacies of these theories and models reflect the complexity of the head injury problem rather than their lack of merits. In the present study, no attempt is made to formulate a conclusive theory for head injury; rather it is the intention of the author to apply existing plausible theories of injury mechanisms toward the

development of a practical model suitable for the prediction of head injury due to one or more possible mechanisms.

1.4 MODELING FOR HEAD INJURY

The human head may be considered a physical system. Given such a system, simulation is resorted to in lieu of direct experimentation with the system itself. This is obviously necessary since experimentation with the human head cannot exceed the tolerances of volunteers, and therefore results of such experiments have limited values. Simulation implies conducting experiments on some model, which is a simplified representation of the real system. The human head, like any other physical system, consists of physical elements of various characteristics or properties which interact according to certain relationships or physical laws. The complexity of these characteristics and relationships, and often the lack of data describing them, necessitates that "reasonable" assumptions and simplifications be made prior to the conception of any representative model.

A distinction must be drawn at this point between two approaches to modeling, one resulting in a "model of the head," another in a "model for head injury." The first one attempts to represent the physical and structural characteristics of the head, and assumes that the structural similarities between model and head imply similarities of responses. The second model gives minor importance to the structural similarities, and concerns itself primarily with the reproduction of those responses which are critical to the prediction of an injury. The first type of modeling may thus be considered as "structural," the second as "functional." If the two approaches are sound, they should then reach similar predictions of injury when the respective models are subjected to similar loading or boundary conditions.

1.4.1 Structural Head Models

The heads of anthropometric dummies may be considered gross representations of the complex structure of the human head. Nevertheless, these dummies [7] provide an excellent visual aide to the kinematics of motion of a passenger in a car accident. Rectilinear and rotational motions of their heads could either be used by themselves to judge the severity of the crash, or as inputs to more sophisticated head models.

Other models have been physically built to validate a specific hypothesis or theory of injury [8,9]. Spherical shells filled with fluids were built either to monitor the motion of the fluid inside the shell, simulating that of the brain inside the skull, or to measure the pressure distribution in the fluid for evidence of cavitation theory of injury.

These models are more or less easier to monitor mathematically. Consequently, analytical models were conceived to extend the choice of properties of those physical models, as well as the spectrum of variables to monitor.

The mathematical formulation of the physical head must be based on great simplifications of its material properties. The model becomes an interesting, but often a difficult problem in applied mechanics. The human skull is far from a spherical shell, and it is debatable whether the brain is a fluid filling a spherical shell. Yet, these simple representations have enough mathematical complexities without implementing irregularities of the skull, non homogeneity and anisotropy of the skull and brain materials. It is not surprising

to find that most of the previous work in continuum mechanics modeling of the head has been limited to simple spherical shapes, and to homogenous and isotropic materials.

The earliest analytical models [10,11] consisted of rigid spherical shells filled with non-viscous liquids. These models were criticized and suggestions were made [3] that the elasticity of the skull should be taken into consideration. Following these suggestions, the rigid shell was replaced by an elastic one [12], and later by a membrane [13]. None of these models provided for damping of the skull and brain materials, and most of them restricted the boundary conditions to axisymmetric or radial loadings. Later, some of these models were extended and other ones formulated [14] to account for the viscoelastic properties of the brain, and to study the response of the model under torsional loads. All these models treated the two-dimensional problem, but later, extension to three-dimensional spherical model was made [15] at the cost of returning to the elastic shell theory.

1.4.2 Functional Head Injury Criteria

Instead of reproducing the structural characteristics of the head, and later associating certain responses of the models with injury, a functional or "black-box" model emphasizes the relationship between an input and an output. The input is usually a mathematical description of the impacting load, and the output is some indication of injury.

In order for these criteria to predict injury accurately, they must be validated against known injury cases. The predominant and principal tolerance criterion was, for a long time, the Wayne-State

Tolerance Curve (WST) [16,17]. This WST curve, (figure 2) was generated initially by impacting the frontal bone of human cadaver heads against unyielding flat surfaces. Linear skull fracture was used as the criteria of minimum injury. This injury assessment is based on the average recorded acceleration and pulse duration.

The WST curve may be considered as a model for head injury since it describes an input (acceleration)-output (injury or non-injury) relationship. Because of the difficulties associated with the practical interpretation of the WSTC the severity index was introduced by Gadd [18], which is essentially a mathematical model fit to the WST curve. Gadd found that an approximate mathematical expression of a good portion of the WST curve is:

$$1000 = \int_0^{\tau} [a(t)]^{2.5} dt$$

where

a(t): head A-P acceleration, in g-units,

dt : time differential, in seconds

τ : duration of acceleration pulse,

2.5 : weighting exponent, found to fit best the WST curve.

To determine whether an acceleration pulse a(t) is severe enough to cause injury, a severity index, GSI, is computed according to the right hand side of the above aquation. If the computed GSI is higher than threshold value of 1000, the acceleration is judged to be injurious, otherwise it is not.

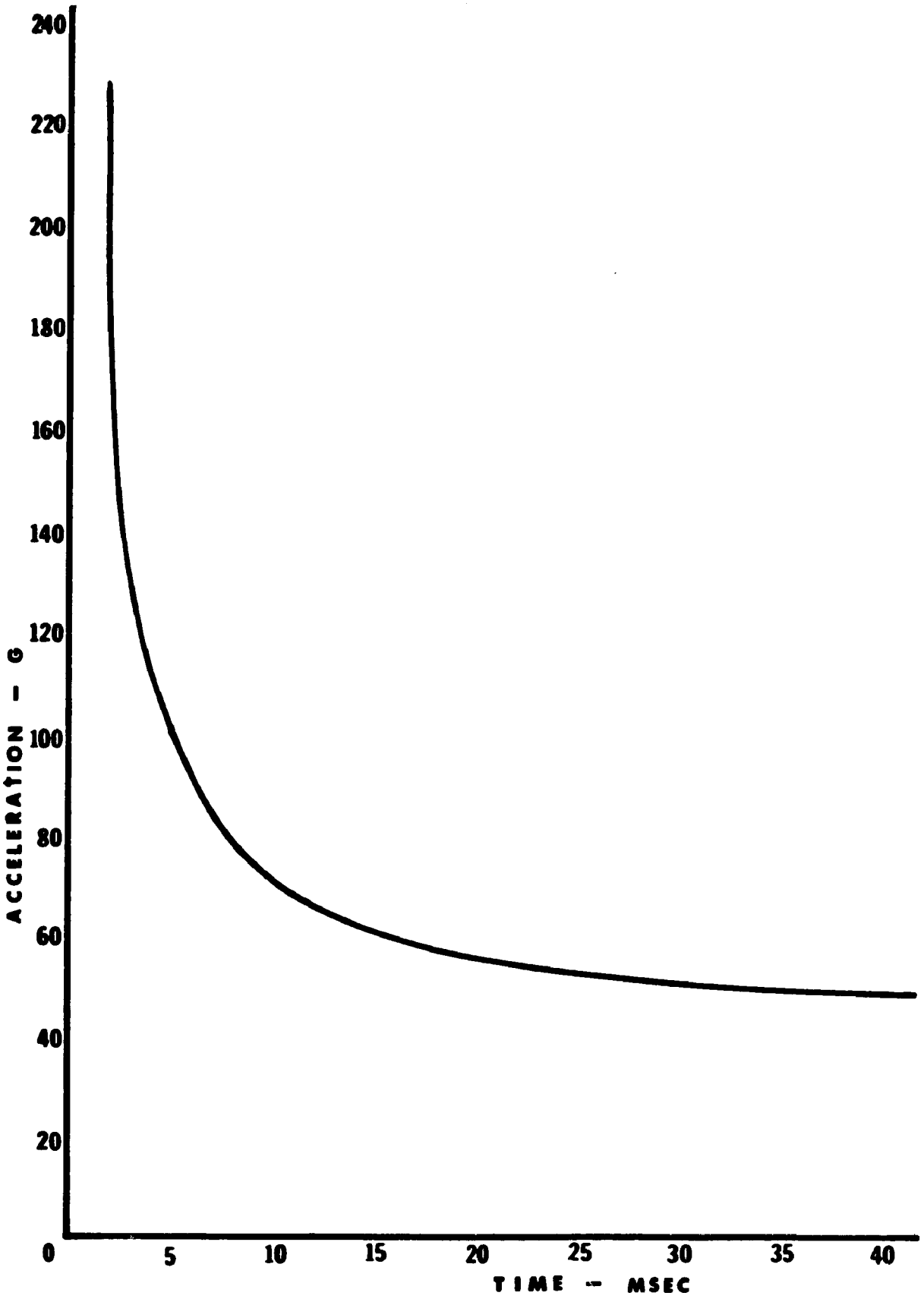


Figure 2. Wayne-State Tolerance Curve

The GSI works well if the impact conditions, under which the acceleration record a(t) is obtained, are similar to those used to generate the WST curve. These conditions are: (a) the impact is frontal, and the recorded acceleration is in the A-P direction; (b) a single pulse is recorded, i.e. no separate, multiple pulses are recorded.

Because of the limited applicability of the Severity Index, a more generalized index was proposed first by Versace, and then modified by NHTSA [19,20]. The new proposed index, Head Injury Criterion (HIC), for a given acceleration pulse a(t) is:

$$HIC = (\bar{A}_{1,2})^{2.5} \quad \Delta t$$

where

$$\bar{A}_{1,2} = \frac{\int_{t_1}^{t_2} a(t)\, dt}{\Delta t}$$

a(t) = resultant acceleration, g units

t = time, in seconds

t_1 = any arbitrary time point in the pulse

t_2 = for a given time t_1, a time point in the pulse, which maximizes HIC

Δt = $(t_2 - t_1)$

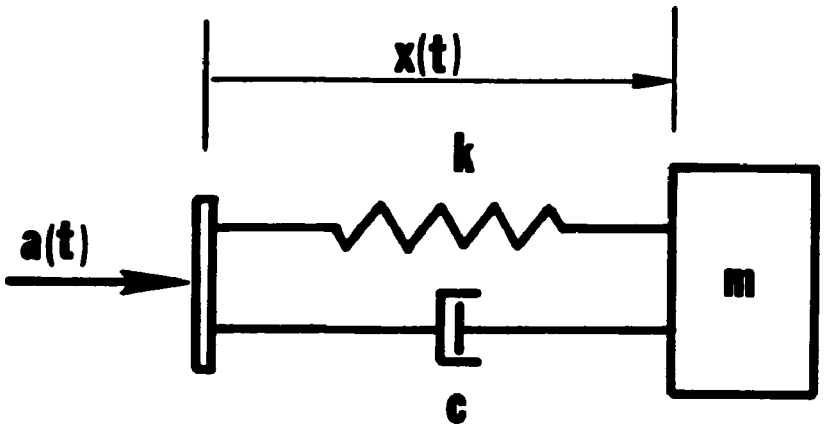
Again, HIC = 1000 is taken as the threshold value of tolerance, with the same consequences as the GSI computations.

The GSI and HIC may be classified as weighted-impulse criteria, where 2.5 is the weighting exponent. These criteria of injury are perhaps the most abstract functional models for head injury. They are mathematical abstractions of the experimental results of actual injury cases.

1.4.3 Functional Head Injury Models

Other functional models, based more or less on some physical reality have been also developed. These are lumped-parameter models with various degrees of lumpings and different bases for selections of parameters. Currently, there are four different lumped-parameter models, which accept acceleration as input, and generate a physical response whose maximum is taken as an indication of impact severity. Three of these models consist of a single mass to which acceleration is applied through a Kelvin viscoelastic element (a spring and a dash-pot in series), shown in figure 3; the fourth model, figure 4, consists of two masses connected by a Kelvin element. These models, their bases and usages are discussed individually in the next paragraphs. Although these models are physical systems of physical elements, their applications are confined to a single input, namely an acceleration pulse recorded under certain conditions, and therefore, they assess head injury only for these loading conditions. The first model is a single degree-of-freedom model, and was introduced by Slattenschek, et. al. [21], of the Vienna Institute of Technology. The equation of motion of this model is

$$\ddot{x} + 2\zeta\omega\dot{x} + \omega^2 x = -a(t)$$



EQUATION OF MOTION:

$$\ddot{x} + 2\zeta\omega\dot{x} + \omega^2 x = -a(t)$$

a(t): input acceleration to model

x(t): output parameter of model

$\omega = \sqrt{k/m}$: natural frequency

$\zeta = \omega c/2k$: daming ratio

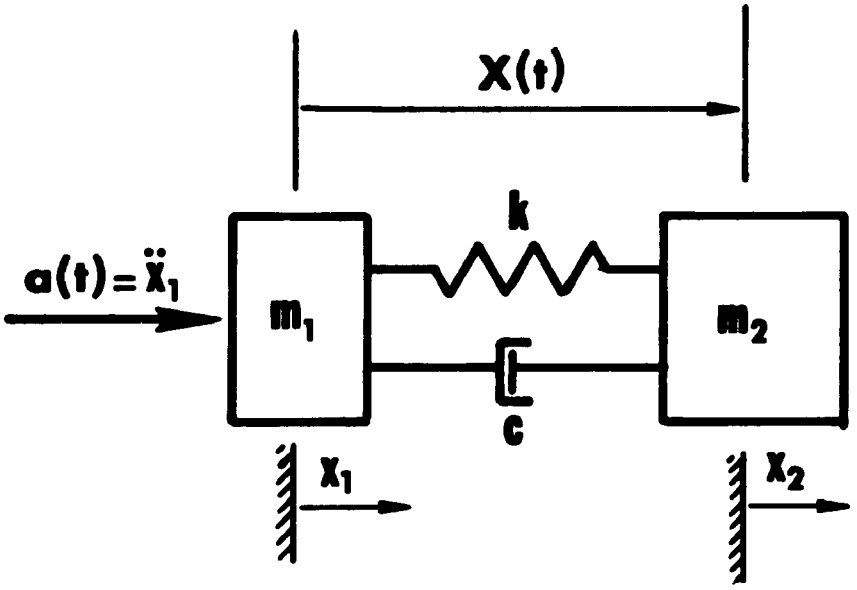
m: mass

c: damping constant

k: spring stiffness

} viscoelastic Kelvin element

Figure 3. One-Mass Head Injury Model



EQUATIONS OF MOTION:

$$\left.\begin{aligned} m_1\ddot{x}_1 + c(\dot{x}_1-\dot{x}_2) + k(x_1-x_2) &= 0 \\ m_2\ddot{x}_2 + c(\dot{x}_2-\dot{x}_1) + k(x_2-x_1) &= 0 \end{aligned}\right\} \text{ for } t > \tau$$

and

$$\ddot{X} + \frac{c}{m_2}\dot{X} + \frac{k}{m_2}X = -a(t) \qquad \text{for } 0 \le t \le \tau$$

where $X = x_2 - x_1$

$a(t)$: input accelration pulse, $\ddot{x}_1(t)$, of duration τ

$X(t)$: response of model

m_1, m_2, c and k: model constants obtained by impedance methods

Figure 4. Two-Mass Head Injury Model

where $x(t)$ is the spring deflection, interpreted as the brain-skull relative motion, ω and ζ are the natural frequency and the damping ratio of the system, respectively, and $a(t)$ is the acceleration time-history, recorded during an actual test and used as the forcing function to the model.

The equation of motion may be solved either with a closed form solution for simple shaped $a(t)$, e.g., sinusoidal pulse, or with numerical techniques if the pulse is irregular as is usually the case. The maximum response X_{max} is taken as an indication of injury associated with a certain force, elongation or pressure occurring in the brain. A J-Tolerance Index (JTI) is then defined as:

$$JTI = \frac{X_{max}}{X_{tol}}$$

where $X_{tol} = 0.092$ inches, for $\omega = 635$ rad/sec and $\zeta = 1$. The values for ω, ζ, and X_{tol} are so chosen as to achieve the closest fit to the Wayne State Tolerance Curve. Thus, there is no physical basis for the choice of these parameters, even though a value of JTI = 1 disagrees with no more than 4% with the WST curve, which is a much better fit than the Gadd Severity Index.

To give the parameters of such a model some physical basis, Fan [22] modified the previous model's parameters to approximate published material properties of the brain. This Revised Brain Model (RBM) estimates that the damping coefficient is 0.4, with a natural frequency of 175 rad/sec. For such a model, it was estimated, based on the long duration portion of the WSTC, that a spring deflection of 1.25 inches is the maximum tolerable value, while for the

short duration (less than 20 msec) portion of the WSTC, the deflection has no significance, but the velocity $\dot{x}(t)$ becomes important and must not exceed 135.3 in/sec.

Another attempt by Brinn and Staffeld [23] to match the WST curve resulted in what they called the Effective Displacement Index (EDI). The same single degree of freedom model is used, but the natural frequency and damping ratio are suggested to be ω = 482 rad/sec and ζ = 0.707. These values produced a deflection of 0.15 inches for short duration pulses (3-5 msec) on the WST curve. Since the model was to be used in designs and testings associated with dummy heads, and because of the unhuman-like response of these heads, higher values of the EDI were accepted as tolerable. Thus for the dummy head's A-P acceleration, the maximum tolerable EDI became 0.17 inches, and for the resultant dummy's head acceleration, 0.20 inches.

The three previous models, i.e., the Slattenschek, Fan and Brinn models, emanate from the WST curve. Slattenschek's gives a "perfect" fit to the curve when the input is a triangular pulse; the other two match portions of the same curve using different parameters, and thus producing different maxima for the response. The last model that will be discussed next is based on the physical response of actual heads in vivo and vitro. Thus the parameters obtained to describe it are derived from actual tests on various cadaver and subhuman heads. The "tolerable" values presented are based on impact survival tests of primates, which are then extrapolated to possible human tolerable values.

Stalnaker and McElhaney [24,25] conducted a series of tests to measure the mechanical impedance of the head, by subjecting it to forced sinusoidal vibrations. By varying the frequency of motion of the exciting probe, they found that the mechanical impedance of the head being tested varies with the frequency. In an attempt to describe in a more general and compact form most of the recorded responses, a simple mathematical model was conceived. This model consisted of two masses connected by a spring and a dashpot in series. At low frequencies, this model behaved as a mass equal to that of the head, while at high frequencies, it behaved as a much smaller mass, which was interpreted as the mass of the segment of skull bone to which the exciting probe was attached. By varying the damping constant and the spring stiffness, they were able to match satisfactorily the impedance curves of the model to those obtained from the actual tests (see figure 5).

Because of the wide frequency range for which the impedance curves were generated (5-5000 Hertz), the model was assumed to be good for corresponding wide range of impact durations. A shock spectrum of this model, for a given acceleration pulse and a given maximax value (largest of absolute values of a maximum or a minimum) had the same basic shape of the WST curve, that is, flat for long durations and dropping sharply with short durations. The remaining problem was then to determine the maximum tolerable value of relative displacement between the two masses. To obtain this value, a series of head impacts to sub-human primates, with various degrees of severity, were conducted, and accelerations of the head were recorded along with a clinical injury index (see section 1.3). The impacts at the threshold

of survival fell in the proximity of a tolerance curve (shock spectrum of constant output parameter), which was generated for a certain maximum spring deflection.

A series of tolerance curves, shown in figure 6, or equivalently, a series of maximum strains were obtained for subhuman primates of various species and weights. Scaling parameters were then introduced to extrapolate the findings to human head, which resulted in a tolerance curve for human head, associated with a maximum strain of 0.0061 in/in for an average human head length of 5.75 inches in the A-P direction.

The Maximum Strain Criterion (MSC) model was validated against known injury cases, and against tests conducted on various human and sub-human heads. It was also used to generate tolerance curves for human heads under lateral impacts (L-R direction). It should be remembered, however, that these curves were developed for blunt impacts where the contact area with the impactor approximates that area of the existing probe used in generating the impedance curves. Extension of the MSC to padded impacts or to impulsive loadings should be done cautiously, since other injury mechanisms may be involved, which are not the basis for developing the model. The same remarks apply to all the models discussed in this section and the previous one. All the criteria and models have a limited range of application. When impact conditions change, so must the criteria of injury. What is needed then is a model that can accomodate various loading conditions, and which can predict injury under one or more criteria based on one or more injury mechanisms.

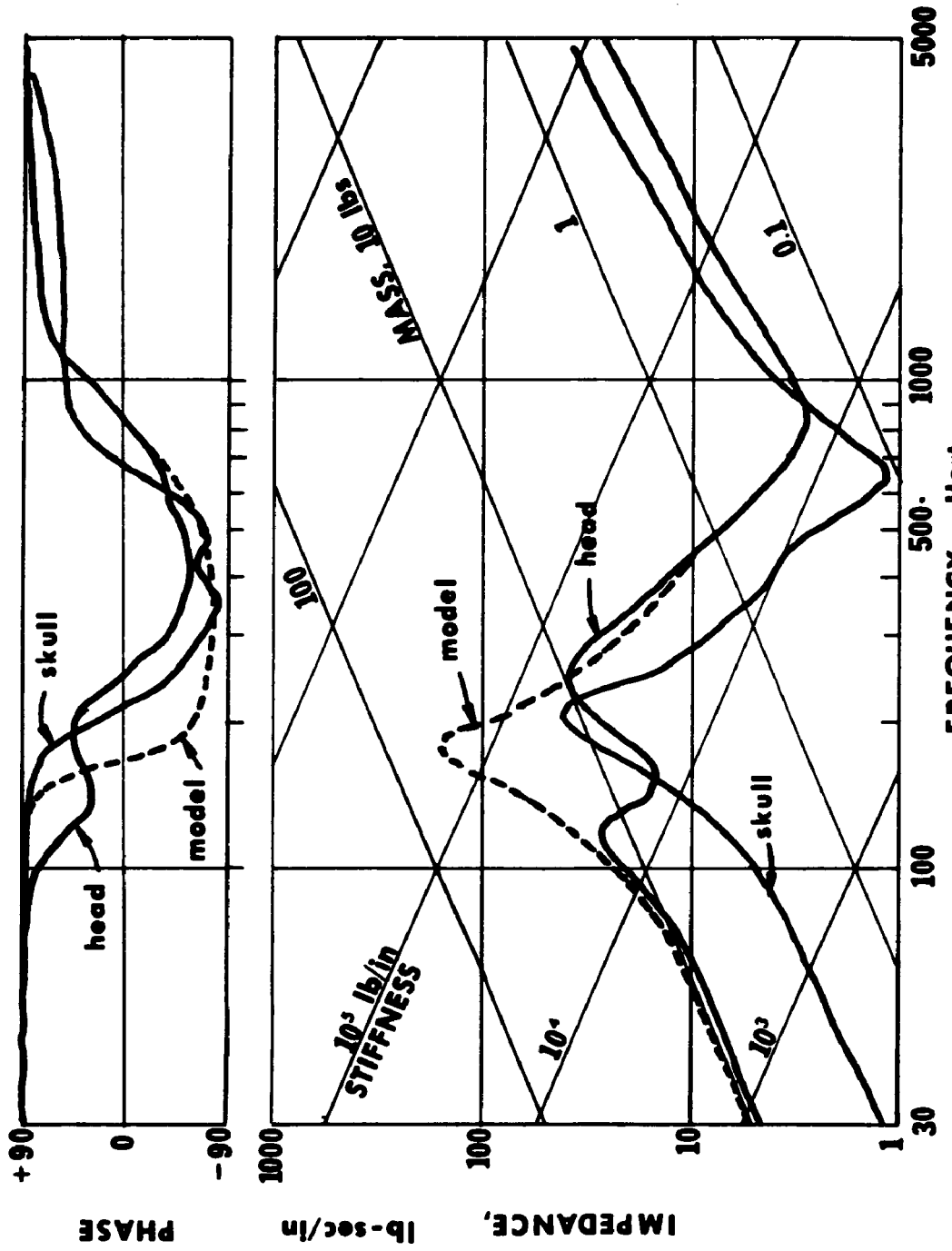


Figure 5. Impedance Curves for Model and Cadaver Head

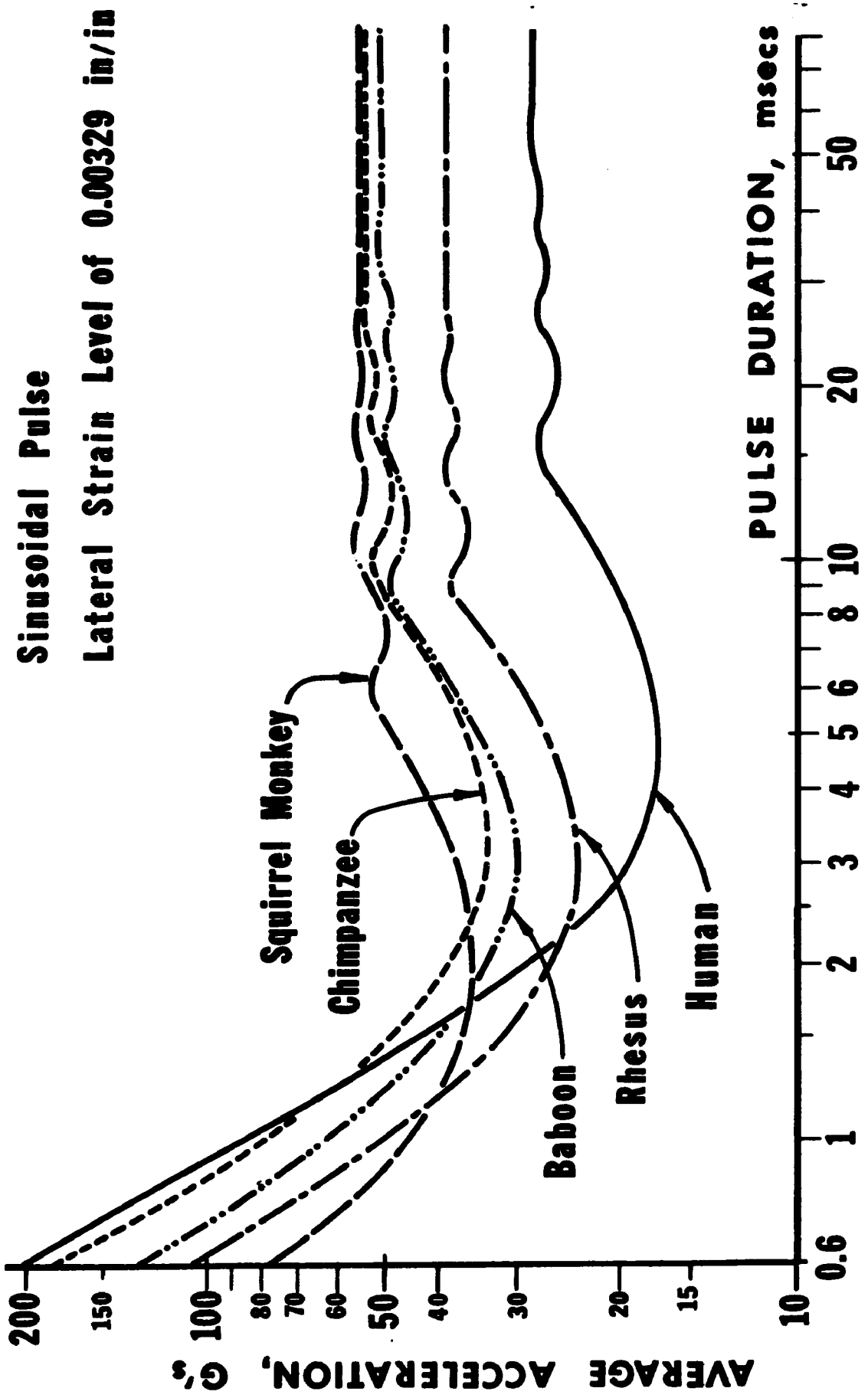


Figure 6. Maximum Strain Criterion Tolerance Curves

CHAPTER 2

A PROPOSED HEAD INJURY MODEL

The background presented in the previous chapter suggests that certain needs in head injury prediction techniques are not satisfied. First, there is a need for a model (or technique) which is capable of simulating various possible injury mechanisms. Second, this model should have the flexibility of accepting a variety of impact loading conditions. Third, such a model should be easy to use, and its responses readily interpreted. In order to meet these needs, a head injury model has been developed. This chapter describes the important features of this model and the rationale associated with its development.

2.1 INJURY MECHANISMS TO BE SIMULATED

Most head injury hypotheses suggest that the motion of the brain inside the skull is of critical importance. This motion is therefore given primary consideration in the proposed model. Translation and rotation of the brain relative to the skull, as well as a measure of the forces acting on the brain stem and the upper cervical cord are predicted.

The skull deflection, and its possible fracture, is another possible mode of head injury that is simulated.

In addition to brain motion and skull deflection, the overall motion of the head about the first and second cervical vertebrae is simulated to give an indication of a possible neck injury.

2.2 PHYSICAL PARAMETERS OF MODEL

The anatomy of the head and neck is geometrically too complex to simulate in detail in a practical model. More or less gross approximations and idealizations must be made in order to achieve a practical model which is capable of simulating the desired injury mechanisms.

Roughly speaking, the head consists of a brain surrounded by a skull, which is mounted on a neck. The characteristics of these elements (brain, skull and neck) and their interconnections, as they relate to the injury mechanisms of concern, may be lumped in a model consisting of rigid bodies, concentrated masses and viscoelastic elements connecting them. Consequently, the model proposed here is a lumped-parameter one, where the parameters are obtained from the actual anatomy of the head, published and measured head responses, and, as necessary, actual measurements of these parameters.

The actual human neck consists of seven cervical vertebrae joined by ligaments, fiber cartilages, and membranes to form a curved beam column. The relative movements of the individual vertebra are lumped in one single movement between the first and second vertebrae (atlas and epistropheus) and the seventh cervical one. Thus, the multi-element curved neck is simulated by a single straight column. The bending characteristic of the neck itself is simulated by a torsional viscoelastic element at the cervical-thoracic articulation, and the compression-tension properties of the intervertebral

ligaments and fibrocartilages are represented by two translational viscoelastic elements along the axis of the simulated straight neck. Finally, the inertial properties of the neck are represented by a concentrated mass placed at the junction of the two translational elements. This mass is equal to that of the neck, and its location along the axis of the neck determines the moment of inertia property of the simulated neck. The sub-model of the neck is shown in figure 7(A).

For the purposes of head injury simulation, the cerebral cranium, which consists of occipital, lateral, temporal, spheroid and ethmoid bones may be considered as an enclosure housing the brain. The eight bones of the cerebral cranium and the visceral cranium are lumped into an enclosure shown in figure 7(B). This sub-model simulates the skull and provides "walls" to which the brain can be attached. In addition, the inertial and viscoelastic properties of this enclosure represent similar characteristics of the actual skull itself. First, the two masses m_1 and m_2 are connected by a Kelvin translational element and may be considered as the lateral walls of the skull. The third mass m_3 may be considered as the "roof" of the skull, and the m_1-m_2 axis as the "floor." The three masses are so lumped as to match impedance characteristics of the skull and their distances are so selected as to give the skull sub-model the same moment of inertia of the actual "rigid" skull. The four imaginary surfaces formed by the three lumped masses of the skull are constrained by relatively stiff viscoelastic Kelvin elements as shown in figure 7(B).

The proposed model is a 2-dimensional (planar) one. The actual movement of the skull relative to the neck is usually a combination of rolling, gliding and rotation, which results in forward-backward pitching, left-right bending (or rolling) and left-right twisting (or yawing). Since the model is planar, the yaw motion is not modeled, and only pitching and rolling are allowed for the A-P and L-R models, respectively.

For the pitching motion of the skull, there is no precise axis of rotation because this motion is a mixed gliding and rolling of the two condyles of the occipital bones about the two articular pits of the atlas (1st cervical vertebra). However, the gliding is so small that it may be lumped with the rolling motion into a simple rotation about the lateral axis passing through the atlanto-occipital articulation. The cartilages, membranes and muscles effecting the motion of this articulation are all lumped into a single torsional viscoelastic element.

The rolling motion is also considered as a pure rotation, even though the mechanics of this left-right motion are not precisely a simple rotation. When the skull "rolls" about the neck, the atlas remains almost fixed to the occipital condyles and the skull-atlas combination rotates about a pair of lateral atlanto-epistrophic joints, symmetrically situated on either side of the middle line. In the model, this motion is considered as a simple rotation about an A-P axis passing through a point half-way between the pair of lateral atlanto-epistrophic (first and second vertebrae) joints. The viscoelastic properties

of cartilages, muscles and ligaments are represented by a single torsional Kelvin element.

Finally, the brain is simulated by a rigid body with mass and moment of inertia. The attachment of the brain to the skull is so designed as to allow three types of motion of the brain relative to the skull. Two translational Kelvin elements secure the brain to the two vertical "walls" of the skull and control the horizontal brain-skull motion. Two other viscoelastic elements attach the brain to the "roof" and the "floor" of the skull and control the vertical relative motion between the skull and the brain. The rotation of the brain inside the skull is controlled by a single torsional Kelvin element, which is grounded to an axis parallel to the m_1-m_2 axis of the skull. The sub-model of the brain and its attachments is shown in figure 7(C).

2.3 THE ASSEMBLED HEAD-NECK INJURY MODEL

When the sub-models of figure 7 are assembled, they form a model of the head which may be used to simulate the motion of the brain, skull and neck under impact conditions. This head-neck model, figure 8, is a two-dimensional one, and therefore would represent a planar motion either in the L-R or the A-P vertical planes. The constants of the model (values for masses, springs, dashpots and distances) would then have to be different for an A-P impact from those for an L-R impact. This does not mean a change in the structure of the model, but a change in the values of the model's parameters.

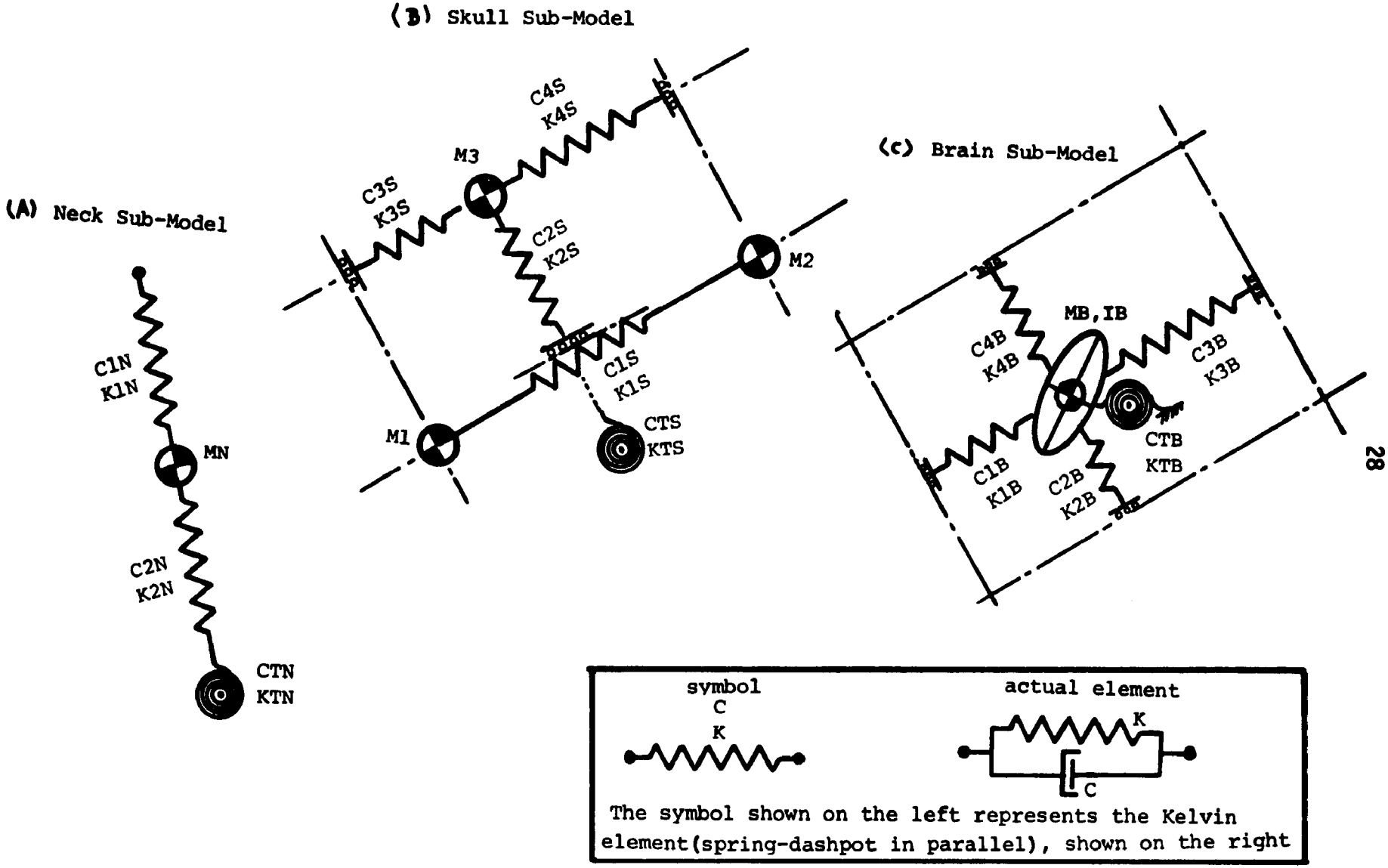


Figure 7. Sub-Models of Neck, Skull and Brain

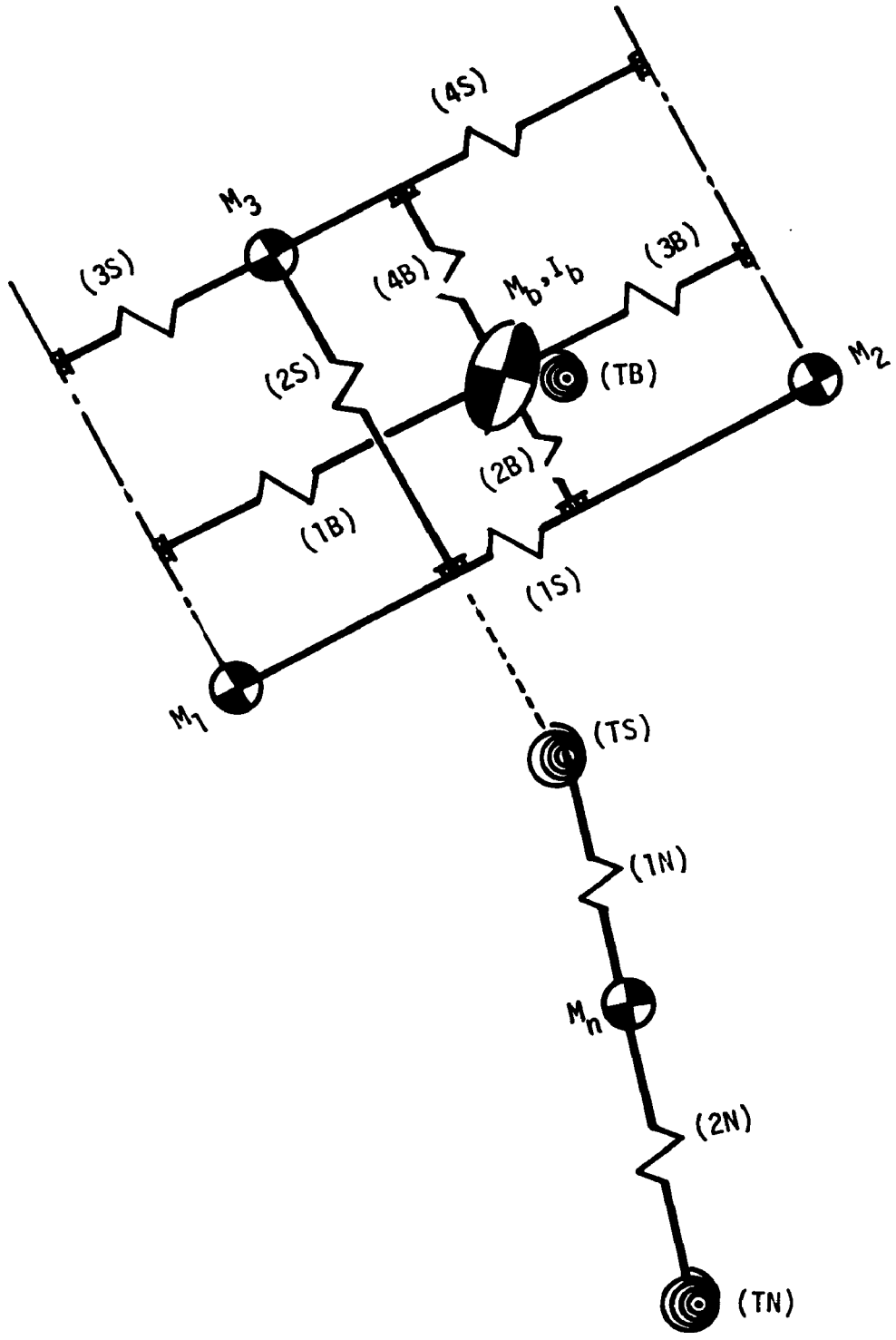


Figure 8. Proposed Head Injury Model

The methods of obtaining the constants of the model are discussed thoroughly in the next chapter. Briefly, there are three classes of these constants that must be determined: (a) masses and moments of inertia, (b) distances and lengths and (c) viscoelastic properties modeled by Kelvin elements which consist each of a spring and a dashpot in parallel. The masses and moments of inertia are obtained from anatomical measurements and the lumping of the masses by impedance methods and simple calculations. Impedance methods and free vibrations are also sources of the viscoelastic properties of the interconnections between the various "lumps" of the head. Distances are essentially based on anatomical measurements, but may be modified to match the inertial properties and the dynamic responses observed in the actual head.

2.4 ALLOWED TYPES OF IMPACTS

The proposed head injury model is designed to simulate injury mechanisms under impact conditions. The most common types of impacts are blows to the skull (direct impact) and sudden stops of the torso (indirect impact) exemplified by whiplash injuries.

In order to keep the input to the model as simple as practicable, while providing enough flexibility of varying the impact conditions, the following forces, torques and accelerations are allowed:

a) Three forces P_1, P_2 and P_3 may be applied to the skull at m_1, m_2 and m_3 respectively. The point of application of each force is at a distance (u,v) relative to its corresponding mass, and its direction is denoted by an angle α from the horizontal axis of the skull.

b) A torque T_s may be applied to the enclosure formed by m_1, m_2 and m_3; i.e., the torque acts on the skull as a rigid body.

c) A torque T_n may be applied to the neck, usually at the neck-torso joint, but could be interpreted to act on the angle of the neck.

d) At the neck-torso articulation, chosen as the inter-vertebral joint between the seventh cervical and first thoracic vertebrae, two types of inputs are allowed. Either vertical and horizontal forces may be applied at this joint, or its vertical and horizontal motions are specified. The rationale behind specifying the motion of this point is the difficulty of obtaining experimental measurements of the forces acting at this joint, and the relative ease of obtaining its time-history motion.

2.5 METHODS OF FORMULATION AND SOLUTION

In this section, only a brief discussion of the methods used to formulate the equations of motion and to solve them is presented. The mathematical details are in appendices A and B.

The proposed model is a mechanical system consisting of masses, springs and dashpots, and has 12 degrees of freedom, of which two may be specified as input. The equations of motion of this system are obtained by the classical Lagrange method which makes use of generalized coordinates and yields directly these equations. The solution produces the time-histories of all the coordinates used, along with some desired moments and forces which would have been difficult to obtain otherwise.

2.5.1 Formulation of Lagrange's Equations of Motion

The Lagrange method of writing the equations of motion allows the use of as many coordinates as convenient.

The Lagrange equation of motion is

$$\frac{d}{dt}\frac{\partial T}{\partial \dot{q}_k} + \frac{\partial D}{\partial \dot{q}_k} + \frac{\partial V}{\partial q_k} + F_k = Q_k \quad ; \qquad k = 1, 2, \ldots, N \tag{2.1}$$

where

T : kinetic energy of the system,

D : dissipation function,

V : potential energy,

N : number of generalized coordinates used, $N > N_o$; N_o being the degrees-of-freedom of the system,

Q_k: generalized force applied externally along the coordinate q_k, and

F_k: constraint force along the q_k coordinate.

The expressions of T, D and V are written in terms of coordinates which are not all independent. The total number of generalized coordinates used to formulate the problem is N = 29. Since the system has N_o = 12 degrees-of-freedom, the difference $N - N_o$ = 17 is the number of non-independent coordinates, and is also the number of independent constraint relationships which must be written to express geometrical dependencies between all 29 generalized coordinates.

In the expression of potential energy, found in appendix A, the gravity effect is neglected. This is a reasonable omission because the model is designed for impacts which could reach as high as 200 g's, and makes the addition of 1-g gravity a mathematical burden with no appreciable effects on the impact response of the head.

The generalized forces Q_k in equation 2.1 are obtained systematically by

$$Q_k = \sum_{j=1}^{N_a} \vec{P}_j \cdot \frac{\partial}{\partial q_k}(\vec{r}_j) \qquad (2.2)$$

where N_a = 7 is the number of externally applied forces, and $\vec{r}_j$ is the position vector of the point of application of the force $\vec{P}_j$, both expressed in the inertial reference frame. Thus, each generalized force Q_k, is the sum of the components of the external forces (or torques) along the k^{th} generalized coordinate.

Finally, the constraint forces F_k are constructed in a similar fashion. Each constraint force F_k, acting along the k^{th} coordinate, is the sum of all the contributions from 17 constraint relations. In other words, given the constraint relations

$$f_j(q_1, q_2, \ldots, q_N) = 0 \qquad j = 1, 2, \ldots (N-N_0)$$

to obtain a constraint force F_k, the Lagrange undetermined multipliers are introduced such that

$$F_k = \sum_{j=1}^{N-N_0} \lambda_j \frac{\partial f_j}{\partial q_k} \tag{2.3}$$

Obviously, the undetermined multipliers λ's are additional unknowns to be determined along with other unknowns of the problem. This is no burden since many of these multipliers represent forces and moments which are of interest to head injury assessment.

The mechanical system proposed as model for head injury is described then by Lagrange equations and constraint equations. In the next paragraphs, the methods employed for the solution are presented, but the details of the solution are given in appendix B.

2.5.2 Methods of Solution

The mathematical description of the system results in as many equations as there are unknowns. The detailed presentaion of these equations is given in Appendix A; the solution, in Appendix B. Only a brief look at the solution is given in this section.

Digital methods for integrating the differential equations are used. The accuracy of these methods, and the flexibility in handling the various parameters and variables offers an advantage over analogue or other methods of solution.

Since the model is to be used for parametric studies as well as repeated predictions of head injury, pre-packaged programs and simulation languages were not used because of their generality and expense. Instead, a set of computer subroutines were written to handle all phases of the simulation, with the exception of the integration subroutine.

The method of solution was chosen as to avoid as much as possible matrix handling and particularly matrix inversion. This was done because the matrix of coefficients of the equations to be solved is large and sparse, which would add storage cost and inversion cost to the total cost of the simulation. Instead, simple back-substitutions were used whenever possible, and special reduced-size matrix operations were introduced.

The order of these steps and the complexity of the solution depends on the type of input. Thus, a force input at the cervical-thoracic joint (x_0, y_0) requires one method of solution, while an acceleration input of $\ddot{x}_0(t)$ and $\ddot{y}_0(t)$ requires another. The details of this solution are presented in appendix B.

2.6 THE "HEAD" SIMULATION PROGRAM

Finally, in this section, a brief outline of the computer program "HEAD" is presented.

In order to simulate an impact to the head, one must know the following:

(a) The characteristic constants of the modeled head.

(b) The boundary conditions, or parameters of the impact.

(c) The simulation paramerters relating to accuracy, duration, etc...

(d) The type of output desired.

This information is used by the HEAD program, which processes it for the solution, performs the solution(integration), then outputs the requested results.

The HEAD computer program is descibed in more or less details in the appendices. Briefly, each simulation conducted by HEAD consists of three phases. In the first phase, the program reads the input data and prepares it for the next phase. The second phase is the solution itself, controlled by a standard integration subroutine which uses two user-written subroutines to compute the derivatives and to output the results. The third and final phase of the simulation is devoted exclusively to the presentation of the results in legible forms.

CHAPTER 3

DETERMINATION OF MODEL CONSTANTS

Once the structural configuration of the proposed model is conceived, the task of descibing the characteristics of its discrete elements begins. This is done in such a manner that the overall properties of the actual head, whenever known, are conserved in the lumped-parameter model.

Many valid questions are raised at this point: What experimental data can serve as a basis for obtaining parameters for the model? How valid is tha available data? Which parameters, if any, can be directly measured? What methods and rationale are used to lump the observed properties into discrete constants? How representative is a selected set of constants? These and other questions form the basis of this chapter.

3.1 VALIDITY OF OBSERVED PROPERTIES AND SELECTED CONSTANTS

Because of wide variations in the biological properties and observed responses between various human heads, it is difficult to ascertain the statistical value of the measured properties. This is further compounded by the limitations in obtaining human responses to impact beyond voluntary tolerance levels.

It seems, therefore, that no set of constants obtained from this data can result in a single model which can be matched by an actual human head. However, the selection of constants can be made from ranges or bands of acceptable experimental data, bearing in mind that, while the resulting model may not duplicate a human head, it can serve effectively to show trends in responses and patterns of injury

mechanisms under varying impact conditions.

Experimental head injury on primates should be included in this discussion. Many researchers, including the author, feel that of all sub-human animals, primates have impact responses closest to humans. This experimental research is valuable in providing insights to the injury mechanisms in humans and their relations to the physical parameters involved in injurious impacts. The major problem, however, is the correlation between humans and primates; though not firmly established, such correlation does appear to exist. Since much of the data necessary to describe and validate a human head injury model extends beyond human voluntary levels, additional gains are obtained from primate research. Furthermore, impact conditions and response measurements can easily be controlled in a laboratory atmosphere. As with humans, there is a wide variation between responses of various species; and within a single species, properties and responses vary with size, age and sex. The drawback in such variations is offset by the benefits gained from extending impact conditions beyond voluntary levels, an extension not feasible with human volunteers.

Given a set of constants describing the model, it should be pointed out that the choice of the constants is based on experimental data recorded under specific impact conditions. It has been shown that when these conditions change, it is very likely that the corresponding responses also change. This justifies the need for different models to be used for different impacts. Thus, an A-P model should not be used for side impacts, instead, an L-R model must be used for these impacts. Such separation is perfectly acceptable

since the model is conceived for short-duration impacts, during which the initial motions are essentially planar.

For the reasons discussed above, two heads are modeled, each in two directions. The four resulting sets of constants (or models) are then: human A-P, human L-R, Rhesus A-P and Rhesus L-R. The choice of the Rhesus monkey's head to be modeled is simply a result of the availability of experimental data obtained with this primate.

3.2 AVAILABLE EXPERIMENTAL DATA

The experimental data available for developing the present model may either be used to obtain constants of the model or to validate its dynamic response to impact. However, some of this data may serve the two stated purposes. This section concerns the first type of data which is used, primarily, to obtain constants of the model.

Most of the anatomical properties of human and Rhesus heads have been measured and published. These are properties relevant to the model and include such inertial properties as average head weights, average brain weights, moments of inertia of the head about various axes. Dimensions of the skull, neck have also been measured; but data on the locations of the skull c.g., brain c.g., and distance between neck-skull articulation to skull c.g. is rare in the literature. This may be attributed to the controversy about the precise axis of rotation of the skull about the atlas, and possibly to the difficulty of pinpointing the exact location of the skull c.g. relative to some well known bone "landmark." Modelers had to assume reasonable values for these distances. Therefore, in addition to actual measurements, assumed values which have been used

in similar models, are used in the present model as initial estimate of many of its parameters. Table 1 gives some of the available properties, their numerical values (when they can be represented by a single constant), and their sources.

The geometrical and inertial properties of the head are only partial requirements to describe the model. Other information is needed about the dynamic behavior of the head. Such information is usually available in the form of load-deflection curves under quasi-static or dynamic loading, natural motion of the brain inside the skull, steady-state response of the head to forced vibrations given in the form of impedance-frequency curves, and occasionaly impact-response of the head given as acceleration-time histories. This type of data cannot be used directly to obtain the constants of the elements of the model; nevertheless the needed information is contained implicitly in these curves. Since most of this data cannot be given as single constants, a series of curves are given instead in figures 9 through 13 and are self-explanatory.

Several observations should be made at this point about the experimental data. First, the spread in most of reported data is wide, which decreases the confidence in the validity of any selected set of constants. Second, many of the "constants" of the model are neither constant nor linear. This is not uncommon in modeling situations where idealizations and simplifying assumptions are usually made in order to develop a simple and practical model. However, some elements, critical to the performance of the model, have been so designed that they may be described by nonlinear piece-wise load-deflection curves. Third it should be pointed out that in a discrete-

PROPERTY (Average of Reported)*	HUMAN	REFERENCE	RHESUS	REFERENCE	UNITS
Neck weight	3.5	HSRI**	0.8	HSRI	lbs
Neck length (Straight line)	4.35	[35]***	1.5	HSRI	inches
Max. Voluntary Flexion	50.	[35]	---	---	degrees
Max. Voluntary Extension	55.	[35]	---	---	degrees
Head Weight (with brain)	10.	[25]	2.1	HSRI	lbs
Brain Weight	2.5	[25]	0.2	HSRI	lbs
Head Mass Moment of inertia (a-p)	0.20	[27]	---	---	$lb\text{-}in\text{-}sec^2$
Head Length (A-P)	7.5	[25]	2.32	HSRI	inches
Head Width (L-R)	6.0	[25]	2.18	HSRI	inches
Head Height (S-I)	5.5	[25]	1.75	HSRI	inches

NOTES: * values given lies within reported extremes, usually, the average.

** HSRI: Biosciences Division of Highway Safety Research Institue's files.

*** Numbers in [ ] are references given at the end of this paper.

Table 1. Some Available Anatomical Data on Head (Human and 20-lbs Rhesus)

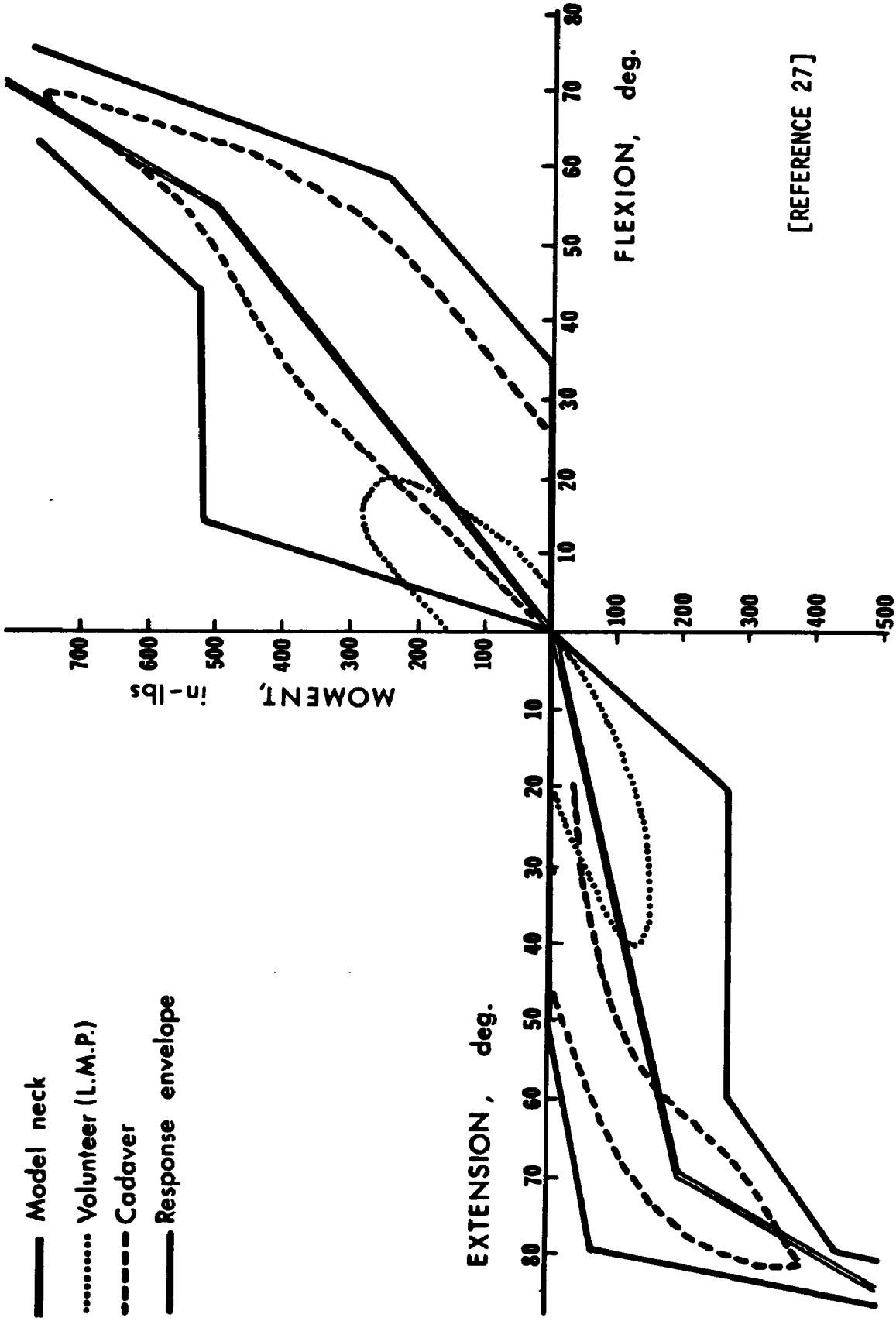


Figure 9. Moment(about occ. condyles) versus Head-Torso Angle

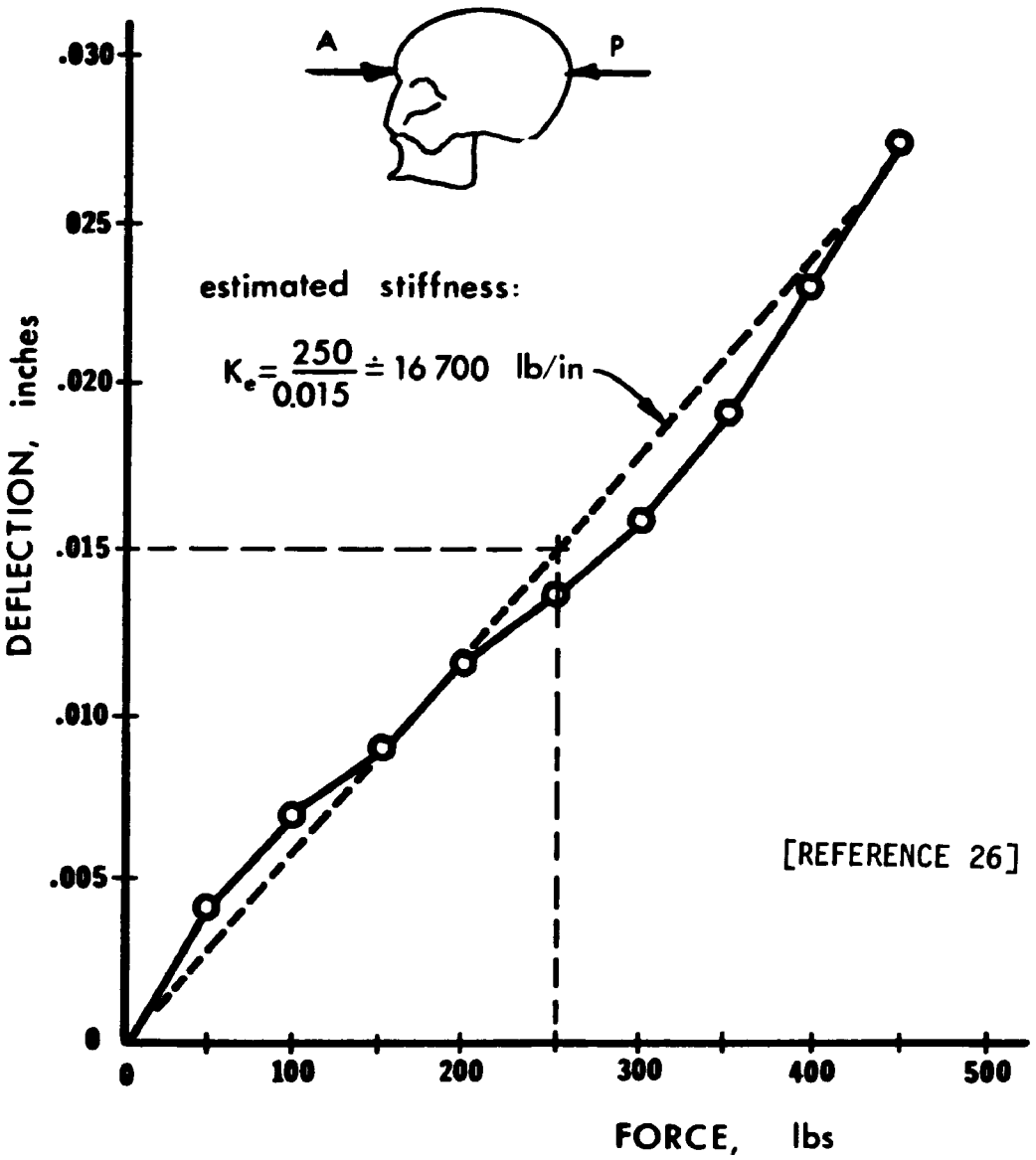


Figure 10. Static Load-Deflection Curve of Human Skull

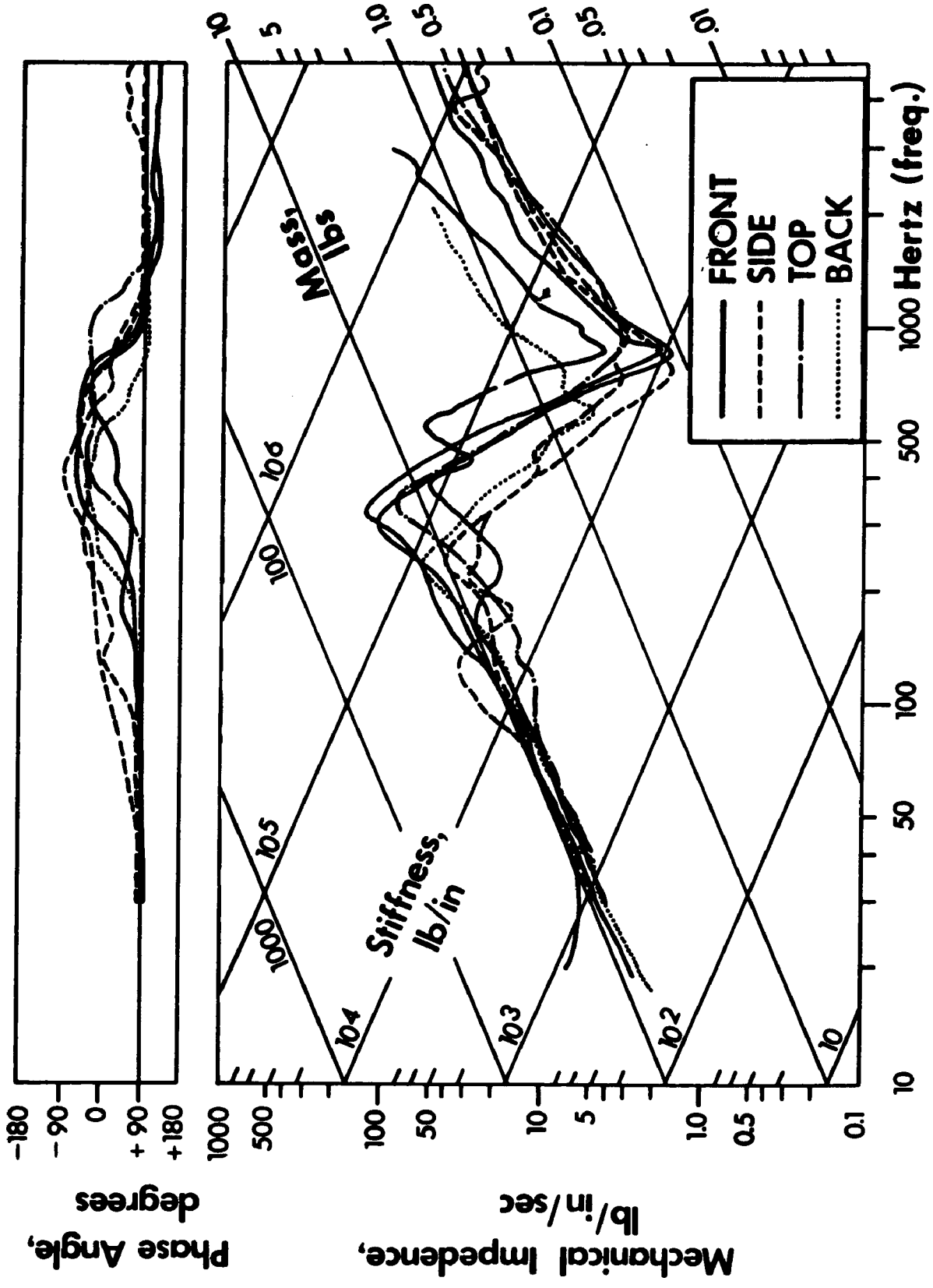
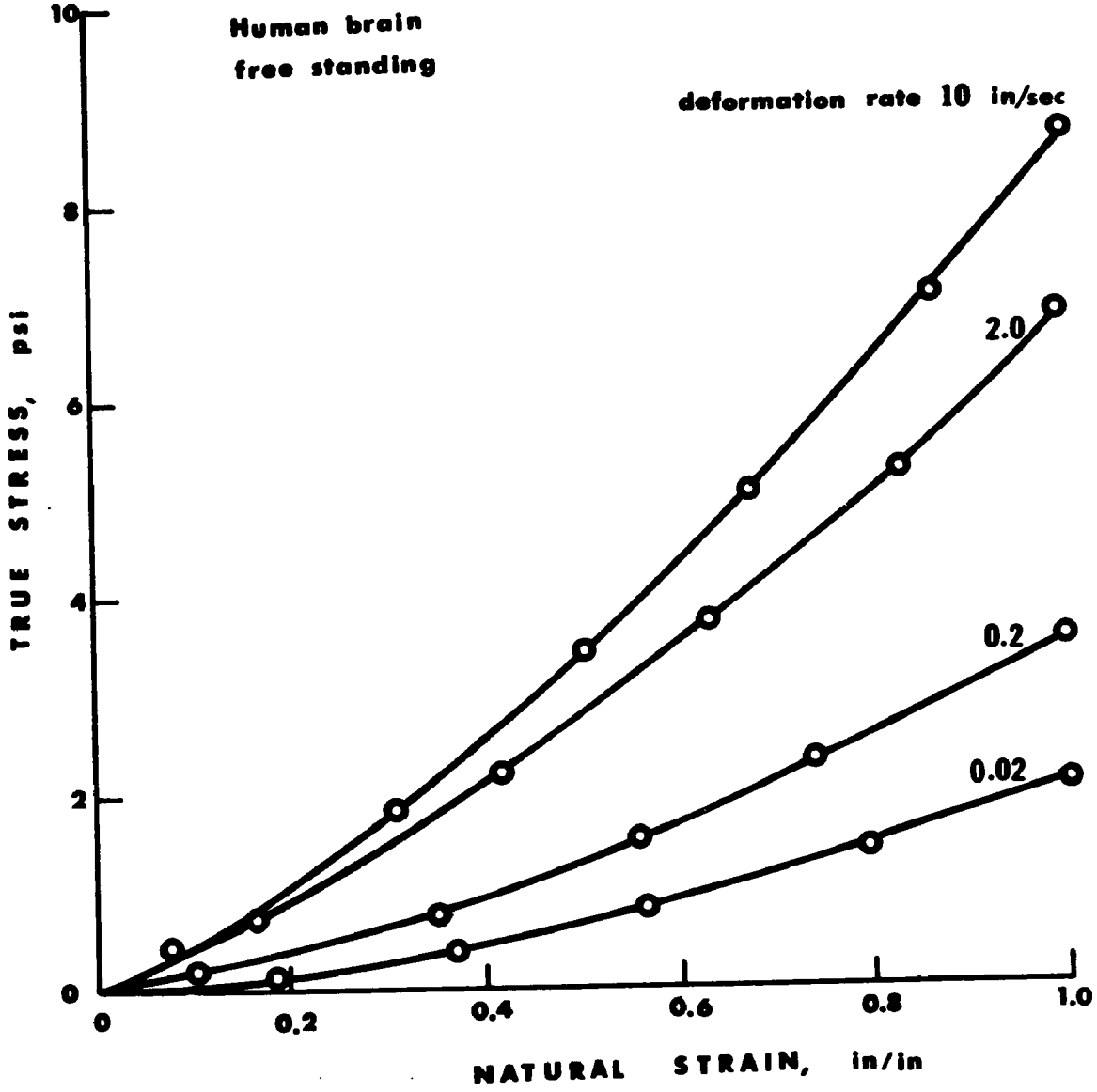


Figure 11. Mechanical Impedance of Cadaver Head [SOURCE: 34]



[REFERENCE 32]

Figure 12. Free Standing Compression of Human Brain Tissue

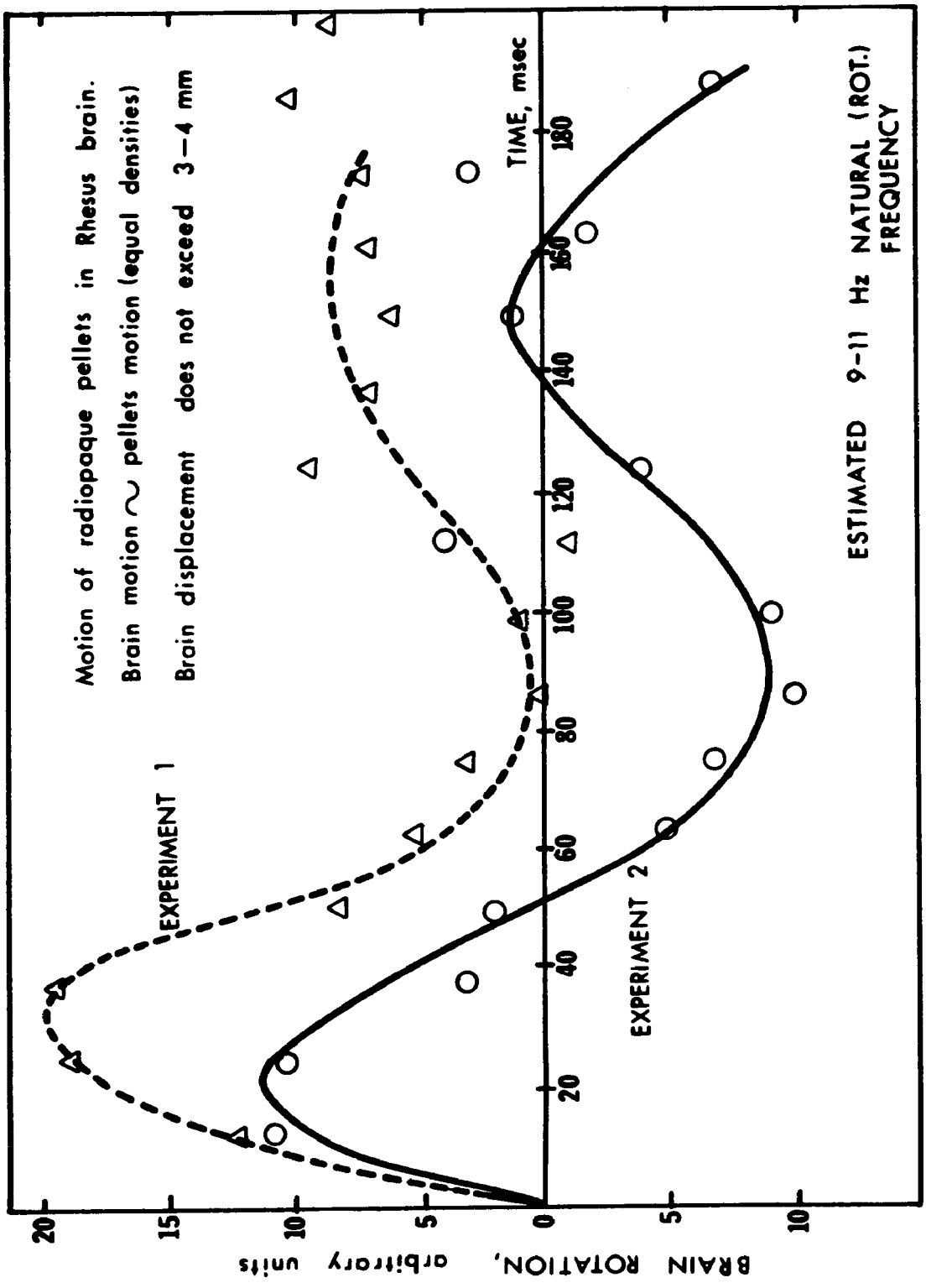


Figure 13. Rotation of Rhesus Brain Relative to Skull [REFERENCE: 6]

element model, many of the elements are conceptual and do not physically exist. By the virtue of "creating" these elements, the problem of assigning properties to them always arises. Some arbitrary, but reasonable, values must be chosen. This choice may later be adjusted during the validation phase of model development.

3.3 LUMPING OF PARAMETERS

The proposed model requires the specification of 6 inertial properties, 13 viscoelastic (spring-dashpot) elements and 12 independent distances to describe it completely. While it is mandatory to specify all inertial and viscoelastic elements, the model requires the input of 3 easily identifiable distances, the other dimensions are calculated automatically within the programmed model according to a predetermined method.

3.3.1 Neck Properties

Inertial. The mass of the neck, MN, is about 3.5 lbs for a 10-lb human head, and about 0.8 lbs for a 20-lb Rhesus monkey which has an average head weight of 2.3 lbs. The moment of inertia of the neck is not included in the formulation. It was felt that inertial effects of the neck on the motion of the brain are sufficiently represented by a concentrated mass, and terms of the form $m\ell^2$ which are implicitly included in the formulation.

Lengths. The neck assembly of seven vertebrae is not in a straight line. However, the neck is simulated by a straight-line connection between the skull-neck and neck-torso articulations. This distance

represents the "length" of the neck and is about 4.35 inches in humans and 1.5 inches in Rhesus monkeys. This distance is used for both the L-R and A-P model, even though as explained in section 2.2, the two axes of L-R roll and A-P pitch do not pass through the same point. The difference, however, is so small that, for all practical purposes, it can be neglected. The total neck length must be divided into two segments L1 and L2 which locate the c.g. relative to C1 and C7, respectively. As initial estimate, the two lengths are assumed equal, i.e. L1=L2=2.17 inches for a human neck, and L1=L2=0.75 inches for the Rhesus.

Springs. Load-deflection responses of the neck suggest that none of the 3 required stiffnesses is linear. Dynamic tests show that the neck is stiffer in compression than it is in tension. Flexion-extension properties, represented in the model by the torsional visco-elastic element, are different for flexion and extension. Furthermore, these properties show a "stiffening" effect with increasing deflection. In figure 14 and table 2, the load-deflection characteristics of K1N, K2N, KTN used in the model are shown for the four models. The rationale for estimating the torsional spring KTN is discussed in section 3.3.2, along with the skull-neck torsional coupling.

Damping. Very little data is available to describe, quantitatively, the effects of damping in the neck. The presence of damping is uncontested, but its type (frictional or viscous) and its amount has not been firmly determined. Because of the lack of such data, viscous damping is assumed, and the values initially adopted are C1N=C2N=1.0 lb-sec/in, CTN=2.0 lb-in-sec/rad for a human A-P and L-R heads and

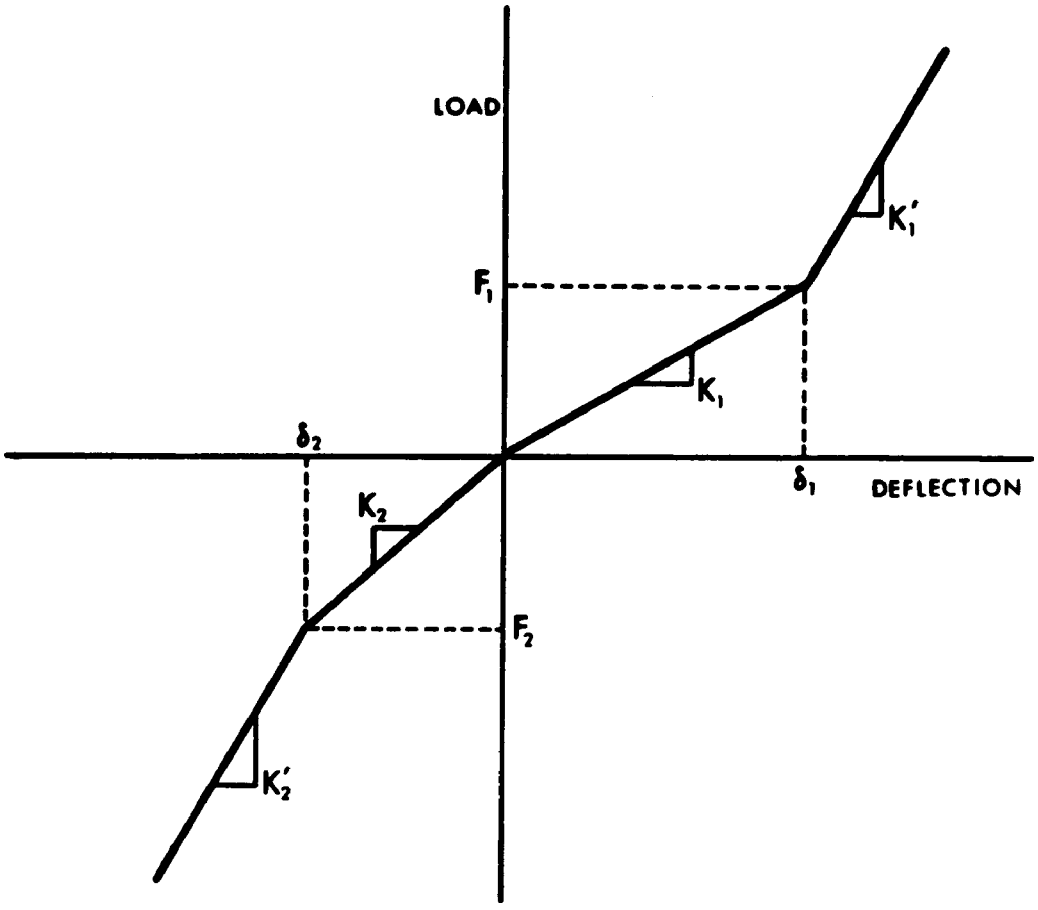


Figure 14. General Load-Deflection (Spring) Characteristics

C1N=C2N=0.5 lb-sec/in, CTN=1 lb-in-sec/rad for Rhesus A-P and L-R.

3.3.2 Skull Properties

Inertial. Normally, the weight of the brain is subtracted from the total weight of the head to obtain that of the skull. For an average 10-lb human head, with a brain of 3 lbs, this operation leaves 7 lbs to represent the skull. This number is much higher than the average weight of a human skull, when all the soft tissues are removed. The model, however, is intended to represent the whole head-neck assembly. Adjustments must be made to the weight of the modeled "skull," as well as to the "brain." After such adjustments are made, the skull weight is taken as 6.0 lbs for a human head. The next step is to lump this weight into 3 concentrated masses M1, M2 and M3.

Consider the human A-P model, to illustrate how this lumping is done. Driving-point impedance tests on human cadaver heads in the A-P direction, where the vibrating probe is mounted on the frontal bone, show that at high frequencies, the head behaves in a mass-like manner of 0.8 lbs. This is simulated in the model by taking M1=0.8 lbs. When the driving direction changes to P-A, (probe mounted on the occipital bone), the value of the driven mass becomes 1.2 lbs. It is therefore reasonable to assume that M2=1.2 lbs, with the understanding that M1 represents the anterior of the head, and M2, the posterior. It seems now logical that similar tests in the S-I direction should yield a value for M3. This may be true if the model is conceived in a different configuration, and if the S-I tests were conducted on a free-free head. However, neither condition has been met, and the only remaining way of obtaining M3

is to subtract M1 + M2 from the total "assumed" weight of the skull, to yield M3 = 4.0 lbs.

Similar arguments and methods are used to obtain the 3 masses for the three remaining models.

Distances The model requires the input of 3 dimensions: D1, D2 and HC. The first two are the horizontal and vertical "diameters" of the skull. Actually, these two distances must be adjusted in order to conserve the moment of inertia of the skull, which is reported to be about 0.08 lb-in-sec^2. The third dimension HC, is the vertical distance between the c.g. of the skull to the neck-skull articulation. It was assumed in conceiving the model that the skull c.g. lies directly above this articulation and that the mass M3 of the skull lies on the same line. Once D1, D2 and HC are given, as well as the 3 masses M1, M2, M3, the center of gravity of the skull is well defined and the relative locations of the 3 masses can be easily calculated.

In order to illustrate the method of adjusting D1 and D2 for a given set of M1, M2 and M3, consider the A-P model for a human head, for which M1=0.8 lbs, M2=1.2 lbs, and M3=4.0 lbs. Assume that D1 is given as 8.0 inches and D2 as 6.0 inches, as illustrated in figure 15.

Simple statics equations are used to compute the resulting skull moment of inertia. Thus D3 and D4 are obtained from:

$$\frac{D3}{D4} = \frac{M_2}{M_1} = \frac{1.2}{0.8} = 1.5$$

and D3 + D4 = D1 = 8.0 inches,

so that D3 = 4.8 inches and D4 = 3.2 inches.

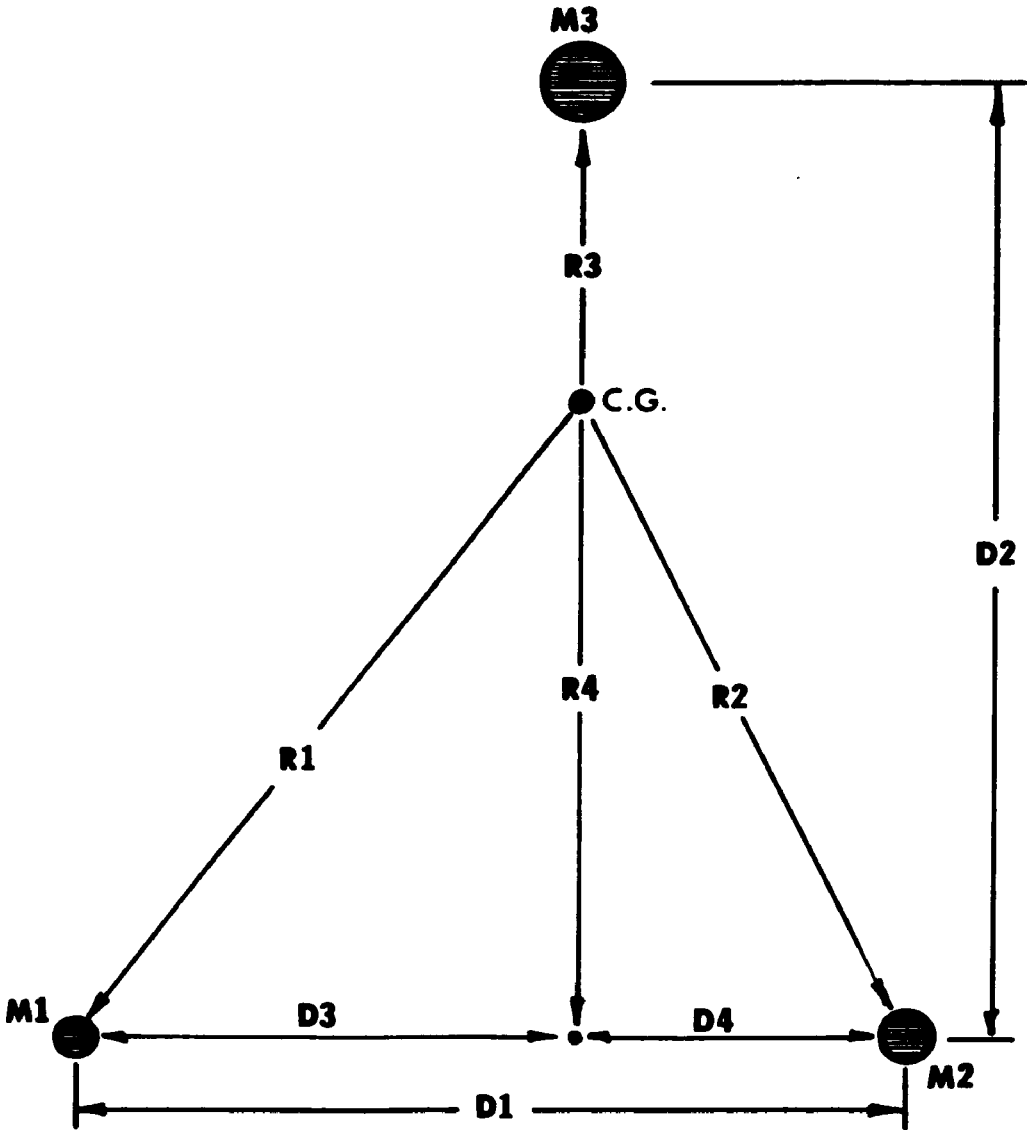


Figure 15. Adjusting D1 and D2 to Match Skull Moment of Inertia

Next, compute R3 and R4 from

$$\frac{R3}{R4} = \frac{M1+M2}{M3} = \frac{2.0}{4.0} = 0.5$$

and R3 + R4 = D2 = 6.0 inches, to obtain R3 = 2.0 inches and R4 = 4.0 inches.

Now it is possible to compute an equivalent moment of inertia about its c.g.:

$$I_s = M1[R1]^2 + M2[R2]^2 + M3[R3]^2$$

where $(R1)^2 = (4.0)^2 + (4.8)^2 = 39.0$

$(R2)^2 = (4.0)^2 + (3.2)^2 = 26.1$

$(R3)^2 = (2.0)^2 = 4.0$

Thus,

$$I_s = (0.8)\ (39.0) + (12)\ (26.1) + (4.0)\ (4.0) = 78.5 \text{ lb-in}^2$$

This calculated value of 78.5 lb-in^2 or 0.203 lb-in-sec^2 seems too high for the estimated skull moment of inertia. Some adjustment must be made to one or more of the parameters affecting the result. If the values of 0.8, 1.2 and 4.0 lbs are considered appropriate, then D1 and/or D2 must be reduced. After such reduction is made, D1 and D2 are taken as 4.0 and 4.8 inches, respectively. These assumed values result, according to the method outlined above, in a calculated moment of inertia of skull, about 39.05 lb-in^2 or 0.102 lb-in-sec^2. This number is a better approximation to the estimate of the skull's moment of inertia.

To complete the illustration, a value of HC = 2.65 inches puts the M1-M2 axis about half an inch below the neck-skull pivot point. This is acceptable and simply means that the distribution of M1, M2 and M3 is such that M1-M2 line falls below the axis of rotation

of the skull about the neck. In order to have this pivot point below the M1-M2 line, the three masses must be redistributed.

Similar rationales and methods are applied to obtain values of M1, M2, M3, D1, D2 and HC for the 3 other models of human L-R, Rhesus A-P and L-R heads. The symmetry of both human and Rhesus heads in the L-R direction provides additional simplifications to the lumping of masses and distances.

Translational Springs. The masses of the skull are interconnected by 4 translational springs: K1S, K3S and K4S in the horizontal direction, and K2S in the vertical direction. The network of springs and masses is assumed rigid in torsion but is allowed to rotate about the neck-skull pivot; a rotation resisted by the torsional spring KTS.

In order to obtain values for the 4 translational springs, two types of measurements are used: (a) static load-deflection curves, such as the one given in figure 10, and (b) the dynamic steady-state response of the skull.

The overall stiffness of the human skull in the A-P direction, when a static compressive load is applied, is estimated from figure 10 at 16,700 lb/in. This stiffness is a static one. It is likely that the dynamic stiffness which is needed for the model is higher. This is confirmed by impedance-frequency curves obtained for the human skull. Assume then that 20,000 lb/in is the overall stiffness. The next step is to lump this stiffness into the 3 horizontal springs so that their equivalent spring constant is in fact 20,000 lb/in. Since the 3 springs form two parallel branches,

it would seem reasonable to let the two branches transmit equal loads. And since one of the branches is formed by two springs, K3S and K4S series, a reasonable first approximation is to assume them to be equal. Thus K1S = 10,000 lbs/in, and K3S = K4S = 20,000 lbs/in.

Parametric study of the effects of K1S, K3S and K4S on the impedance of the model shows that, when M1 is the driven mass, the effect of K4S is megligible, while K1S and K3S which are directly connected to M1, are of critical importance. The model, however, is designed for impacts to any of the 3 masses, therefore all translational springs must be treated with equal importance, unless it is known, a priori, that the impact is applied to one specific mass.

The vertical skull spring, K2S, represents the dynamic stiffness of the skull in the S-I direction. Skull injury patterns suggest that the skull is weaker in the S-I direction than it is in the A-P direction. A tentative value of 15,000 lbs/in is therefore used for K2S.

In the L-R direction, the human skull is expected to be weaker than in the A-P direction. Thus an overall stiffness for the human L-R skull is assumed to be about 15,000 lbs/in, which is lumped into 3 spring constants applying the same reasoning used for the A-P model. The result is K1S = 7500, K2S = 15,000, K3S = 15,000 and K4S = 15,000 lbs/in for the L-R human skull.

For the Rhesus A-P and L-R models, the only reliable basis for obtaining the various spring constants is driving-point impedance tests. Starting with overall stiffnesses of 40,000 lbs/in for the A-P model and 30,000 for the L-R, proportional lumping of these values into the 4 required spring constants were performed, then the values were refined to produce model impedance curves which matched

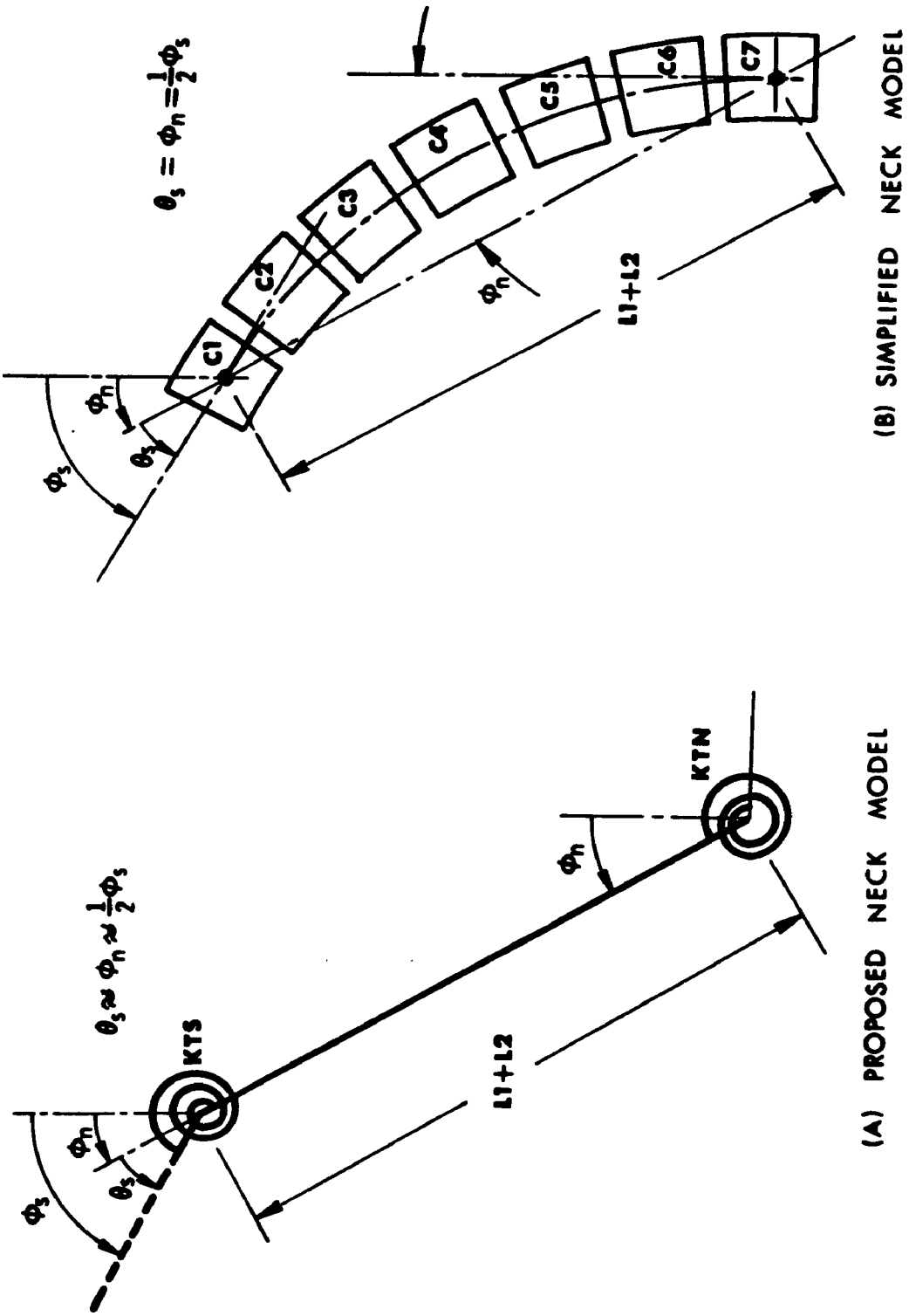


Figure 16. Estimation of Torso-Neck and Neck-Skull Angles from Head-Torso Angle

closely those measured in the laboratory.

Torsional Springs. The rotation of the head is usually described in the published experimental data as a moment about the occipital condyles versus the angular deflection of the head relative to the torso. It is difficult to define exactly the head-torso angle or to measure the moment at the condyles. Nevertheless, the model lumps this total angle into two separate angles: one representing the neck-torso angle, denoted by ϕ_n, the other representing the neck-skull angle and denoted by θ_s. Clearly, the head-torso angle ϕ_s would be the sum of the two angles, i.e. $\phi_s = \phi_n + \theta_s$.

The bending characteristics of the neck structure is lumped, then, into two torsional springs, KTS and KTN, which act in series along θ_s and ϕ_n, respectively.

In order to specify KTS and KTN separately, given their combined effects, one must make some assumptions as to the two angles θ_s and ϕ_n, which would result in a reasonable lumping of KTS and KTN.

Consider therefore a simplified model of the neck which consists of seven cubes representing the 7 cervical vertebrae. Assume that when the neck is bent, it forms a circular arc, as shown in figure 16(b). Simple geometry shows that by the time the angle of the neck has reached a value ϕ_n, the orientation of the 1st "cube" or vertebra has reached twice that value. It is not unreasonable then to assume that the difference θ_s between ϕ_s and ϕ_n is "at least" equal to ϕ_n; the words "at least" being used to indicate that the rotation of the skull relative to the 1st vertebra was not taken into account in the crude estimation of a relationship between θ_s and ϕ_n.

This simple analysis provides a basis to assume that KTS = KTN, and since they act in series, that each would be twice the overall bending stiffness obtained from experimental moment-angle curves. Figure 9 shows the dynamic flexion-extension properties of a human neck. It should be pointed out that the L-R bending properties have not been established as well as the A-P ones. The overall bending stiffness of the neck in side impacts must however, be assumed, then lumped into 2 equally stiff springs.

A general comment about all the springs of the skull and the neck should finally be made. Experimental static and dynamic testing of the neck and skull show that their properties are not linear. This is evidenced by a "softening" effect when the skull is cracked under increasing loads, and a "hardening" effect when the head undergoes hyperflexion or hyperextension. The model provides for the specification of a spring of the general type, such as the one shown in figure 14. This hopefully brings the behavior of the model closer to the actual dynamic behavior of the head.

Damping. Impedance tests on human and Rhesus skulls provide an excellent source for the lumped dashpot constants, associated with the various translational springs. Parametric studies of the effects of these constants on the model's impedance, and trial and error, are in fact the basis for obtaining the values given in table 3.

Torsional damping constants CTN and CTS can only be estimated from the available dynamic behavior of the neck, since no torsional impedance tests were conducted. This estimate may, however, be refined when attempting to validate the model, and when more data

SYMBOL* (UNITS)	SPRING	HUMAN A-P	HUMAN L-R	RHESUS A-P	RHESUS L-R
K_1 (lb-in/rad)	KTS and KTN	1040.	1430.	800.	800.
δ_1 (degrees)		27.5	20.	28.	28.
K_1' (lb-in/rad)		2250.	2500.	1200.	1200.
K_2 (lb-in/rad)		330.	1430.	800.	800.
δ_2 (degrees)		-35.	-20.	-28.	-28.
K_2' (lb-in/rad)		2250.	2500.	1200.	1200.
K_1 (lb/in)	K1N , K2N	2000.	2000.	1500.	1500.
K_2 (lb/in)		6000.	6000.	4000.	4000.
K_1, K_2 (lb/in)	K1S	10000.	7500.	15000.	10000.
$\delta_1, -\delta_2$ (inches)		0.15	0.15	0.1	0.1
K_1', K_2' (lb/in)		8000.	6000.	10000.	8000.
K_1, K_2 (lb/in)	K2S	15000.	12000.	15000.	18000.
$\delta_1, -\delta_2$ (inches)		0.15	0.15	0.1	0.1
K_1', K_2' (lb/in)		12000.	10000.	10000.	15000.
K_1, K_2 (lb/in)	K3S and K4S	20000.	15000.	30000.	20000.
$\delta_1, -\delta_2$ (inches)		0.15	0.15	0.1	0.1
K_1', K_2' (lb/in)		15000.	12000.	20000.	18000.

*See figure 14 for definitions of symbols.

Table 2. Nonlinear Characteristics of Various Model Springs

pertinent to this specific model becomes available.

3.3.3 Brain Properties

Of all head components, the brain motion is perhaps the most difficult to measure in vivo. Any attempt to describe this motion in quantitative terms is at best an approximation.

Evidence of brain rotation and translation have been found by many investigators; however, only the motion of Rhesus brain have been quantitatively described (curve form) so that it could be used as a basis of a lumped parameter model. Brain material properties have been measured, but these can only provide lower and upper bounds of the lumped parameters, which are obtained after making many assumptions.

Inertial. Estimates of the human brain weight vary but center about 2.5 lbs; those of a Rhesus brain, about 0.2 lbs. The lumping of the skull and brain into discrete masses should take into account all the tissues and bones of the head. Thus, the brain weight, as modeled by MB should be increased to 3.5 lbs so that the total model weight would be about the 10 lbs nominal weight of a human head. The Rhesus brain weight is increased for the same reasons to 0.3 lbs.

An approximate moment of inertia (MOI) of the brain is assumed to be the difference between the MOI of the head (skull and brain) and the MOI of the skull (brain removed). A value of 0.2 lb-in-sec^2 is thus obtained for the human A-P model and 0.05 for the Rhesus A-P model. The two MOI of the brain in the L-R direction are assumed to be the same as in the A-P direction. These values are only approximate, but given enough samples, they could be measured accurately.

Distances. One of the difficult distances to measure is the location of the brain c.g. relative to the skull c.g. The model requires the specification of BSX and BSY as the A-P (or L-R) and S-I components of this distance.

Data is rare about these two distances, however, many modelers and investigators use BSX=0.8 inches and BSY=1.0 inches for the A-P model of the human head. The L-R model would have BSX=0 because of the symmetry of the head, but BSY remains 1.0 inches. For the Rhesus monkey, these two distances are so small that they may be considered zero for both L-R and A-P models.

Torsional Springs and Dashpots

The coupling of the brain to the skull, in rotation, is lumped into a single torsional Kelvin element, KTB and CTB. To obtain values for these two constants, one must be able to measure the dynamic response of the brain inside the skull, a very difficult task. Such measurement has been conducted on the Rhesus monkey, and the result, shown in figure 13, forms the basis of obtaining KTB and CTB, given the moment of inertia IB.

The curve of figure 13 is essentially a free damped vibration, with an estimate of 10 Hz for the natural frequency. Using the classical method of logarithmic decrement, an equivalent damping ratio is obtained from

$$\zeta = \frac{1}{\left[1 + \left(\frac{2\pi}{\delta}\right)^2\right]^{1/2}}$$

where δ is the logarithmic decrement (ratio of two successive peaks). Since the number of peaks is not enough for accurate measurement, δ may be approximated by the ratio of the only two successive

peak-to-peak values. Thus $\delta \simeq 0.5$ and the damping is about 0.6% off the critical damping. Therefore it may be calculated that the brain-skull torsional coupling is critically damped. Carrying out the computations of KTB and CTB, for the given ω_n = 5Hz, ζ = 1.0, and IB = 0.2 lb-in-sec^2:

$$\omega_n^2 = KTB/IB \simeq 100. \quad ,$$

$$\zeta^2 = \frac{(CTB)^2}{4(KTB)(IB)} \simeq 1.0$$

yields KTB ≈ 2.25 lb-in/rad

and CTB ≈ 1.0 lb-in/rad/sec, for the Rhesus brain model in the A-P direction.

The human brain-skull torsional coupling is more difficult to obtain since less data is available for humans than for monkeys. However, the natural frequency of the human brain has been estimated to be 4-5 Hz. This ω_n, together with the human brain moment of inertia, IB=0.2 lb-in-sec^2, yields an estimate for KTB:

$$KTB = IB(\omega_n)^2 \simeq 2.5 \quad \text{lb-in/rad}$$

Furthermore, there has been no significant difference in the reported tissue properties between human and Rhesus brain. It is assumed, therefore, that the human brain is also critically damped, which yields a lumped damping constant CTB = 1.35 lb-in/rad/sec.

The values of KTB obtained with this reasoning are much lower than the torsional constants of the neck, obtained with a different reasoning. One may expect the brain to rotate much more than would the neck. While this is entirely possible with these values in this model, one should bear in mind that all the values used are estimated from data recorded for other purposes than to obtain the parameters of this model. The parameters used are only a starting

point in obtaining a valid model. The procedure for lumping should form a basis for conducting further measurements and any available or would-be available experimental response should be the basis for refining the parameters used in the model.

Translational Springs and Dashpots. Most of the data available to describe the translational motion of the brain inside the skull is qualitative. The model on the other hand requires numerical values of the coupling between the skull and brain; namely, it requires the specification of 2 horizontal springs K1B and K3B, 2 vertical springs K2B and K4B, as well as the corresponding dashpot constants C1B, C3B, C2B and C4B. Against this requirement, there is the problem of interpreting the brain tissue properties, which have been measured, in terms of a gross motion of the brain as a whole.

Consider the following background. The brain's bulk modulus has been reported to be similar to water, which is 3×10^5 psi. This suggests that if the brain's enclosure (skull) is rigid and closed, the brain would not compress significantly, and therefore it would undergo no translational motion. This however has been shown not to be true; for the skull is not rigid but very stiff ($K_s \approx 17{,}000$ lb/in), and it is not completely closed with the foramen magnum providing an opening for the brain to flow through. In addition, some experimental results show that the brain translates and rotates inside the skull, when the head is subjected to impact.

Next consider the stiffness of the head under static compression. It is most likely that this stiffness is largely due to the stiffness of the skull, and that the brain's presence contributes very little to the overall stiffness. Thus, in the model, any equivalent brain

stiffness should be much smaller than the adopted skull stiffness of 20 000 lb/in, say not more than 5 percent. This leads to an upper bound of 1000 lb/in. The viscoelastic properties of brain tissue may be interpreted by representing the tissue by a massless Kelvin element. A spring constant of less than 2 lb/in may be estimated from the published data using this model. It is difficult to conceive of a scheme or a method for obtaining a lumped brain-skull coupling from the brain tissue model. However, this value of 2 lb/in could be interpreted as a lower bound on the desired lumped overall brain-skull spring.

Another consideration must be made in relation to lumping the brain motion into a single degree-of-freedom model. While it is necessary to obtain numerical values for the spring and dashpot constants, the important factor in determining or validating an injury hypothesis, is the type of brain motion more so than its amplitude. It is more likely that the various spring constants would effect the amplitudes but not so much the general shapes of the response curves. This makes shapes of the respone curves. This makes the selection of a spring constant almost arbitrary, but limited by the upper and lower bounds discussed earlier.

All these considerations lead to the selection of an equivalent spring coupling of 500 lb/in for the translation of the brain relative to the skull. The next step is to break this stiffness between two horizontal springs, and then, using the same stiffness, obtain the two vertical springs. It is assumed that the brain resistance to motion is equal in all directions, i.e. K1B = K3B and K2B = K4B. Since each two springs act in parallel between the skull and the

brain, each spring would have 1/2 the adopted equivalent stiffness, i.e.

$K1B = K3B = 250$ lb/in,

and $K2B = K4B = 250$ lb/in.

The damping constants are obtained by assuming that the brain, in translation as well as in rotation, is critically damped. This leads to an equivalent damping constant of

$$C^2 = 4.K.M$$

with $M = 2.5$ lbs,

$$C^2 = 4(500.)(2.5/386.) \simeq 13.$$

or

$$C \simeq 3.6 \text{ lb/in/sec}$$

This equivalent damping is broken into two dashpots in parallel in the horizontal and vertical directions to give:

$C1B = C3B = 1.8$ lb/in/sec

and $C2B = C4B = 1.8$ lb/in/sec.

Throughout the discussion of brain-skull coupling properties, the human A-P model was used to give the various values. For the L-R human model, it can be assumed that the various constants would have the same values as they did for the A-P human model. The rhesus brain model must take into account the inertial properties to obtain damping constants, if the same stiffnesses are to be used for both L-R and A-P Rhesus models:

$K1B = K2B = K3B = K4B \simeq 250$ lb/in

and $C1B = C2B = C3B = C4B \simeq 1.0$ lb/in/sec

SPRING	UNITS	HUMAN A-P & L-R	RHESUS A-P & L-R
K1B	lb/in	250.	250.
K2B	lb/in	250.	250.
K3B	lb/in	250.	250.
K4B	lb/in	250.	250.
KTB	lb-in/rad	2.5	2.25
C1B	lb/(in/sec)	1.8	1.0
C2B	lb/(in/sec)	1.8	1.0
C3B	lb/(in/sec)	1.8	1.0
C4B	lb/(in/sec)	1.8	1.0
CTB	(in-lb)/(rad/sec)	1.35	1.0

Table 3. Estimated Contants of Brain-Skull Couplings

3.4 CONCLUDING REMARKS

It should be clear to the reader of sections 3.2 and 3.4 that many basic, and sometimes arbitrary, assumptions were made to interpret the available data in the context of the proposed model. The constants assigned to each of the 4 models must not be taken on their "face value." Instead, they should be used to study the general behavior of the model, as it would relate to injury patterns and mechanisms.

The experimental data used to obtain constants for the model is the result of years of research and experimentation by many individuals and institutions. The fact that most of this data cannot directly result in the desired constants of the model, shows that more experiments should be conducted to specifically measure the parameters required by this model. The difficulty of measuring the motion of the brain in vivo, for example, may be surmounted by designing an experimental set-up which can in fact monitor this motion. The model provides a basis for conducting these experiments and, when more reliable data becomes available, may be used for actual simulations of the head. As it is now, it can only be used to study the effects of the physical parameters of impact on head injury, and to draw some general conclusions about it.

CHAPTER 4

RESPONSES OF THE MODEL

The immediate result of the present study is the generation of time-response of the proposed model, by numerically solving the equations of motion. This initial result has both academic and practical values. The academic value lies in the methods used to obtain a solution to a complex mechanical system. More important are the practical applications of the model, where the solution plays an essential role.

In this chapter, the results of a couple of impact simulations are discussed and presented in graphical form. The sensitivity of the model's impedance (frequency-response) to some of the model's constants, as well as the effects of one of the physical parameters of impact on the model's time-response are also discussed in this chapter. These presentations and discussions are intended to be illustrative rather than complete, with the objective of paving the way towards more complete studies in the future.

4.1 IMPEDANCE PARAMETRIC STUDY

The impedance-frequency curve of a mechanical system is an implicit description of most of its elements. It is therefore the most powerful single property which describes a mathematical model or a real system.

The driving-point impedance is one of the mechanical properties of the head which have been measured. The same property may easily be obtained for the model by the reduction techniques presented in appendix C. It is accurate to state that a valid model should, at

least, have impedance characteristics which match those of the real system being modeled. This match is possible because of the sensitivity of the impedance to the values assigned to the various masses, springs and dashpots of the model.

To illustrate this sensitivity, consider the A-P human head model. It is assumed that the exciting sinusoidal force, which is applied to the forehead (M_1), is small enough to adopt linear springs and dashpots. Thus, given a set of constants describing the elements of the model, each constant is allowed to vary while all other constants are held fixed at their base values. Impedance-frequency curves are generated for several values of each constant by using the methods of appendix C.

4.1.1 General Observations

The immediate, but not surprising, observation is that the impedance-frequency curve of the model depends, indeed, on the values assigned to the various constants. An important implication is that these constants can be tuned, as finely as desired but within the limitations of the model, to match the measured impedance of a real head.

Another observation is that the resonances and antiresonances, generally obtained in an impedance test and which could not previously be explained by Stalnaker's 2-mass model (see chapter 1), can now be explained by the present model. However, the maximum number of resonances that can be generated by the model is three, which corresponds to the three natural frequencies of the horizontal model. One of these frequencies is very low (3-5 Hz) and does not appear on most of the measured impedance curves. This frequency is

attributed to the motion of the brain (heavy mass) inside the skull (soft coupling springs).

It is interesting to note that not all the elements of the model have significant effects on the generated impedance curve. As might have been expected, the further an element gets away from the driven point, the less effect it has on the frequency response of the driving-point impedance.

In general, stiffer springs tend to shift the mid-portion of the curve to the right (higher frequency), and heavy dampings tend to "round off" the peaks of the curve (lower anti-resonance and higher resonance). Masses have various effects, but basically shift the curve upwards when their values are increased.

4.1.2 Effects of Some Springs and Dashpots

The driving-point impedance curve for the A-P human head model is compared in figure 17 to an impedance curve obtained in an actual test on a human cadaver head. It is clear that the base model, initially developed in chapter 3, needs some tuning before assuming that the resulting model is close enough to represent the particular head on which the actual impedance test was conducted. The variations observed between various cadavers, (see figure 11 in chapter 3), makes it almost impossible to assert that any given "tuned" model represents a specific head. Therefore, unless a reproduction of a particular head is necessary, it is satisfactory to use the base model as a "typical" head model for the purposes of this study.

For those cases where a closely matched impedance is desired, it is helpful to have a guide as to the effects, on the impedance, of

variations in the model's constant. To this end, some of these effects are shown in figures 18 through 24.

In figures 18, 19 and 20, the effects of K1S, K3S and K1B are shown. Recall that these three springs connect directly the driven mass M1 to the three other masses of the horizontal model. The couplings K4S (between M3 and M2) and K1B (between MB and M2) have secondary effects on the driving-point impedance and therefore are not shown. The effects of damping on the impedance are shown in figures 21 through 24. Note that even though the dashpot C3B is not directly connected to the driven mass M1, it does have some effects on the anti-resonance peak but little effect on the resonance, as shown in figure 24.

Usually, some quantitative description of these effects would be desirable. However, there are two major problems associated with the generation of conventional 2- or 3-dimensional parametric graphs. The first is the characterization of the impedance curve. It is difficult to describe the impedance curve by quantitative terms without loosing some of its details. Even when it can be so described by maxima, minima, natural frequencies, slopes or other measurable features, the other problem is the large number of graphs which are necessary to describe the impedance-parameters relationships; for, each graph cannot practically show more than two dependency relationships.

The graphs shown in figures 18 through 24 are more basic, simple and attractive alternative to a conventional guide to adjust constants. Several trials (and errors) can bring the model's impedance to a satisfactory match of an experimental impedance curve.

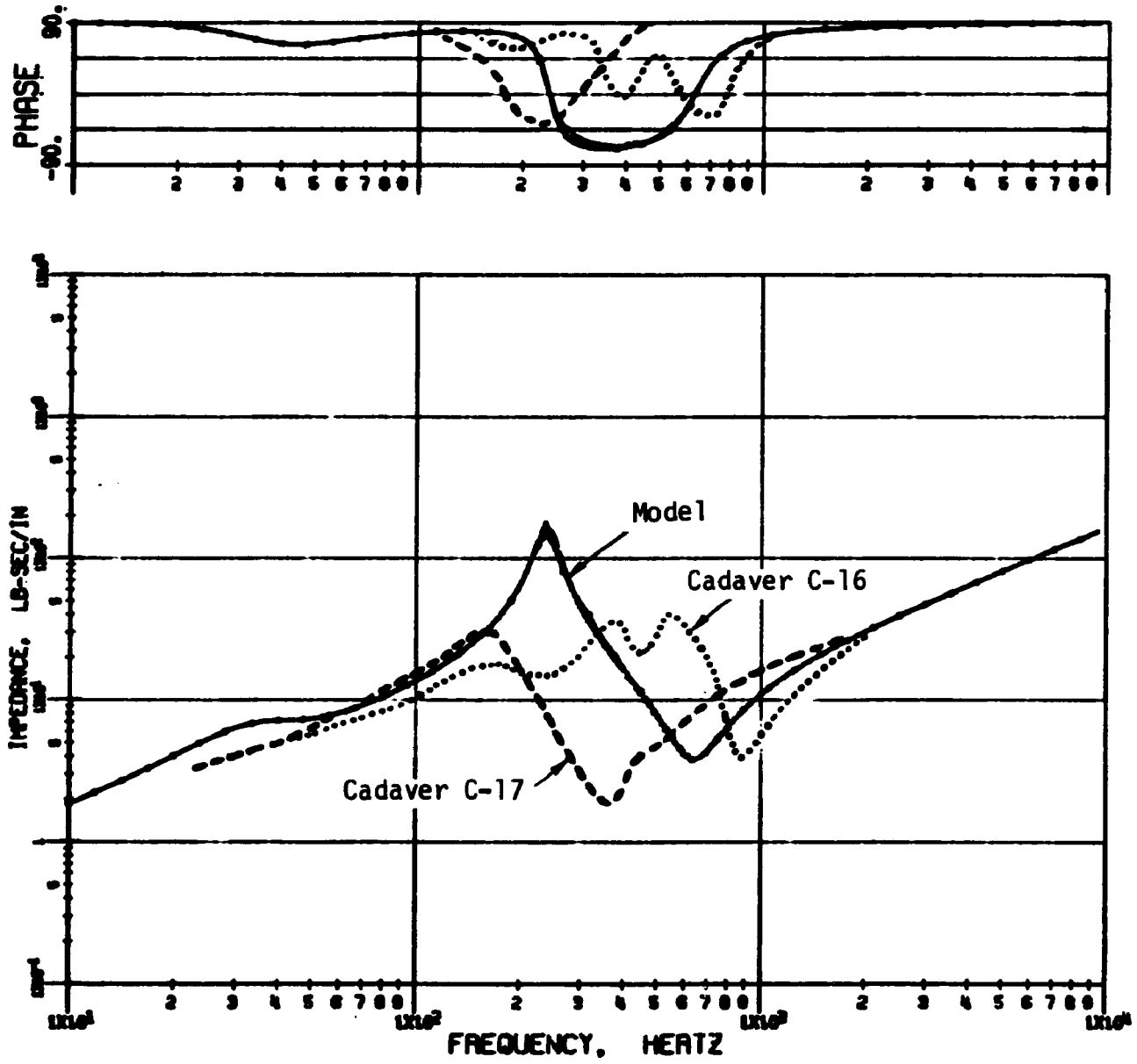


Figure 17. Impedance of Human A-P Model
Compared with Two Actual Cadaver Impedances.

K1S _ ① 40000.000 ----------

K1S _ ② 20000.000 ----------

K1S _ ④ 5000.000 ----------

K1S _ ⑤ 1000.000 ----------

K1S _ ③ 10000.000 ———————— (BASE)

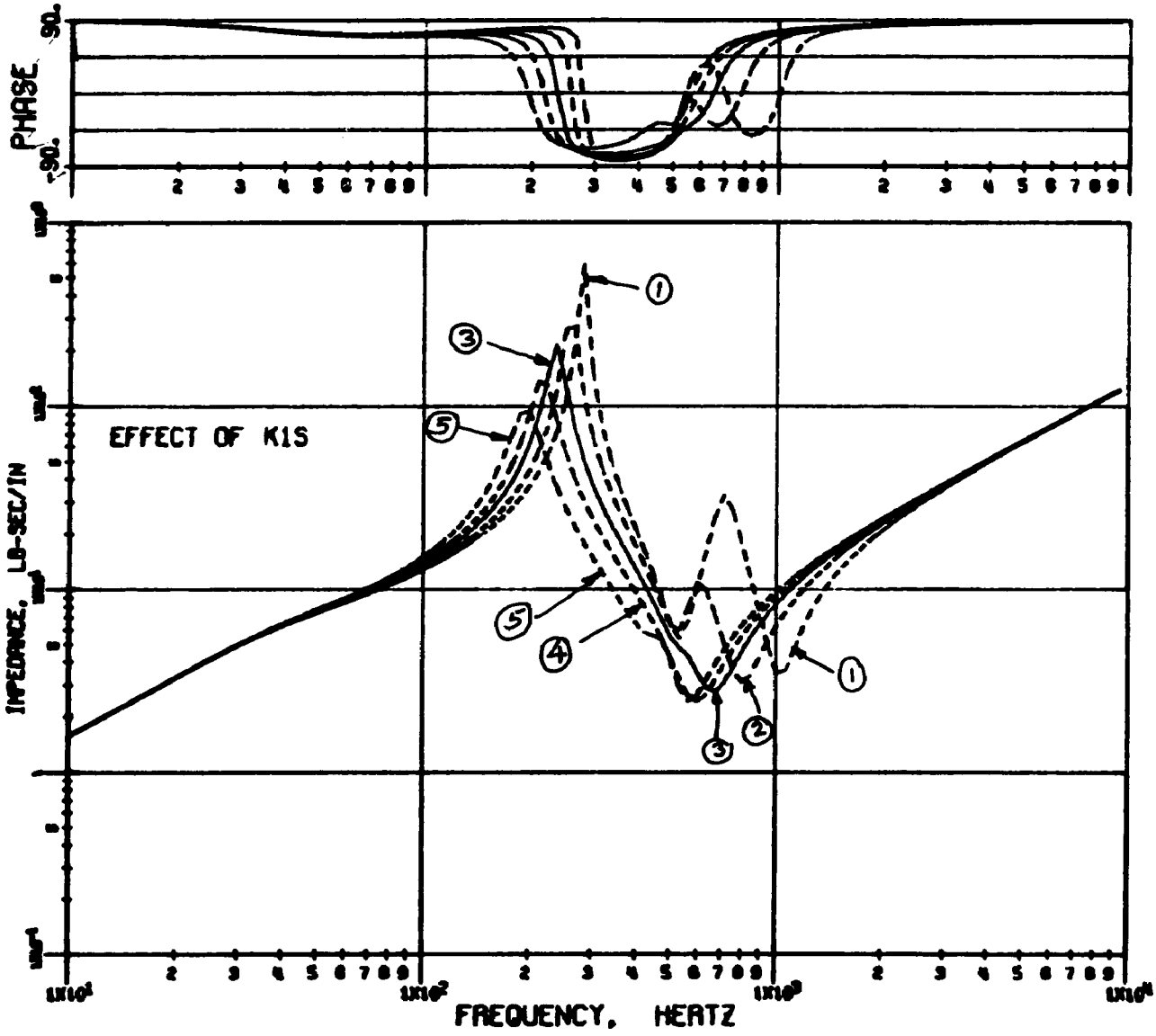


Figure 18. Effects of K1S (M1-M2 Spring).

K3S _ ① 80000.000 ----------

K3S _ ② 40000.000 ----------

K3S _ ④ 10000.000 ----------

K3S _ ⑤ 5000.000 ----------

K3S _ ③ 20 000.00 ———————— (BASE)

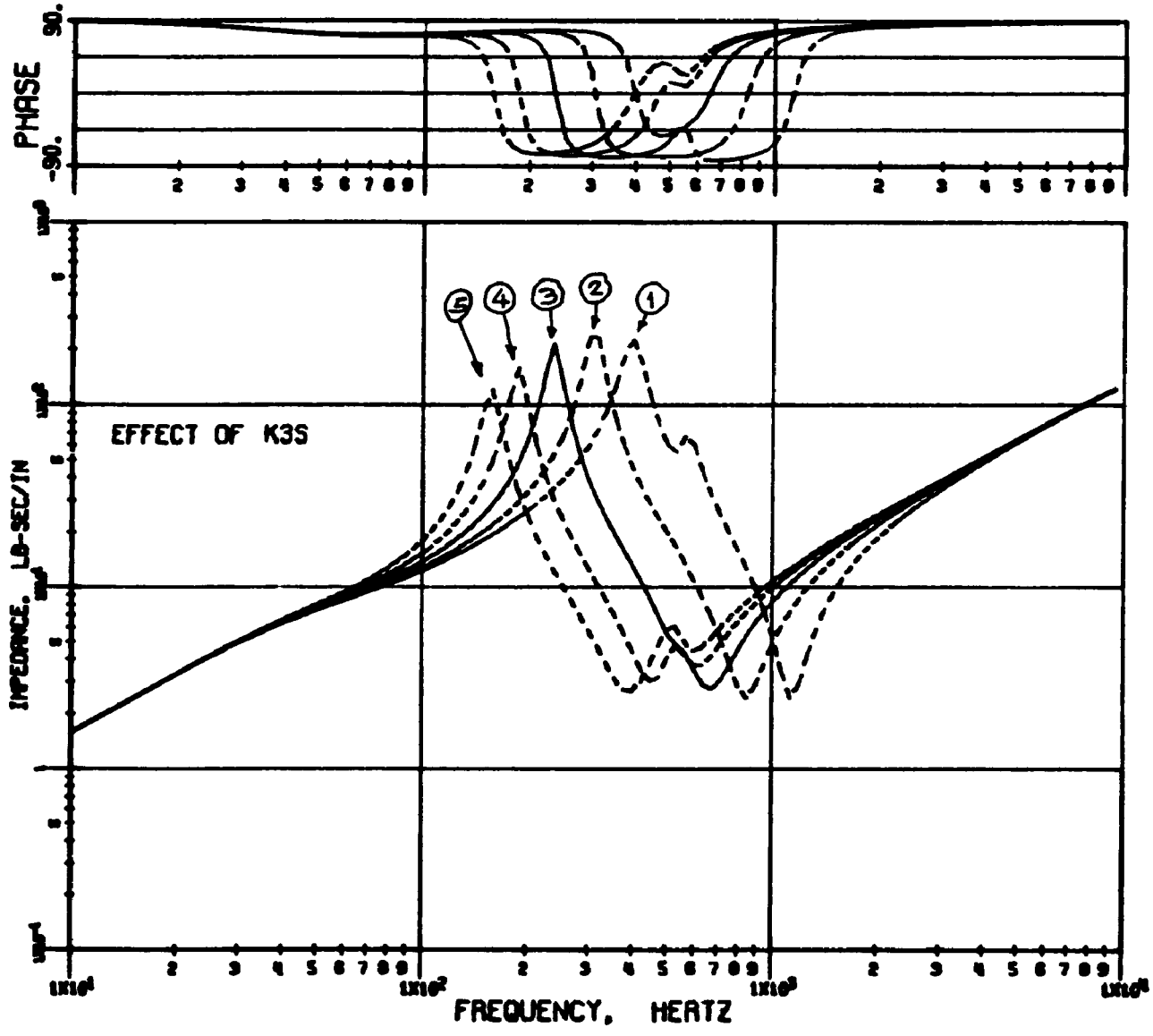


Figure 19. Effects of K3S (M1-M3 Spring).

K1B _① 1000.000 ----------

K1B _② 500.000 ----------

K1B _④ 125.000 ----------

K1B _⑤ 25.000 ----------

K1B _③ 250. ———————— (BASE)

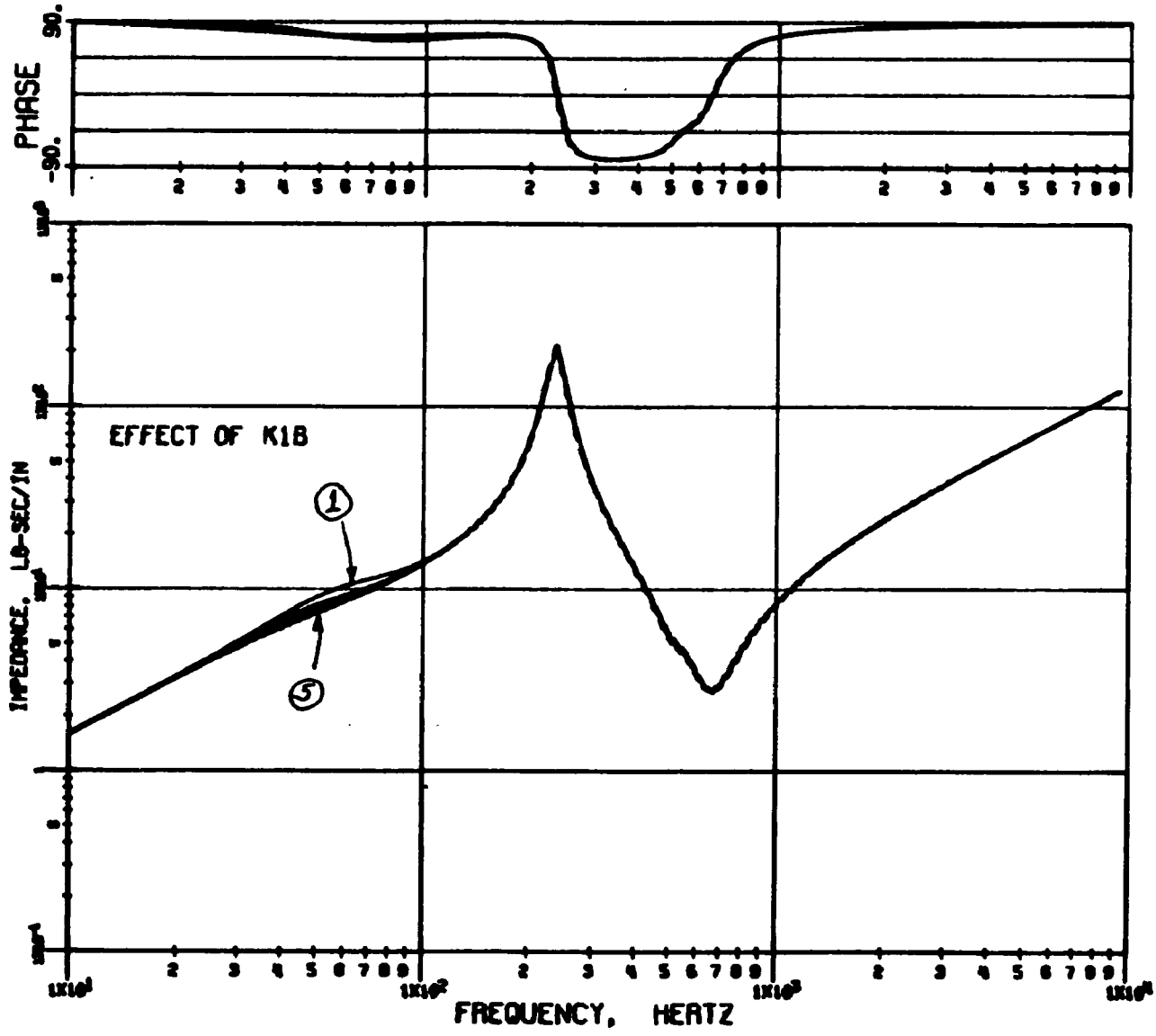


Figure 20. Effect of K1B (M1-MB Spring).

C1S – ① 10.000 ----------

C1S – ② 1.000 ----------

C1S – ④ .500 ----------

C1S – ⑤ .100 ----------

C1S – ③ 0.25 ———————— (BASE)

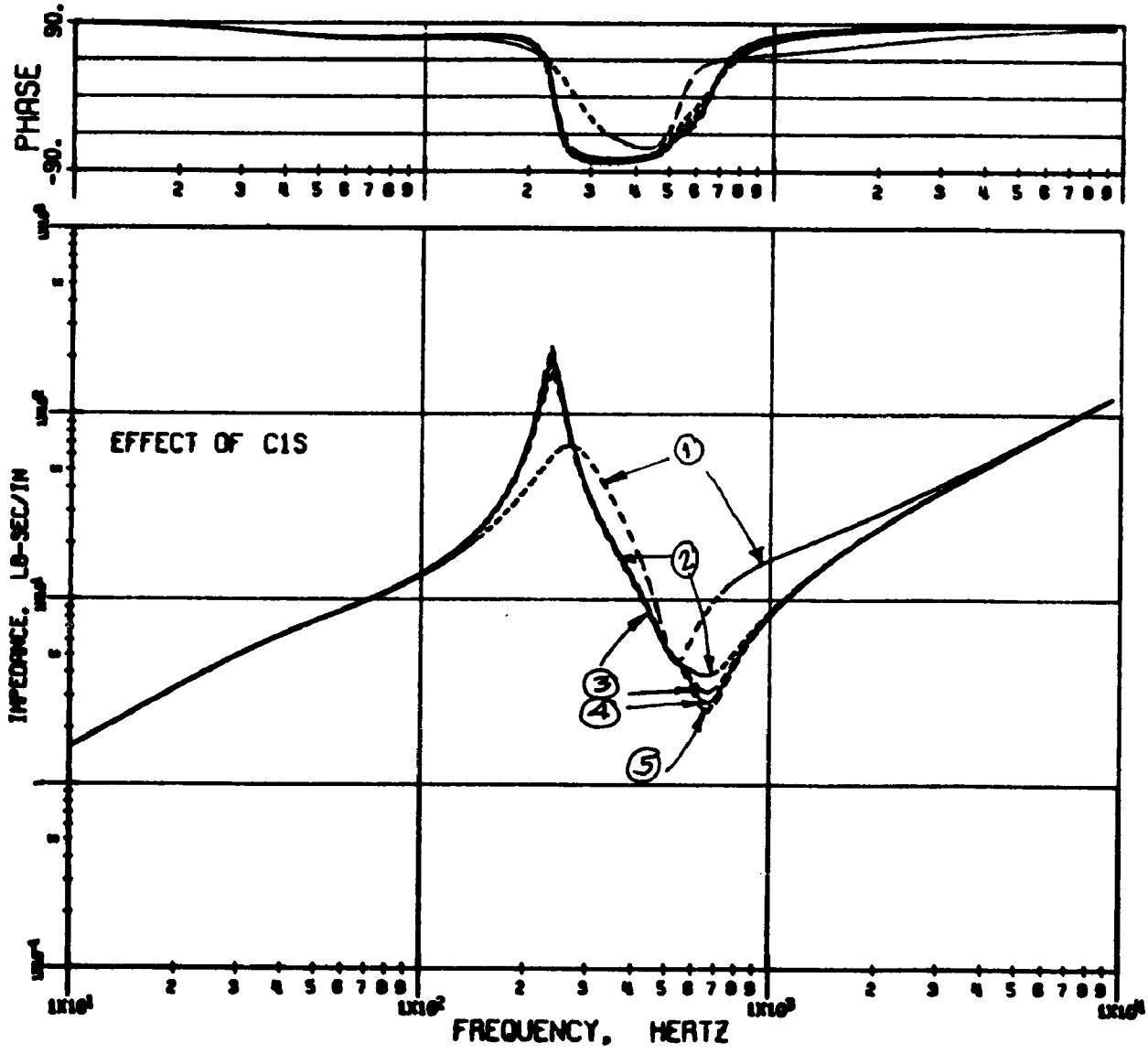


Figure 21. Effects of C1S (M1-M2 Damping).

C3S _ ① 10.000 ----------

C3S _ ② 1.000 ----------

C3S _ ④ .500 ----------

C3S _ ⑤ .100 ----------

C3S _ ③ 0.25 ———————— (BASE)

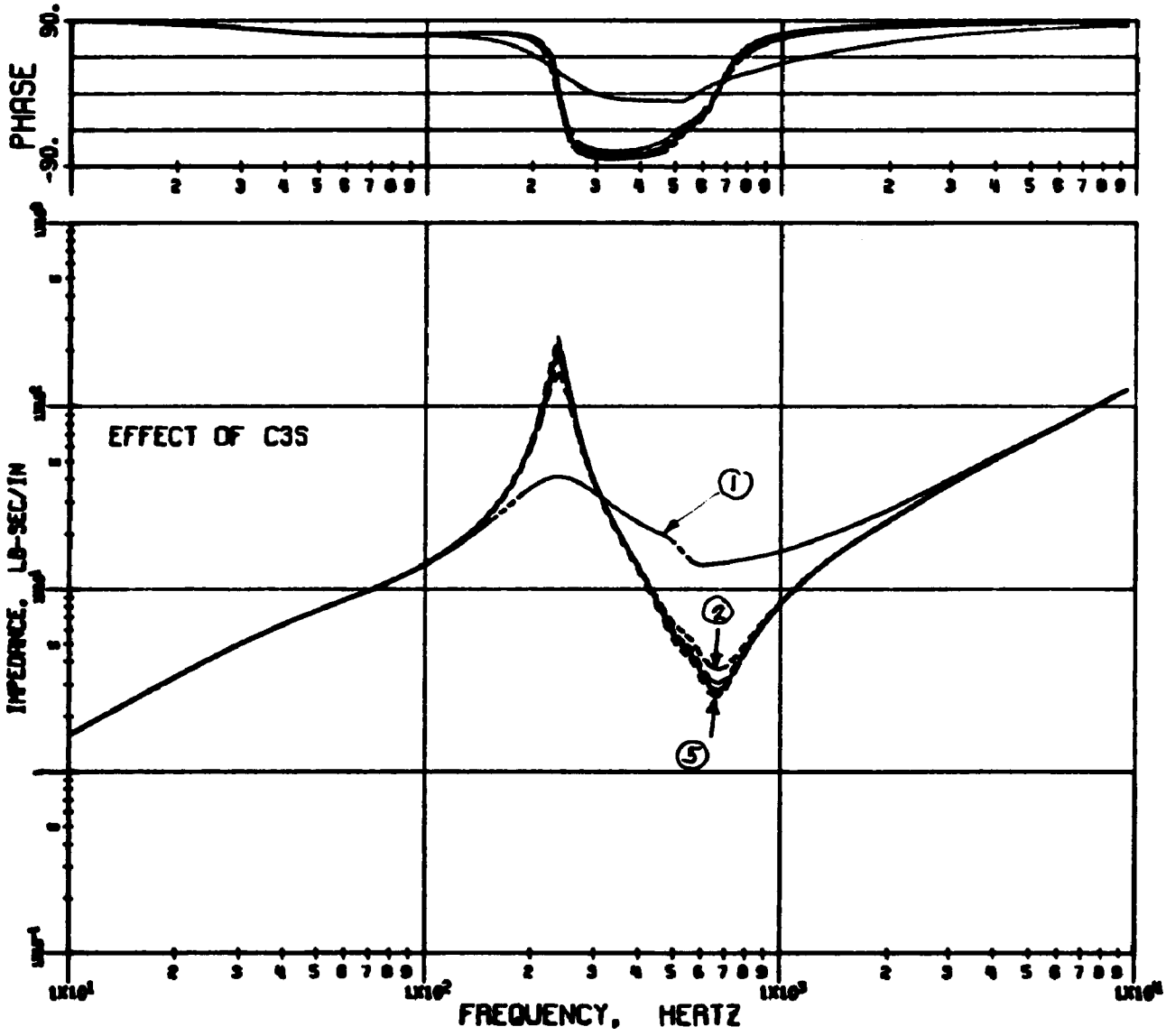


Figure 22. Effects of C3S (M1-M3 Damping).

C1B _ ① 10.000 ----------

C1B _ ② 5.000 ----------

C1B _ ④ 1.000 ----------

C1B _ ⑤ .250 ----------

C1B _ ③ 1.8 ———————— (BASE)

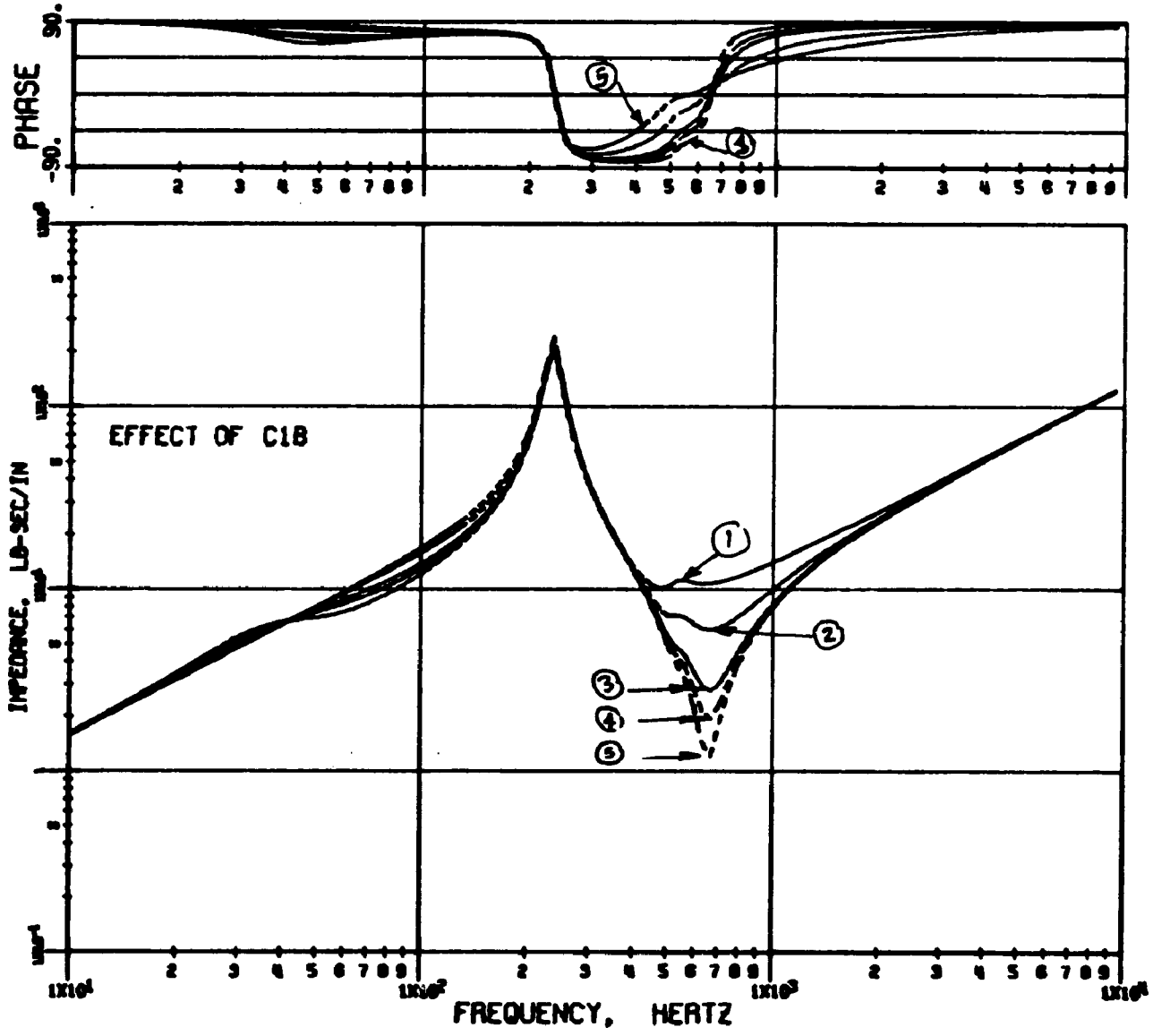


Figure 23. Effects of C1B(M1-MB Damping).

C3B – ① 10.000 ----------

C3B – ② 5.000 ----------

C3B – ④ 1.000 ----------

C3B – ⑤ .250 ----------

C3B – ③ 1.8 ———————— (BASE)

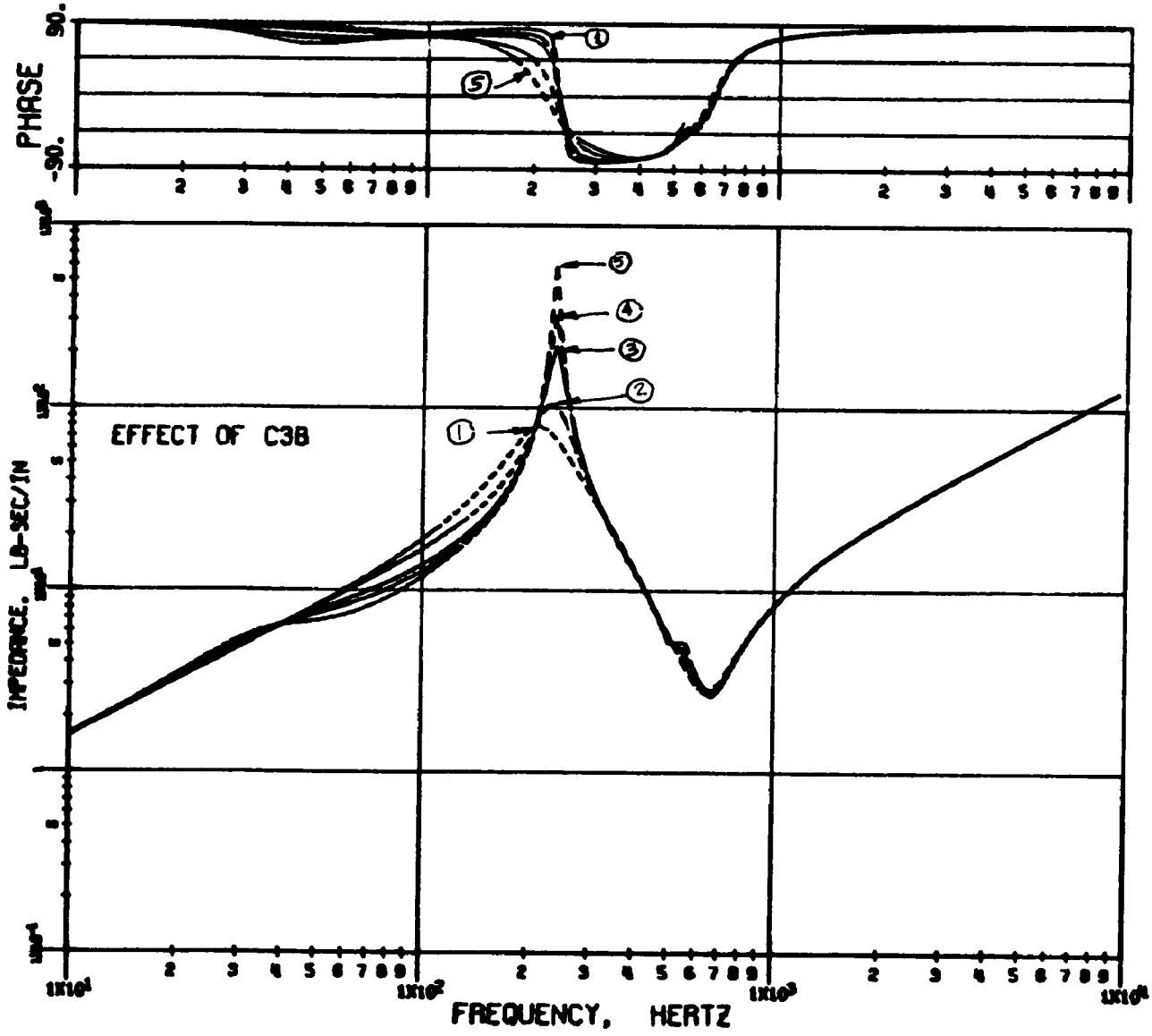


Figure 24. Effects of C3B (MB-M2 Damping).

4.2 TWO TYPICAL IMPACT SIMULATIONS

In order to demonstrate the use of the model in simulating impact situations, two impact cases are presented in this section. The first one is a direct side impact to the skull, performed on the Rhesus L-R model. The second is a simulation of "whiplash" undergone by the human A-P model. Selected output is presented and some comments about the response are made.

4.2.1 Side Impact to Rhesus Head

This simulation is based on one of a series of side impact tests conducted by Stalnaker [37] at the Highway Safety Research Institute. The test is selected to be simulated because the weight of the Rhesus head is 2.1 lbs which is close to the Rhesus head model developed in the previous chapter.

Reportedly, the impact force, which is almost triangular in shape, had a duration of 3.5 milliseconds and a peak of 2050 lbs. This resulted in a maximum head acceleration of 940 g's, a maximum head angular acceleration of 75000 rad/sec^2, a maximum angular velocity of 180 rad/sec. The injury was reported just at the threshold of survival (index 3 on a scale of 1 to 5), with no skull fractures or loss of consciousness.

The purpose of this simulation is to compare the results of the model to the experimental result. The biggest problem in re-creating the impact conditions is the description of the forces (or accelerations at the bottom of the neck, which were not measured during the experimental test. Therefore, some reasonable boundary conditions must be assumed in order to run the model.

Consider the experimental results of test RH-70-22. These show that peak recorded forces and accelerations are reached within 3 milliseconds from the beginning of the impact. Examination of the high-speed film of the event shows that the torso, because of its large inertia, remains almost stationary while the head moves, and the peaks are reached during the initial period of 3 milliseconds. Therefore, it is reasonable to assume that the accelerations of the neck-torso pivot are zero, at least during the first few critical milliseconds. Furthermore, forces which act on this point are not zero. but must "balance" the impact force. This leads to the conclusion that, insofar as the initial period of the simulation is concerned, the boundary conditions at the neck-torso point are zero accelerations and unknown forces, which calls for a type II solution of the equations.

The input data to program HEAD for this simulation is shown in figure 25. Most of the results of the simulation are shown in graphical forms in figures 26 through 40. Based on these results, the following conclusions and comments may be made.

1) The maximum velocity (680 in/sec), attained by the skull in the simulation, compares well with the reported head maximum velocity of 670 in/sec. The skull velocity, figure 26, and the brain velocity figure 27, are almost in phase, but the brain reaches a higher peak (780 in/sec). The settling velocity of both skull c.g. and brain c.g., which was not reached during the simulation, seems to be about 450 in/sec (26 mph).

2) The skull and brain angular velocities, shown in figures 28 and 29, show that the skull reaches a substantially higher peak angular velocity than the brain. In the actual test, the reported experimental "head" angular velocity of 180 rad/sec is much lower than the simulated 950 rad/sec of the skull.

3) The reported maximum head acceleration for test RH-70-22 is 940 g's. The simulation shows a maximum of 780 g's for the skull and 950 g's for the brain. Here, there seems to be an agreement between the results of the simulation and the actual test.

4) Angular accelerations have been the center of much of the attention in head injury assessment. The simulation predicts (figures 32 and 33) that the skull would reach a peak 550,000 rad/sec^2 angular acceleration, while the brain reaches a peak 18,500 rad/sec^2. In the actual test RH-70-22, it is reported that the head angular acceleration reaches a peak of 75,000 rad/sec^2.

5) The motion of the brain relative to the skull, is shown as a translational (vector sum) between the c.g. of the 3 masses of the skull and the c.g. of the brain in figure 34, and as an angular deflection of the brain-skull coupling spring in figure 35. These two curves convey two ideas: (a) the brain does indeed move inside the skull and (b) the motion seems to be much higher than anticipated. While there is not enough experimental quantitative measurements of this motion, the peaks reached seem to be unreasonable.

6) There are many possible explanations for the discrepencies between the results of the simulation and the actual test. First, the impact conditions imposed on the model are, apparently, much more violent than the actual impact conditions of test RH-70-22. The assumption of zero acceleration profiles at the bottom of the neck is only speculative, since no boundary conditions were measured at this point in the actual test. In a separate simulation, the Rhesus A-P model, which has the same brain-skull couplings as the L-R model, was impacted by a 200-lbs force, 10 msec, half-sine force at the occiput. The difference in the boundary conditions was that in this simulation (A-P), the forces at the bottom of the neck were assumed to be zero. This resulted in no more than 4 degrees brain-skull angular deflection, as shown in figure 35(A). The point being made here is that the boundary conditions have a great effect on the results of the simulation.

Discrepencies between the results of test RH-70-22 and the simulation may be attributed to the location of the impact force. In the simulation, the 2000 lbs force was applied directly to mass M1, along the M1-M2 line. This line, is much lower than the level of the c.g. of the head. The impact may therefore be described as an eccentric impact, causing the skull to rotate violently while the brain remains virtually stationary. Although the model provides for any orientation or direction of the impact, by specifying appropriate α_1 and v_1, no attempt was made at specifying v_1 so that the force $\vec{P}_1$ passes through the c.g. of the head, since, in the actual test, the force of impact is spread over a finite area of the impacting rigid surface, and hence, the location or point

of application cannot be pinpointed.

A third possible explanation for these discrepencies or "unreasonable" values obtained, are the spring constants chosen for the skull-brain couplings. By choosing stiffer springs, the brain-skull relative motion may be reduced. However, the lack of experimental measurements of this motion would make any choice a "good" choice, provided that the results of the simulation are properly and carefully interpreted.

7) The skull horizontal deflection, figure 36, is the distance between M1 and M2. This distance is comparable to the distance between the two masses of Stalnaker's Maximum Strain Criterion Model (see figure 4 in chapter 1). In this impact simulation, the deflection reached a maximum of 0.04 inches. When this deflection is used in the same context as the MSC model, it yields a maximum strain of 0.027 in/in, which compares well with the 0.029 in/in established by Stalnaker's study as the threshold tolerance of the Rhesus monkey in side impact. This implies the present model may be used as a substitute for the MSC model, since it offers in addition to the maximum strain, other variables which could be used as criteria for injury, under a variety of impact conditons.

8) In a direct impact test, some of the variables that might offer a clue to head injury tolerance are the forces and moment at the occipital condyles, simulated in the present model by the skull-neck pivot point. Figures 38, 39 and 40 show the moment, axial and shear forces acting on this joint. These are typical variables which are difficult to measure experimentally, but can easily be obtained

in the simulation. The peaks are approximately 3100 in-lbs for the moment, 1400 lbs for the axial force and 1100 for the shear force. While there is no experimental records to compare against these results, these values are not unreasonable, considering the 2000 lbs force applied as input. The irregular behavior of these three curves is a result of two facts. First the head is attached to a neck which oscillates such that its acceleration (neck-torso pivot) is zero. Second, the neck-skull pivot is characterized by the model by non-linear springs. However, it could be safely assumed that the responses in the initial period (2 or 3 times the durations of the impact pulse) are reliable, at least as far as most of the experimentally available results show.

9) Finally, it is clear from studying the time-response of the various variables that the model needs tuning. The basis for tuning must ultimately be experimental measurements. The results presented in this section serve to point out the direction in which experimental measurements should be oriented. Apparently, two measurements, which are critical to a "reasonable" simulation, are: (a) the boundary conditions at the T1-C7 joint, in the form of accelerations or forces, and (b) the motion of the brain inside the skull under various conditions, e.g., free vibrations, translational and torsional steady-state forced vibrations, and impact response.

```
*MODEL      RHESUS L-R HEAD MODEL
 &NECK     WN=0.6, L1=0.75, L2=0.75,
           K1N=0.5,400.,1200.,9*0.,    C1N=0.5,
           K1N=1500.,5*0.,4000.,5*0., C1N=0.5,
           K2N=1500.,5*0.,4000.,5*0.,C2N=0.5     &END
 &SKULL    W1=0.1, W2=0.1, W3=1.5,
           D1=2.1, D2=2.1, HC=0.75
           K1S=0.5,400.,1200.,9*0.,    C1S=0.5,
           K1S=0.1,1000.,8000.,9*0.,  C1S=0.25,
           K2S=0.1,1800.,15000.,9*0., C2S=0.25,
           K3S=0.1,2000.,18000.,9*0., C3S=0.25,
           K4S=0.1,2000.,18000.,9*0., C4S=0.25  &END
 &BRAIN    WB=0.3,IB=0.05,
           BSX=0., BSY=0.,
           K1B=2.5,C1B=1.0,
           K1B=250.,K2B=250.,K3B=250.,K4B=250.,
           C1B=1.,  C2B=1.,  C3B=1.,  C4B=1.     &END
*TITLE     DIRECT SIDE IMPACT SIMULATION
*INI        ZERO-ACCELERATIONS AT NECK-TORSO
 &INCON   XZ=0.  &END
*FOR        3.5 MSEC, 2000 LBS IMPACT TO SKULL
 &FORCES  TYPE=2,
          JP1=2,P1=3.5,2000.,114*0. ,
          JXC=0, JYO=0  &END
 &OUTPUT  PLT=1,5*0, PRT=6*0 &END
 &TIMER   FINTIM=28., DELOUT=0.4,
          DELTIM=0.1, AESEPR=0.25  &END
*RUN
```

Figure 25. Input Data to Side Impact Simulation.

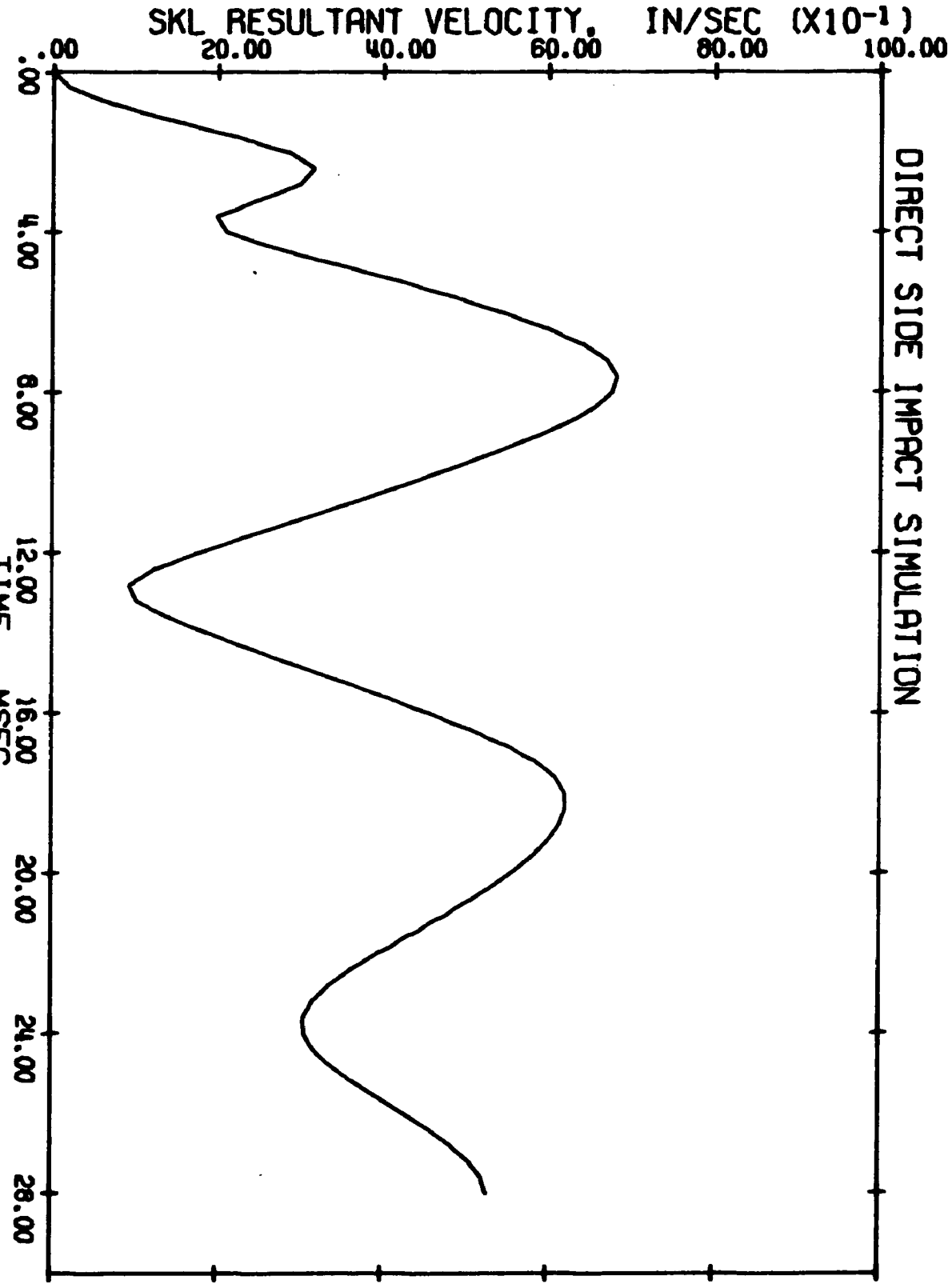


Figure 26. Resultant Absolute Velicity of Skull.

RHESUS L-R HEAD MODEL
ZERO-ACCELERATIONS AT NECK-TORSO
3.5 MSEC. 2000 LBS IMPACT TO SKULL

NOV 13, 1973

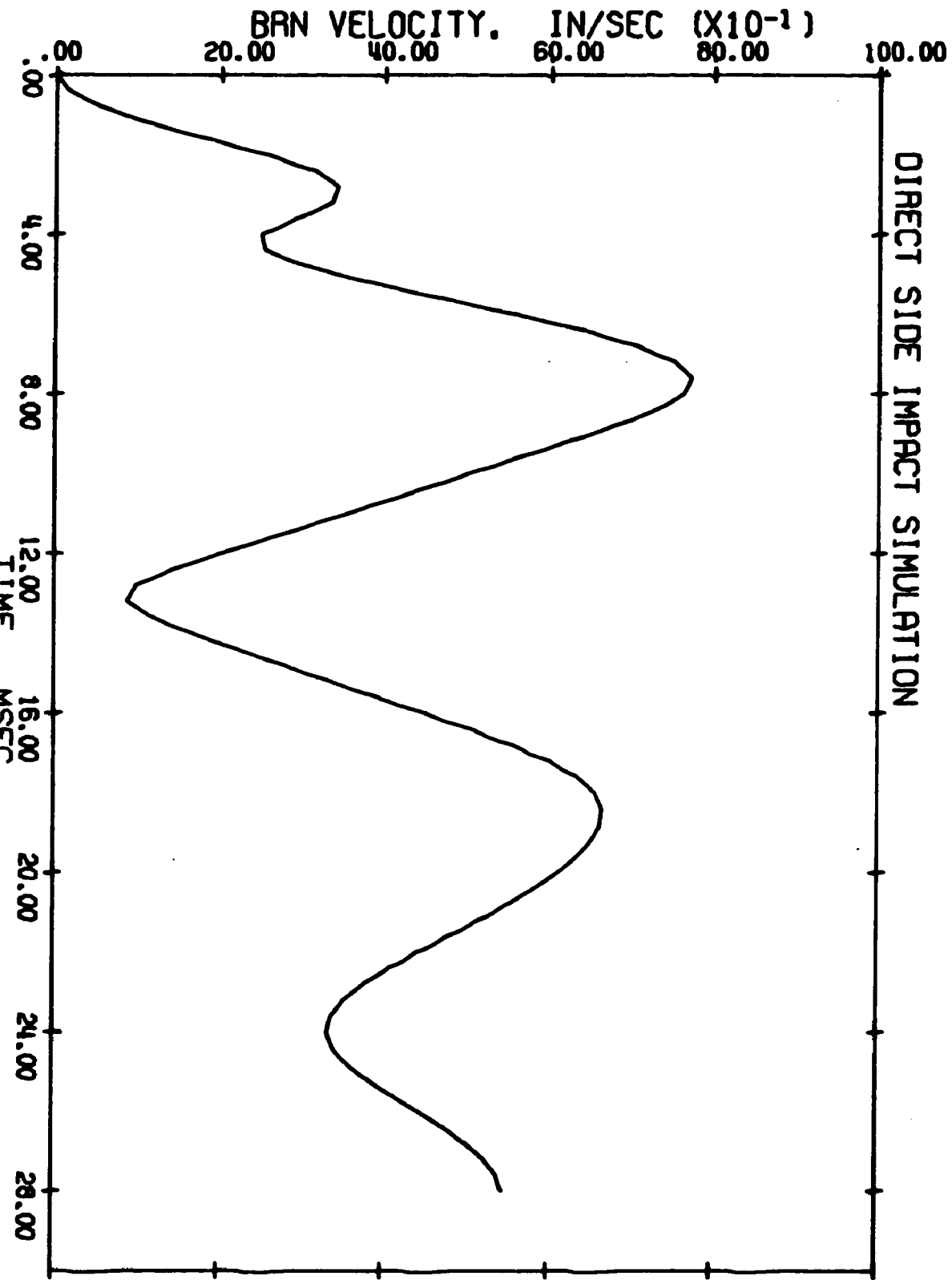


Figure 27. Brain Absolute Velocity.

RHESUS L-R HEAD MODEL
ZERO-ACCELERATIONS AT NECK-TORSO
3.5 MSEC. 2000 LBS IMPACT TO SKULL

NOV 13, 1973

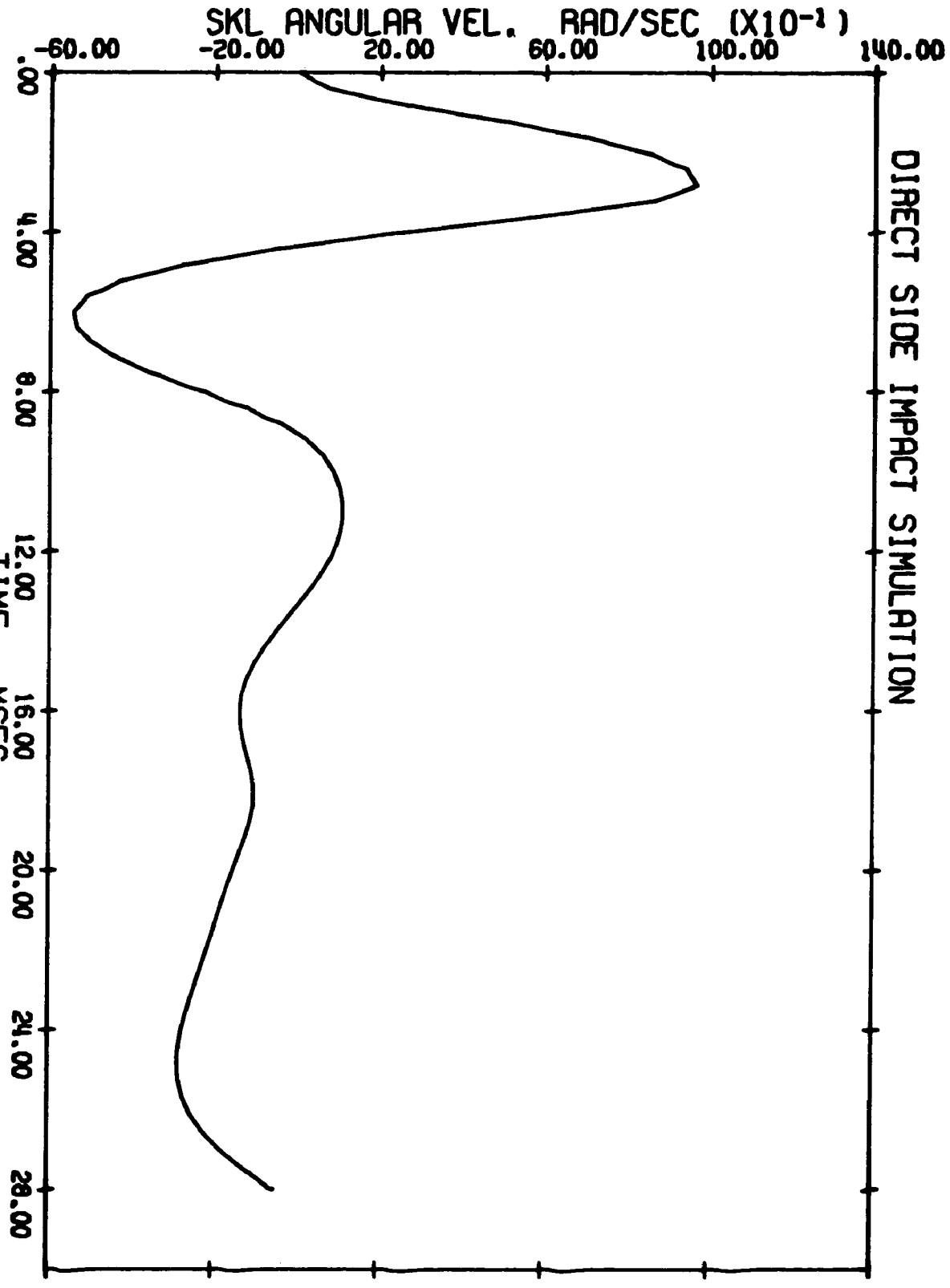


Figure 28. Skull Absolute Angular Velocity.

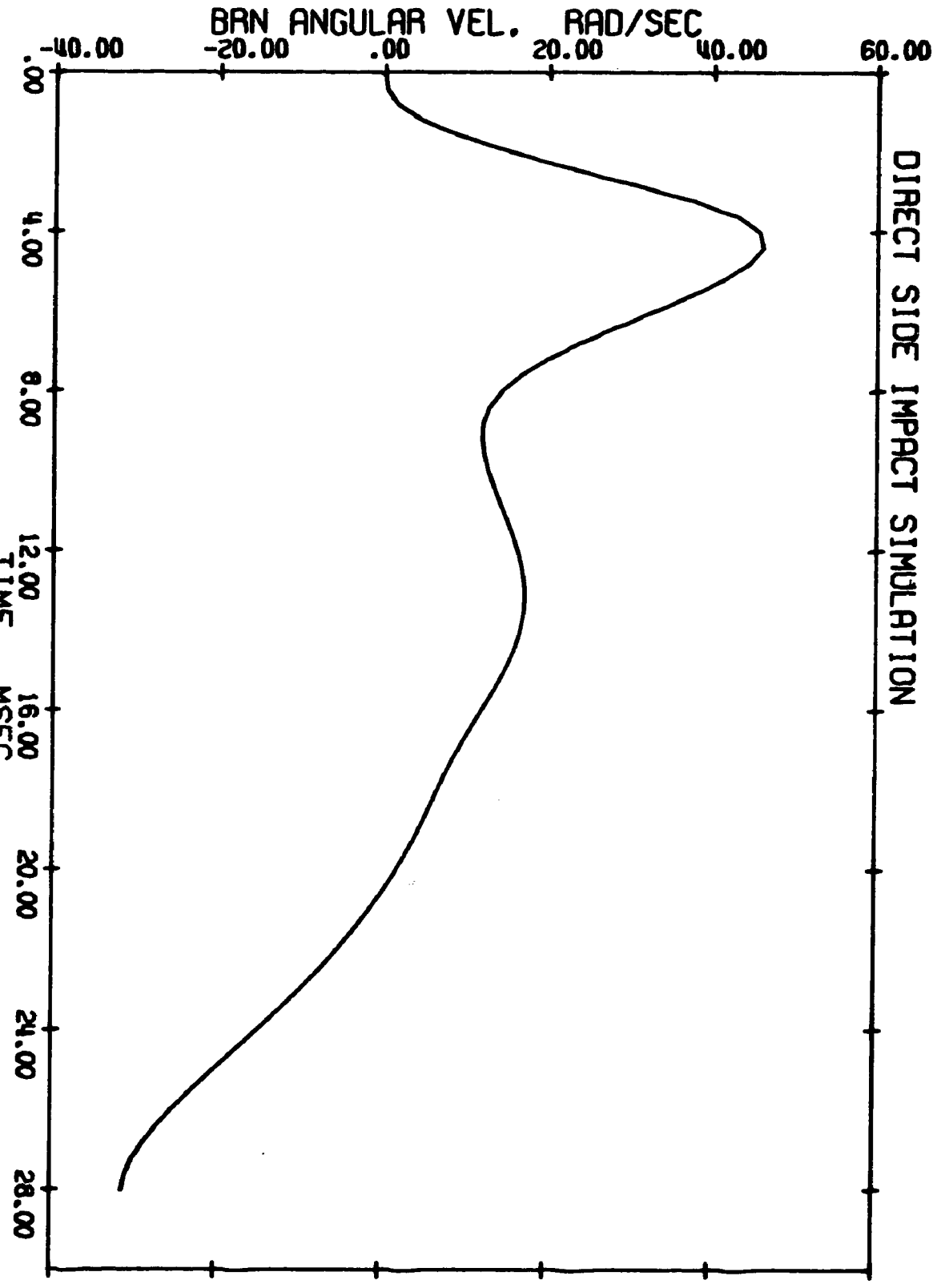


Figure 29. Brain Absolute Angular Velocity.

RHESUS L-R HEAD MODEL
ZERO-ACCELERATIONS AT NECK-TORSO
3.5 MSEC. 2000 LBS IMPACT TO SKULL

NOV 13, 1973

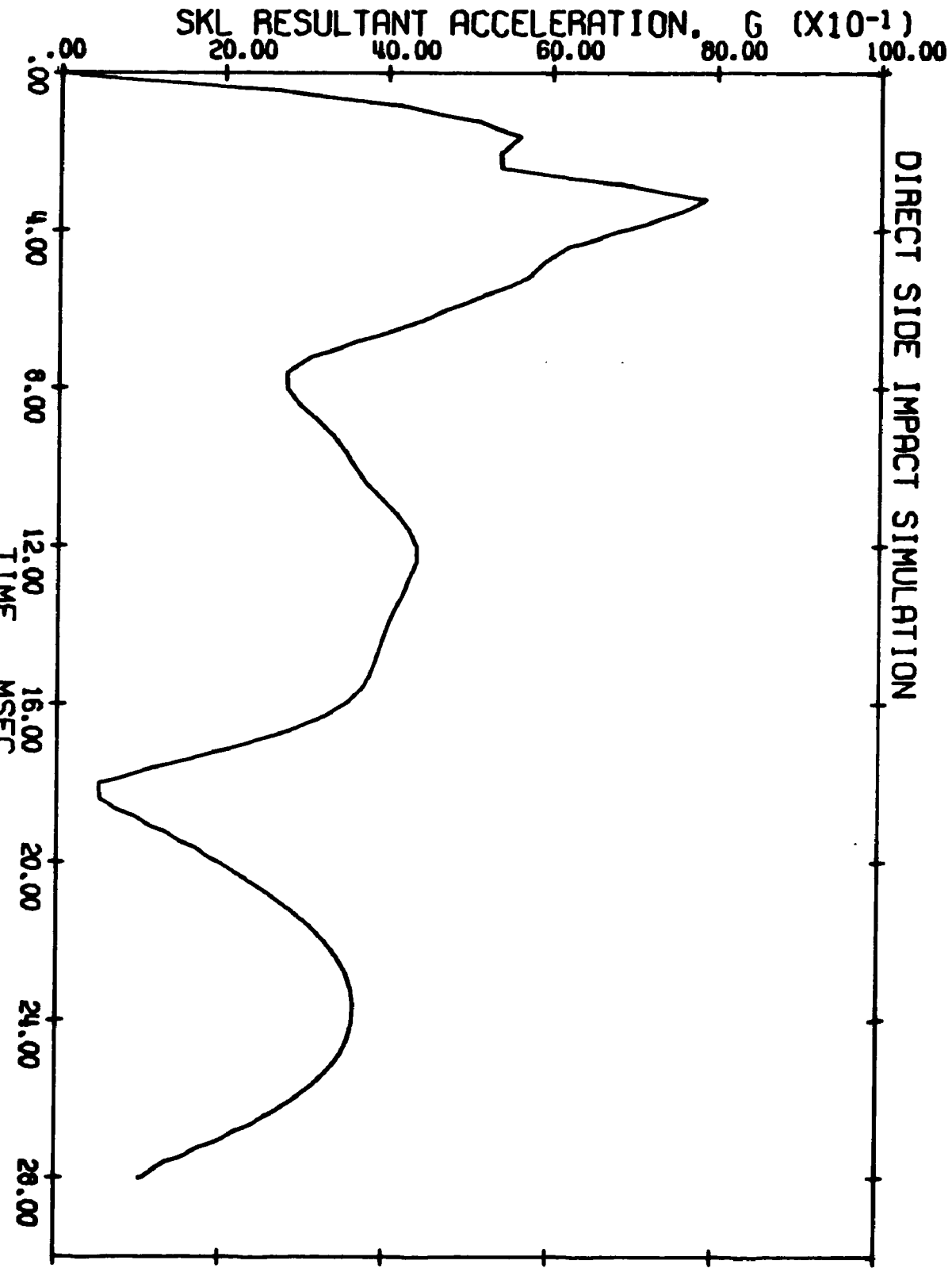


Figure 30. Resultant Absolute Acceleration of Skull.

RHESUS L-A HEAD MODEL
ZERO-ACCELERATIONS AT NECK-TORSO
3.5 MSEC. 2000 LBS IMPACT TO SKULL

NOV 13, 1973

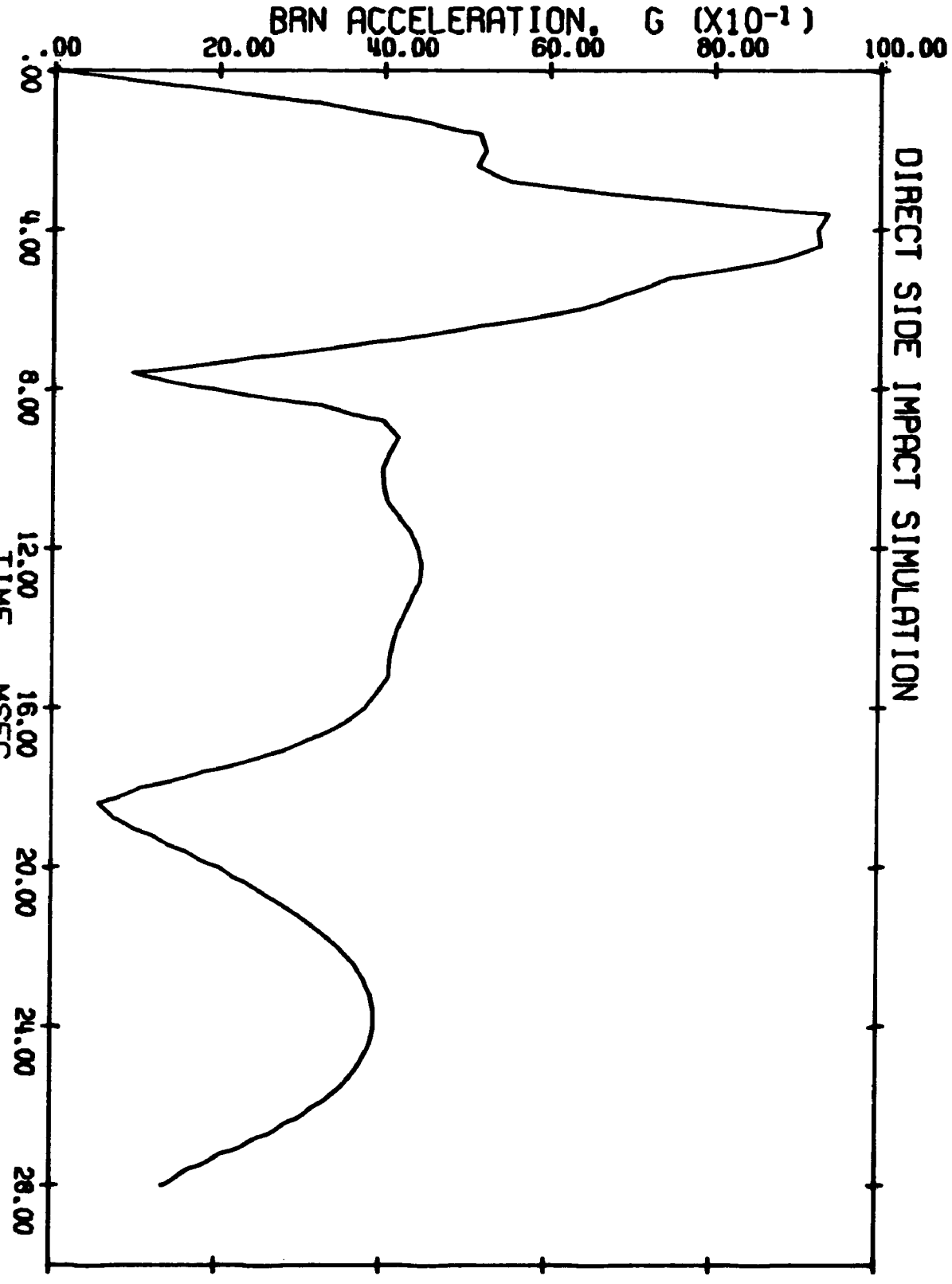


Figure 31. Brain Absolute Acceleration.

RHESUS L-R HEAD MODEL
ZERO-ACCELERATIONS AT NECK-TORSO
3.5 MSEC. 2000 LBS IMPACT TO SKULL

NOV 13, 1973

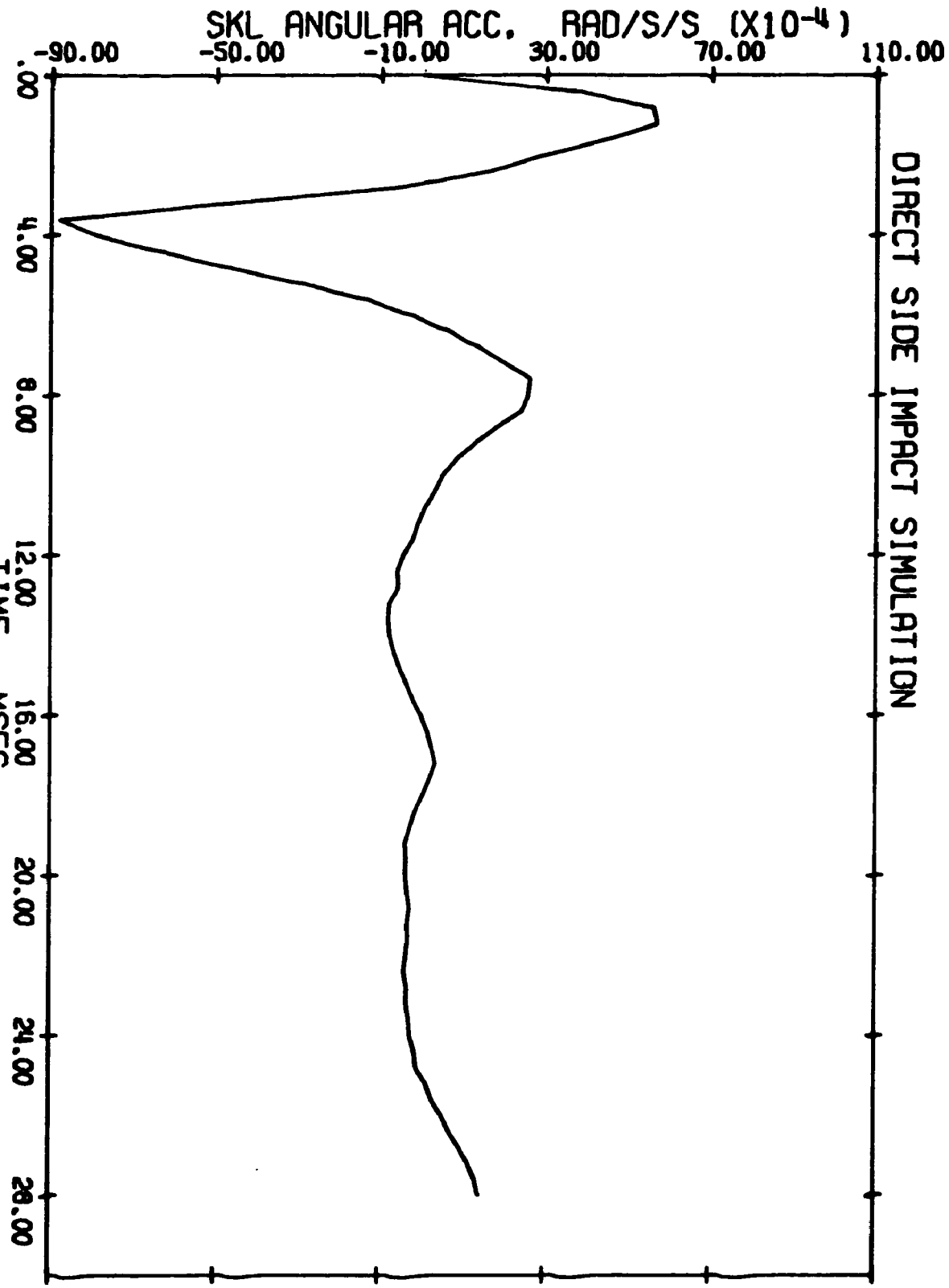


Figure 32. Skull Absolute Angular Acceleration.

RHESUS L-R HEAD MODEL
ZERO-ACCELERATIONS AT NECK-TORSO
3.5 MSEC. 2000 LBS IMPACT TO SKULL

NOV 13, 1973

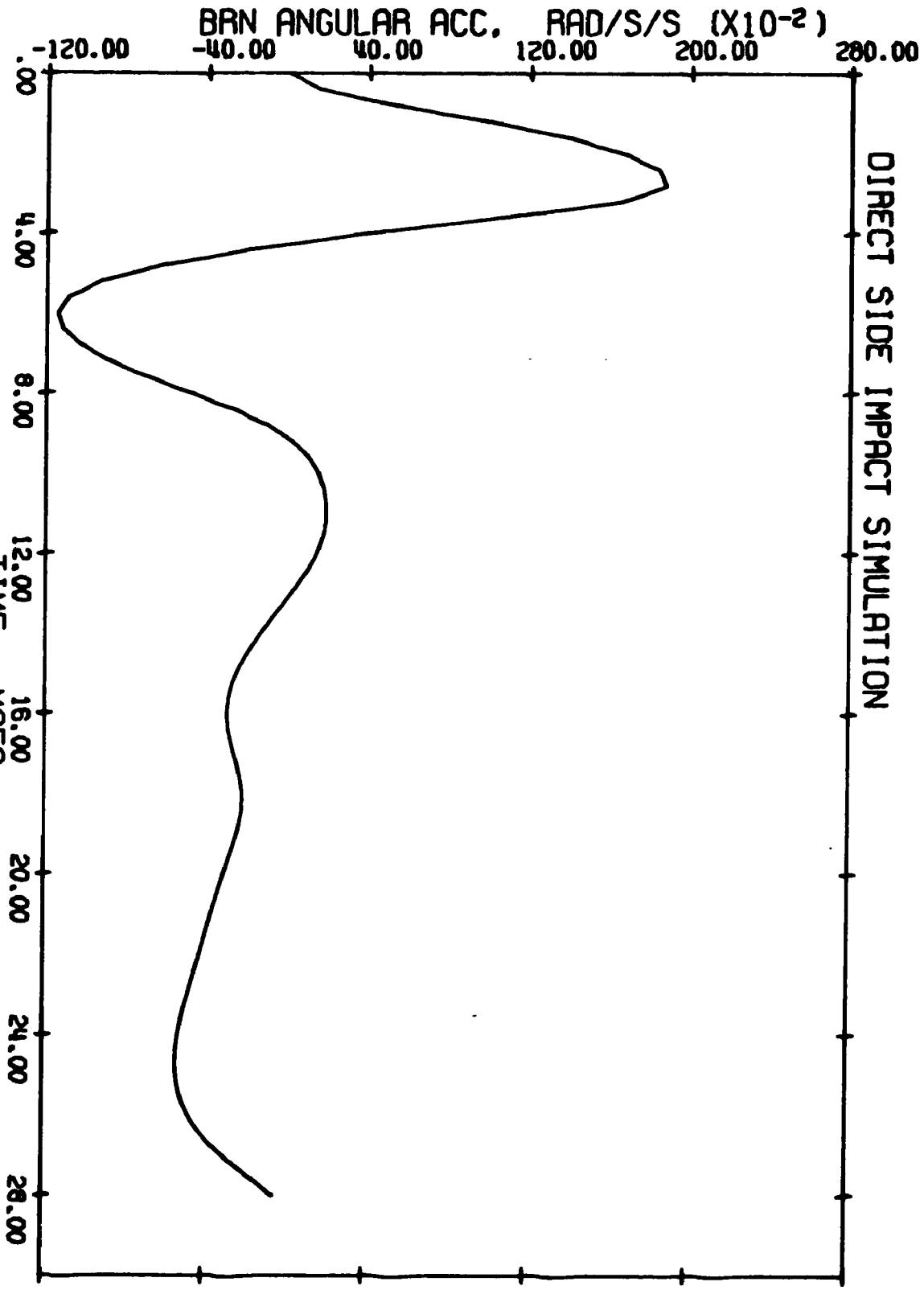


Figure 33. Brain Absolute Angular Acceleration.

RHESUS L-R HEAD MODEL
ZERO-ACCELERATIONS AT NECK-TORSO
3.5 MSEC. 2000 LBS IMPACT TO SKULL

NOV 13, 1973

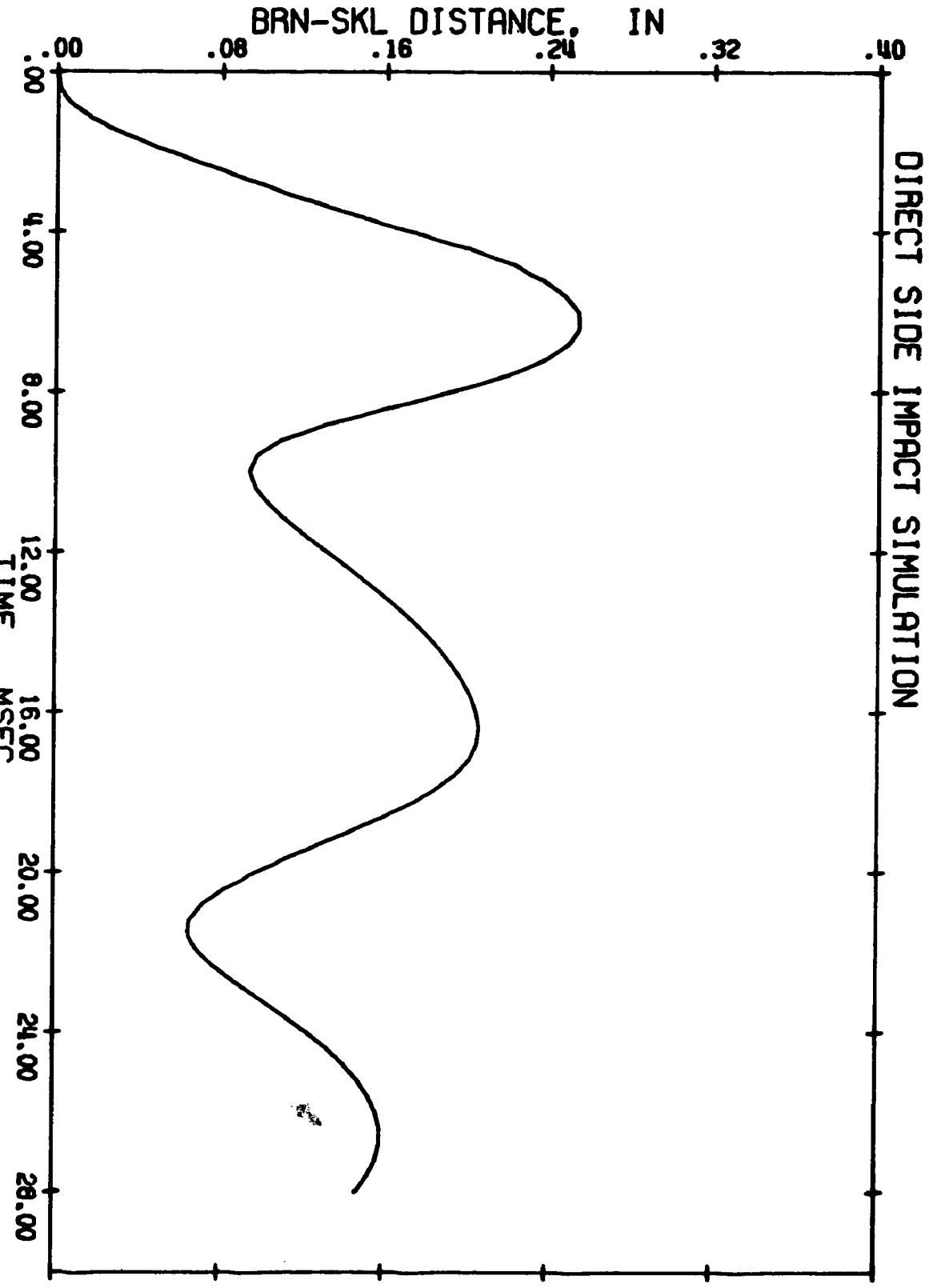


Figure 34. Distance of Brain Relative to Skull.

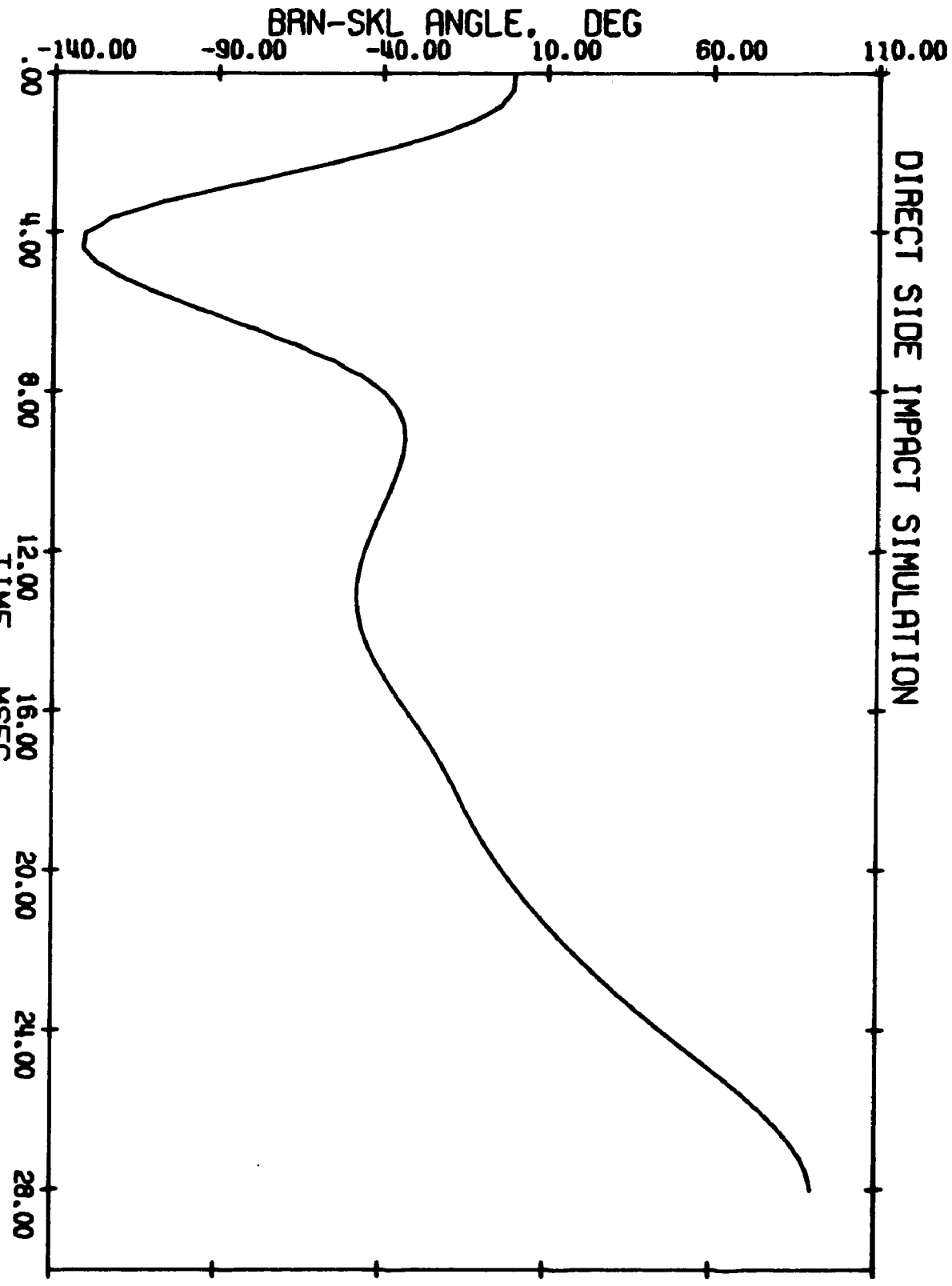


Figure 35. Brain-Skull Angle.

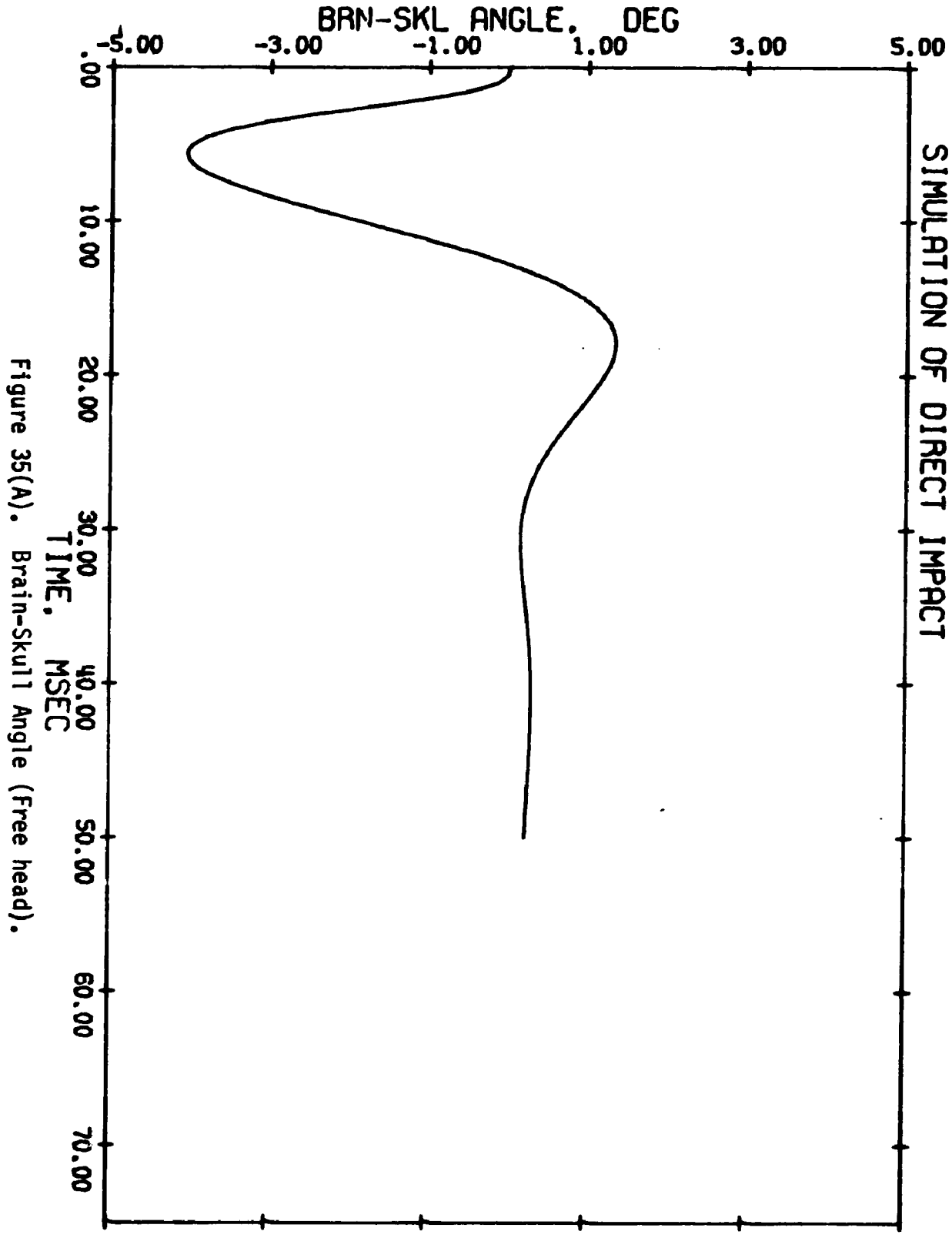


Figure 35(A). Brain-Skull Angle (Free head).

RHESUS A-P HEAD MODEL
FREE HEAD
HALF-SINE, 200-LB PEAK AT OCCIPUT (P-A)

NOV 4, 1973

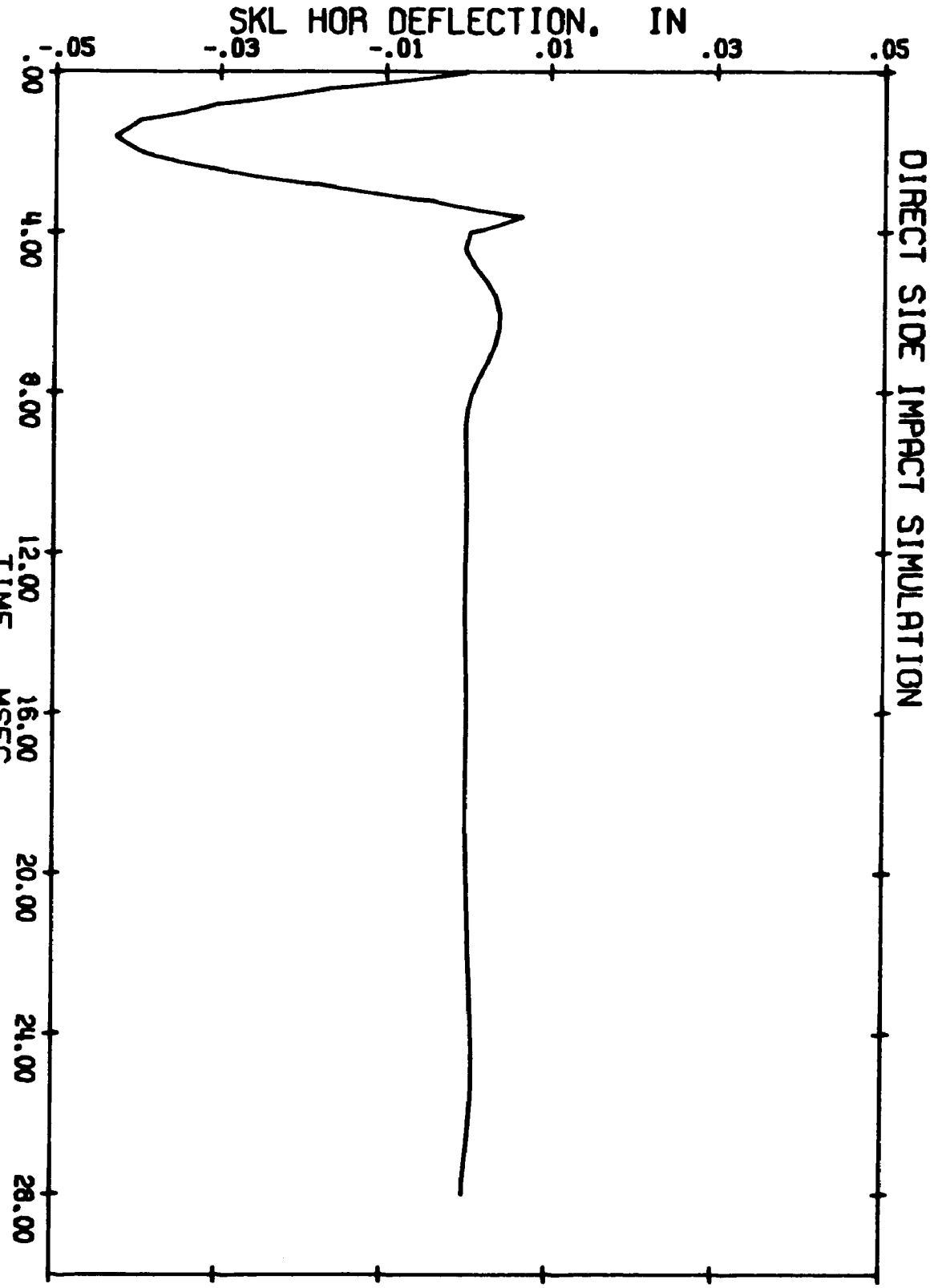


Figure 36. Skull Horizontal (L-R) Deflection.

RHESUS L-R HEAD MODEL
ZERO-ACCELERATIONS AT NECK-TORSO
3.5 MSEC. 2000 LBS IMPACT TO SKULL

NOV 13. 1973

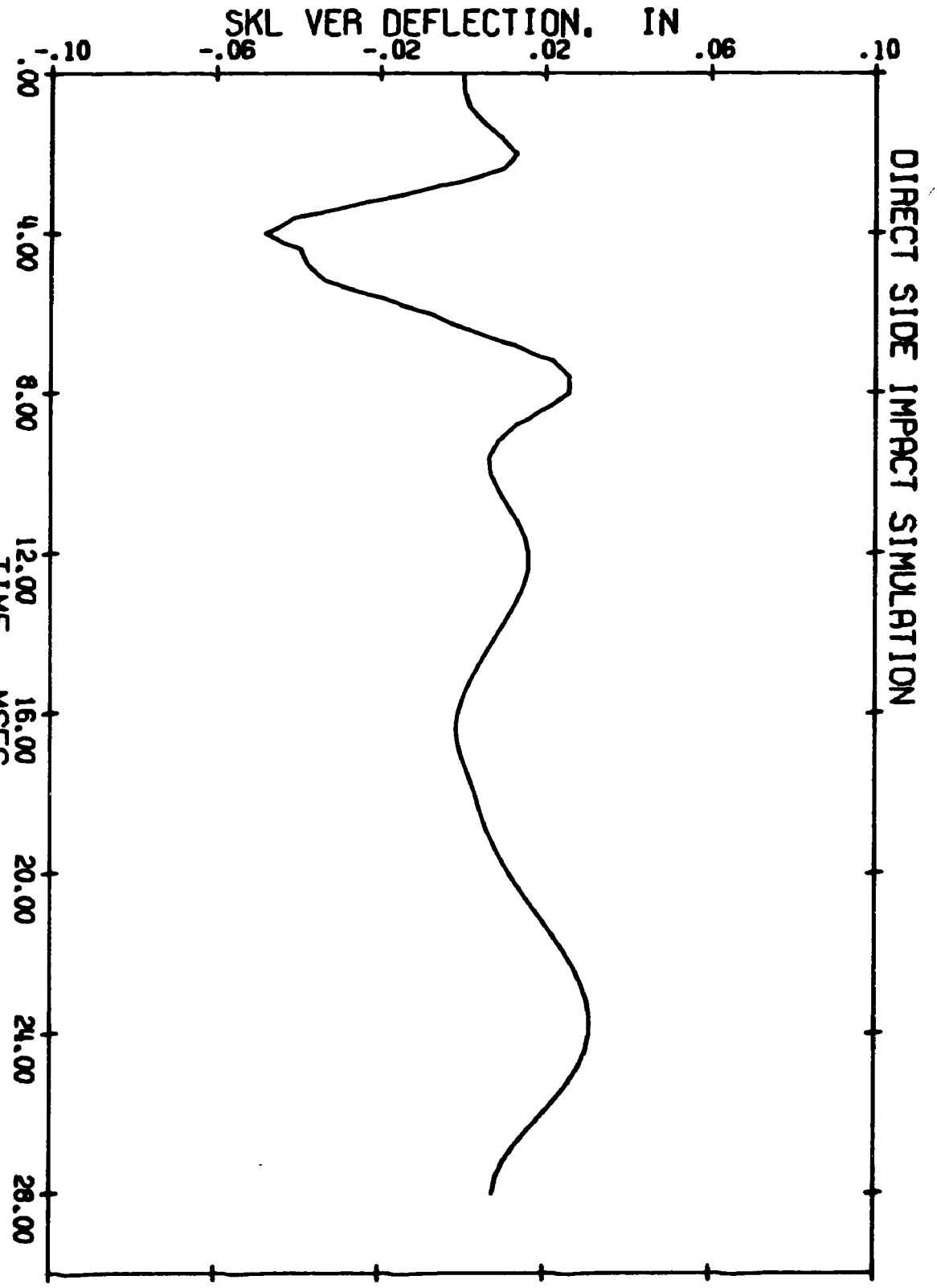


Figure 37. Skull Vertical (S-I) Deflection.

RHESUS L-R HEAD MODEL
ZERO-ACCELERATIONS AT NECK-TORSO
3.5 MSEC. 2000 LBS IMPACT TO SKULL

NOV 13, 1973

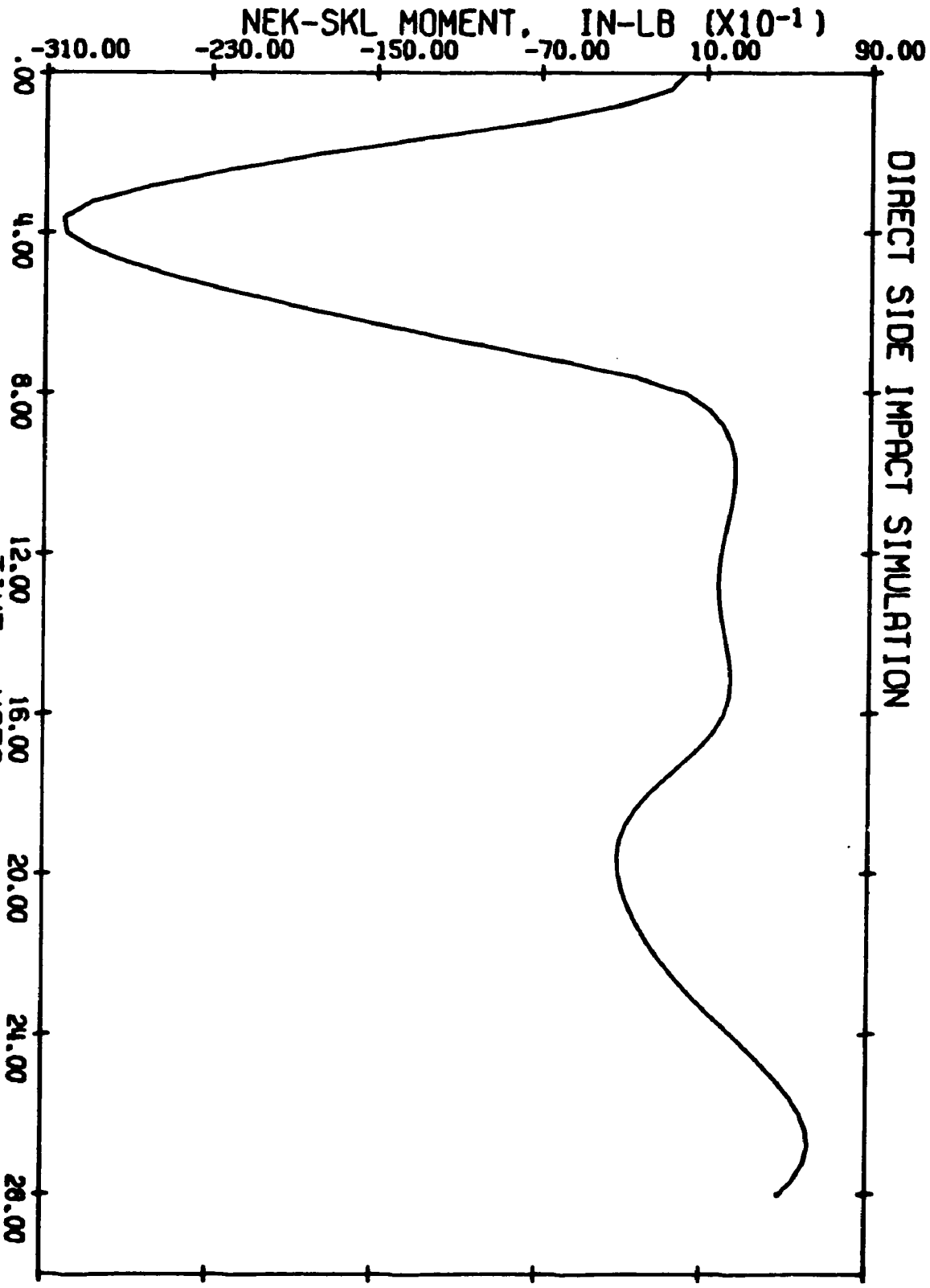


Figure 38. Moment at Neck-Skull Joint.

RHESUS L-R HEAD MODEL
ZERO-ACCELERATIONS AT NECK-TORSO
3.5 MSEC. 2000 LBS IMPACT TO SKULL

NOV 13, 1973

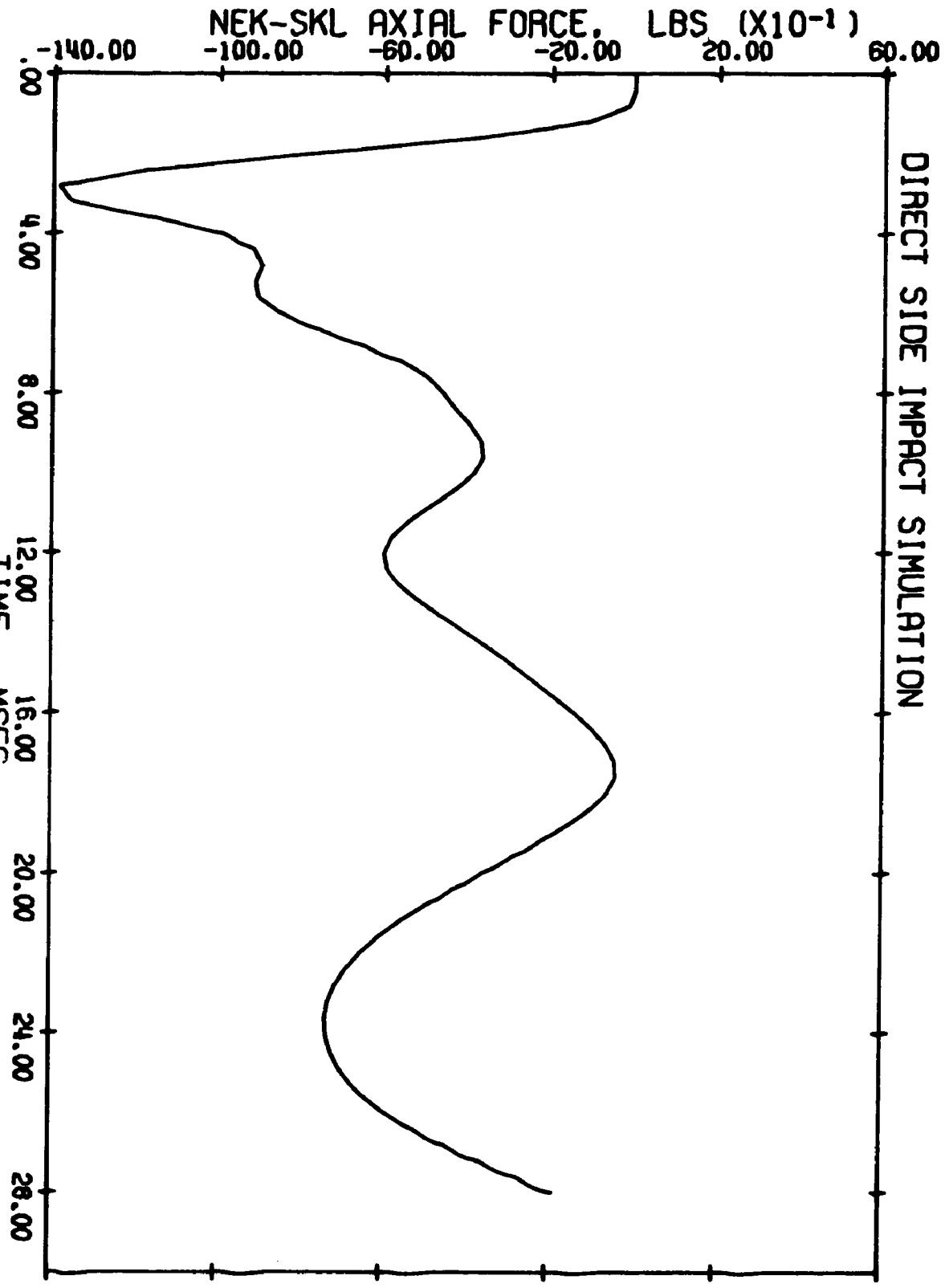


Figure 39. Axial (S-I) Force at Neck-Skull Joint.

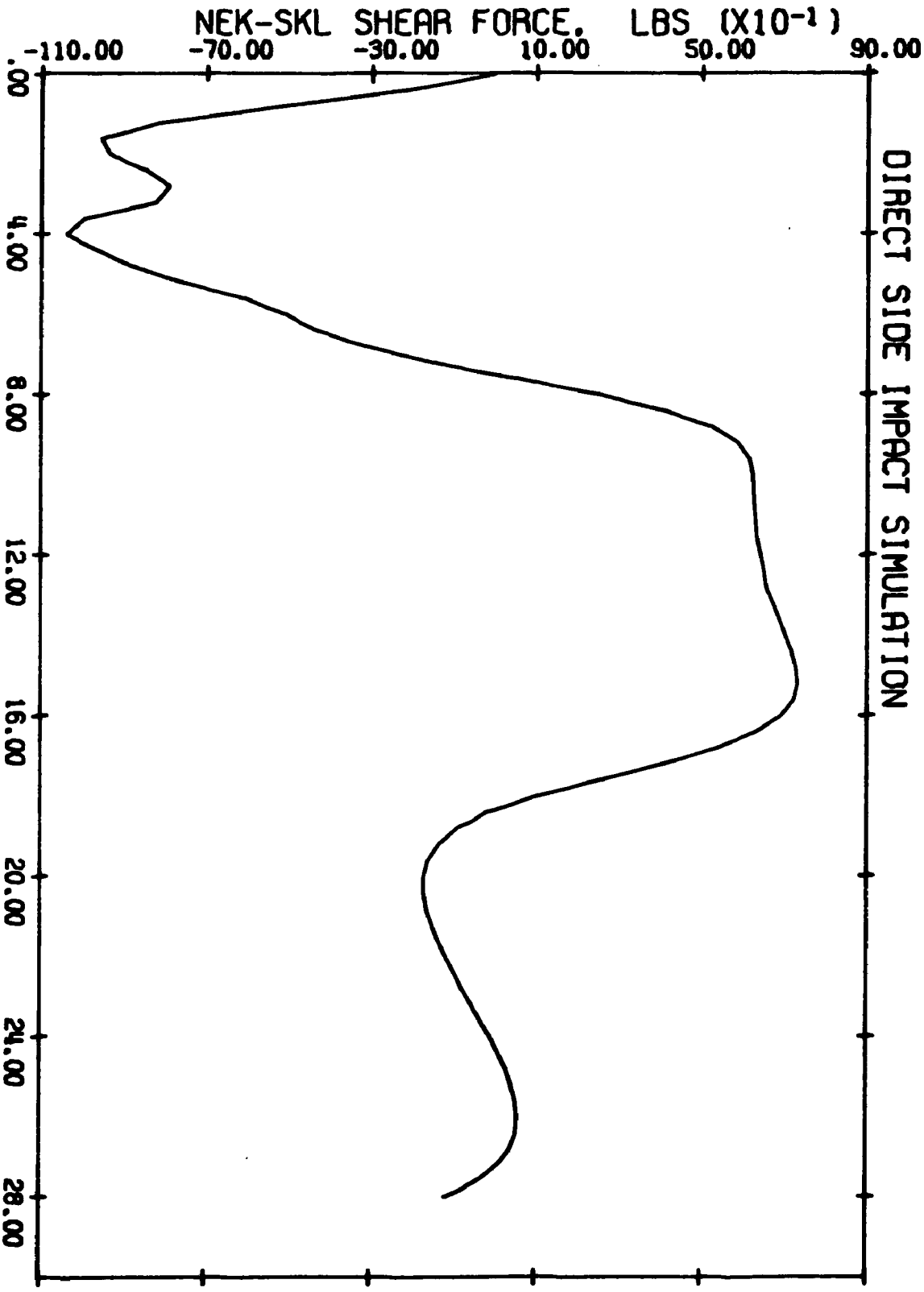


Figure 40. Shear (L-R) Force at Neck-Skull Joint.

4.2.2 Whiplash Simulation of Human Head

The term "whiplash" generally refers to the motion of the head of a passenger in an automobile which is struck from the rear. This motion, which may be attributed to forces transmitted through the torso of the passenger to the bottom of his head-neck assembly, is essentially in the A-P vertical plane of the head.

The purpose of this simulation is to study the general behavior of the model's variable in hypothetical and typical whiplash situations. The human A-P model, whose constants were developed in chapter 3, is subjected to a hypothetical half-sine horizontal acceleration pulse. This pulse, shown in figure 42, has a duration of 10 msec and a peak of 5 g's.

The data describing the model's constants and simulation's parameters is given in figure 41. Attention should be drawn to the non-linear spring characteristics of the neck (hardening springs) and those of the skull (softening springs), as well as to the brain-skull torsional couplings. These spring constants were later changed (increased) to study their effect on some variables of the model. Results of the first simulation are shown in figures 43 through 56. The following comments may be made about these and other results.

1) The duration (60 msec) of the simulation is not enough to allow all or most, of the variables to reach their settling values. Typically, a whiplash experiment may last as long as 200 or 300 msec. Extension of the simulation period, while keeping the same accuracy of the integration subroutine, puts a financial burden that was not feasible. It was assumed that the critical variables, e.g., brain rotation, neck forces, would reach their peaks during the 60 msec.

This assumption, however, was found not to be true.

2) As with direct impact simulation, the boundary conditions play an important role in reproducing a realistic whiplash simulation. To show this effect, two simulations were conducted using forces as input at the bottom of the neck (type I). The data was obtained from McKenzie, et. al. whiplash model [29], where more or less realistic forces at a low inter-vertebral joint were used as input to the present model. The duration of the input pulses (FXO, FYO, TN), was 125 msec, and the simulation was allowed to last 140 msec. Results of these two simulations showed that the time, at which peaks occurred, varied from 125 msec to 140 msec, with some of the peaks occurring about 50 and 60 msec. It should be noted that FXO had a peak of 100 lbs at t = 50 msec, FYO had a peak of 45 lbs at t = 38 msec, and TN had a peak of 100 in-lb at t = 60 msec. All three pulses may be approximated by half-sine pulses of duration 125 msec.

3) Neck axial deflection, the neck-torso angle and the skull-torso angle, shown in figures 43, 44 and 45. It is interesting to note that, even after 20 or 30 msec from the end of the acceleration pulse, the angles didn't exceed 5 degrees.

4) The skull deformations (vertical and horizontal) are shown in figures 46 and 47. The horizontal deformation had its peak of 0.04 thousandths of an inch at t = 45 msec, while the vertical deformation was twice that much, but occurred at the same time. The strong oscillations of these variables, at a time long after

the end of the input acceleration pulse, suggests that inertial forces acting on the neck, along with the imposed zero-accelerations on its bottom, drive the system in what seems to be unstable response. This, however, may be explained by recalling that the spring constants of the neck (KTS and KTN) have unequal values for positive and negative deflections. Thus, each time the neck-torso or the skull-neck angles cross zero (change sign), the resulting moment undergoes a sharp change. This is also true for the axial deformation of the neck where the two springs K1N and K2N have unequal spring constants for compression and tension. Eventually, with the presence of damping, these violent oscillations should die out.

5) Figures 48 and 49 indicate that even when the skull is not directly impacted, the brain does move relative to the skull. The magnitudes of this motion depend on the characteristics of the skull-brain couplings.

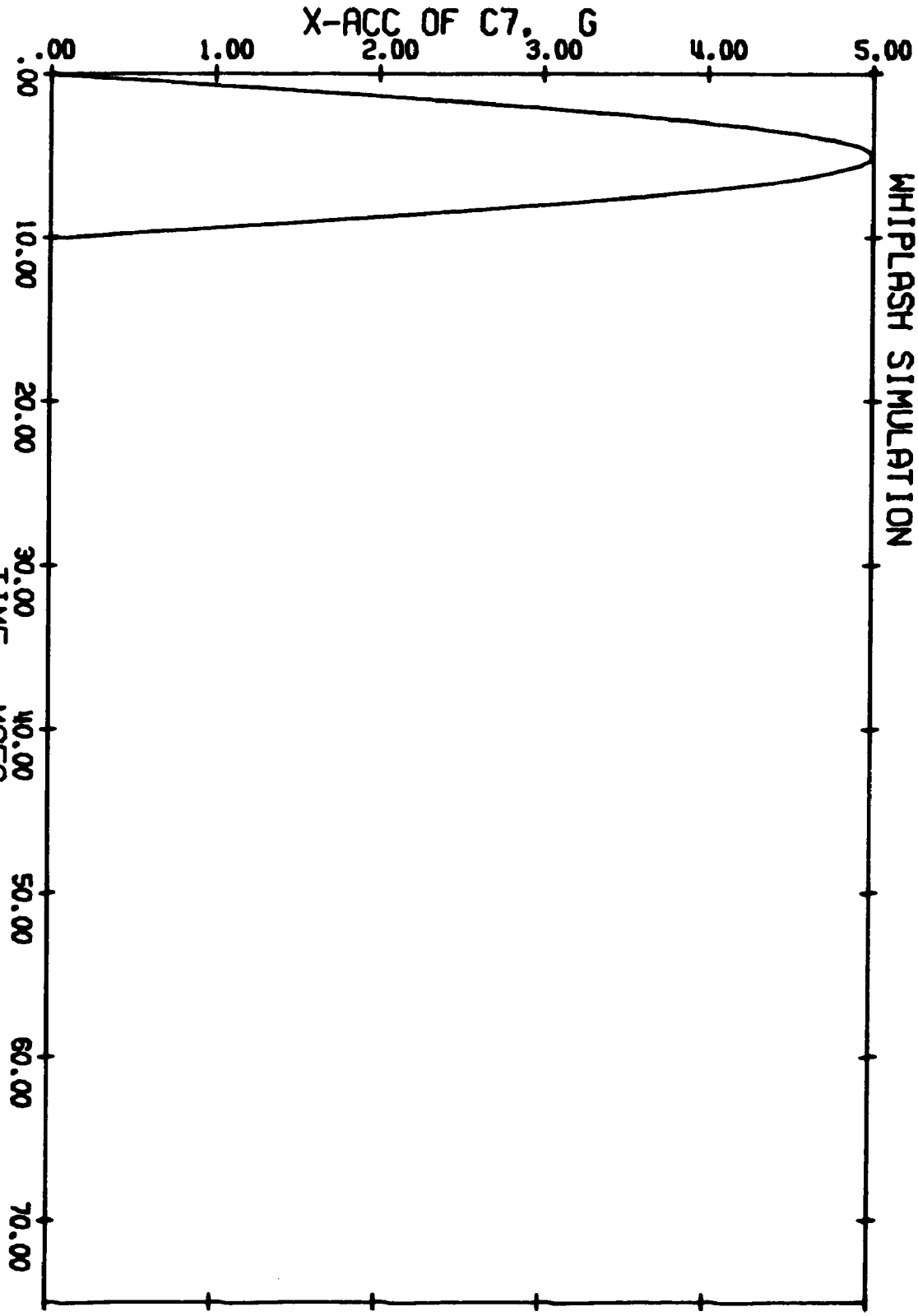
6) The skull and brain absolute angular velocities (figures 50 and 51), and accelerations (figures 52 and 53) show relatively low peaks. It is suspected that under realistic boundary conditions, these peaks would be higher.

7) With the acceleration input specified for this simulation, it is interesting to observe the forces which are necessary to maintain the prescribed motion. These forces are shown in figures 54, 55 and 56. Note that the horizontal force has two "breaks." The first break occurs at 10 msec, when the half-sine pulse ends; the time of the second break (about 35 msec) coincides with the crossing of zero of the skull-neck angle.

8) In order to provide a contrast to the results of this simulation, 3 typical results of another simulation are given in figures 49(A), 50(A) and 54(A). These curves were generated in a similar whiplash simulation, where the peak acceleration input was 10 g's, and the ABSERR was 5.0. The increase in the acceleration level is reflected in the peaks, and the decrease of the accuracy in the integration subroutine shows up in the periodic "jerking" of the response. It can be concluded that the specified accuracy effects the smoothness of the response but not its general behavior. This suggests that an optimum accuracy, which compromises cost for smoothness, may be found by making a few parametric runs.

```
*MODEL      HUMAN A-P HEAD MODEL
 &NECK     WN=3.5, L1=2.17, L2=2.17,
           KTN=0.48,500.,2250.,3*0.,
               -0.611,-200.,1115.,3*0., CTN=0.5,
           K1N=2000.,5*0.,6000.,5*0.,   C1N=0.5,
           K2N=2000.,5*0.,6000.,5*0.,   C2N=0.5  &END
 &SKULL    W1=0.8, W2=1.2, W3=4.0,
           D1=4.0,  D2=4.8,  HC=2.65,
           KTS=0.48,500.,2250.,3*0.,
               -0.611,-200.,1115.,3*0., CTS=0.5,
           K1S=0.15,1500.,8000.,9*0.,   C1S=0.25,
           K2S=0.15,2250.,12000.,9*0.,  C2S=0.25,
           K3S=0.15,3000.,15000.,9*0.,  C3S=0.25,
           K4S=0.15,3000.,15000.,9*0.,  C4S=0.25  &END
 &BRAIN    WB=3.5,  IB=0.2,
           BSX=-0.5,  BSY=1.0,
           KTB=2.5, CTB=1.35,
           K1B=250.,K2B=250.,K3B=250.,K4B=250.,
           C1B=1.8, C2B=1.8, C3B=1.8, C4B=1.8     &END
*TIT        WHIPLASH SIMULATION
*INI        HORIZONTAL ACCELERATION INPUT
 &INCON PHN=0.  &END
*FOR        REAR IMPACT, HALF-SINE: 5 G'S, 10 MSEC
 &FORCES TYPE=2,
          JXO=2,XO=10.,5.,104*0.  &END
 &TIMER FINTIM=60., DELOUT=0.4,
        DELTIM=0.1, ABSERR=0.25   &END
 &OUTPLT PRT=6*0, PLT=1,5*0 &END
*RUN
```

Figure 41. Input Data to Whiplash Simulation.



HUMAN A-P HEAD MODEL
HORIZONTAL ACCELERATION INPUT
REAR IMPACT. HALF-SINE: 5 G'S, 10 MSEC

NOV 13, 1973

Figure 42. Input Acceleration at Neck-Torso Joint.

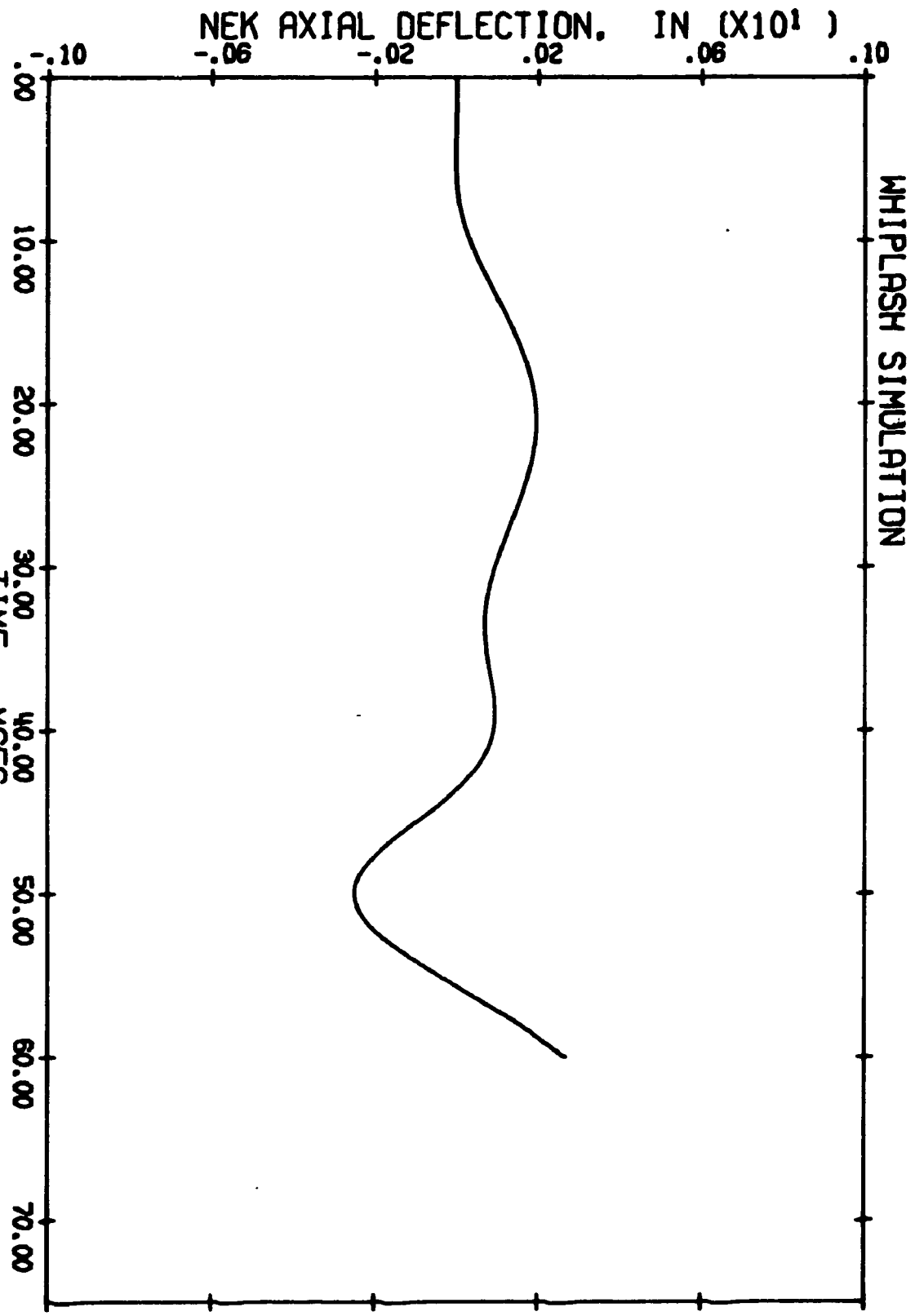


Figure 43. Neck Axial Deformation.

HUMAN A-P HEAD MODEL
HORIZONTAL ACCELERATION INPUT
REAR IMPACT, HALF-SINE: 5 G'S, 10 MSEC

NOV 13, 1973

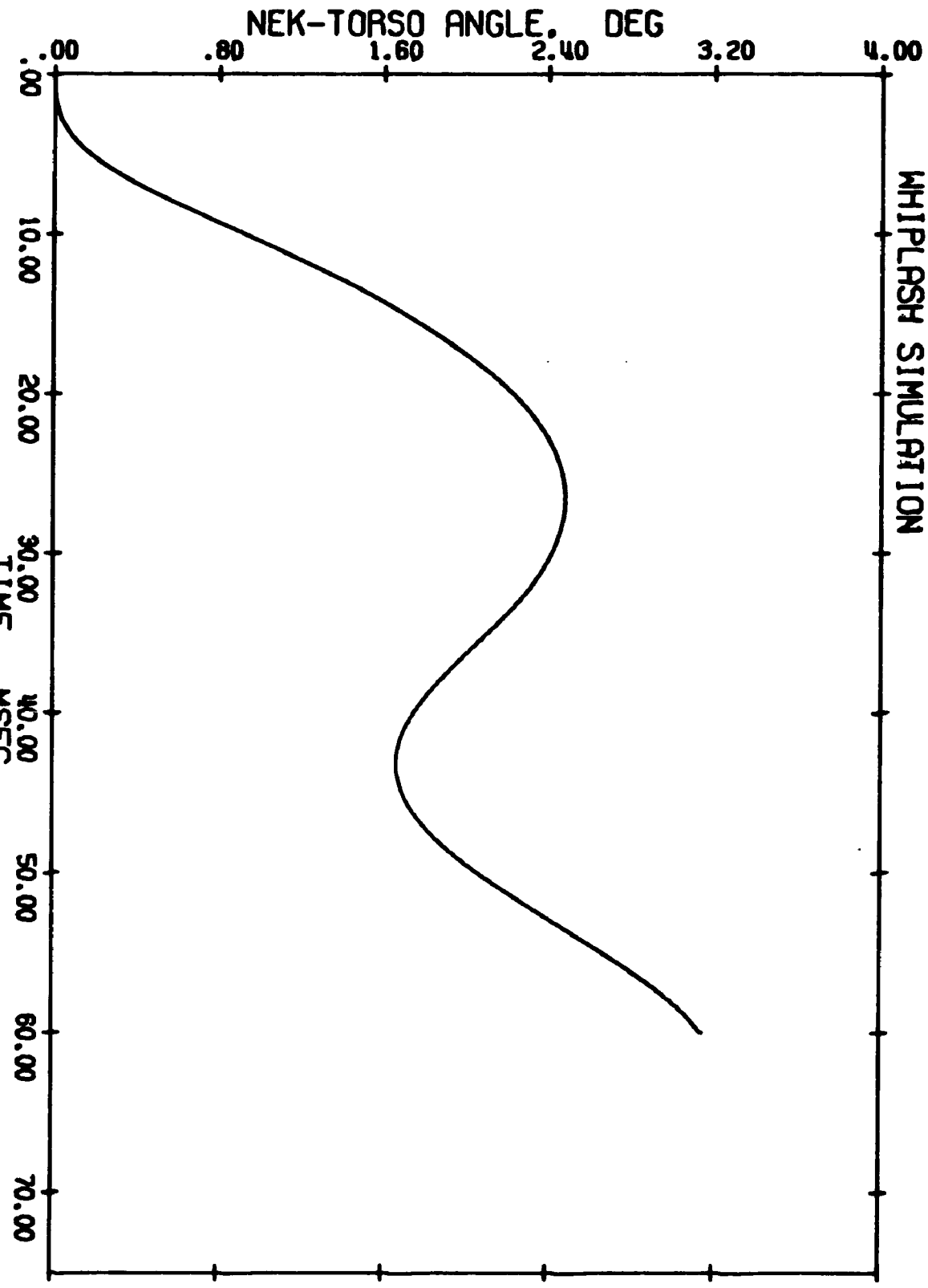


Figure 44. Orientation of Neck (Relative to Torso).

HUMAN A-P HEAD MODEL
HORIZONTAL ACCELERATION INPUT
REAR IMPACT, HALF-SINE: 5 G'S, 10 MSEC

NOV 13, 1973

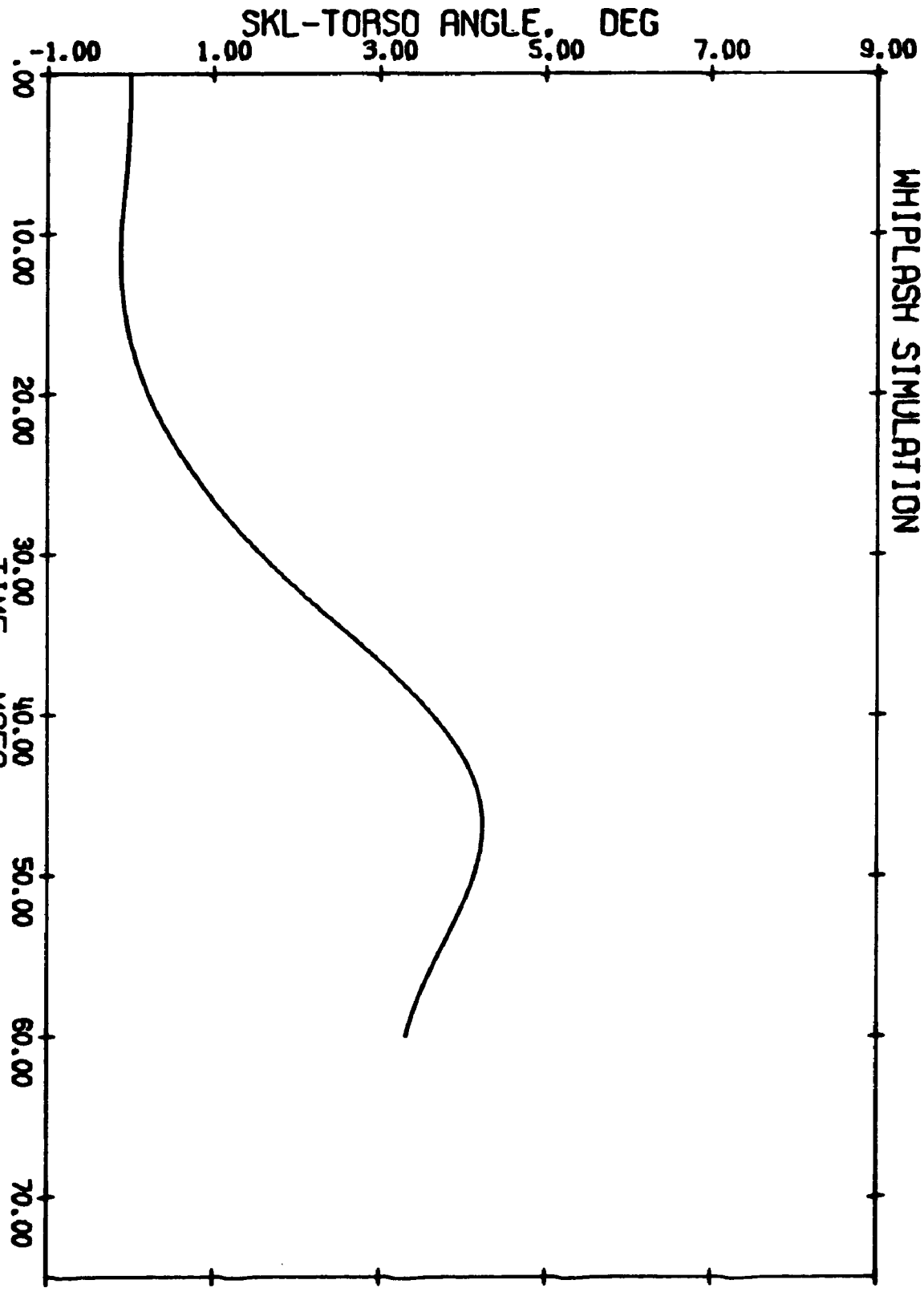


Figure 45. Angle of Skull Relative to Torso.

HUMAN A-P HEAD MODEL
HORIZONTAL ACCELERATION INPUT
REAR IMPACT, HALF-SINE: 5 G'S, 10 MSEC

NOV 13, 1973

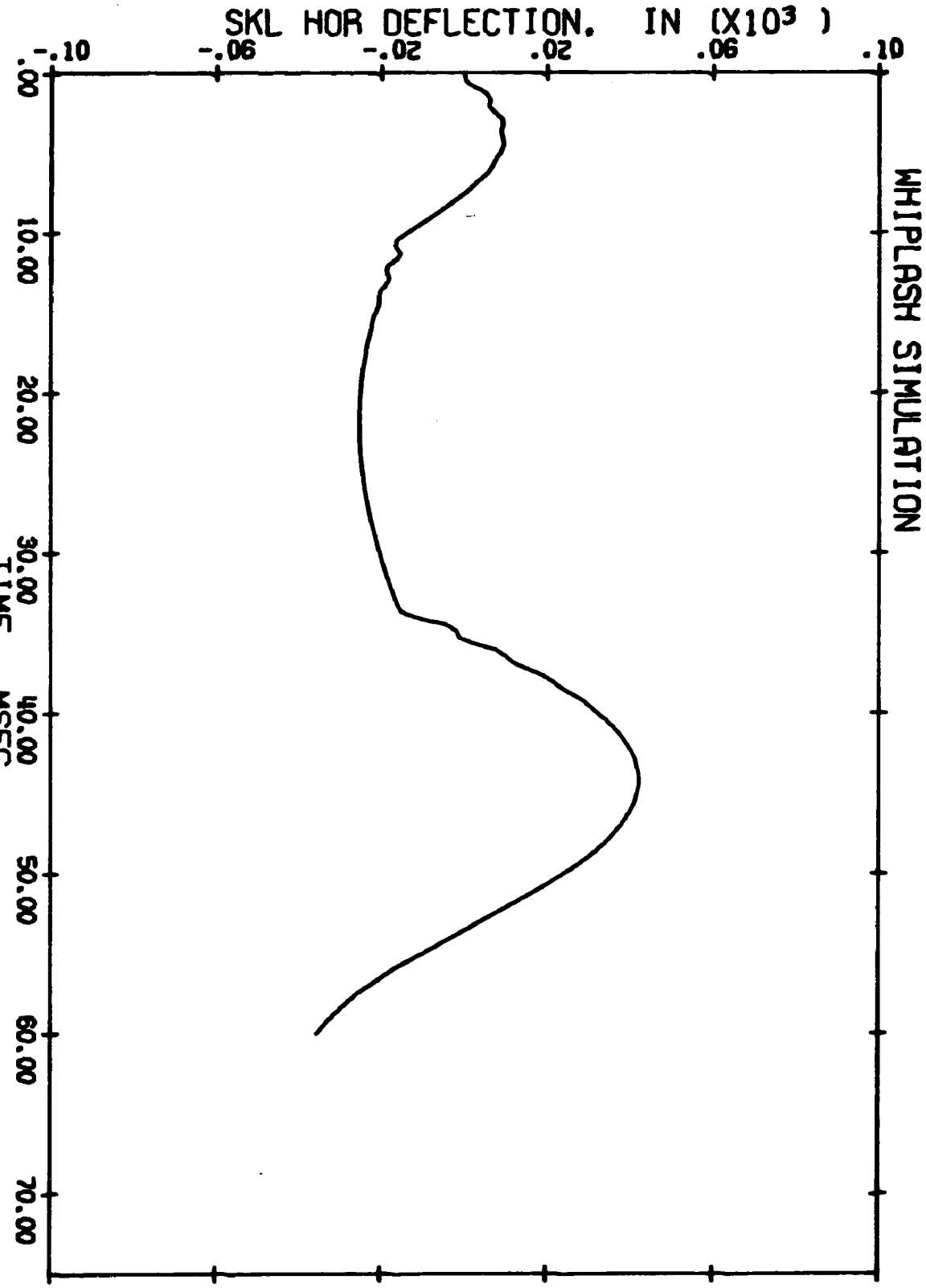


Figure 46. Horizontal (A-P) Skull Deformation

HUMAN A-P HEAD MODEL
HORIZONTAL ACCELERATION INPUT
REAR IMPACT, HALF-SINE: 5 G'S, 10 MSEC

NOV 13, 1973

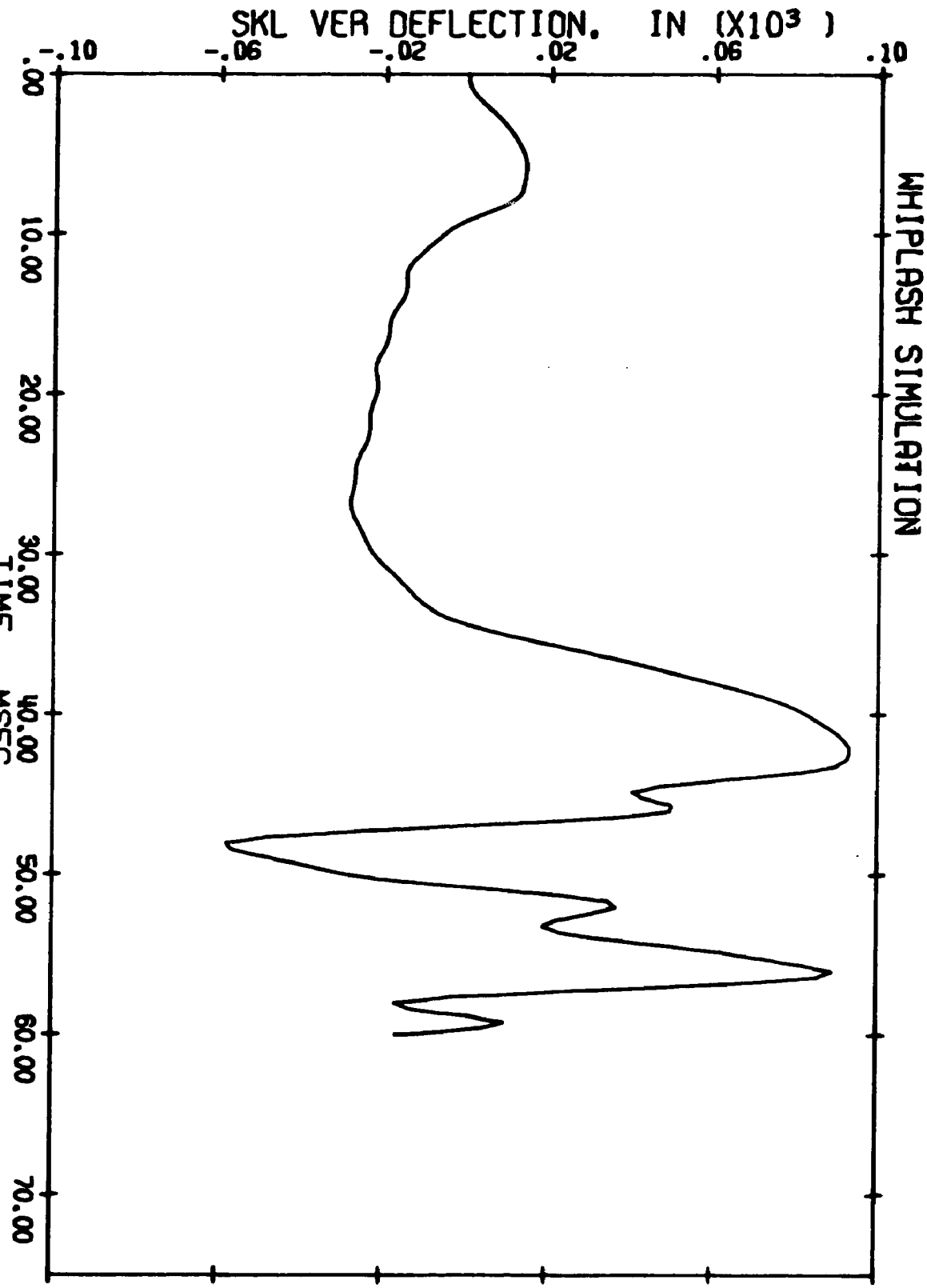


Figure 47. Vertical (S-I) Skull Deformation.

HUMAN A-P HEAD MODEL
HORIZONTAL ACCELERATION INPUT
REAR IMPACT, HALF-SINE: 5 G'S, 10 MSEC

NOV 13, 1973

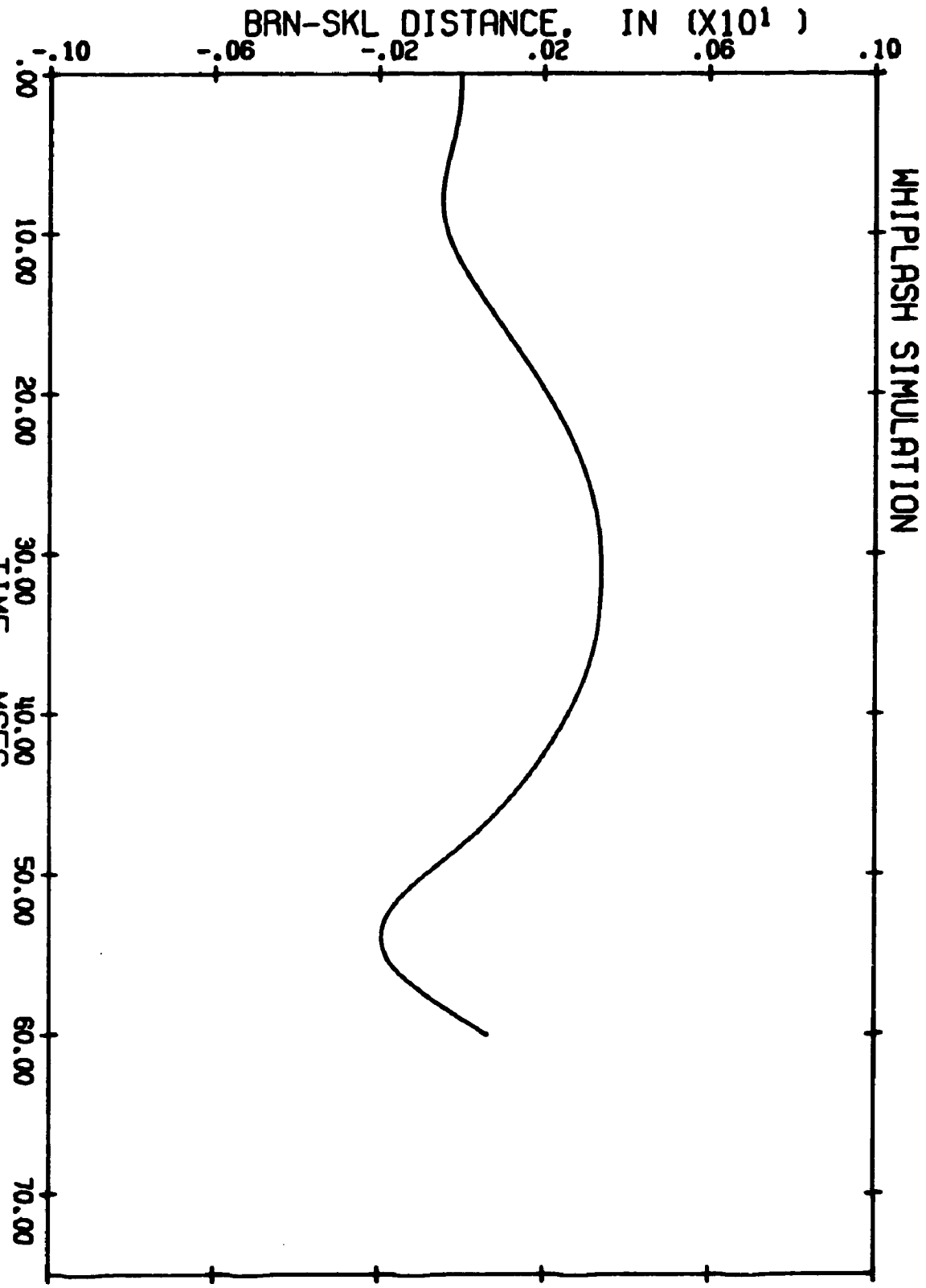


Figure 48. Motion (Distance) of Brain Relative to Skull.

HUMAN A-P HEAD MODEL
HORIZONTAL ACCELERATION INPUT
REAR IMPACT, HALF-SINE: 5 G'S, 10 MSEC

NOV 13, 1973

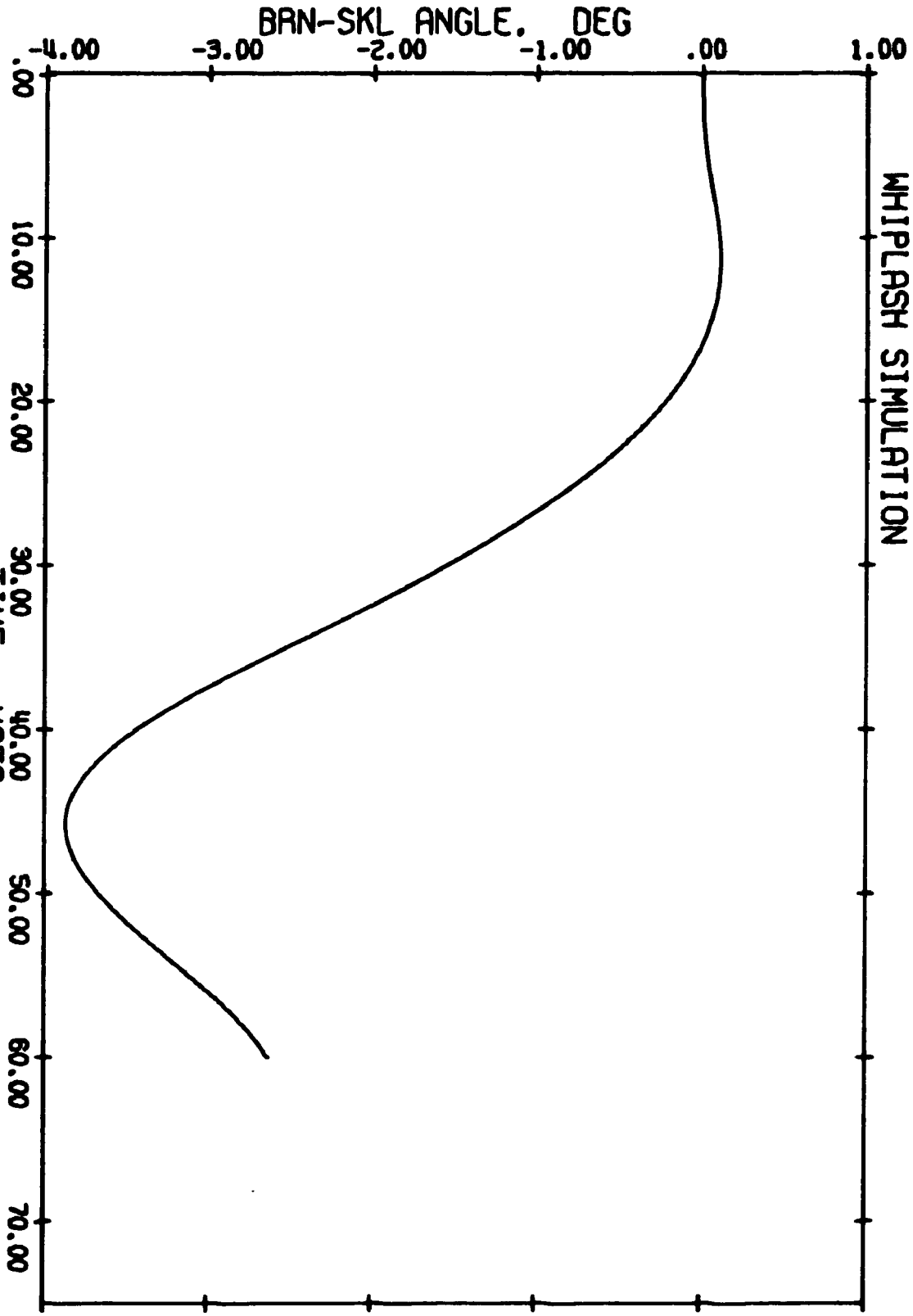


Figure 49. Motion (Angle) of Brain Relative to Skull.

HUMAN A-P HEAD MODEL
HORIZONTAL ACCELERATION INPUT
REAR IMPACT, HALF-SINE: 5 G'S, 10 MSEC

NOV 13, 1973

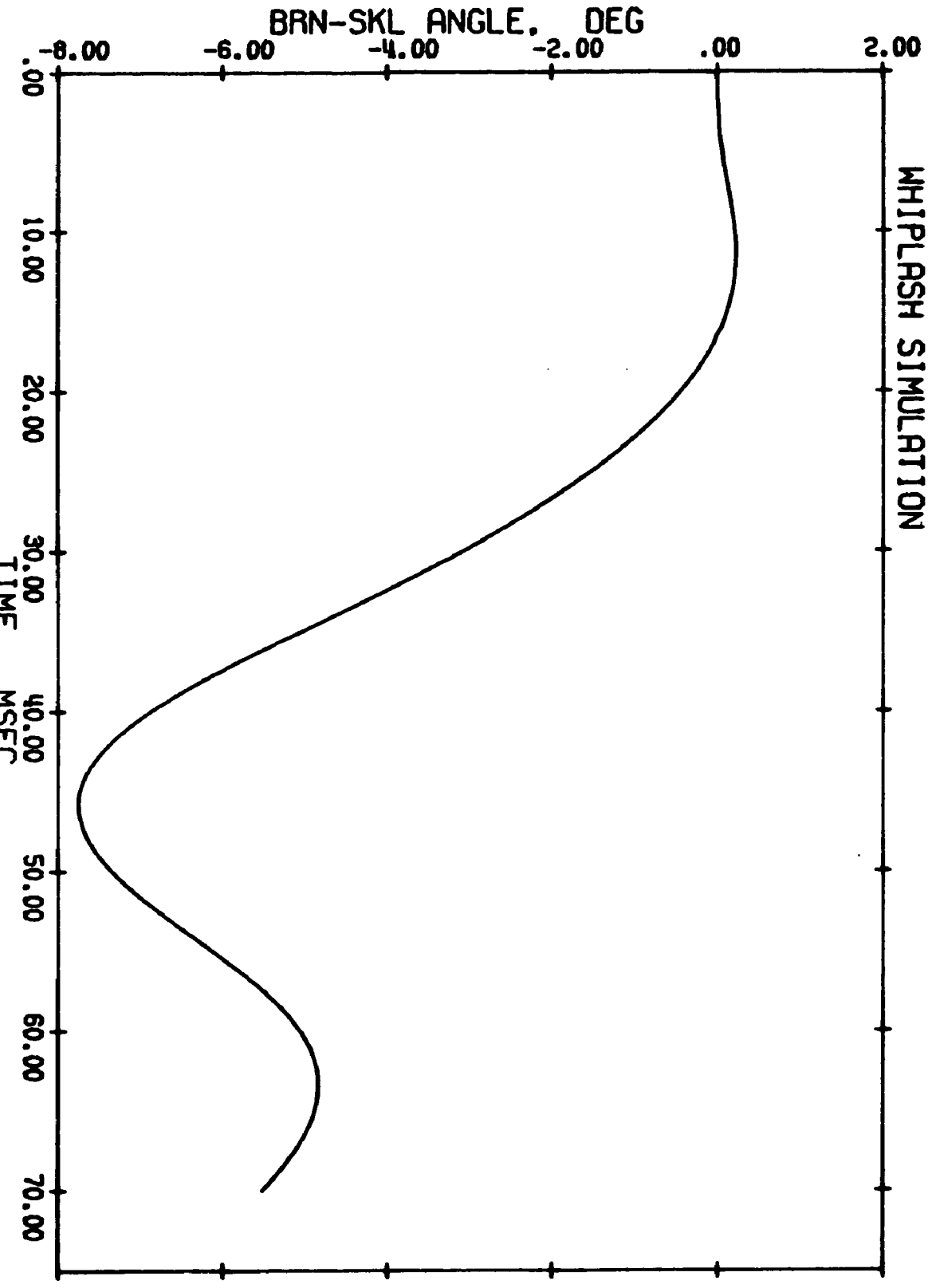


Figure 49 (A). Brain-Skull Angle (10-g Acc. Input).

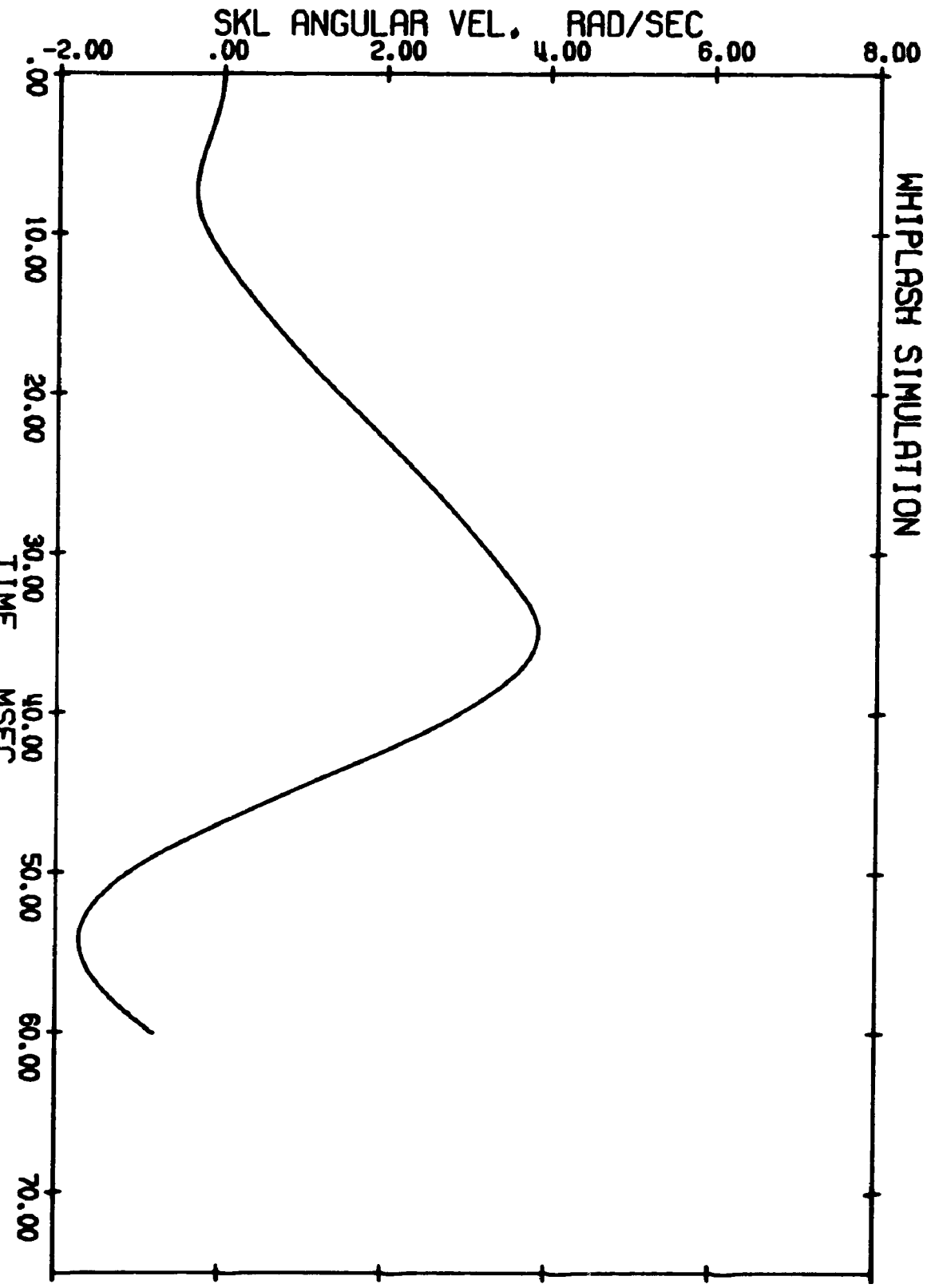


Figure 50. Absolute Angular Velocity of Skull.

HUMAN A-P HEAD MODEL
HORIZONTAL ACCELERATION INPUT
REAR IMPACT, HALF-SINE: 5 G'S, 10 MSEC

NOV 13, 1973

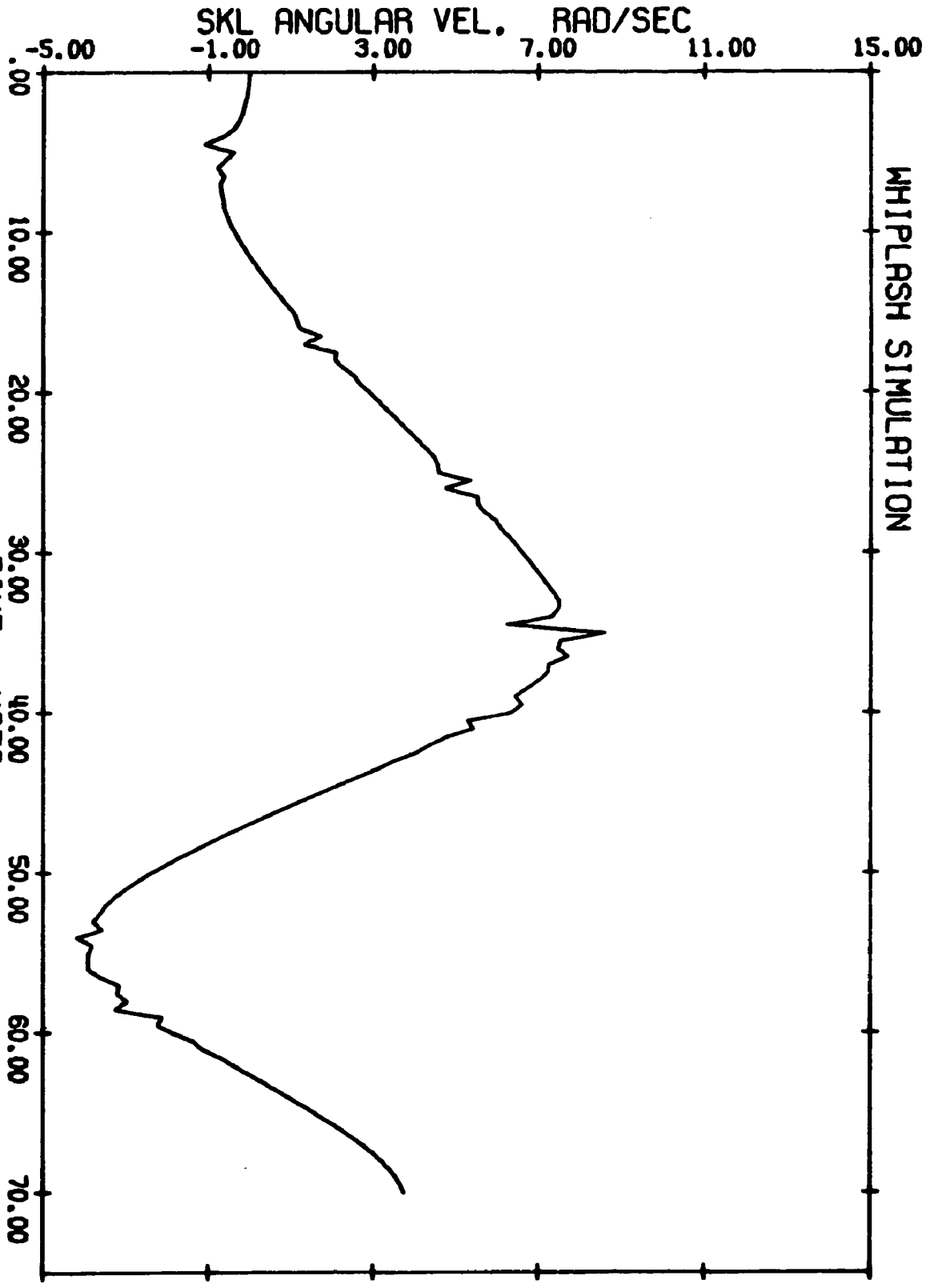


Figure 50 (A). Skull Angular Velocity (10-g Acc. Input)

HUMAN A-P HEAD MODEL
HORIZONTAL ACCELERATION INPUT
REAR IMPACT. HALF-SINE: 20 G'S. 20 MSEC

NOV 8, 1973

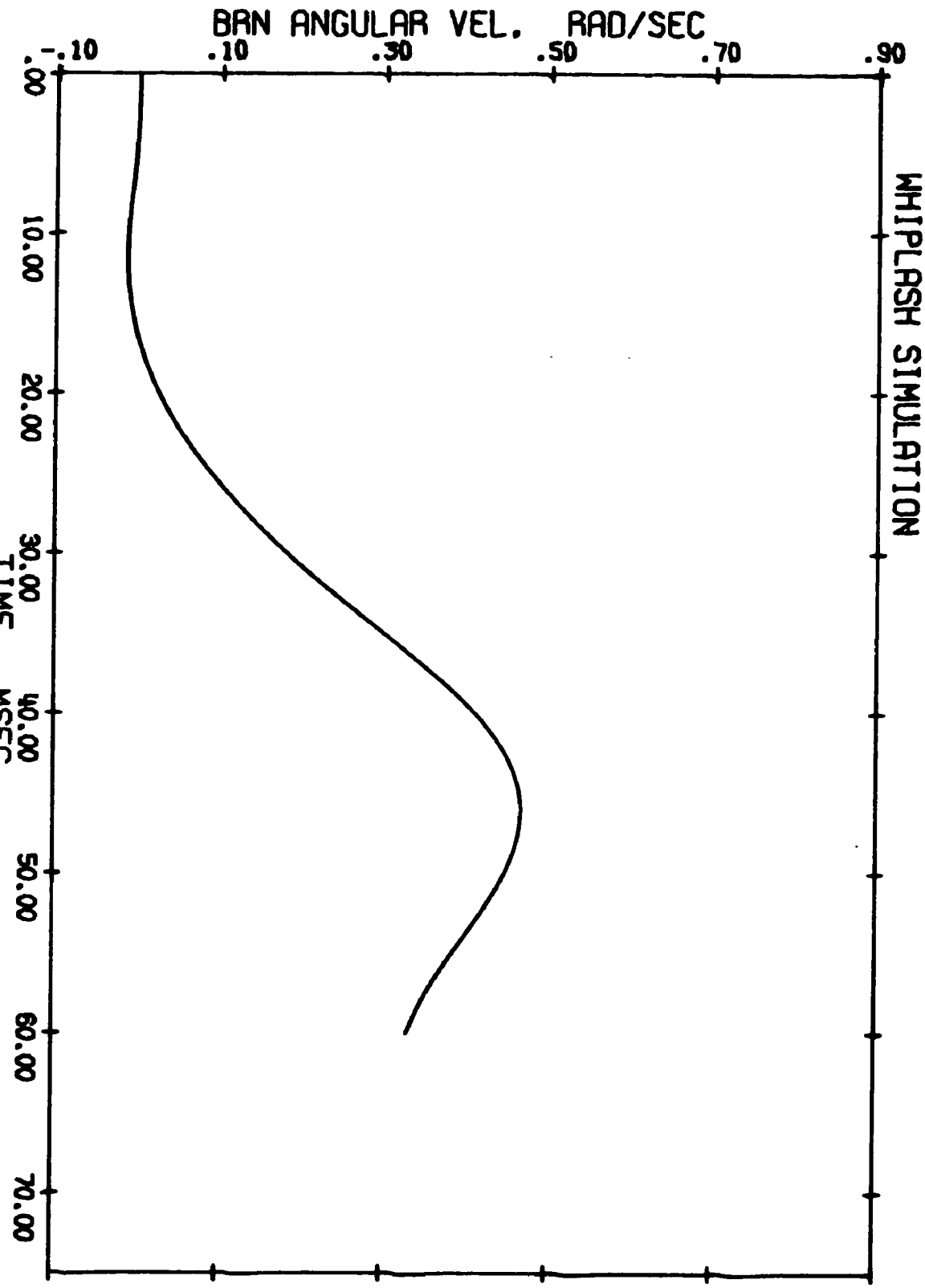


Figure 51. Brain Absolute Angular Velocity.

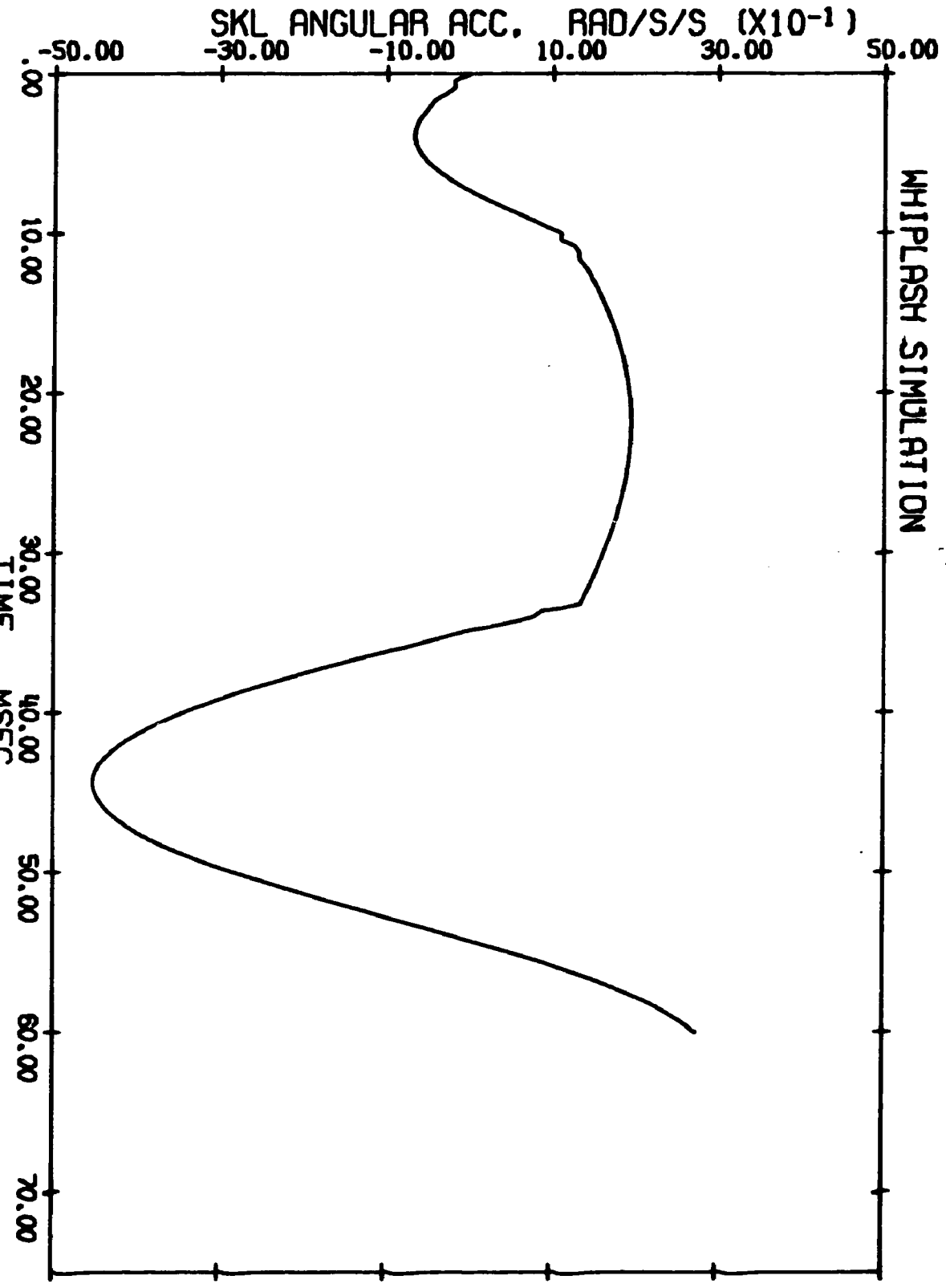


Figure 52. Skull Absolute Angular Acceleration.

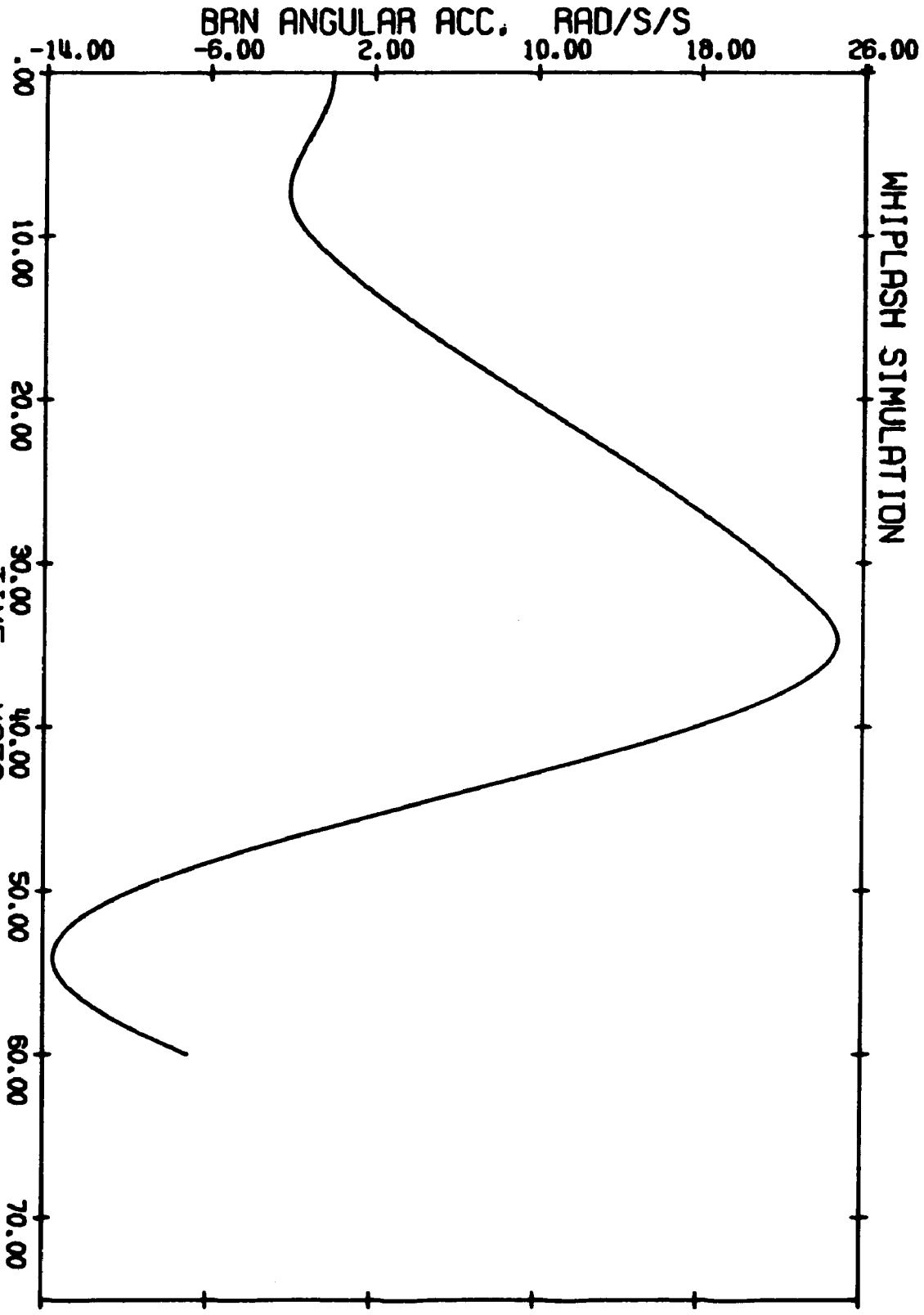


Figure 53. Brain Absolute Angular Acceleration.

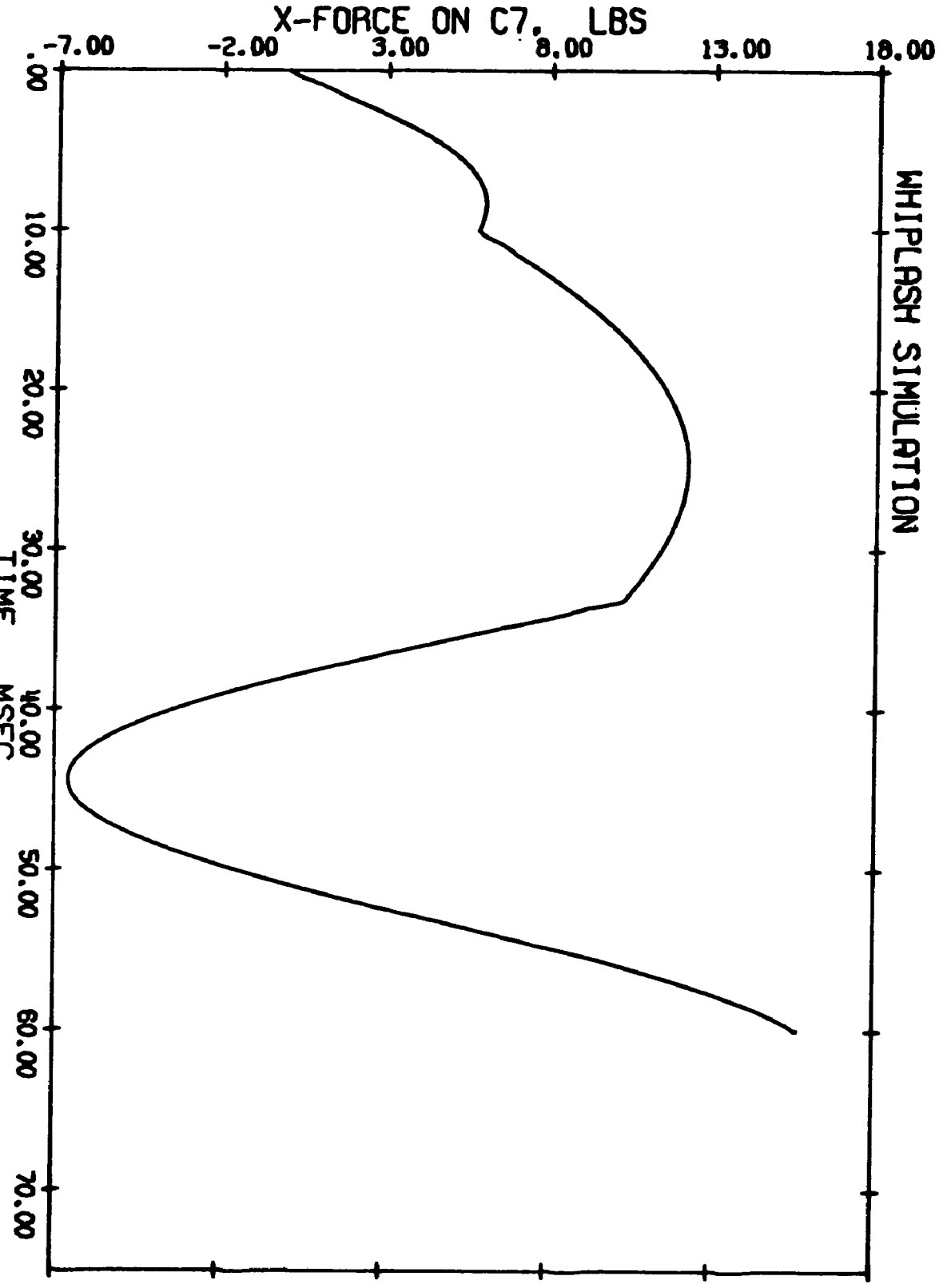


Figure 54. Constraint Force on XO.

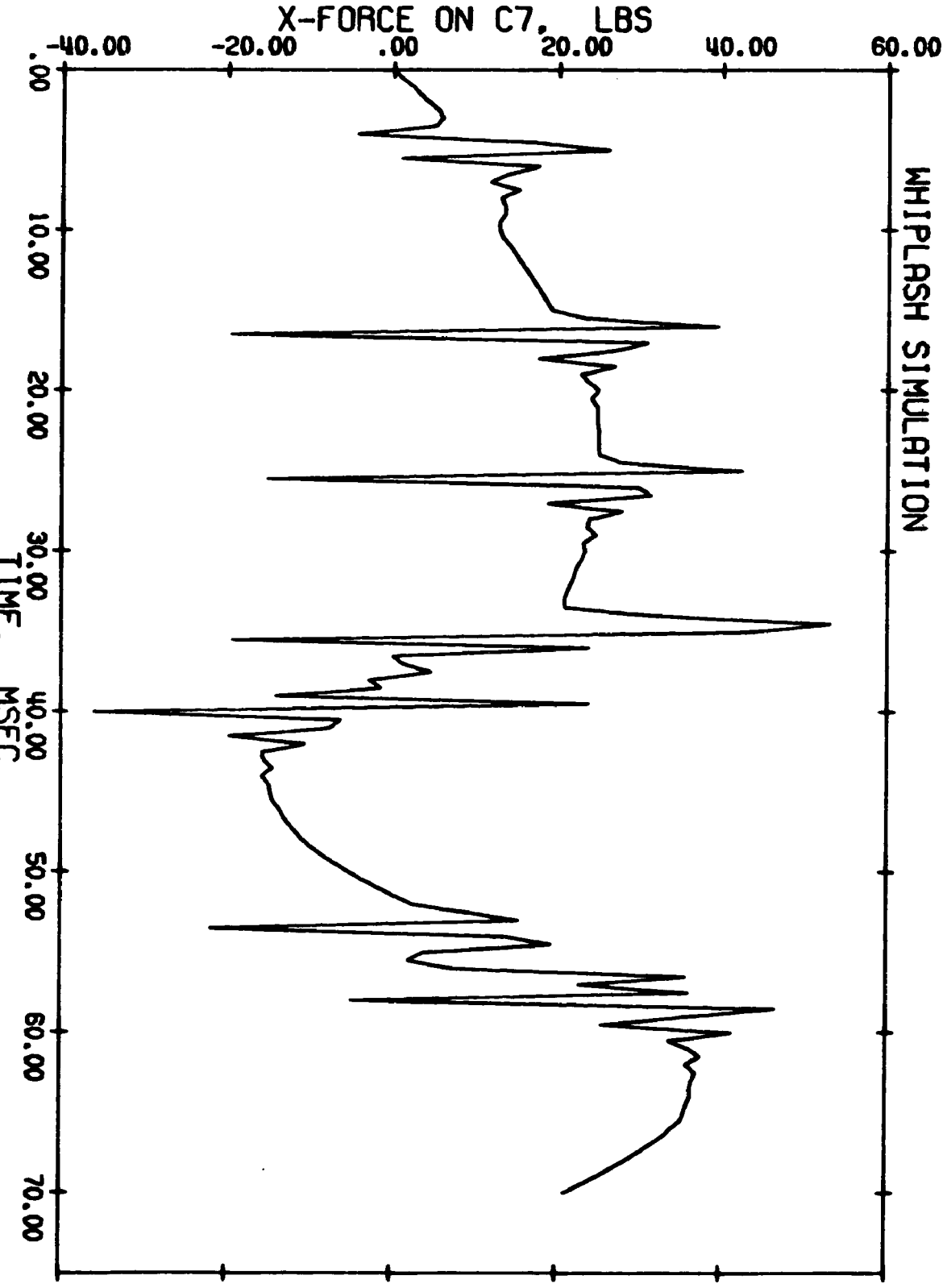


Figure 54 (A). XO-Constraint Force (10-g, Less Accuracy).

HUMAN A-P HEAD MODEL
HORIZONTAL ACCELERATION INPUT
REAR IMPACT, HALF-SINE: 10 G'S, 10 MSEC

NOV 8, 1973

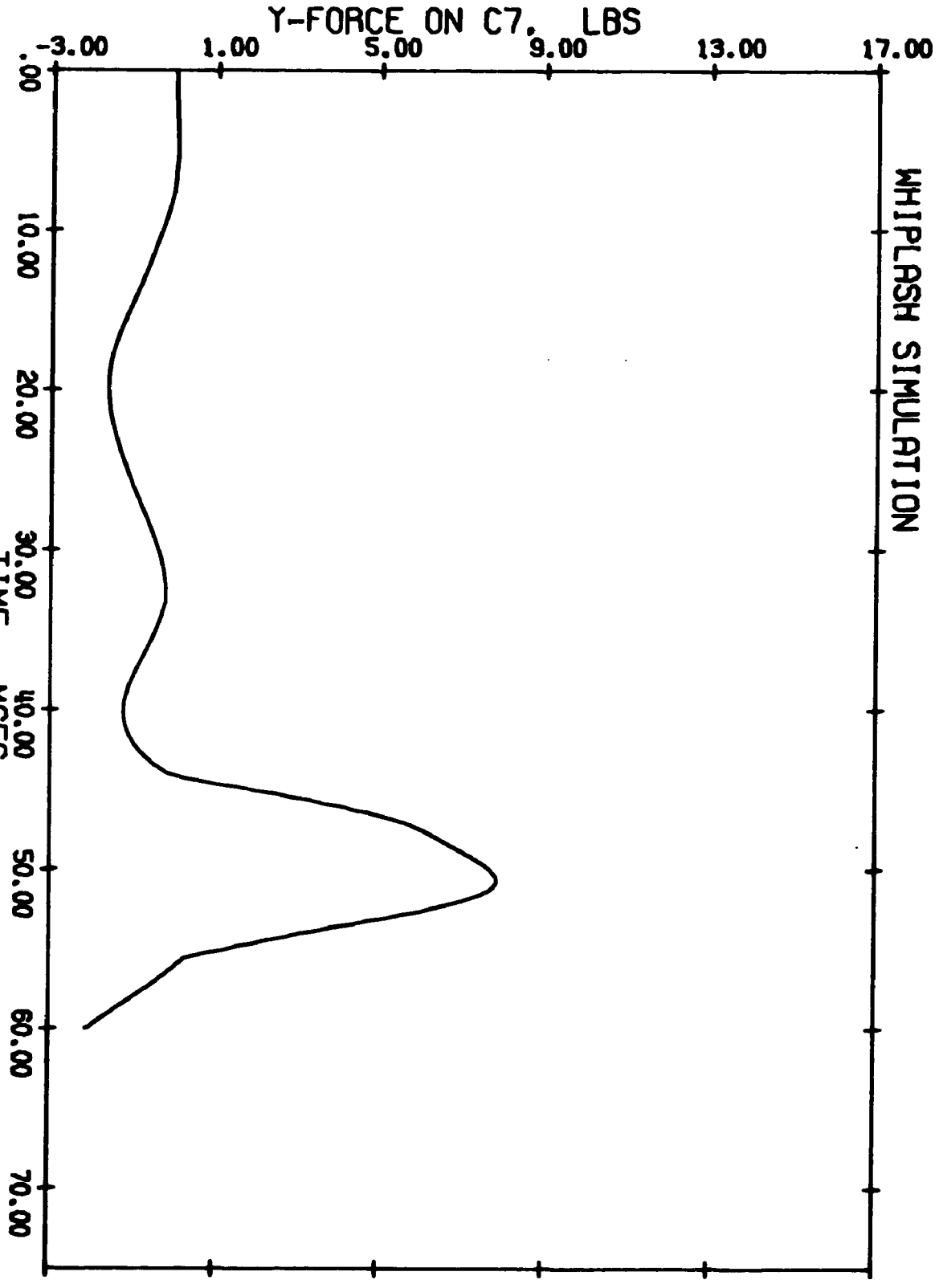


Figure 55. Constraint Force on Y0.

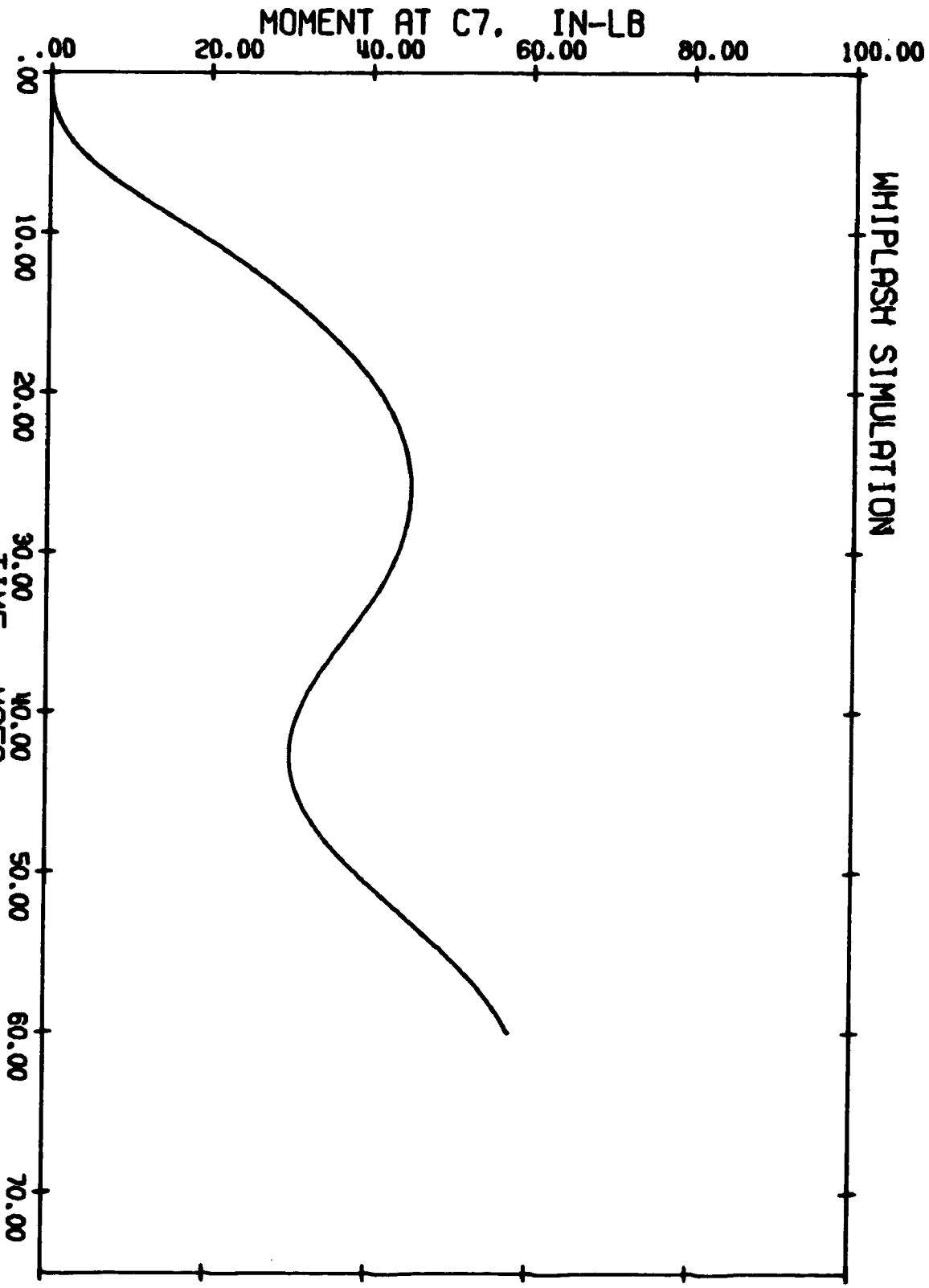


Figure 56. Constraint Moment at (XO,YO).

4.3 COMPARATIVE SIMULATIONS

Two series of simulations were conducted in order to illustrate the relative behavior of the model, (a) when some of the model's constants are changed but the boundary conditions remain unchanged, and (b) when the same model is subjected to similar impacts, with only one of the impact parameters varied.

4.3.1 Whiplash Simulations of Two Heads

The human A-P model was subjected to forces and moment, applied at the bottom of the neck. The data was based on McKenzie's whiplash data [ ]. The horizontal force had a peak of -100 lbs and a duration of 125 msec. The vertical force was downwards with a peak of -50 lbs, started 12 msec later, and lasted 75 msec. The moment, which started at time zero, was about 120 msec long and had a peak of -100 in-lbs. These boundary conditions seemed to be more realistic, even though they were generated by a mathematical model.

With these inputs, two simulations were conducted. The first one used the same spring constants shown in figure 41, with the exception of KTB, which was changed from 2.5 to 25.0 in-lb/rad. In the second simulation, the input forces were kept unchanged, but KTB was increased from 25 to 100 in-lb/rad, KTS and KTN were doubled. The results of these two simulations are partially given in table 4.

Stiffening of springs had most obvious effects on the angular motion of the brain. While the angular deflection of the brain relative to the skull was reduced from 94 degrees to 64 degrees by stiffening KTB, the angular acceleration almost doubled. The neck-skull angular deflection was reduced from 5.3 to 017 degrees by increasing the stiffnesses of KTN and KTS.

	PEAK RESPONSES	
	Soft Springs	Stiff Springs
Brain Absolute Motion:		
result. vel. (in/sec)	237	245
result. accel. (g's)	17	16
angular vel. (rad/sec)	-23	-36
angular accel. (rad/s/s)	-327	-614
Brain Relative to Skull:		
displacement (inches)	2.17	2.05
angle (degrees)	94	64
Skull Absolute Motion:		
hor. deformation (1000ths in)	0.44	0.46
ver. deformation (1000ths in)	6.5	6.3
resultant vel. (in/sec)	237	241
resultant accel. (g's)	13.2	12.6
angular vel. (rad/sec)	-39.2	-38.6
Neck Motion:		
neck-skull angle (deg)	5.3	0.7
elongation (inches)	0.114	0.109

TABLE 4. COMPARISON OF PEAK RESPONSES OF TWO WHIPLASH SIMULATIONS

This simple comparison illustrates that parametric tests are extremely useful in tuning the model as well as understanding the effects of some of the model's constants on the various responses.

4.3.2 Five Direct Impacts on One Head

Useful information may be obtained by subjecting the model to a series of impacts, in which the model is kept unchanged and only one of the impact parameters is changed.

Five such tests were conducted on the human L-R model. The purpose of this series is to study the effects of the location, relative to the head c.g., of a horizontal impact force, applied to the side of the skull, i.e. to M1. To give the tests some physical reality, the bottom of the neck was assumed to react such that the sum of all forces (and moments) applied to the head are zero. These sums do not include inertial forces, which are unknown. Thus, a force $\vec{P}_1$ is applied to M1 at a vertical distance v_1. The neck is simultaneously subjected to a force equal and opposite to $\vec{P}_1$, i.e., FXO = $-\vec{P}_1$, and to a moment equal and opposite to the couple formed by $\vec{P}_1$ and FXO.

Five such impacts were simulated. In each one, $\vec{P}_1$ was a half-sine pulse with a peak of 100 lbs and a duration of 10 msec. The only distinction between the 5 tests was the height, above M1, of the point of application of P_1. This height, specified by v_1, took on the values 4.0, 3.37, 3.0, 2.0, and 0.35 inches. These values were chosen as follows: for v_1 = 4.0 in, $\vec{P}_1$ passes through the brain c.g.; for v_1 = 3.37 in, the force passes through the skull c.g.; for v_1 = 2.0 in, the impact force is 2 inches below

the brain c.g. level; and for $v_1 = 0.35$, the impact would be at the level of the neck-skull pivot point.

Some of the peak results of these 5 tests are shown in table 5. The general trend is that peak responses drop as the applied force comes closer to the M1-M2 line, and with a dropping of the torque applied to the neck. Since the model has not been completely validated, the actual values obtained in this series of tests can serve only as qualitative indication on how the model would behave under varying conditions. This type of parametric studies can also be used to validate the model, once experimental measurements become available.

P_1 (lbs)	100.	100.	100.	100.	100.
v_1 (inches)	4.0	3.37	3.0	2.0	0.35
T_n (in-lbs)	800.	736.	700.	600.	434.
Brain Absolute:					
resultant vel. (in/sec)	18.0	14.6	12.5	7.6	0.5
resultant accel (g's)	17.0	15.2	14.5	10.1	11.4
angular vel. (rad/sec)	-0.61	-0.50	-0.44	-0.28	0.
angular acc. (rad/s/s)	121	117	91.6	55.6	5.
Brain Rel. to Skull:					
displacement (inches)	0.102	0.085	0.074	0.046	0.002
angle (degrees)	5.1	4.2	3.7	2.3	0.
resultant vel. (in/sec)	23.2	19.1	16.8	10.4	0.9
angular vel. (rad/sec)	18.0	17.4	13.8	8.9	1.4
Skull Absolute:					
hor. deformation (1/1000 in)	3.26	3.30	3.30	3.34	3.36
ver. deformation (1/1000 in)	8.22	5.87	4.67	2.01	0.02
resultant vel. (in/sec)	34.1	28.1	24.5	15.1	0.4
resultant accel. (g's)	32.8	26.4	22.7	18.1	6.3
orientation (deg.)	-5.4	-4.5	-3.9	-2.5	0.
angular vel. (rad/sec)	17.7	17.3	13.5	8.2	2.2
Neck Motion:					
skull-neck angle (deg)	-14.4	-11.9	-10.4	-6.5	0.1
elongation (inches)	0.059	0.100	0.032	0.013	0.001

TABLE 5. COMPARISON OF PEAK RESPONSES OF 5 DIRECT IMPACT TESTS

CHAPTER 5

CONCLUSIONS AND RECOMMENDATIONS

5.1 CONCLUSIONS

The analytical model developed in this study responds to a variety of impact loading conditions and produces a variety of responses. Simpler models do not provide the versatility that this current model does.

Some of the difficulties encountered were the determination of mechanical characteristics of the various elements of the model. Most were overcome by reasonable assumptions based on the available experimental measurements. Results show that the model response shows a qualitative agreement with the measured responses of human and Rhesus heads, but the detailed response of the model cannot be validated unless more measurements, specifically oriented to this end, are made.

The boundary conditions at the neck-torso pivot point seem to play an essential role in a reasonable reproduction of an impact test.

The model was found to be sensitive to its own constants on the one hand, and to the external parameters of the impact on the other. Nonlinear springs are provided for in the model, but sharp breaks in the specified load-deflection curves describing the various springs cause violent oscillations in the model responses.

Tolerance curves were not generated, but possible variables which could be used as criteria for injury are the brain motion (angular and rectilinear), forces at the joints and vertical

and horizontal skull deformations. In fact, such a tolerance curve has been generated for horizontal skull deflection for a 2-mass model. Similar curves could be generated for one variable or a combination of several variables.

Parametric studies are essential in studying the behavior of the model, in generating tolerance curves or simply to tune the model's constants.

In all, this study resulted in a mathematical model which can be used, in more than one way, to study various aspects of the head injury problem.

5.2 RECOMMENDATIONS

Most of the goals set at the beginning of this investigation were accomplished. While a major hurdle has been passed by developing this model, further research must follow it, by using it both as a guide in experimental head injury and as a tool in developing injury criteria. It is suggested that:

1) The motion of the brain be accurately observed during forced and impact vibrations. The state of the art in radio-cinematography is now capable of observing and recording the motion of the brain under these conditions.

2) Torsional forced vibrations tests should be conducted on the head in order to obtain a more reliable experimental basis for determining the brain-skull coupling.

3) Extensive parametric studies of the model should be conducted in order (a) to tune the model, (b) to isolate critical variables that could be used as criteria for injury, and

(c) to generate tolerance curves which could aid in assessing the severity of a given impact.

(4) The specifications of spring constants, which are currently piece-wise linear, may be modified to represent a continuous function, described by polynomials.

(5) Full-size whiplash and direct impact tests must be conducted, and variables be recorded in the light of the detailed responses generated by the model.

LIST OF REFERENCES

1. National Safety Council (1972) Accident Facts, Chicago, Illinois.

2. Caveness, W. F. and Walker, A. E. (1966) Head Injury Conference Proceedings, J. B. Lippincott Co., Philadelphia.

3. Goldsmith, W. (1966) "The Physical Processes Producing Head Injuries," Head Injury Conference Proceedings, Chapter 29, J. B. Lippincott Co., Philadelphia.

4. Patrick, L. M. (1966) "Head Impact Protection," Head Injury Conference Proceedings, Chapter 4, J. B. Lippincott Co., Philadelphia.

5. Kihlberg, J. K. (1966) "Head Injury in Automobile Accidents," Head Injury Conference Proceedings, Chapter 2, J. B. Lippincott Co., Philadelphia.

6. Hirsch, A. E., Ommaya, A. K. and Mahone, H. M. (1970) "Tolerance of Subhuman Primate Brain to Cerebral Concussion," Impact Injury and Crash Protection, Chapter XVI, C. C. Thomas, publisher, Springfield.

7. Alderson, S. W. (1967) "The Development of Anthropomorphic Test Dummies to Match Specific Human Responses to Accelerations and Impacts," Proc. 11th Stapp Car Crash Conference, pp. 62-67, Society of Automotive Engineers.

8. Suh, C. C., Yang, W. J. and McElhaney, J. H. (1972) "Refraction of Liquids in a Spherical Shell Due to Local Radial Loads with Application to Brain Damage," Journal of Biomechanics, vol. 5, pp. 181-189.

9. Kenner, V. H. and Goldsmith, W. (1972) "Dynamic Loading of a Fluid-Filled Spherical Shell," Journal of Biomechanics, vol. 14, pp. 557-568.

10. Anzelius, A. (1943) "The Effect of an Impact on a Spherical Liquid Mass," Acta Path. Microbiol. Scand., suppl. 48, pp. 153-159.

11. Guttinger, W. (1950) "Der Stosseffekt auf eine Flussigkeitskugel als Grundlage einer Physikalischen Theorie der Entstehung von Gehirnverletzungen," Zeit. f. Naturforschung, 5a, 622-628.

12. Engin, A. E. (1969) "The Axisymmetric Response of a Fluid-Filled Spherical Shell to a Local Radial Impulse -- A Model for Head Injury," Journal of Biomechanics, vol. 2, pp. 325-341.

13. Benedict, J. V., Harris, E. H. and von Rosenberg (1970) "An Analytical Investigation of the Cavitation Hypothesis of Brain Damage," Journal of Basic Engineering, vol. 92, pp. 597-603.

14. Lee, Y. C. and Advani, S. H. (1970) "Transient Response of a Sphere to Torsional Loading -- A Head Injury Model," Math. Biosc., vol. 6, pp. 473-486.

15. Hickling R. and Wenner, M. L. (1973) "Mathematical Model of a Head Subjected to an Axisymmetric Impact," Journal of Biomechanics, vol. 6, pp. 115-132.

16. Gurdgian, E. S., Lissner, H. R. and Patrick, M. S. (1962) "Protection of the Head and Neck in Sports," Journal of American Medical Assoc., vol. 182, pp. 509-512.

17. Gurdgian, E. S. et. al., (1961) "Intracranial Pressure and Acceleration Accompanying Head Impacts in Human Cadavers," Surg. Gyn. Obstet., vol. 113, p. 185.

18. Gadd, C. W. (1966) "Use of Weighted-Impulse Criterion for Estimating Injury Hazard," Proc. 10th Stapp Car Crash Conference, paper 660793.

19. Versace, J. (1971) "A Review of the Severity Index," Ford Technical Report, No. S-71-43, Ford Motor Co.

20. Department of Transportation, National Highway Traffic Safety Administration, "Occupant Crash Protection Head Injury Criterion," (49 CFR Part 571) Docket No. 69-7; notice 17.

21. Slattenschek, W. T. and Benedikter, G. (1971) "The Quantification of Internal Head Injury by Means of the Phantom Head and the Impact Assessment Methods," Proc. 15th Stapp Car Crash Conference, paper 710879, Society of Automotive Engineers.

22. Fan, W. R. S. (1971) "Internal Head Injury Assessment," Proc. 15th Stapp Car Crash Conference, paper 710870, Society of Automotive Engineers.

23. Brinn, J. and Staffeld, S. E. "The Effective Displacement Index -- An Analysis Technique for Crash Impacts of Anthropometric Dummies," Proc. 15th Stapp Car Crash Conference, pp. 817-824, Society of Automotive Engineers.

24. Stalnaker, R. L. and McElhaney, J. H. (1970) "Head Injury Tolerance for Linear Impacts by Mechanical Impedance Methods," ASME Winter Annual Meeting, paper 70-BHF-21.

25. McElhaney, J.H. et al. (1973) "Biomechanical Aspects of Head Injury." Proc. Symposium on Human Impact Response (W.F. King and H.J. Mertz, editors). Plenum Press, New York, pp. 85-112.

26. Thomas, L.M. et al. (1968) "Static Deformation and Volume Changes in the Human Skull," Proc. 12th Stapp Car Crash Conference, pp. 260-270, Society of Automotive Engineers.

27. Mertz, H.J. and L.M. Patrick (1971) "Strength and Response of the Human Neck," Proc. 15th Stapp Car Crash Conference, pp. 207-255, Society of Automotive Engineers.

28. Tarrière, C. and C. Sapin (1969) "Biokinetic Study of Head to Thorax Linkage," Proc. 13th Stapp Car Crash Conference, pp. 365-380, Society of Automotive Engineers.

29. McKenzie, J.A. and J.F. Williams (1971) "The Dynamic Behavior of the Head and Cervical Spine During 'Whiplash'," J. Biomechanics, Vol. 4, pp. 477-490.

30. Martinez, J.L. and D.J. Garcia (1968) "A Model for Whiplash," J. Biomechanics, Vol. 1, pp. 23-32.

31. Melvin, J.W. et al. (1972) "Evaluation of Dummy Neck Performance," Proc. Symposium on Human Impact Response, (W.F. King and H.J. Mertz, eds.) Plenum Press, N.Y., pp. 247-261.

32. Estes, M.S. (1969) "Mechanical Response of Brain in Free Standing Compression," Master's Thesis, West Virginia University, Morgantown, W. Va.

33. Melvin, J.W. (1967): Unpublished experimental dynamic tests of in vivo Rhesus brain.

34. Stalnaker, R.L. et al. (1973) "Mechanical Impedance Response of Prototype and Production Antropomorphic Dummy Heads," Presented at 1973 Winter Annual Meeting, paper 73-WA/Bio-13, ASME, Detroit.

35. Snyder, R. G., -Anthropometric Measurements of 200 volunteers - data to be published.

36. Stalnaker, R. L., (1970), "Door Crashworthiness Criteria," Final Report, Contract No. FH-11-7288, Highway Safety Research Institute, University of Michigan, Report No. DOT-HS-800-534.

APPENDIX A

FORMULATION OF THE PROBLEM

The mechanical system used as a model for head injury is described by equations and relationships that express the physical laws of motion as well as the imposed constraints on this motion.

The Lagrange formulation is chosen for two main reasons: (a) The coordinates used to describe the system are more than the necessary minimum, i.e. the number of used coordinates far exceeds the degrees-of-freedom of the system and (b) the systematic approach in differentiating energies to obtain the differential equations of motion. The procedure of formulation consists of the following steps (see figure A.1):

1. Write expression for the system's kinetic energy, dissipation function and potential energy, using any convenient coordinates.
2. Write constraint equations.
3. Obtain the generalized forces of constraint.
4. Obtain the generalized applied forces.
5. Construct the Lagrange equations of motion.

A.1 GENERALIZED COORDINATES

The system's configuration is completely specified if the following coordinates are defined:

x_b, y_b, φ_b : define the position of the brain

x_1, y_1 : define the position of m_1

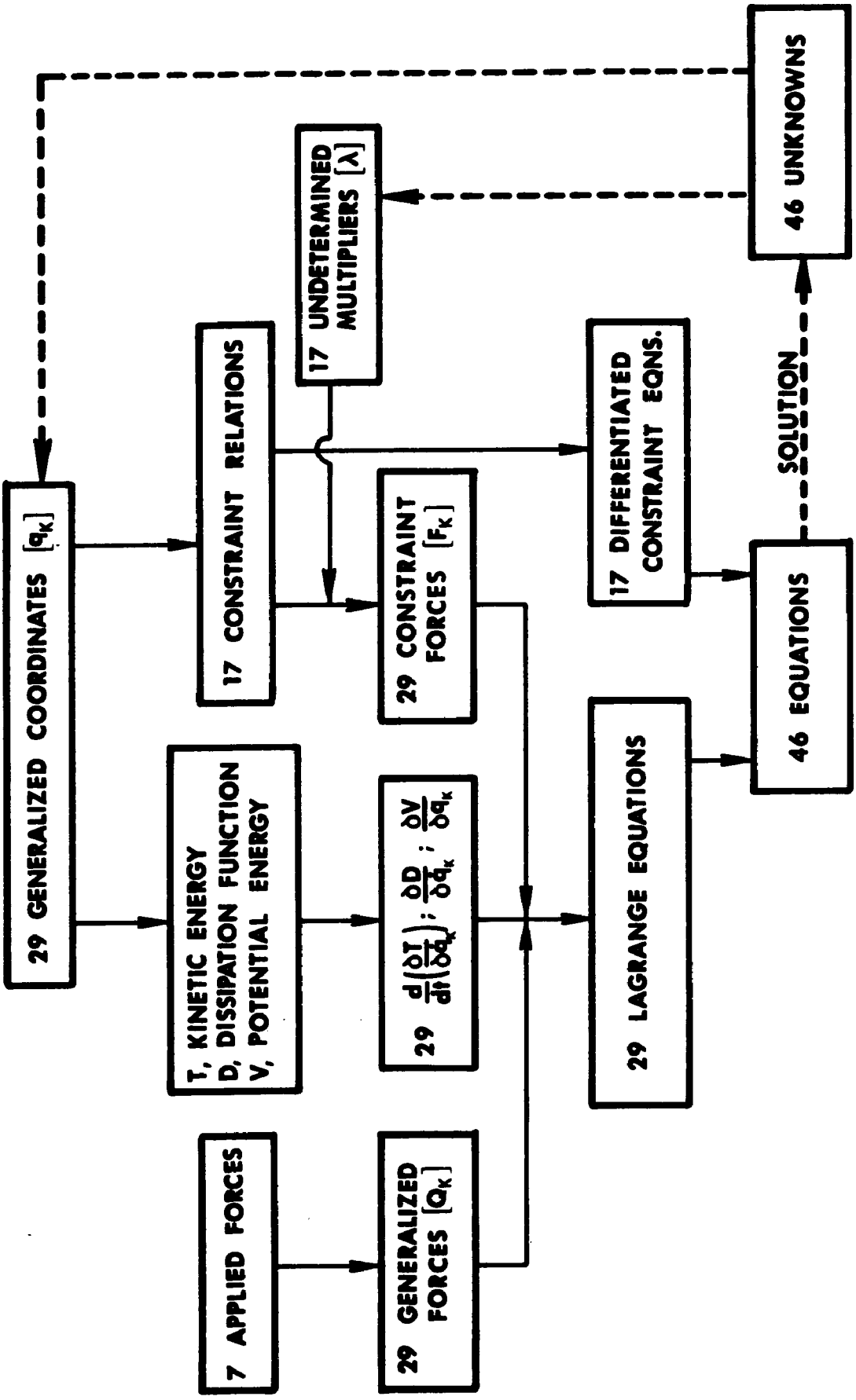


Figure A.1. Formulation Diagram of the Problem

x_2 , y_2 : define the position of m_2

x_3 , y_3 : define the position of m_3

x_n , y_n : define the position of m_n

l_2 : defines the position of the (x_0, y_0) pivot

These 12 coordinates constitute a complete set of independent generalized coordinates and may be termed the "degrees of freedom" of the system.

Other coordinates (12 more to be exact) are used to express the potential energy and the dissipation function of the system. Specifically, there are the lengths (or angles) of the springs in the system.

b_1 , b_2 , b_3 , b_4 : lengths of K1B, K2B, K3B and K4B, respectively

d_1 , d_2 , d_3 , d_4 : lengths of K1S, K2S, K3S and K4S respectively

l_1 : length of K1N. The length of l_2 of K2N is already counted as an independent coordinate.

θ_b : brain-skull angular deflection acting on KTB

θ_s : skull-neck angular deflection acting on KTS

φ_n : neck-torso angular deflection acting on KTN.

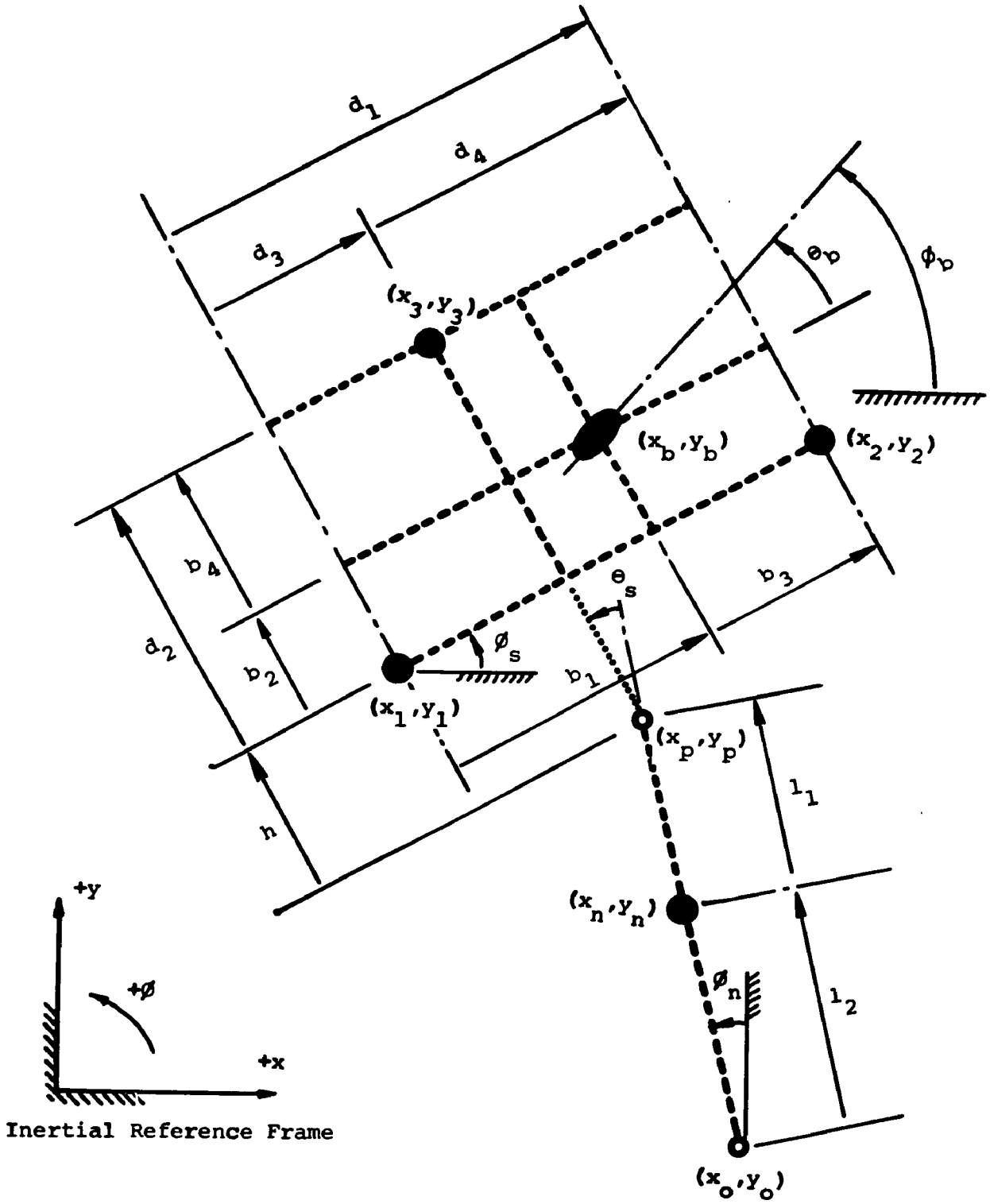


Figure A.2. Coordinates Used in the Formulation

In addition to the above 24 coordinates which enter in the expressions of KE, DF and PE, 5(five) more coordinates are used to express dependency relationships between the various coordinates. These are:

φ_s	: orientation of the skull (m_1- m_2 axis)
x_p , y_p	: position of the skull-neck pivot
x_o , y_o	: position of the neck-torso pivot

Thus, there are 29 generalized coordinates used, of which only 12 are independent, and 17 are "dependent," and related to other coordinates by 17 constraint relations. The coordinates used in this problem are shown in figure A.2.

A.2 KINETIC AND POTENTIAL ENERGIES, DISSIPATION FUNCTION

The general expression of the kinetic energy is:

$$T = \frac{1}{2} \sum_k m_k \dot{q}_k^2$$

where $\dot{q}_k$ is the absolute velocity of coordinate q_k which has an inertia of m_k. Thus,

$$\begin{aligned} T = {} & \tfrac{1}{2} m_1 (\dot{x}_1^2 + \dot{y}_1^2) + \tfrac{1}{2} m_2 (\dot{x}_2^2 + \dot{y}_2^2) \\ & + \tfrac{1}{2} m_3 (\dot{x}_3^2 + \dot{y}_3^2) + \tfrac{1}{2} m_n (\dot{x}_n^2 + \dot{y}_n^2) \\ & + \tfrac{1}{2} m_b (\dot{x}_b^2 + \dot{y}_b^2) + \tfrac{1}{2} I_b \dot{\varphi}_b^2 \end{aligned}$$

The potential energy is the sum of all the energy stored in the springs. Potential energy due to elevation is neglected because of the small distances involved and since the model is primarily designed for impacts involving much higher acceleration levels than the 1-g

earth gravity. The potential energy is formed by adding terms of the form

$$\frac{1}{2} K (q - q_o)^2$$

where K is the spring constant, and $(q - q_0)$ is the amount of spring deflection. Thus

$$\begin{aligned} V = {} & \tfrac{1}{2} K_{1S} (d_1 - d_{10})^2 + \tfrac{1}{2} K_{2S} (d_2 - d_{20})^2 + \tfrac{1}{2} K_{3S} (d_3 - d_{30})^2 \\ & + \tfrac{1}{2} K_{4S} (d_4 - d_{40})^2 + \tfrac{1}{2} K_{1B} (b_1 - b_{10})^2 + \tfrac{1}{2} K_{2B} (b_2 - b_{20})^2 \\ & + \tfrac{1}{2} K_{3B} (b_3 - b_{30})^2 + \tfrac{1}{2} K_{4B} (b_4 - b_{40})^2 \\ & + \tfrac{1}{2} K_{1N} (\ell_1 - \ell_{10})^2 + \tfrac{1}{2} K_{2N} (\ell_2 - \ell_{20})^2 \\ & + \tfrac{1}{2} K_{tB} (\theta_b - \theta_{bo})^2 \\ & + \tfrac{1}{2} K_{ts} (\theta_s - \theta_{so})^2 \\ & + \tfrac{1}{2} K_{tN} (\varphi_n - \varphi_{no})^2 \end{aligned}$$

The dissipation function which enters in the Lagrange equation is a mathematical "potential" of the velocities. A non-conservative system, such as the present model, may be treated mathematically as a conservative one by adding damping forces derived from this "kinetic potential," called the dissipation function. Just as in the potential energy, terms of the form

$$\frac{1}{2} C \dot{q}^2$$

are added for all the dashpots in the system. Therefore, the dissipation function is:

$$\mathcal{D} = \tfrac{1}{2} C_{1S} \dot{d}_1^2 + \tfrac{1}{2} C_{2S} \dot{d}_2^2 + \tfrac{1}{2} C_{3S} \dot{d}_3^2 + \tfrac{1}{2} C_{4S} \dot{d}_4^2$$
$$+ \tfrac{1}{2} C_{1B} \dot{b}_1^2 + \tfrac{1}{2} C_{2B} \dot{b}_2^2 + \tfrac{1}{2} C_{3B} \dot{b}_3^2 + \tfrac{1}{2} C_{4B} \dot{b}_4^2$$
$$+ \tfrac{1}{2} C_{1N} \dot{l}_1^2 + \tfrac{1}{2} C_{2N} \dot{l}_2^2$$
$$+ \tfrac{1}{2} C_{tB} \dot{\theta}_b^2 + \tfrac{1}{2} C_{tS} \dot{\theta}_s^2 + \tfrac{1}{2} C_{tN} \dot{\varphi}_n^2$$

A.3 CONSTRAINT RELATIONS

One way of describing these relations is calling them "vector closure" equations of the coordinates of the system. Essentially, constraint equations are expressions describing the geometrical relationships between the generalized coordinates used to formulate the model. These expressions are then written in the form of an equation

$$f(q_1, q_2, q_3, \cdots, q_{29}) = 0$$

The constraint equations must meet two conditions:

(a) They must be independent.

(b) Their number must be equal to the difference between the total number of coordinates used, and the degrees-of-freedom of the system.

Therefore, 17 independent constraint equations must be written, so that, given 12 independent coordinates, the 17 constraint equations should uniquely define the remaining 17 unknown coordinates.

The constraint equations are:

$$f_1 : \quad x_1 - x_2 + d_1 \cos\varphi_s = 0$$

$$f_2 : \quad y_1 - y_2 + d_1 \sin\varphi_s = 0$$

$$f_3 : \quad x_1 - x_3 + d_3 \cos\varphi_s - d_2 \sin\varphi_s = 0$$

$$f_4 : \quad y_1 - y_3 + d_3 \sin\varphi_s + d_2 \cos\varphi_s = 0$$

$$f_5 : \quad x_p - x_3 - (h + d_2) \sin\varphi_s = 0$$

$$f_6 : \quad y_p - y_3 + (h + d_2) \cos\varphi_s = 0$$

$$f_7 : \quad x_n - x_p - l_1 \sin\varphi_n = 0$$

$$f_8 : \quad y_n - y_p + l_1 \cos\varphi_n = 0$$

$$f_9 : \quad x_o - x_n - l_2 \sin\varphi_n = 0$$

$$f_{10} : \quad y_o - y_n + l_2 \cos\varphi_n = 0$$

$$f_{11} : \quad \theta_b + \varphi_s - \varphi_b = 0$$

$$f_{12} : \quad d_4 + d_3 - d_1 = 0$$

$$f_{13} : \quad x_1 - x_b + b_1 \cos\varphi_s - b_2 \sin\varphi_s = 0$$

$$f_{14} : \quad y_1 - y_b + b_1 \sin\varphi_s + b_2 \cos\varphi_s = 0$$

$$f_{15} : \quad b_3 - b_1 - d_1 = 0$$

$$f_{16} : \quad b_4 + b_2 - d_2 = 0$$

$$f_{17} : \quad \theta_s + \varphi_n - \varphi_s = 0$$

In preparing for the solution, these constraint equations must be differentiated at least once, and depending on the type of input, a second differentiation may be necessary. Therefore, the constraint equations in 1st- and 2nd-order differentiated form are given below.

A.3.1 First-Order-Differentiated Constraints

$$\dot{x}_1 - \dot{x}_2 + \dot{d}_1 \cos\varphi_s - \dot{\varphi}_s d_1 \sin\varphi_s = 0$$

$$\dot{y}_1 - \dot{y}_2 + \dot{d}_1 \sin\varphi_s + \dot{\varphi}_s d_1 \cos\varphi_s = 0$$

$$\dot{x}_1 - \dot{x}_3 + \dot{d}_3 \cos\varphi_s - \dot{\varphi}_s d_3 \sin\varphi_s - \dot{d}_2 \sin\varphi_s - \dot{\varphi}_s d_2 \cos\varphi_s = 0$$

$$\dot{y}_1 - \dot{y}_3 + \dot{d}_3 \sin\varphi_s + \dot{\varphi}_s d_3 \cos\varphi_s + \dot{d}_2 \cos\varphi_s - \dot{\varphi}_s d_2 \sin\varphi_s = 0$$

$$\dot{x}_p - \dot{x}_3 - \dot{d}_2 \sin\varphi_s - \dot{\varphi}_s (h + d_2) \cos\varphi_s = 0$$

$$\dot{y}_p - \dot{y}_3 + \dot{d}_2 \cos\varphi_s - \dot{\varphi}_s (h + d_2) \sin\varphi_s = 0$$

$$\dot{x}_n - \dot{x}_p - \dot{\ell}_1 \sin\varphi_n - \dot{\varphi}_n \ell_1 \cos\varphi_n = 0$$

$$\dot{y}_n - \dot{y}_p + \dot{\ell}_1 \cos\varphi_n - \dot{\varphi}_n \ell_1 \sin\varphi_n = 0$$

$$\dot{x}_o - \dot{x}_n - \dot{\ell}_2 \sin\varphi_n - \dot{\varphi}_n \ell_2 \cos\varphi_n = 0$$

$$\dot{y}_o - \dot{y}_n + \dot{\ell}_2 \cos\varphi_n - \dot{\varphi}_n \ell_2 \sin\varphi_n = 0$$

$$\dot{\theta}_b + \dot{\varphi}_s - \dot{\varphi}_b = 0$$

$$\dot{d}_4 + \dot{d}_3 - \dot{d}_1 = 0$$

$$\dot{x}_1 - \dot{x}_b + \dot{b}_1 \cos\varphi_s - \dot{\varphi}_s b_1 \sin\varphi_s - \dot{b}_2 \sin\varphi_s - \dot{\varphi}_s b_2 \cos\varphi_s = 0$$

$$\dot{y}_1 - \dot{y}_b + \dot{b}_1 \sin\varphi_s + \dot{\varphi}_s b_1 \cos\varphi_s + \dot{b}_2 \cos\varphi_s - \dot{\varphi}_s b_2 \sin\varphi_s = 0$$

$$\dot{b}_3 + \dot{b}_1 - \dot{d}_1 = 0$$

$$\dot{b}_4 + \dot{b}_2 - \dot{d}_2 = 0$$

$$\dot{\theta}_s + \dot{\varphi}_n - \dot{\varphi}_s = 0$$

A.3.2 Second-Order-Differentiated Constraints

Although not all of these equations are pertinent to the solution, they are given here for the sake of completeness.

$$\ddot{x}_1 - \ddot{x}_2 + \ddot{d}_1 \cos\varphi_s - 2\dot{\varphi}_s \dot{d}_1 \sin\varphi_s - \ddot{\varphi}_s d_1 \sin\varphi_s - \dot{\varphi}_s^2 d_1 \cos\varphi_s = 0$$

$$\ddot{y}_1 - \ddot{y}_2 + \ddot{d}_1 \sin\varphi_s + 2\dot{\varphi}_s \dot{d}_1 \cos\varphi_s + \ddot{\varphi}_s d_1 \cos\varphi_s - \dot{\varphi}_s^2 d_1 \sin\varphi_s = 0$$

$$\ddot{x}_1 - \ddot{x}_3 + \ddot{d}_3 \cos\varphi_s - 2\dot{\varphi}_s \dot{d}_3 \sin\varphi_s - \ddot{\varphi}_s d_3 \sin\varphi_s - \dot{\varphi}_s^2 d_3 \cos\varphi_s$$
$$- \ddot{d}_2 \sin\varphi_s - 2\dot{\varphi}_s \dot{d}_2 \cos\varphi_s - \ddot{\varphi}_s d_2 \cos\varphi_s + \dot{\varphi}_s^2 d_2 \sin\varphi_s = 0$$

$$\ddot{y}_1 - \ddot{y}_3 + \ddot{d}_3 \sin\varphi_s + 2\dot{\varphi}_s \dot{d}_3 \cos\varphi_s + \ddot{\varphi}_s d_3 \cos\varphi_s - \dot{\varphi}_s^2 d_3 \sin\varphi_s$$
$$+ \ddot{d}_2 \cos\varphi_s - 2\dot{\varphi}_s \dot{d}_2 \sin\varphi_s - \ddot{\varphi}_s d_2 \sin\varphi_s - \dot{\varphi}_s^2 d_2 \cos\varphi_s = 0$$

$$\ddot{x}_p - \ddot{x}_3 - \ddot{d}_2 \sin\varphi_s - 2\dot{\varphi}_s \dot{d}_2 \cos\varphi_s - \ddot{\varphi}_s (h + d_2)\cos\varphi_s + \dot{\varphi}_s^2 (h + d_2)\sin\varphi_s = 0$$

$$\ddot{y}_p - \ddot{y}_3 + \ddot{d}_2 \cos\varphi_s - 2\dot{\varphi}_s \dot{d}_2 \sin\varphi_s - \ddot{\varphi}_s (h + d_2)\sin\varphi_s - \dot{\varphi}_s^2 (h + d_2)\cos\varphi_s = 0$$

$$\ddot{x}_n - \ddot{x}_p - \ddot{l}_1 \sin\varphi_n - 2\dot{\varphi}_n \dot{l}_1 \cos\varphi_n - \ddot{\varphi}_n l_1 \cos\varphi_n + \dot{\varphi}_n^2 l_1 \sin\varphi_n = 0$$

$$\ddot{y}_n - \ddot{y}_p + \ddot{l}_1 \cos\varphi_n - 2\dot{\varphi}_n \dot{l}_1 \sin\varphi_n - \ddot{\varphi}_n l_1 \sin\varphi_n - \dot{\varphi}_n^2 l_1 \cos\varphi_n = 0$$

$$\ddot{x}_o - \ddot{x}_n - \ddot{l}_2 \sin\varphi_n - 2\dot{\varphi}_n \dot{l}_2 \cos\varphi_n - \ddot{\varphi}_n l_2 \cos\varphi_n + \dot{\varphi}_n^2 l_2 \sin\varphi_n = 0$$

$$\ddot{y}_o - \ddot{y}_n + \ddot{l}_2 \cos\varphi_n - 2\dot{\varphi}_n \dot{l}_2 \sin\varphi_n - \ddot{\varphi}_n l_2 \sin\varphi_n - \dot{\varphi}_n^2 l_2 \cos\varphi_n = 0$$

$$\ddot{\theta}_b + \ddot{\varphi}_s - \ddot{\varphi}_b = 0$$

$$\ddot{d}_4 + \ddot{d}_3 - \ddot{d}_1 = 0$$

$$\ddot{x}_1 - \ddot{x}_b + \ddot{b}_1 \cos\varphi_s - 2\dot{\varphi}_s \dot{b}_1 \sin\varphi_s - \ddot{\varphi}_s b_1 \sin\varphi_s - \dot{\varphi}_s^2 b_1 \cos\varphi_s$$
$$- \ddot{b}_2 \sin\varphi_s - 2\dot{\varphi}_s \dot{b}_2 \cos\varphi_s - \ddot{\varphi}_s b_2 \cos\varphi_s + \dot{\varphi}_s^2 b_1 \sin\varphi_s = 0$$

$$\ddot{y}_1 - \ddot{y}_b + \ddot{b}_1 \sin\varphi_s + 2\dot{\varphi}_s \dot{b}_1 \cos\varphi_s + \ddot{\varphi}_s b_1 \cos\varphi_s - \dot{\varphi}_s^2 b_1 \sin\varphi_s$$
$$+ \ddot{b}_2 \cos\varphi_s - 2\dot{\varphi}_s \dot{b}_2 \sin\varphi_s - \ddot{\varphi}_s b_2 \sin\varphi_s - \dot{\varphi}_s^2 b_2 \cos\varphi_s = 0$$

$$\ddot{b}_3 + \ddot{b}_1 - \ddot{d}_1 = 0$$

$$\ddot{b}_4 + \ddot{b}_2 - \ddot{d}_2 = 0$$

$$\ddot{\theta}_s + \ddot{\varphi}_n - \ddot{\varphi}_s = 0$$

A.4 CONSTRAINT FORCES

The kinematic relationships between the various coordinates of the system, as expressed by the constraint equations, are maintained by forces that are unknown directly, but known by the kinematic effects they produce. These forces can be eliminated if the Lagrange equations are written in terms of 12 independent coordinates. An alternative to the elimination of the extra coordinates, is the use of the Lagrange multipliers idea.

By keeping all 29 coordinates, the constraint forces are included in the Lagrange equations. These forces produce no actual work, and may be computed by virtual work methods. Thus, when one coordinate q_k is allowed a virtual displacement δq_k, there would be a constraint force F_k made up of unknown contributions from all the constraint relations. Each contribution of $f_j(q_1, q_2, q_3, \cdots, q_{29})=0$ has the form

$$\lambda_j \frac{\partial f_j}{\partial q_k} ,$$

The multipliers λ_j are undetermined, and obviously are additional unknowns to be determined along with the other 28 generalized coordinates. The forces F_k are constructed systematically by

$$F(q_k) = F_k = \sum_{j=1}^{17} \lambda_j \frac{\partial f_j}{\partial q_k} , \quad k=1,2,\ldots,29$$

The 29 constraint forces are then:

$$F_1 = F(x_b) = -\lambda_{13}$$

$$F_2 = F(y_b) = -\lambda_{14}$$

$$F_3 = F(\varphi_b) = -\lambda_{11}$$

$$F_4 = F(x_1) = \lambda_1 + \lambda_3 + \lambda_{13}$$
$$F_5 = F(y_1) = \lambda_2 + \lambda_4 + \lambda_{14}$$

$$F_6 = F(x_2) = -\lambda_1$$
$$F_7 = F(y_2) = -\lambda_2$$

$$F_8 = F(x_3) = -\lambda_3 - \lambda_5$$
$$F_9 = F(y_3) = -\lambda_4 - \lambda_6$$

$$F_{10} = F(x_n) = \lambda_7 - \lambda_9$$
$$F_{11} = F(y_n) = \lambda_8 - \lambda_{10}$$

$$F_{12} = F(b_1) = \lambda_{13}\cos\varphi_s + \lambda_{14}\sin\varphi_s + \lambda_{15}$$
$$F_{13} = F(b_2) = -\lambda_{13}\sin\varphi_s + \lambda_{14}\cos\varphi_s + \lambda_{16}$$
$$F_{14} = F(b_3) = \lambda_{15}$$
$$F_{15} = F(b_4) = \lambda_{16}$$

$$F_{16} = F(d_1) = \lambda_1\cos\varphi_s + \lambda_2\sin\varphi_s - \lambda_{12} - \lambda_{15}$$
$$F_{17} = F(d_2) = -\lambda_3\sin\varphi_s + \lambda_4\cos\varphi_s - \lambda_5\sin\varphi_s + \lambda_6\cos\varphi_s - \lambda_{16}$$
$$F_{18} = F(d_3) = \lambda_3\cos\varphi_s + \lambda_4\sin\varphi_s + \lambda_{12}$$
$$F_{19} = F(d_4) = \lambda_{12}$$

$$F_{20} = F(\ell_1) = -\lambda_7\sin\varphi_n + \lambda_8\cos\varphi_n$$
$$F_{21} = F(\ell_2) = -\lambda_9\sin\varphi_n + \lambda_{10}\cos\varphi_n$$
$$F_{22} = F(\theta_b) = \lambda_{11}$$
$$F_{23} = F(\theta_s) = \lambda_{17}$$

$$F_{24} = F(\varphi_n) = -\lambda_7 \ell_1 \cos\varphi_n - \lambda_8 \ell_1 \sin\varphi_n - \lambda_9 \ell_2 \cos\varphi_n - \lambda_{10} \ell_2 \sin\varphi_n + \lambda_{17}$$

$$F_{25} = F(x_p) = \lambda_5 - \lambda_7$$

$$F_{26} = F(y_p) = \lambda_6 - \lambda_8$$

$$F_{27} = F(x_o) = \lambda_9$$

$$F_{28} = F(y_o) = \lambda_{10}$$

(see note below)

$$F_{29} = F(\varphi_s) = -\lambda_1 d_1 \sin\varphi_s + \lambda_2 d_1 \cos\varphi_s - \lambda_3 [d_3 \sin\varphi_s + d_2 \cos\varphi_s] + \lambda_4 [d_3 \cos\varphi_s - d_2 \sin\varphi_s] - \lambda_5 (h + d_2) \cos\varphi_s - \lambda_6 (h + d_2) \sin\varphi_s + \lambda_{11} - \lambda_{13} [b_1 \sin\varphi_s + b_2 \cos\varphi_s] + \lambda_{14} [b_1 \cos\varphi_s - b_2 \sin\varphi_s] - \lambda_{17}$$

A.5 GENERALIZED APPLIED FORCES

External forces and torques applied to the system are shown in figure (A.3):

$\vec{P}_{ox}$ applied at (x_o, y_o), in the (+x)-direction

$\vec{P}_{oy}$ applied at (x_o, y_o), in the (+y)-direction

$\vec{P}_1, \vec{P}_2, \vec{P}_3$ applied to m_1, m_2 and m_3

T_s torque applied to the skull, in the $(+\varphi_s)$-direction

T_N torque applied to the neck, in the $(+\varphi_n)$-direction

The generalized force $Q_k(q_k)$ corresponding to a generalized coordinate q_k, k + 1,2, ..., 29, is given by

$$Q_k = Q(q_k) = \sum_i \vec{P}_i \cdot \frac{\partial \vec{r}_i}{\partial q_k}$$

If $\vec{P}_i$ is a force, then $\vec{r}_i$ is the position vector of its point of application. If $\vec{P}_i$ is a torque along an angle q_k, then Q_k is simply equal to that applied torque.

The applied forces and their points of application's position vectors are:

$$\vec{P}_{ox} = P_{ox}\,\hat{I} \quad ; \quad \vec{P}_{oy} = P_{oy}\,\hat{J}$$
$$\vec{r}_{ox} = x_o\,\hat{I} + y_o\,\hat{J} = \vec{r}_{oy}$$

$$\vec{P}_1 = P_1 \cos(\varphi_s + \alpha_1)\,\hat{I} + P_1 \sin(\varphi_s + \alpha_1)\,\hat{J}$$
$$\vec{r}_1 = (x_1 + u_1 \cos\varphi_s - v_1 \sin\varphi_s)\,\hat{I} + (y_1 + u_1 \sin\varphi_s + v_1 \cos\varphi_s)\,\hat{J}$$

$$\vec{P}_2 = P_2 \cos(\varphi_s + \alpha_2)\,\hat{I} + P_2 \sin(\varphi_s + \alpha_2)\,\hat{J}$$
$$\vec{r}_2 = (x_2 + u_2 \cos\varphi_s - v_2 \sin\varphi_s)\,\hat{I} + (y_2 + u_2 \sin\varphi_s - v_2 \cos\varphi_s)\,\hat{J}$$

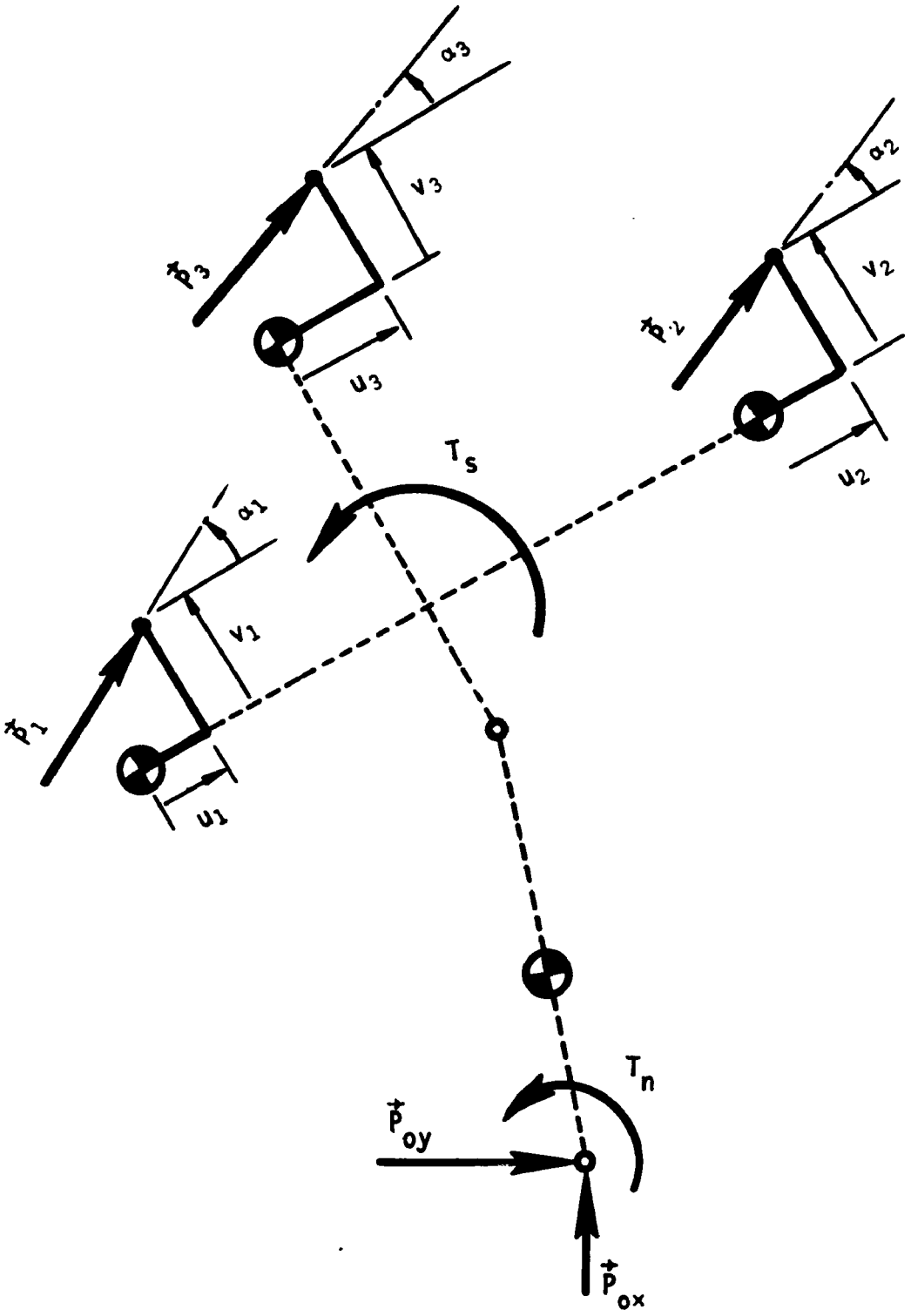


Figure A.3. External Inputs to the Model

$$\vec{P}_3 = P_3 \cos(\varphi_s+\alpha_3)\ \hat{I} + P_3 \sin(\varphi_s+\alpha_3)\ \hat{J}$$
$$\vec{r}_3 = (x_3 + u_3\cos\varphi_s - v_3\sin\varphi_s)\hat{I} + (y_3 + u_3\sin\varphi_s - v_3\cos\varphi_s)\hat{J}$$

Note that the orientation of the forces is fixed relative to the skull, so that their absolute orientations are ($\varphi_s+\alpha$). Also note that the point of applications are at constant distances from the corresponding masses. The 29 generalized forces $Q(q_k)$ are constructed systematically. they are

$$Q_1 = Q(x_b) = 0 \quad ; \qquad Q_{10} = Q(x_n) = 0$$
$$Q_2 = Q(y_b) = 0 \quad ; \qquad Q_{11} = Q(y_n) = 0$$
$$Q_3 = Q(\varphi_b) = 0$$
$$Q_4 = Q(x_1) = P_1 \cos(\varphi_s+\alpha_1)$$
$$Q_5 = Q(y_1) = P_1 \sin(\varphi_s+\alpha_1)$$
$$Q_6 = Q(x_2) = P_2 \cos(\varphi_s+\alpha_2)$$
$$Q_7 = Q(y_2) = P_2 \sin(\varphi_s+\alpha_2)$$
$$Q_8 = Q(x_3) = P_3 \cos(\varphi_s+\alpha_3)$$
$$Q_9 = Q(y_3) = P_3 \sin(\varphi_s+\alpha_3)$$

$$Q_{12} = Q(b_1) = 0$$
$$Q_{13} = Q(b_2) = 0$$
$$Q_{14} = Q(b_3) = 0$$
$$Q_{15} = Q(b_4) = 0$$

$$Q_{16} = Q(d_1) = 0$$
$$Q_{17} = Q(d_2) = 0$$
$$Q_{18} = Q(d_3) = 0$$
$$Q_{19} = Q(d_4) = 0$$
$$Q_{20} = Q(l_1) = 0$$
$$Q_{21} = Q(l_2) = 0$$
$$Q_{22} = Q(\theta_b) = 0$$
$$Q_{23} = Q(\theta_s) = 0$$

$$Q_{24} = Q(\varphi_n) = T_n$$

$$Q_{25} = Q(x_p) = 0$$
$$Q_{26} = Q(y_p) = 0$$
$$Q_{27} = Q(x_o) = P_{ox}$$
$$Q_{28} = Q(y_o) = P_{oy}$$
$$Q_{29} = Q(\varphi_s) = T_s + P_1(u_1 \sin\alpha_1 - v_1 \cos\alpha_1) + P_2(u_2 \sin\alpha_2 - v_2 \cos\alpha_2) + P_3(u_3 \sin\alpha_3 - v_3 \cos\alpha_3)$$

A.6 LAGRANGE EQUATIONS OF MOTION

Finally, the 29 Lagrange equations of motion may be constructed. Each equation corresponds to a generalized coordinate q_k, and has the form

$$\frac{d}{dt}\frac{\partial T}{\partial \dot{q}_K} + \frac{\partial D}{\partial \dot{q}_K} + \frac{\partial V}{\partial q_K} + F(q_K) = Q(q_K) \; ; \quad K = 1, 2, \ldots, 29$$

These equations are:

GEN'D. COORD.	EQUATION OF MOTION
x_b	$m_b \ddot{x}_b - \lambda_{13} = 0$
y_b	$m_b \ddot{y}_b - \lambda_{14} = 0$
φ_b	$I_b \ddot{\varphi}_b - \lambda_{11} = 0$
x_1	$m_1 \ddot{x}_1 + \lambda_1 + \lambda_3 + \lambda_{13} = P_1 \cos(\varphi_s + \alpha_1)$
y_1	$m_1 \ddot{y}_1 + \lambda_2 + \lambda_4 + \lambda_{14} = P_1 \sin(\varphi_s + \alpha_1)$
x_2	$m_2 \ddot{x}_2 - \lambda_1 = P_2 \cos(\varphi_s + \alpha_2)$
y_2	$m_2 \ddot{y}_2 - \lambda_2 = P_2 \sin(\varphi_s + \alpha_2)$
x_3	$m_3 \ddot{x}_3 - \lambda_3 - \lambda_5 = P_3 \cos(\varphi_s + \alpha_3)$
y_3	$m_3 \ddot{y}_3 - \lambda_4 - \lambda_6 = P_3 \sin(\varphi_s + \alpha_3)$
$\ddot{x}_n$	$m_n \ddot{x}_n + \lambda_7 - \lambda_9 = 0$
y_n	$m_n \ddot{y}_n + \lambda_8 - \lambda_{10} = 0$
b_1	$c_{1b} \dot{b}_1 + K_{1b}(b_1 - b_{10}) + \lambda_{13} \cos\varphi_s + \lambda_{14} \sin\varphi_s + \lambda_{15} = 0$
b_2	$c_{2b} \dot{b}_2 + K_{2b}(b_2 - b_{20}) - \lambda_{13} \sin\varphi_s + \lambda_{14} \cos\varphi_s + \lambda_{16} = 0$
b_3	$c_{3b} \dot{b}_3 + K_{3b}(b_3 - b_{30}) + \lambda_{15} = 0$
b_4	$c_{4b} \dot{b}_4 + K_{4b}(b_4 - b_{40}) + \lambda_{16} = 0$
d_1	$c_{1s} \dot{d}_1 + K_{1s}(d_1 - d_{10}) + \lambda_1 \cos\varphi_s + \lambda_2 \sin\varphi_s - \lambda_{12} - \lambda_{15} = 0$
d_2	$c_{2s} \dot{d}_2 + K_{2s}(d_2 - d_{20}) - \lambda_3 \sin\varphi_s + \lambda_4 \cos\varphi_s - \lambda_5 \sin\varphi_s + \lambda_6 \cos\varphi_s - \lambda_{16} = 0$
d_3	$c_{3s} \dot{d}_3 + K_{3s}(d_3 - d_{30}) + \lambda_3 \cos\varphi_s + \lambda_4 \sin\varphi_s + \lambda_{12} = 0$
d_4	$c_{4s} \dot{d}_4 + K_{4s}(d_4 - d_{40}) + \lambda_{12} = 0$

$$\ell_1 \quad C_{1n}\dot{\ell}_1 + K_{1n}(\ell_1-\ell_{10}) - \lambda_7 \sin\varphi_n + \lambda_8 \cos\varphi_n = 0$$

$$\ell_2 \quad C_{2n}\dot{\ell}_2 + K_{2n}(\ell_2-\ell_{20}) - \lambda_9 \sin\varphi_n + \lambda_{10} \cos\varphi_n = 0$$

$$\theta_b \quad C_{tb}\dot{\theta}_b + K_{tb}(\theta_b-\theta_{b0}) + \lambda_{11} = 0$$

$$\theta_s \quad C_{ts}\dot{\theta}_s + K_{ts}(\theta_s-\theta_{s0}) + \lambda_{17} = 0$$

$$\varphi_n \quad C_{tn}\dot{\varphi}_n + K_{tn}(\varphi_n-\varphi_{n0}) - \lambda_7 \ell_1 \cos\varphi_n - \lambda_8 \ell_1 \sin\varphi_n - \lambda_9 \ell_2 \cos\varphi_n - \lambda_{10} \ell_2 \sin\varphi_n + \lambda_{17} = T_n$$

$$x_p \quad \lambda_5 - \lambda_7 = 0$$

$$y_p \quad \lambda_6 - \lambda_8 = 0$$

$$x_o \quad \lambda_9 = P_{ox}$$

$$y_o \quad \lambda_{10} = P_{oy}$$

$$\varphi_s \quad \left.\begin{aligned} &-\lambda_1 d_1 \sin\varphi_s + \lambda_2 d_1 \cos\varphi_s \\ &-\lambda_3[d_3 \sin\varphi_s + d_2 \cos\varphi_s] \\ &+\lambda_4[d_3 \cos\varphi_s - d_2 \sin\varphi_s] \\ &-\lambda_5[(h+d_2)\cos\varphi_s] \\ &-\lambda_6[(h+d_2)\sin\varphi_s] \\ &-\lambda_{13}[b_1 \sin\varphi_s + b_2 \cos\varphi_s] \\ &+\lambda_{14}[b_1 \cos\varphi_s - b_2 \sin\varphi_s] \\ &+\lambda_{11} - \lambda_{17} \end{aligned}\right\} = T_s + \begin{cases} P_1(u_1\cos\alpha_1 - v_1\sin\alpha_1) \\ P_2(u_2\cos\alpha_2 - v_2\sin\alpha_2) \\ P_3(u_3\cos\alpha_3 - v_3\sin\alpha_3) \end{cases}$$

APPENDIX B

SOLUTION OF THE PROBLEM

The equations describing the motion of the proposed model were derived in appendix A. These equations consist of first- and second-order non-linear differential equations and some zero-order ones.

Alternatives considered to solve these equations included analog and digital methods. Digital simulation methods were chosen primarily for their numerical accuracy and their ease in handling model parameters and input/output data. Cost was also a factor effecting this choice. It was felt that with analog simulation, the savings in the intended exercises of the model would not offset the cost and time consumed to set up the analog computer circuit.

The solution was therefore programmed for a digital computer, by writing a package of subroutines in Fortran IV language, and a main program to control the various phases of the simulation using these subroutines. The program was then compiled, tested and run on the MTS computer facilities at the University of Michigan. Although the package uses some MTS-device support subroutines, it can easily be adapted to any IBM-360 system.

B.1 EXAMINATION OF EQUATIONS AND UNKNOWNS

The 29 Lagrange equations may be combined with a compatible form of the 17 constraint equations (differentiated twice) to form a set of 46 simultaneous equations for 46 unknowns. To

prepare these equations for a solution, they may be rearranged so that only terms in the 29 unknown accelerations and 17 undetermined multipliers remain on the left hand sides of the equations, while all other "known" quantities are moved to the right hand sides. This results in a system, represented compactly by

$$[A]\{X\} = \{B\}$$

The column vector $\{X\}$ of unknowns consist of 29 unknown accelerations followed by the 17 multipliers. The right hand side $\{B\}$ is a 46-element vector of the right hand sides of the 46 rearranged equations. The matrix [A] of coefficients is a 46 x 46 symmetric matrix, whose elements are non-linear and must be known before the integration. This matrix is shown symbolically in figure B.1.

Normally, such an algebra-differential set of equations is solved numerically by combining standard methods for solving simultaneous, linear algebraic equations with numerical integration methods. The idea is to divide the desired duration of simulation into small time increments, starting with the instant at which initial conditions are given, then treat the equations as a linear set of equations for each time step. The procedure is to compute all the elements of [A] and $\{B\}$, and invert [A] to obtain:

$$\{X\} = [A]^{-1} \{B\} .$$

Once the elements of $\{X\}$ are obtained, a numerical integration of the accelerations is performed in order to predict

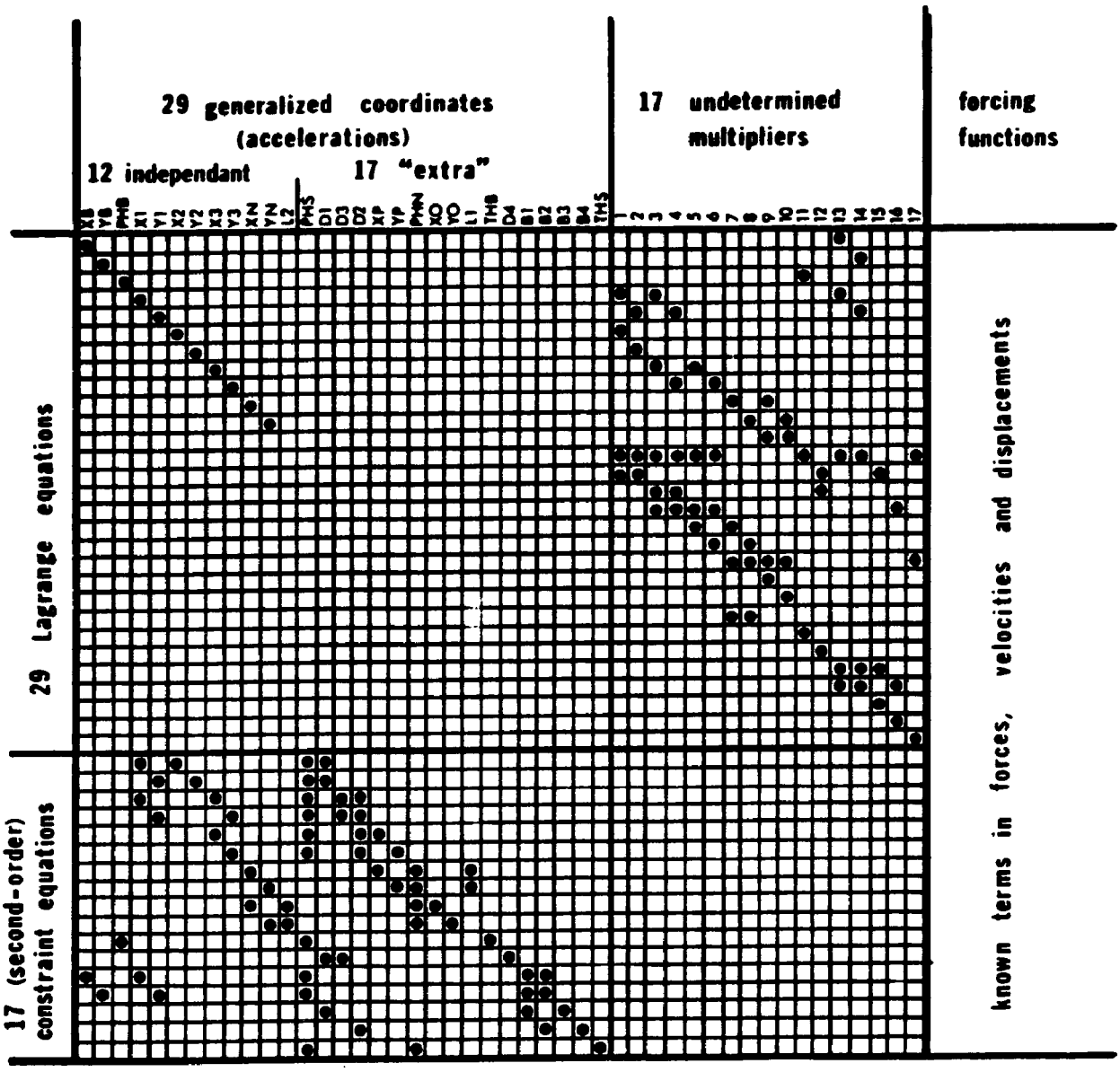


Figure B.1. Symbolic Form of the Matrix of Problem's Equations

velocities and displacements which are taken as initial conditions for the next time step.

This method is straight forward but presents several drawbacks considering the form of [A]. First, the size of the matrix (46 x 46) is large enough to give second thoughts about a straight matrix inversion, regardless of the efficiency of the inversion method and the symmetry of the matrix. Second, this matrix is so sparse (only 145 out of 2116 terms are non-zero), that over 93% of the required computer storage is wasted. The author does not know of an efficient technique or method that has been developed to handle the inversion of large, sparse matrices. Third, the integration of 29 accelerations to obtain 29 displacements is actually a total of 58 distinct integrations, which are usually costly to perform. Finally, not all the 29 accelerations obtained in a complete solution are relevant to head injury prediction or assessment.

An efficient solution must take these points into consideration by minimizing, or avoiding if possible, large matrix inversion, wasted computer storage and unnecessary computations of unknowns which are not relevant to the intended applications of the model. It is believed that such a solution has been obtained. The following sections present this solution.

B.2 PREPARATION AND OUTLINE OF SOLUTION

Depending on the type of input, the solution takes one of two procedures. This is necessary because the model is designed, as mentioned in chapter 2, for two types of inputs:

Type I: 7 input forces

Type II: 5 input forces and 2 motion inputs at (x_o, y_o).

For Type I input, $x_o(t)$, $y_o(t)$ are unknowns and have to be determined in the solution, given the boundary conditions $P_{ox}(t)$ and $P_{oy}(t)$. On the other hand, when $x_o(t)$ and $y_o(t)$ are prescribed (Type II), by giving their accelerations $\ddot{x}_o(t)$ and $\ddot{y}_o(t)$, they are no longer unknowns and the problem of degrees of freedom is reduced by 2; however $P_{ox}(t)$ and $P_{oy}(t)$ are new unknowns added to the problem, since they represent constraint forces necessary to maintain the prescribed motion $x_o(t)$ and $y_o(t)$.

There is no change in the structure of the equations when either type I or II inputs is given; only the method of solution due to the rearrangement of the unknowns changes.

An array of 12 elements, Q(12), is reserved for those coordinates, whose accelerations are necessarily given or computed. With this arrangement, actually 2 arrays must be created for the integration: Q(24) and QD(24). Other coordinates that do not have to be integrated, but may algebraically be computed, are assigned the symbols R(17) and RD(17). The numbers in parenthesis are the number of elements in each array, and the "D" stands for the "dot" in the familiar time-derivative symbolic writing. The correspondence table between these arrays and the symbols used in the equations is given in Table B.1. Note that in this table, the same elements of the array are used for either type of input, with some, given in parenthesis, to indicate that they are used exclusively in the solution for Type II input.

The method of solution avoids matrix inversion altogether, but does make use of numerical integration to obtain velocities and displacements. The solution is performed essentially in the following order:

1. Given initial positions and velocities of 12 independent coordinates, compute the remaining 17 coordinate velocities and displacements using the constraint equations.

2. Obtain the undetermined multipliers by using those Lagrange equations which do not contain accelerations.

3. Solve for the accelerations.

4. Integrate accelerations and velocities to obtain new velocities and displacements.

5. Repeat this procedure for the next time step until the duration of the simulation is spanned.

This gross outline is detailed in section B.5.

B.3 INPUT DATA

The data required by the program is handled by subroutine RPDATA which reads, prints the input cards, performs preliminary computations and generally initializes and prepares the program to start the simulation. Each simulation requires information about the model's constraints, the initial conditions, the loading conditions and certain parameters relevant to the performance, duration and types of desired outputs of the simulation itself.

B.3.1 Constants of the Model

These constants describe the masses, springs, dashpots and the geometrical configuration of the model at rest.

The required masses (and moment of inertia) are M1, M2, M3, MB, IB, and MN. None of these can be zero.

The load-deflection characteristics that must be described are K1S, K2S, K3S, K4S, K1B, K2B, K3B, K4B, K1N, K2N, KTS, KTB and KTN. These spring characteristics can be a single number representing a linear spring rate and may be zero except K2N which cannot be zero when type II input is given. Furthermore, those springs (translational and torsional) associated with the skull and the neck may be given non-linear characteristics by describing piece-wise linear (not more than 6 pieces per curve) load-deflection curves. Subroutine STORK prepares the input for later use in function FORK, which obtains the spring force for a given deflection.

It was felt that a better approximation of the real behavior of the neck and skull may be obtained by the non-linear modeling of their load-deflection characteristics. The brain springs, however, are kept strictly linear, primarily because of the lack of experimental data describing its "load-deflection" properties as the model requires.

The viscous damping of the model, represented by dashpots, must also be given as input. Those are C1S, C2S, C3S, C4S, C1B, C2B, C3B, C4B, C1N, C2N, CTS, CTB and CTN. Since these constants have not been directly measured, it was felt that linear damping is adequate enough to add the damping effects observed in dynamic measurements of the impacted heads.

The head model is not complete without describing its geometric configuration at rest. Since there are 29 coordinates

whose positions and velocities must be initially specified, it is difficult and impractical to input all of them. One reason for the difficulty is that not all 29 coordinates are independent, thus the freedom in the specification of initial conditons is truly limited to 12 coordinates. Furthermore, many of these 12 independent coordinates would have the same initial values for each intended simulation; thus, only a limited number of them are actually inputted; the remaining ones are either assigned commonly used values or computed via the constraint relations.

Therefore, for practical reasons, the distances that must be given as input are:

L1, L2 : lengths of sections of neck above and below its c.m., respectively.

HC : the distance between the skull c.m. and the neck-skull pivot.

D1, D2 : horizontal and vertical "diameters" of the skull, adjusted as to conserve the moment of inertia of the skull.

BSX,BSY : horizontal and vertical distances between the skull c.m. and the brain c.m.

B.3.2 Initial Conditions

Theoretically, 29 generalized velocities and 29 generalized coordinates must be initially specified. These initial conditions must also be consistent with the constraint relations. The possibility of error, along with the impracticality of large input, makes it necessary to limit the initial conditions to the following:

XO, YO: absolute position of bottom of neck.

PHS: absolute orientation of skull

PHN: absolute orientation of neck

The initial velocities XOD, YOD, PHSD, PHND of these coordinates may also be given. The rest of the "work" is done by subroutine DPREP which either assigns or computes the remaining initial positions and velocities, consistant with the configuration of the model and the constraint equations.

B.3.3 Loading Conditions

It was mentioned in appendix A that 7 forcing functions may be applied (or specified) to the model. These are PXO, PYO, P1, P2, P3, TS and TN. Associated with each "force" is a switch J which must be given one of three values: 0, 1 or 2. The first value (J=0) indicates that throughout the simulation, the corresponding force (or acceleration) is zero. The second value (J=1) indicates that the function is sinusoidal. The third (J=2) is used to indicate that the function is described in a tabular form, in which case, up to 100 points must be described.

The type of input at (XO,YO) is indicated by a switch, TYPE, which can equal either 1 or 2. When TYPE=1, PXO and PYO are treated as forces, and when TYPE=2, they are taken as accelerations of XO and YO respectively.

B.3.4 Simulation Parameters

These parameters consist of information required by the integration subroutine DHPCG and by the various output subroutines. The following is a partial list of these parameters:

FINTIM : duration of the simulation

DELTIM : maximum initial time increment

DELOUT : time increment for printing the results

ABSERR : a criterion of accuracy for the integration subroutine.

PLT : 6 switches to turn on or off six plotting routines

PRT : 6 ON-OFF switches for 6 printing routines.

The above presentation of the input data is not a complete one. It is the intention here to present an idea about the capabilities of the model and its flexibility in handling various simulation requirements, rather than giving a "user's manual" for the program.

B.4 PHASES OF THE SIMULATION

The first phase of the simulation is the initialization of all problem variables. This is done by subroutines DPREP and IPREP. The first one computes initial values from input data, as well as those constants and factors that will be used repeatedly during the simulation; the second one prepares the program for integration.

The second phase of the simulation is the actual integration, performed by a standard subroutine DHPCG. Once this phase has begun, DHPCG controls the simulation until the problem duration has reached its end, or an error condition is encountered. This integration subroutine is one of the IBM-360/SSP (Scientific Subroutines Package) and is well documented there; hence, it shall not be described here. However, it should be noted that DHPCG has

given satisfactory, and in most instances, excellent results in other simulations developed by the author and by many of his associates.

The integration subroutine DHPCG requires two user-written subroutines. The first one, FCT, is to compute accelerations and velocities, given velocities and displacements by using the equations of motion; the second subroutine, DHPOUT, to record the output results once an integration step is successful. At each time increment which is controlled by DHPCG, FCT is called to perform its computation of the higher derivatives. FCT returns to DHPCG with new computed derivatives, which attempts to predict numerical integrals. This is usually repeated until a desired accuracy is reached, at which time DHPOUT is called to record the results. The same procedure is repeated for each time increment until all of the duration of the simulation is spanned.

The third and final phase of the simulation is printing out the results. A variety of printouts and plots may be produced by reading the raw results (recorded by DHPOUT) and presenting them in the desired formats.

The three phases are diagrammed in figure B.2. Clearly, the second phase of the simulation is the most important one.

At the heart of this phase, is subroutine FCT, which controls the sequence of solution. Actually, subroutine FCT itself is a short 20-card program and serves as the entry/exit point of a package of subroutines which are separated to perform specific "blocks" of computations.

The next section describes the details of the solution and gives the names of the subroutines which perform the corresponding "blocks" of computations. Note that the sequence in computation must be

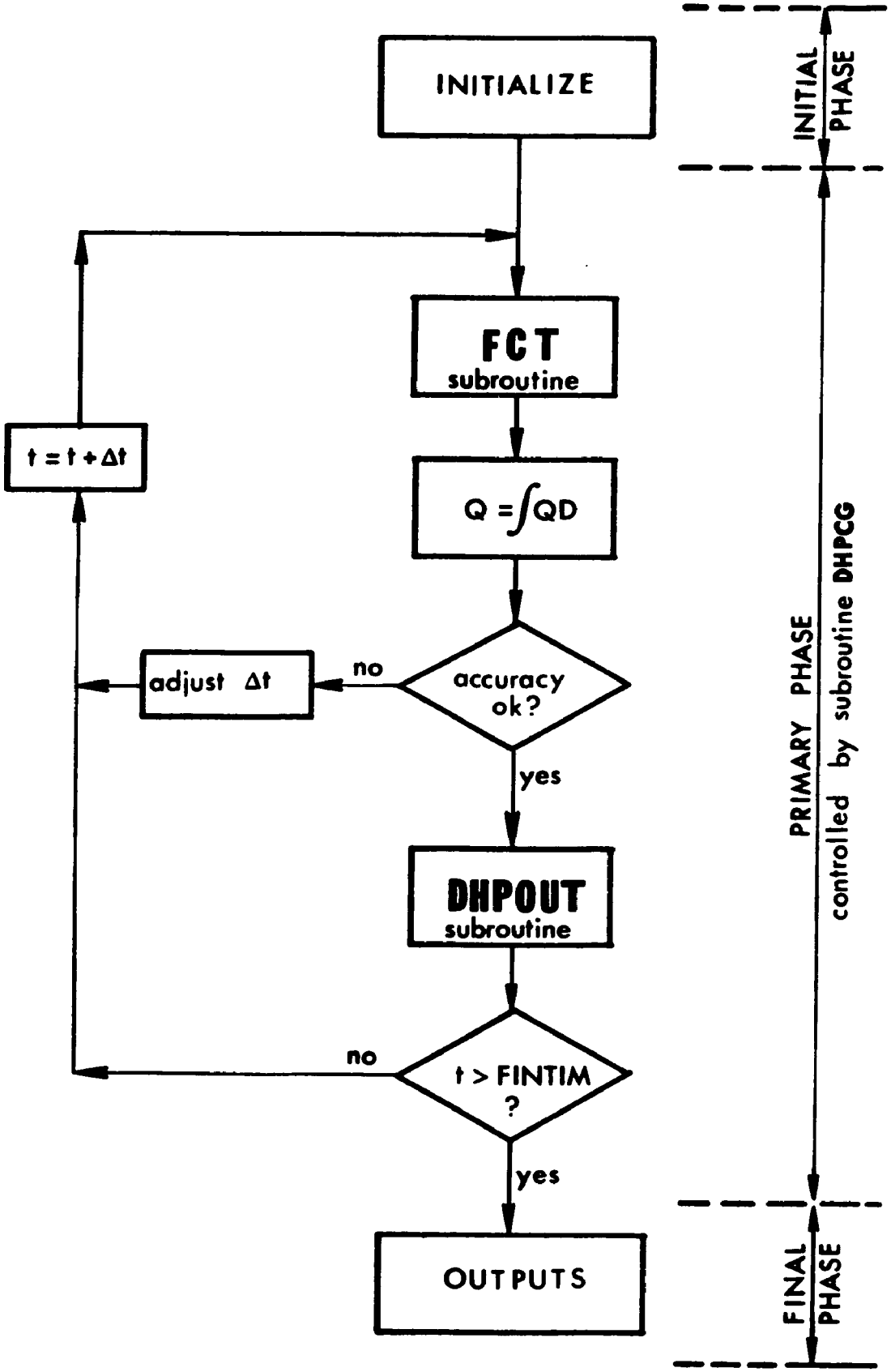


Figure B.2. Phases of the Simulation

followed in the given order, since the next step of the solution uses variables and unknowns computed in previous steps.

B.5 SOLUTION OF THE EQUATIONS

The "blocks" of computations in the solutions are presented in this section under the name of the subroutine which performs them.

B.5.1 Subroutine EXCITE

At the current instant of time, the seven input forces (or accelerations) are computed in this subroutine. The returned values are FXO(t), FYO(t), P1(t), P2(t), P3(t), TS(t) and TN(t). Each one is generated by subroutine FGEN which uses data prepared in the initialization phase.

B.5.2 Subroutine RELQ

This subroutine computes all the "relative" coordinates and their derivatives, using the constraint equations. Most of the computations are identical for both type I and type II inputs. The 12 independent coordinates (and their velocities) which are given are:

type I : x_b y_b ϕ_b x_1 y_1 x_2 y_2 x_3 y_3 x_n y_n ℓ_2

type II: x_b y_b ϕ_b x_1 y_1 x_2 y_2 x_3 y_3 x_o y_o ℓ_2

Then,

$$\varphi_s = \tan^{-1}\left[(y_2-y_1)/(x_2-x_1)\right]$$

$$d_1 = (x_2-x_1)\cos\varphi_s + (y_2-y_1)\sin\varphi_s$$

$$d_3 = (x_3-x_1)\cos\varphi_s + (y_3-y_1)\sin\varphi_s$$

$$d_2 = -(x_3-x_1)\sin\varphi_s + (y_3-y_1)\cos\varphi_s$$

$$x_p = x_3 - (h+d_2)\sin\varphi_s$$

$$y_p = y_3 - (h+d_2)\cos\varphi_s$$

Now, for type I (x_n, y_n) are given, thus

$$\varphi_n = \tan^{-1}[(x_n - x_p)/(y_p - y_n)]$$
$$x_o = x_n + [l_2] \sin\varphi_n$$
$$y_o = y_n - [l_2] \cos\varphi_n$$

For type II input, (x_0, y_0) are given:

$$\varphi_n = \tan^{-1}[(x_o - x_p)/(y_p - y_o)]$$
$$x_n = x_o + [-l_2] \sin\varphi_n$$
$$y_n = y_o - [-l_2] \cos\varphi_n$$

Note that the expressions of ϕ_n, x_n, y_n have the same form regardless of the known quantities. This is helpful in the actual programming of these expressions. The remaining coordinates are:

$$l_1 = (x_n - x_p)\sin\varphi_n + (y_p - y_n)\cos\varphi_n$$
$$\theta_b = \varphi_b - \varphi_s$$
$$d_4 = d_1 - d_3$$
$$b_1 = (x_b - x_1)\cos\varphi_s + (y_b - y_1)\sin\varphi_s$$
$$b_2 = -(x_b - x_1)\sin\varphi_s + (y_b - y_1)\cos\varphi_s$$
$$b_3 = d_1 - b_1$$
$$b_4 = d_2 - b_2$$
$$\theta_s = \varphi_s - \varphi_n$$

The constraint equations are used now in their 1st order differentiated forms to obtain the velocities of the relative coordinates. Thus:

$$\dot{\varphi}_s = (1/d_1)\left[-(\dot{x}_2 - \dot{x}_1)\sin\varphi_s + (\dot{y}_2 - \dot{y}_1)\cos\varphi_s\right]$$
$$\dot{d}_1 = (\dot{x}_2 - \dot{x}_1)\cos\varphi_s + (\dot{y}_2 - \dot{y}_1)\sin\varphi_s$$
$$\dot{d}_3 = (\dot{y}_3 - \dot{y}_1)\sin\varphi_s + (\dot{x}_3 - \dot{x}_1)\cos\varphi_s + \dot{\varphi}_s d_2$$
$$\dot{d}_2 = (\dot{y}_3 - \dot{y}_1)\cos\varphi_s - (\dot{x}_3 - \dot{x}_1)\sin\varphi_s - \dot{\varphi}_s d_3$$
$$\dot{x}_p = \dot{x}_3 + \dot{d}_2 \sin\varphi_s + \dot{\varphi}_s(h + d_2)\cos\varphi_s$$
$$\dot{y}_p = \dot{y}_3 - \dot{d}_2 \cos\varphi_s + \dot{\varphi}_s(h + d_2)\sin\varphi_s$$

At this point the program switches to the appropriate equations, given $(\dot{x}_n, \dot{y}_n)$ for type I or $(\dot{x}_0, \dot{y}_0)$ for type II. Thus for type I:

$$\dot{\varphi}_n = (1/\ell_1)[(\dot{x}_n - \dot{x}_p)\cos\varphi_n + (\dot{y}_n - \dot{y}_p)\sin\varphi_n]$$

$$\dot{x}_0 = \dot{x}_n + \dot{\ell}_2 \sin\varphi_n + \dot{\varphi}_n \ell_2 \cos\varphi_n$$

$$\dot{y}_0 = \dot{y}_n - \dot{\ell}_2 \cos\varphi_n + \dot{\varphi}_n \ell_2 \sin\varphi_n$$

In the expressions of $\dot{x}_0$ and $\dot{y}_0$, the velocity $\dot{\ell}_2$ is not obtained by integration, but rather computed by

$$\dot{\ell}_2 = (1/c_{2n})[-K_{2n}(\ell_2 - \ell_{20}) + P_{x0}\sin\varphi_n - P_{y0}\cos\varphi_n]$$

For type II, $\dot{\ell}_2$ is obtained directly by integration of $\ddot{\ell}_2$. For this type of input

$$\dot{\varphi}_n = [1/(\ell_1 + \ell_2)][(\dot{x}_0 - \dot{x}_p)\cos\varphi_n + (\dot{y}_0 - \dot{y}_p)\sin\varphi_n]$$

$$\dot{x}_n = \dot{x}_0 + [-\dot{\ell}_2]\sin\varphi_n + [-\dot{\varphi}_n \ell_2]\cos\varphi_n$$

$$\dot{y}_n = \dot{y}_0 - [-\dot{\ell}_2]\cos\varphi_n + [-\dot{\varphi}_n \ell_2]\sin\varphi_n$$

The remaining derivatives for both types I and II are:

$$\dot{\ell}_1 = (\dot{x}_n - \dot{x}_p)\sin\varphi_n - (\dot{y}_n - \dot{y}_p)\cos\varphi_n$$

$$\dot{\theta}_b = \dot{\varphi}_b - \dot{\varphi}_s$$

$$\dot{d}_4 = \dot{d}_1 - \dot{d}_3$$

$$\dot{b}_1 = (\dot{y}_b - \dot{y}_1)\sin\varphi_s + (\dot{x}_b - \dot{x}_1)\cos\varphi_s + \dot{\varphi}_s b_2$$

$$\dot{b}_2 = (\dot{y}_b - \dot{y}_1)\cos\varphi_s - (\dot{x}_b - \dot{x}_1)\sin\varphi_s - \dot{\varphi}_s b_1$$

$$\dot{b}_3 = \dot{d}_1 - \dot{b}_1$$

$$\dot{b}_4 = \dot{d}_2 - \dot{b}_2$$

$$\dot{\theta}_s = \dot{\varphi}_s - \dot{\varphi}_n$$

Now it is possible to comput the spring and damping forces of the 13 Kelvin elements of the model.

B.5.4 Subroutine KELVIN

The forces acting through one Kelvin element has the form

$$c\dot{\ell} + K(\ell - \ell_o)$$

where C and K are the dashpot and spring constants, respectively. Since many of the springs of the model have non linear load-deflection characteristics, a subroutine FORK is written to extract the spring force for a given deflection. For convenience, each Kelvin force is given a symbol, and is computed at this stage for later use in the solution. The 13 Kelvin forces are:

$$PTS = C_{ts}\dot{\theta}_s + K_{ts}(\theta_s - \theta_{so})$$
$$P1S = C_{1s}\dot{d}_1 + K_{1s}(d_1 - d_{1o})$$
$$P2S = C_{2s}\dot{d}_2 + K_{2s}(d_2 - d_{2o})$$
$$P3S = C_{3s}\dot{d}_3 + K_{3s}(d_3 - d_{3o})$$
$$P4S = C_{4s}\dot{d}_4 + K_{4s}(d_4 - d_{4o})$$
$$PTB = C_{tb}\dot{\theta}_b + K_{tb}(\theta_b - \theta_{bo})$$
$$P1B = C_{1b}\dot{b}_1 + K_{1b}(b_1 - b_{1o})$$
$$P2B = C_{2b}\dot{b}_2 + K_{2b}(b_2 - b_{2o})$$
$$P3B = C_{3b}\dot{b}_3 + K_{3b}(b_3 - b_{3o})$$
$$P4B = C_{4b}\dot{b}_4 + K_{4b}(b_4 - b_{4o})$$
$$PTN = C_{tn}\dot{\varphi}_n + K_{tn}(\varphi_n - \varphi_{no})$$
$$P1N = C_{1n}\dot{\ell}_1 + K_{1n}(\ell_1 - \ell_{1o})$$
$$P2N = C_{2n}\dot{\ell}_2 + K_{2n}(\ell_2 - \ell_{2o})$$

At this point of the solution, there are radical differences between the procedure to treat a force-input model (type I), and that to treat an acceleration-input (type II). Thus, it was more practical to write two separate subroutines to perform the remaining steps of the solution. However, these two subroutines, SOLVE1 and

SOLVE2, use the same routines EXCITE, RELQ and KELVIN, which have built-in switches for the two types of inputs.

B.5.5 Subroutine SOLVE1

The input is a force PX0, PY0 at (x_0, y_0), along with 5 other inputs at m_1, m_2, m_3, ϕ_s, ϕ_n. First, solve for λ_{11} through λ_{17}

$$\lambda_{17} = -PTS$$
$$\lambda_{16} = -P4B$$
$$\lambda_{15} = -P3B$$
$$\lambda_{13} = (P3B - P1B)\cos\varphi_s - (P4B - P2B)\sin\varphi_s$$
$$\lambda_{14} = (P3B - P1B)\sin\varphi_s + (P4B - P2B)\cos\varphi_s$$
$$\lambda_{12} = -P4S$$
$$\lambda_{11} = -PTB.$$

Now

$$\left.\begin{aligned}\lambda_9 &= PX0\\ \lambda_{10} &= PY0\end{aligned}\right\} \text{ input, type I.}$$

To solve for λ_7 and λ_8, let

$$f_1 = -P1N$$
$$f_2 = TN - PTN + PTS + (PX0)\ell_2\cos\varphi_n + (PY0)\ell_2\sin\varphi_n$$

then,

$$\lambda_7 = -f_1\sin\varphi_n - (f_2/\ell_1)\cos\varphi_n$$
$$\lambda_8 = f_1\cos\varphi_n - (f_2/\ell_1)\sin\varphi_n$$

Now that λ_7 and λ_8 are computed,

$$\lambda_5 = \lambda_7$$
$$\lambda_6 = \lambda_8$$

To solve for λ_3 and λ_4, move all known terms in the Lagrange equations for d_2 and d_3 to the R. H. S., i.e.

$$-\lambda_3\sin\varphi_s + \lambda_4\cos\varphi_s = \lambda_5\sin\varphi_s - \lambda_6\cos\varphi_s - P4B - P2S \equiv f_1$$
$$\lambda_3\cos\varphi_s + \lambda_4\sin\varphi_s = P4S - P3S \equiv f_2$$

thus

$$\lambda_3 = -f_1 \sin\varphi_s + f_2 \cos\varphi_s$$
$$\lambda_4 = f_1 \cos\varphi_s + f_2 \sin\varphi_s$$

Finally, the Lagrange equations for d_1 and ϕ_s are used to compute λ_1 and λ_2:

$$\lambda_1 \cos\varphi_s + \lambda_2 \sin\varphi_s = f_1$$
$$-\lambda_1 d_1 \sin\varphi_s + \lambda_2 d_1 \cos\varphi_s = f_2$$

where

$$f_1 \equiv -P4S - P3B - P1S$$
$$f_2 \equiv \lambda_3 [d_3 \sin\varphi_s + d_2 \cos\varphi_s] - \lambda_4 [d_3 \cos\varphi_s - d_2 \sin\varphi_s]$$
$$+ \lambda_5 [(h+d_2)\cos\varphi_s] + \lambda_6 [(h+d_2)\sin\varphi_s]$$
$$+ \lambda_{13} [b_1 \sin\varphi_s + b_2 \cos\varphi_s] - \lambda_{14} [b_1 \cos\varphi_s - b_2 \sin\varphi_s]$$
$$+ TS + PUVA + PTB - PTS$$

Here, f_1 and f_2 contain known terms only, and PUVA is the only newly introduced symbol:

$$PUVA = P_1 (u_1 \sin\alpha_1 - v_1 \cos\alpha_1)$$
$$+ P_2 (u_2 \sin\alpha_2 - v_2 \cos\alpha_2)$$
$$+ P_3 (u_3 \sin\alpha_3 - v_3 \cos\alpha_3)$$

Therefore

$$\lambda_1 = f_1 \cos\varphi_s - (f_2/d_1) \sin\varphi_s$$
$$\lambda_2 = f_1 \sin\varphi_s + (f_2/d_1) \cos\varphi_s$$

The next step, after computing all the undetermined multipliers, is to use them to solve for the accelerations. In order to reduce the writing, let

$$PX1 = P1 \cos(\varphi_s + \alpha_1)$$
$$PY1 = P1 \sin(\varphi_s + \alpha_1)$$

and let PX2, PY2, PX3, PY3 have similar connotations, then,

$$\ddot{x}_b = (1/m_b)\ \lambda_{13}$$
$$\ddot{y}_b = (1/m_b)\ \lambda_{14}$$
$$\ddot{\varphi}_b = (1/I_b)\ \lambda_{11}$$
$$\ddot{x}_1 = (1/m_1)\ [PX1 - \lambda_1 - \lambda_3 - \lambda_{13}]$$
$$\ddot{y}_1 = (1/m_1)\ [PY1 - \lambda_2 - \lambda_4 - \lambda_{14}]$$
$$\ddot{x}_2 = (1/m_2)\ [PX2 + \lambda_1]$$
$$\ddot{y}_2 = (1/m_2)\ [PY2 + \lambda_2]$$
$$\ddot{x}_3 = (1/m_3)\ [PX3 + \lambda_3 + \lambda_5]$$
$$\ddot{y}_3 = (1/m_3)\ [PY3 + \lambda_4 + \lambda_6]$$
$$\ddot{x}_n = (1/m_n)\ [\lambda_9 - \lambda_7]$$
$$\ddot{y}_n = (1/m_n)\ [\lambda_{10} - \lambda_8]$$

These accelerations are then returned to DHPCG as QD(13), QD(14), ..., QD(23), to be integrated into velocities. The first 12 elements of the array QD are the corresponding velocities and are simply obtained from the last 12 elements of the Q-array. (See table B.1 for correspondence.)

Note that not all the 29 accelerations are computed since they are not absolutely necessary to obtain the primary coordinates. So even with an "incomplete" solution, all relevant accelerations, velocities, displacements, and forces are obtained. There is room however for computing more accelerations if needed. Such accelerations, e.g. $\ddot{\phi}_s$, can be directly obtained from the constraint relations, during the output phase of the simulation.

B.5.6 Subroutine SOLVE2

The program switches to this subroutine if TYPE = 2, i.e. if PX0 = $\ddot{x}_0(t)$. The solution with this type of input requires more

OD(1) =XBD	O(1) =XB	R,RD(1) =PHS,PHSD
OD(2) =YBD	O(2) =YB	R,RD(2) =D1 ,D1D
OD(3) =PHBD	O(3) =PHB	R,RD(3) =D3 ,D3D
OD(4) =X1D	O(4) =X1	R,RD(4) =D2 ,D2D
OD(5) =Y1D	O(5) =Y1	R,RD(5) =XP ,XPD
OD(6) =X2D	O(6) =X2	R,RD(6) =YP ,YPD
OD(7) =Y2D	O(7) =Y2	R,RD(7) =PHN,PHND
OD(8) =X3D	O(8) =X3	R,RD(8) =XO ,XOD
OD(9) =Y3D	O(9) =Y3	(XN ,XND)
OD(10)=XND(XOD)	O(10)=XN(XO)	R,RD(9) =YO ,YOD
OD(11)=YND(YOD)	O(11)=YN(YO)	(YN ,YND)
OD(12)=L2D	O(12)=L2	R,RD(10)=L1 ,L1D
		R,RD(11)=THB,THBD
OD(13)=XBDD	O(13)=XBD	R,RD(12)=D4 ,D4D
OD(14)=YBDD	O(14)=YBD	R,RD(13)=B1 ,B1D
OD(15)=PHBDD	O(15)=PHBD	R,RD(14)=B2 ,B2D
OD(16)=X1DD	O(16)=X1D	R,RD(15)=B3 ,B3D
OD(17)=Y1DD	O(17)=Y1D	R,RD(16)=B4 ,B4D
OD(18)=X2DD	O(18)=X2D	R,RD(17)=THS,THSD
OD(19)=Y2DD	O(19)=Y2D	
OD(20)=X3DD	O(20)=X3D	
OD(21)=Y3DD	O(21)=Y3D	
OD(22)=XNDD(XODD)	O(22)=XND(XOD)	
OD(23)=YNDD(YODD)	O(23)=YND(YOD)	
OD(24)=....(L2DD)	O(24)=...(L2D)	

Table B.1. Correspondance between program arrays and problem coordinates

lengthy procedure since it is necessary to solve for some accelerations which are not relevant to the model head injury prediction, but necessary to uncouple the equations of the problem.

Briefly, the procedure is to compute all the unknowns from the equations which have little or no coupling with the rest of the system of equations. Then, select those unknowns which are indispensable to the solution, then rearrange the corresponding equations so that the matrix of coefficients is almost triangular. Next, "triangulize" this matrix so that the half below the principal diagonal contains only zeros. The final step is solving for the unknowns by simple back-substitution.

After examining the equations, it becomes clear that λ_{11}, λ_{12}, ...λ_{17} may be obtained immediately in the same manner detailed in the previous section. Thus, up to this point in the solution, EXCITE, RELQ, KELVIN and solving for $\lambda(11,...,17)$ is performed and the results may be considered known quantities.

Next it becomes clear that the equations involving the following unknowns are so coupled that they must be solved by some matrix method:

$$\ddot{x}_p \quad \ddot{y}_p \quad \ddot{d}_2 \quad \ddot{\varphi}_s \quad \ddot{x}_1 \quad \ddot{y}_1 \quad \ddot{x}_2 \quad \ddot{y}_2 \quad \ddot{x}_3 \quad \ddot{y}_3$$
$$\lambda_1 \quad \lambda_2 \quad \lambda_3 \quad \lambda_4 \quad \lambda_5 \quad \lambda_6$$
$$\ddot{x}_n \quad \ddot{y}_n \quad \ddot{l}_2 \quad \ddot{\varphi}_n$$
$$\lambda_7 \quad \lambda_8 \quad \lambda_9 \quad \lambda_{10}$$

The 24 equations involving these coordinates are extracted from matrix [A] given in section B.1, and are written so that the vector of unknowns is in the above given sequence. Normally, this

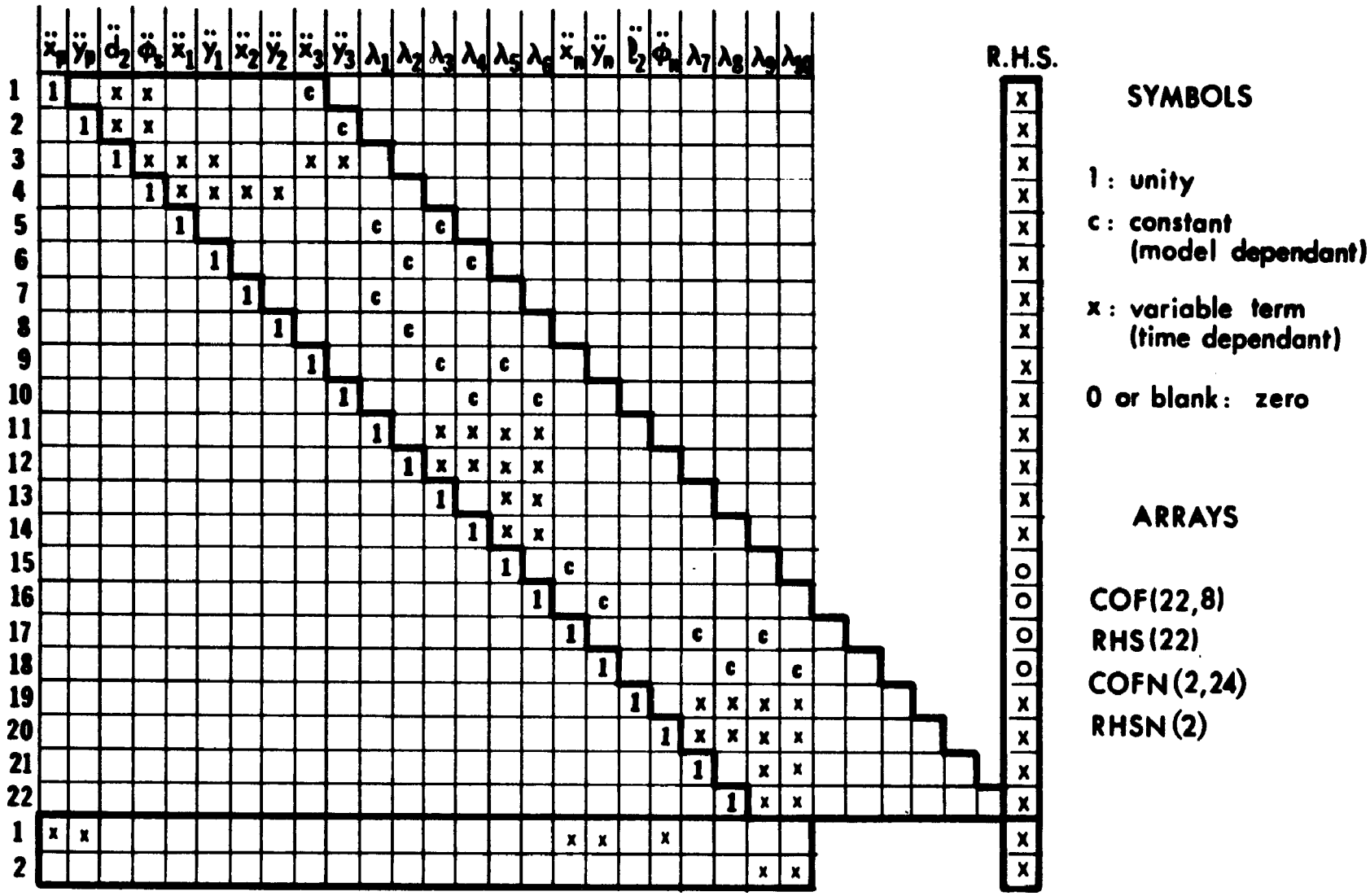


Figure B.3. Symbolic Matrix for Type II Input Solution of 24 Coupled Equations

results in a 24 x 24 matrix of coefficients, but with some preparation of the equations, it is possible to eliminate many of the terms so that the final "appearance" of these 24 equations becomes as shown in figure B.3. The storage requirements are thus reduced, the diagonal is normalized down to the 22nd element, and special subroutine BAKSUB was written to handle the diagonalization of the last two equations and solving by back-substitution for the unknowns.

After selection of the necessary equations and appropriate reductions, the equations that enter in this phase of solution are given below. The circled number to the left of each equation indicate the row of the matrix.

First, the 5th and 6th constraint equations:

$$\textcircled{1}\quad \ddot{x}_p + \ddot{d}_2[-\sin\varphi_s] + \ddot{\varphi}_s[-(h+d_2)\cos\varphi_s] + \ddot{x}_3[-1] = 2\dot{\varphi}_s\dot{d}_2\cos\varphi_s - \dot{\varphi}_s^2(h+d_2)\sin\varphi_s$$

$$\textcircled{2}\quad \ddot{y}_p + \ddot{d}_2[\cos\varphi_s] + \ddot{\varphi}_s[-(h+d_2)\sin\varphi_s] + \ddot{y}_3[-1] = 2\dot{\varphi}_s\dot{d}_2\sin\varphi_s + \dot{\varphi}_s^2(h+d_2)\cos\varphi_s$$

Now combine the 3rd and 4th constraint equations to eliminate $\ddot{d}_3$:

$$\textcircled{3}\quad \ddot{d}_2 + \ddot{\varphi}_s[d_3] + \ddot{x}_1[-\sin\varphi_s] + \ddot{y}_1[\cos\varphi_s] + \ddot{x}_3[\sin\varphi_s] + \ddot{y}_3[\cos\varphi_s] = -2\dot{\varphi}_s\dot{d}_3 + \dot{\varphi}_s^2 d_2$$

Next, eliminate $\ddot{d}_1$ from constraint equations (1) and (2), or differentiate the expression for $\dot{\phi}_s$:

$$\textcircled{4}\quad \ddot{\varphi}_s + \ddot{x}_1\left[-\frac{\sin\varphi_s}{d_1}\right] + \ddot{y}_1\left[\frac{\cos\varphi_s}{d_1}\right] + \ddot{x}_2\left[\frac{\sin\varphi_s}{d_1}\right] + \ddot{y}_2\left[\frac{-\cos\varphi_s}{d_1}\right] = -\frac{2\dot{\varphi}_s\dot{d}_1}{d_1}$$

Now rewrite the Lagrange equation in x_1, y_1, x_2, y_2, x_3, y_3 so that all computed or given terms are moved to the R.H.S.:

⑤ $\ddot{x}_1 + \lambda_1[1/m_1] + \lambda_3[1/m_1] = (1/m_1)[PX1 - \lambda_{13}]$

⑥ $\ddot{y}_1 + \lambda_2[1/m_1] + \lambda_4[1/m_1] = (1/m_1)[PY1 - \lambda_{14}]$

⑦ $\ddot{x}_2 + \lambda_1[-1/m_2] = (1/m_2)[PX2]$

⑧ $\ddot{y}_2 + \lambda_2[-1/m_2] = (1/m_2)[PY2]$

⑨ $\ddot{x}_3 + \lambda_3[-1/m_3] + \lambda_5[-1/m_3] = (1/m_3)[PX3]$

⑩ $\ddot{y}_3 + \lambda_4[-1/m_3] + \lambda_6[-1/m_3] = (1/m_3)[PY3]$

The next two rows need special handling since they contain more terms than other equations. These two equations are obtained from the Lagrange equations for ϕ_s and d_1, but are diagonalized so that the coefficients of λ_1 and λ_2 are both unity.

$$-\lambda_1 \sin\varphi_s + \lambda_2 \cos\varphi_s - \lambda_3 A_1 + \lambda_4 A_2 + \lambda_5 A_3 + \lambda_6 A_4 = F_1/d_1$$

$$\lambda_1 \cos\varphi_s + \lambda_2 \sin\varphi_s = F_2$$

where

$$A_1 \equiv (d_3 \sin\varphi_s + d_2 \cos\varphi_s)/d_1$$

$$A_2 \equiv (d_3 \cos\varphi_s - d_2 \sin\varphi_s)/d_1$$

$$A_3 \equiv [(h+d_2)\cos\varphi_s]/d_1$$

$$A_4 \equiv [(h+d_2)\sin\varphi_s]/d_1$$

$$F_1 \equiv \lambda_{13}(b_1 \sin\varphi_s + b_2 \cos\varphi_s) - \lambda_{14}(b_1 \cos\varphi_s - b_2 \sin\varphi_s) + TS + PUVA - \lambda_{11} - \lambda_{17}$$

$$F_2 \equiv -P4S - P3B - P1S$$

then, the 11th and 12 rows of the matrix become

⑪ $\lambda_1 + \lambda_3[A_1 \sin\varphi_s] + \lambda_4[A_2 \sin\varphi_s] + \lambda_5[A_3 \sin\varphi_s] + \lambda_6[A_4 \sin\varphi_s] = F_2 \cos\varphi_s - (F_1/d_1)\sin\varphi_s$

⑫ $\lambda_2 + \lambda_3[-A_1 \cos\varphi_s] + \lambda_4[A_2 \cos\varphi_s] + \lambda_5[-A_3 \cos\varphi_s] + \lambda_6[A_4 \cos\varphi_s] = F_2 \sin\varphi_s + (F_1/d_1)\cos\varphi_s$

To obtain rows 13 and 14 of the matrix, diagonalize the Lagrange equations for d_3 and d_2 which become

(13) $\lambda_3 + \lambda_5[\sin^2\varphi_s] + \lambda_6[-\sin\varphi_s\cos\varphi_s]$
$= (P4S - P3S)\cos\varphi_s - (P4B - P2S)\sin\varphi_s$

(14) $\lambda_4 + \lambda_5[-\sin\varphi_s\cos\varphi_s] + \lambda_6[\cos^2\varphi_s]$
$= (P4S - P3S)\sin\varphi_s + (P4B - P2S)\cos\varphi_s$

The next four rows are the Lagrange equations of x_p, y_p, x_n and y_n, i.e.

(15) $\lambda_5 + \lambda_7[-1] = 0$

(16) $\lambda_6 + \lambda_8[-1] = 0$

(17) $\ddot{x}_n + \lambda_7[1/m_n] + \lambda_9[-1/m_n] = 0$

(18) $\ddot{y}_n + \lambda_8[1/m_n] + \lambda_{10}[-1/m_n] = 0$

The next two equations are the 9th and 10th constraint equations. Since the leading terms are $\ddot{x}_n$ and $\ddot{y}_n$, they are manipulated as to produce $\ddot{\ell}_2$ and $\ddot{\phi}_2$ as leading terms. They become

(19) $\ddot{\ell}_2 + \lambda_7\left[-\frac{\sin\varphi_n}{m_n}\right] + \lambda_8\left[\frac{\cos\varphi_n}{m_n}\right] + \lambda_9\left[\frac{\sin\varphi_n}{m_n}\right] + \lambda_{10}\left[\frac{-\cos\varphi_n}{m_n}\right]$
$= (PXO)\sin\varphi_n - (PYO)\cos\varphi_n + \dot{\varphi}_n^2\ell_2$

(20) $\ddot{\varphi}_n + \lambda_7\left[\frac{-\cos\varphi_n}{m_n}\right] + \lambda_8\left[\frac{-\sin\varphi_n}{m_n}\right] + \lambda_9\left[\frac{\cos\varphi_n}{m_n\ell_2}\right] + \lambda_{10}\left[\frac{\sin\varphi_n}{m_n\ell_2}\right]$
$= (1/\ell_2)[(PXO)\cos\varphi_n + (PYO)\sin\varphi_n - 2\dot{\varphi}_n\dot{\ell}_2]$

The last two equations that will be diagonalized are the Lagrange equations of ℓ_1 and ϕ_n.

let $f_1 \equiv -(1/\ell_1)[TN - PTN + PTS]$

$f_2 \equiv -P1N$

then

(21) $\lambda_7 + \lambda_9\left[\frac{\ell_2}{\ell_1}\cos^2\varphi_n\right] + \lambda_{10}\left[\frac{\ell_2}{\ell_1}\sin\varphi_n\cos\varphi_n\right] = f_1\cos\varphi_n - f_2\sin\varphi_n$

(22) $\lambda_8 + \lambda_9\left[\frac{\ell_2}{\ell_1}\sin\varphi_n\cos\varphi_n\right] + \lambda_{10}\left[\frac{\ell_2}{\ell_1}\sin^2\varphi_n\right] = f_1\sin\varphi_n + f_2\cos\varphi_n$

The last two rows are left without diagonalization, and subroutine BAKSUB is designed to eliminate the coefficients by proper rows manipulation. Row 23 is a combination of 7th and 8th constraint equations to eliminate $\ddot{\ell}_1$, and row 24 is the Lagrange equation in ℓ_2.

(23) $$\ddot{x}_p[\cos\varphi_n] + \ddot{y}_p[\sin\varphi_n] + \ddot{x}_n[-\cos\varphi_n] + \ddot{y}_n[-\sin\varphi_n] + \ddot{\varphi}_n[\ell_1] = -2\dot{\varphi}_n\dot{\ell}_1$$

(24) $$\lambda_9[-\sin\varphi_n] + \lambda_{10}[\cos\varphi_n] = -P2N$$

It is worth noting here that, in none of the equations, are there more than 8 terms, many of which are either constants or zero. Subroutine BAKSUB requires that the coefficient matrix be defined as COF(22,8) and COFN(2,24) as opposed to a general requirement of A(24, 24). Another noteworthy point is that the arrangement of the coefficients and 18 R.H.S. terms. All other terms are either zeros or constants and are thus defined, only once, at the beginning of the simulation. Finally, note that this arrangement of the equations, formal inversion of the matrix is replaced by a back-substitution method for solution of the system of equations; thus, there is no fear of the nonexistence of an inverse under any circumstance.

Once BAKSUB returns with a solution to the various unknowns (accelerations and lambdas) the same procedure of SOLVE1 is used, in this SOLVE2 subroutine, to define the elements of QD array, which are then returned to DHPCG for their integration.

APPENDIX C

IMPEDANCE REDUCTION TECHNIQUE OF A MECHANICAL NETWORK

When dealing with a multi-element network of masses, springs and dashpots, the expression of the equivalent mechanical impedance between two arbitrary nodes becomes very involved. This expression is usually obtained for the purpose of studying the effect of frequency on the magnitude of the impedance and its phase angle. The result is generally plotted as impedance and phase angle versus frequency.

A technique for obtaining the numerical values of these two curves is given here, with application to the driving-point impedances of the proposed model in the horizontal and vertical directions.

C.1 METHOD

Given a mechanical network of masses, springs and dashpots, such as shown in figure C.1, the physical elements are replaced by a two-part impedance, thus forming a network of impedances, connected at several nodes. The technique is merely a systematic reduction of elements between adjacent nodes until the equivalent mechanical impedance between two desired nodes is obtained.

This reduction procedure is repeated for each frequency value of a desired spectrun of frequencies. The result is a numerical description of impedance as a function of frequency.

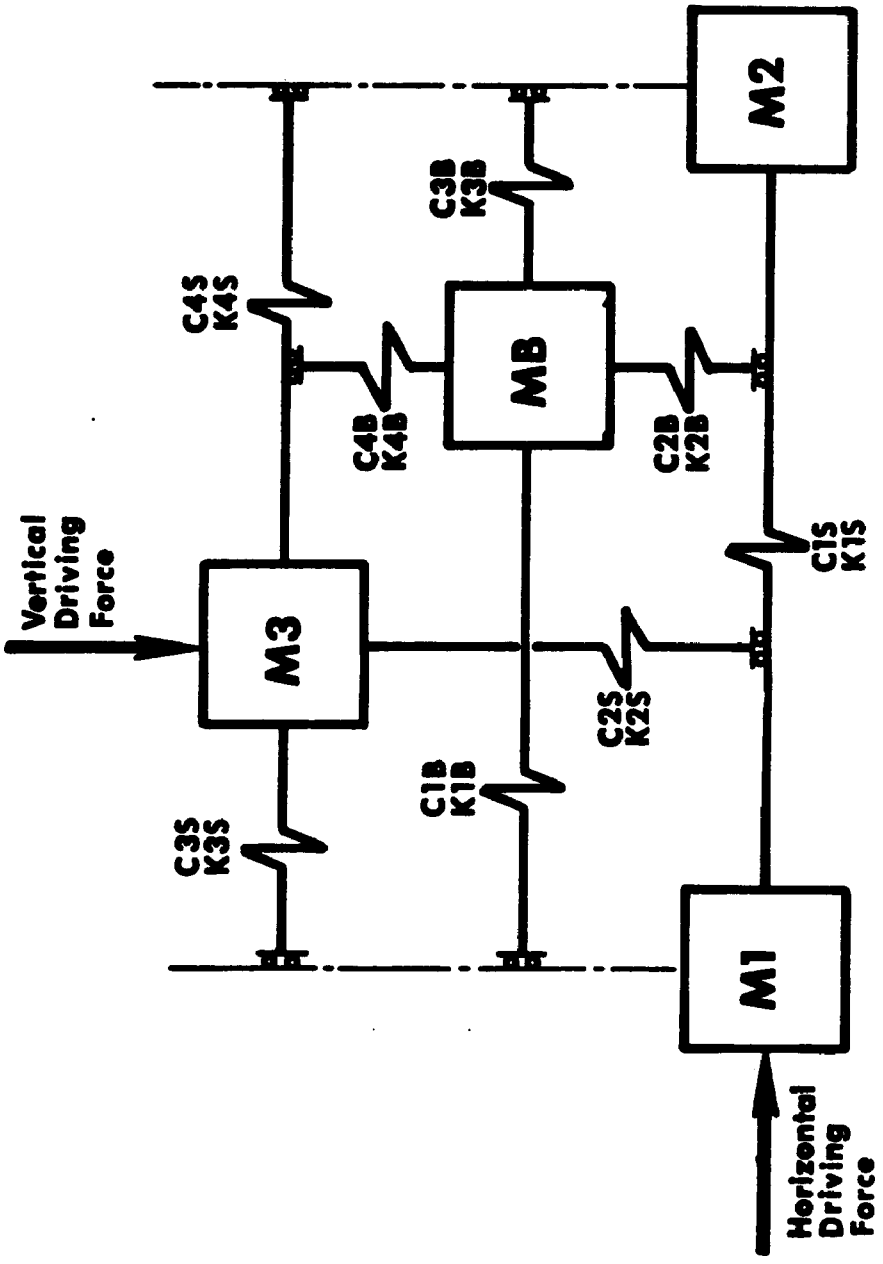


Figure C.1. Mechanical Network of Skull-Brain

Since the impedance is generally a complex number which is a function of frequency, i.e.

$$Z(\omega) = A(\omega) + i\,B(\omega)$$

the four basic operations of addition, subtraction, multiplication and division must always be performed on pairs of numbers. The facility of complex number manipulations on the University of Michigan IBM-360 digital computer were not used, instead, four subroutines were written (ZADD, ZSUB, ZMUL, ZDIV) to perform these operations. Each subroutine accepts (A_1, B_1), (A_2, B_2) and produces a specific result (A,B).

To perform the reduction, for a given frequency and a set of constants m, c, k (masses, dashpots and springs), subroutines to obtain the impedances $Z_m(\omega)$, $Z_c(\omega)$, $Z_k(\omega)$ were written. Then, given two impedances in parallel or in series, subroutines were written to obtain the equivalent parallel or series impedances, respectively. Finally, when 3 impedances are connected in a Y or Δ configuration, another subroutine was written to perform the Y-Δ transformation in either direction.

Now that these basic subroutines are avaliable, a specific subroutine to reduce a given network may be written which calls the various subroutines to perform the reduction. A main program generates the desired frequencies, calls the network subroutine which returns with an over-all equivalent impedance for each frequency, and outputs the results in plots, tables, etc.

C.2 BASIC ELEMENTS

It is assumed here that the concept of mechanical impedance is understood, as it may be found in any vibrations or dynamics textbook.

The impedances of a mass m, a dashpot c, and a spring k are:

$$Z_m = i\omega m$$

$$Z_c = C$$

$$Z_k = -i\frac{k}{\omega}$$

Three subroutines, ZMASS, ZDASH and ZSPRG compute $(0,\omega m)$, $(C,0)$ and $(0, -k/\omega)$ given respectively (ω,m) (ω,c) and (ω,k). These subroutines are called in order to replace the physical elements in the mechanical networks by two-port elements of impedances, thus forming a network of branches (impedances) and nodes (connections). To reduce the resulting network, combinations of two or three elements are replaced by equivalent elements.

C.3 BASIC COMBINATIONS

Two elements in series, Z_1 and Z_2, have an equivalent impedance Z, such that

$$\frac{1}{Z} = \frac{1}{Z_1} + \frac{1}{Z_2}$$

or

$$Z = \frac{Z_1 Z_2}{Z_1 + Z_2}$$

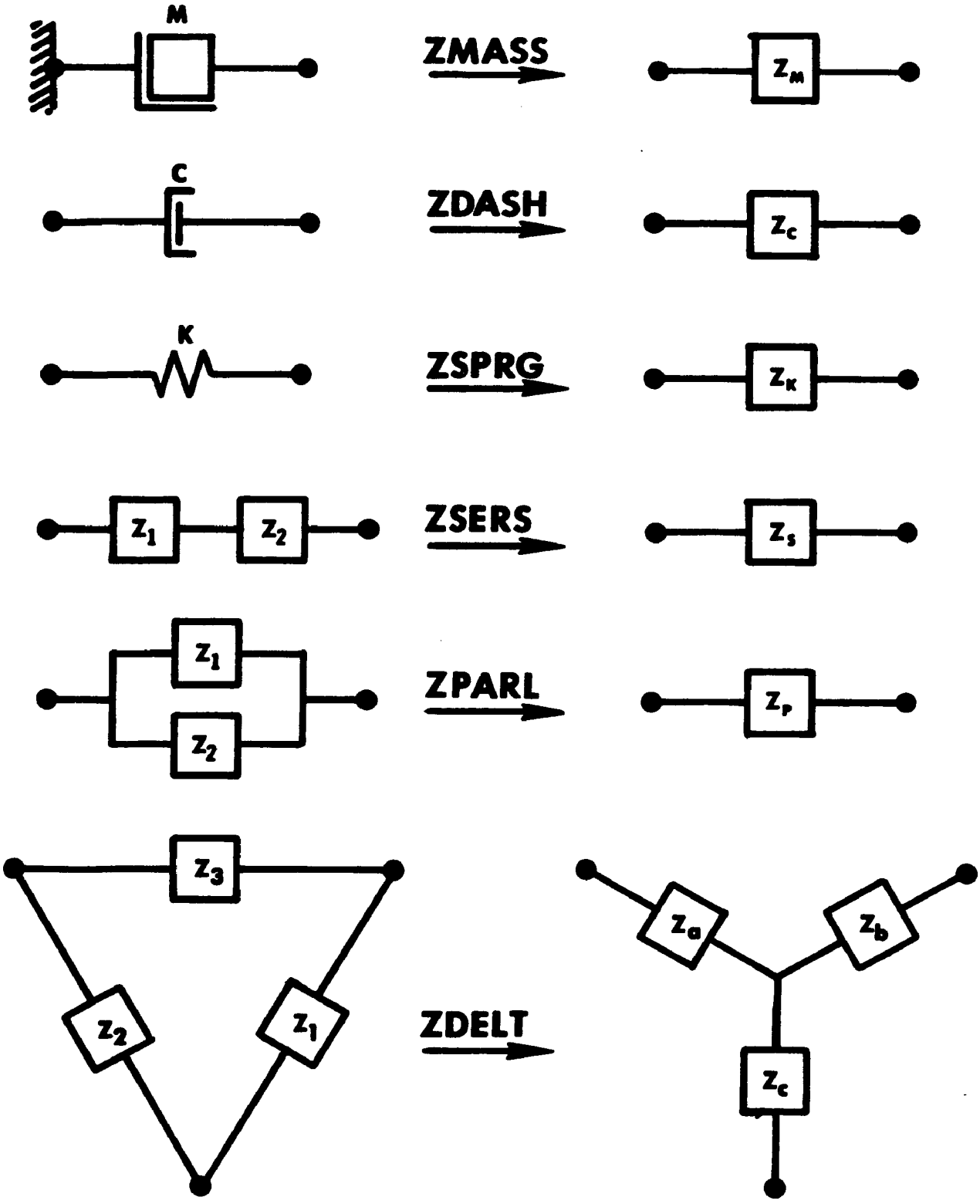


Figure C.2. Transformations of Basic Elements and Networks

Subroutine ZSERS performs this reduction by using addition (ZADD), multiplication (ZMUL) and division (ZDIV) operations.

Two elements in parallel, Z_1 and Z_2, have an equivalent impedance Z

$$Z = Z_1 + Z_2$$

Subroutine ZPARL performs this addition by calling the ZADD subroutine.

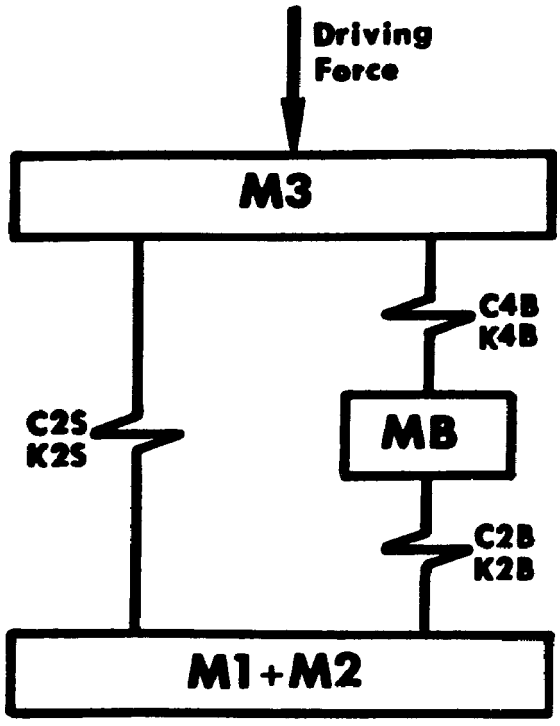
When three elements for a (Δ) between three nodes, an equivalent (Y) between the same nodes is computed by subroutine ZDELT, which adds a fourth node at the center of the transformed (Δ). This transformation is opposite to the "Tee-Pi" transformation in electrical circuits, with mechanical mobilities (reciprocal of impedances) being equivalent to the electrical impedances.

One combination that was used in the proposed model is the spring-dashpot in parallel, which constitutes the viscoelastic Kelvin element. A special subroutine ZKELV was written to accept (ω,k,c) as input and produce directly the equivalent impedance of this viscoelastic element.

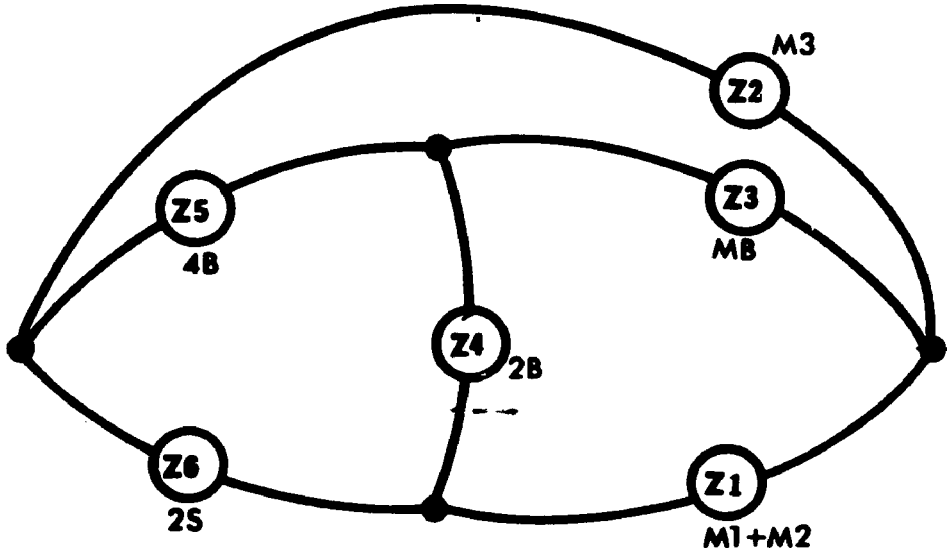
A list of the subroutines written for impedance network reduction is given in figure C.2.

C.4 APPLICATIONS

The driving point impedance of the human head has been measured and published. In order to lump the parameters of the proposed model, its driving point impedance is obtained by the

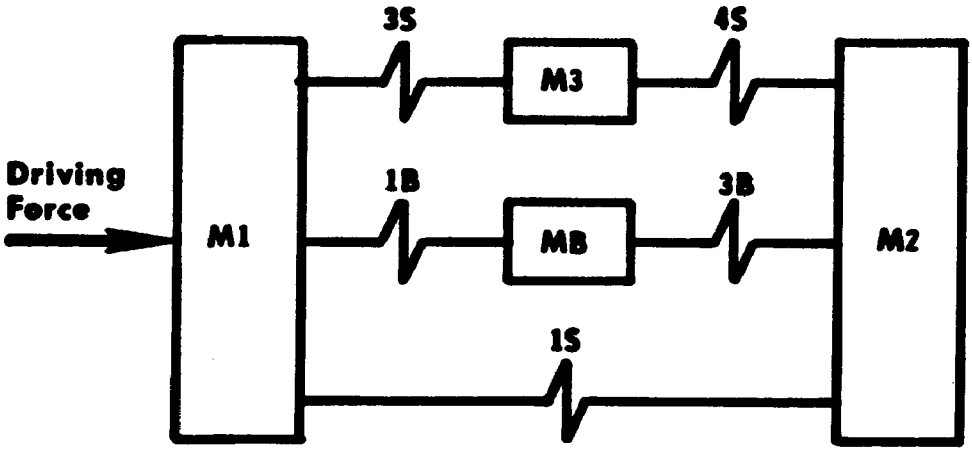


(A) PHYSICAL MODEL

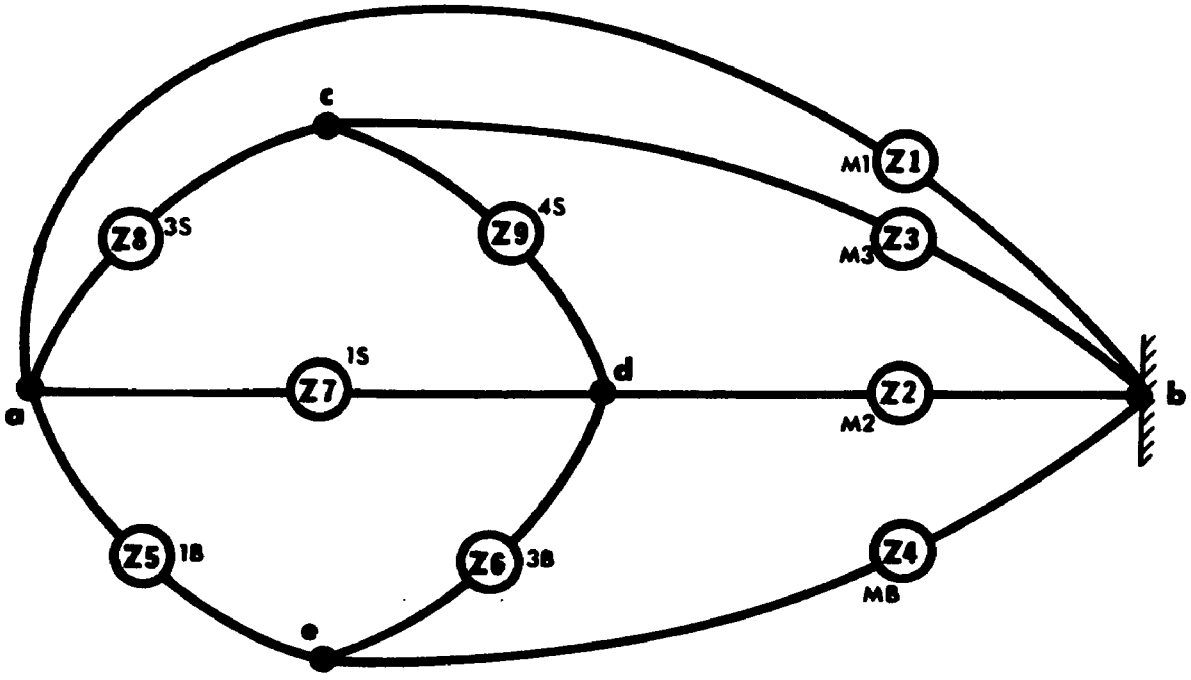


(B) IMPEDANCE NETWORK

Figure C.3 Vertical-direction Impedance



(A) PHYSICAL MODEL



(B) IMPEDANCE NETWORK

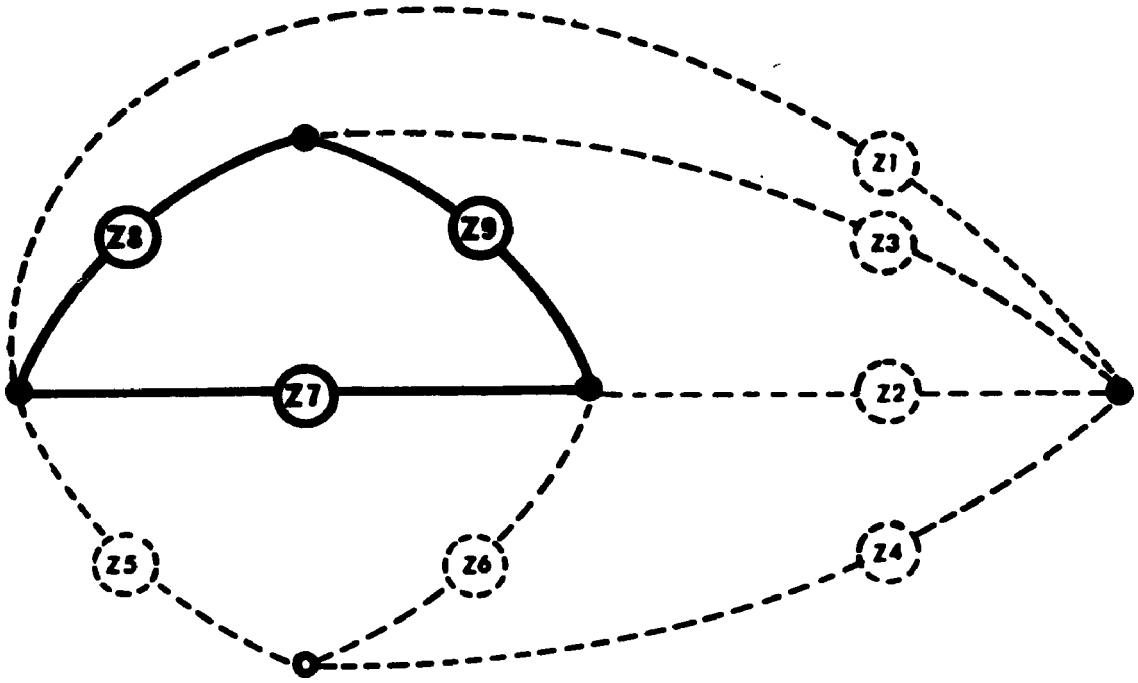
Figure C.4 Horizontal-direction Impedance

technique described in the previous sections, and these parameters modified until a satisfactory match is obtained between the impedance of the model and the actual head.

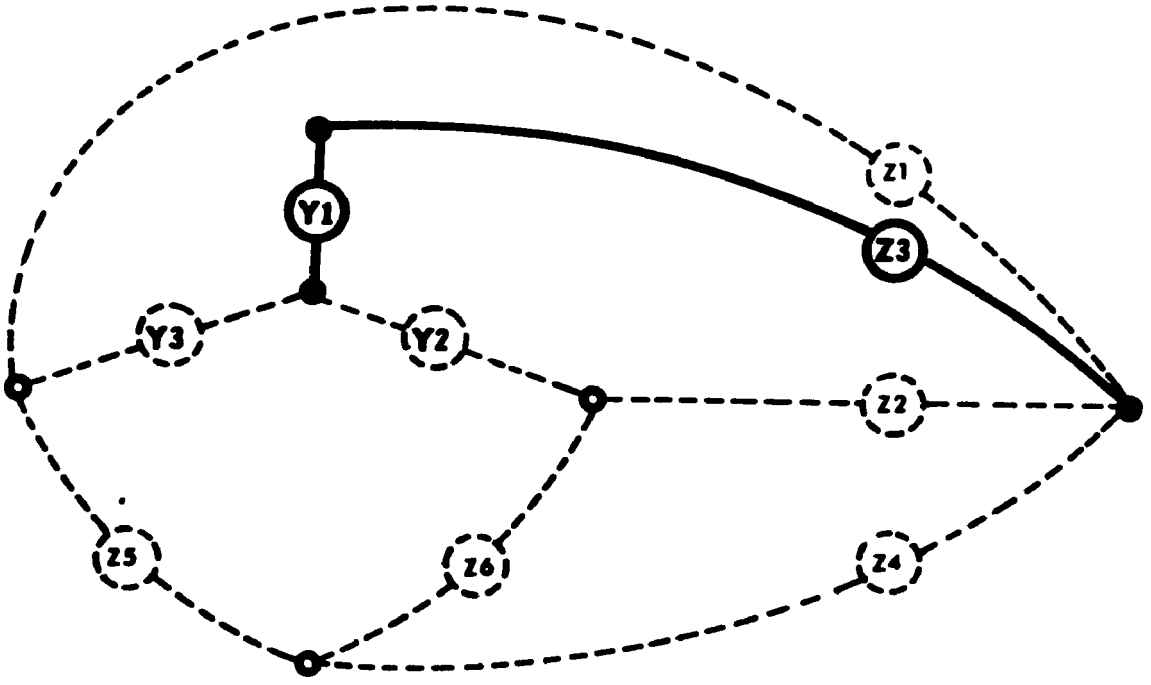
The skull and brain section of the model are shown in figure C.1. When the impedance is obtained in the horizontal direction (either A-P or L-R), only the portions shown in figure C.4(A) effect this impedance. This physical network may be replaced by the impedance network of figure C.4(B) on which successive reductions are performed.

The nodes are labeled a, b, c, d and e and the desired impedance is between node a and node b. Branches are labeled by the labels of the model, i.e. 1S, 3S, 4S, 1B, 3B, M1, M2, M3 and MB. Each transformation changes the configuration of the network until there is one final element between a and b. The "evolution" of the network is given in the following pages.

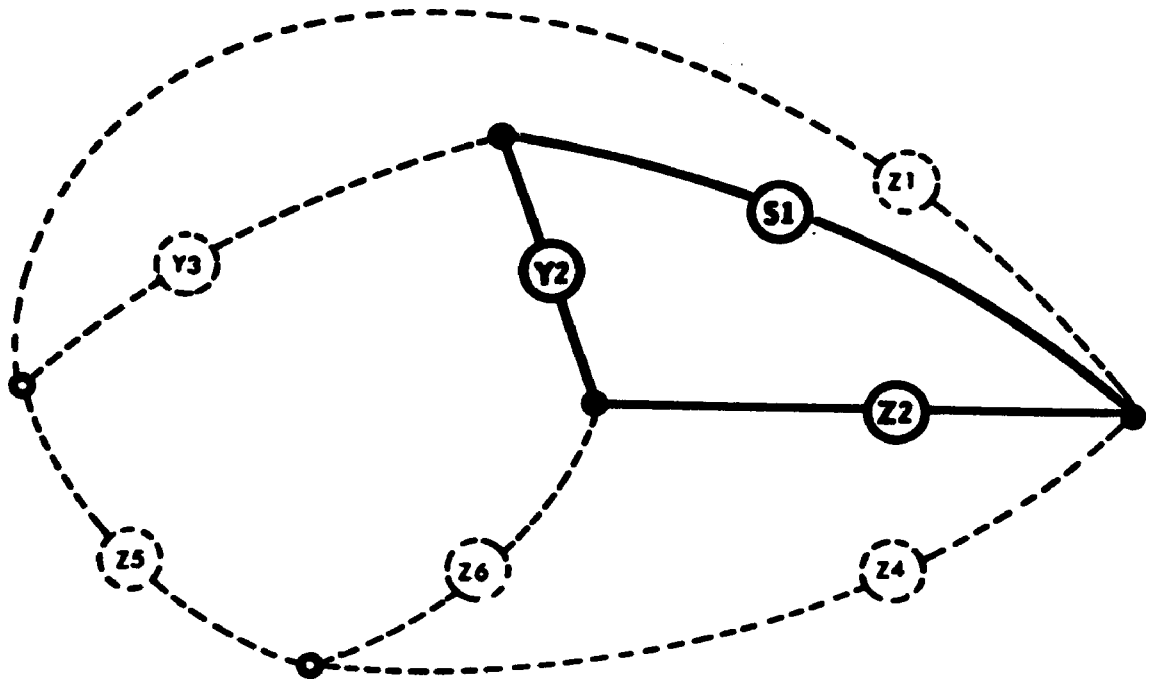
Similar procedure is followed to obtain an equivalent impedance for the brain-skull section in the vertical direction. The physical model of figure C.3(A) is again replaced by an impedance network as shown in figure C.3(B). Then successive reductions, using the basic reduction subroutines, are applied until one single equivalent impedance is obtained. The details of step-by-step reduction is not shown for this S-I network.



STEP 1. Delta(Z7,Z8,Z9) is transformed into a wye(Y1,Y2,Y3)

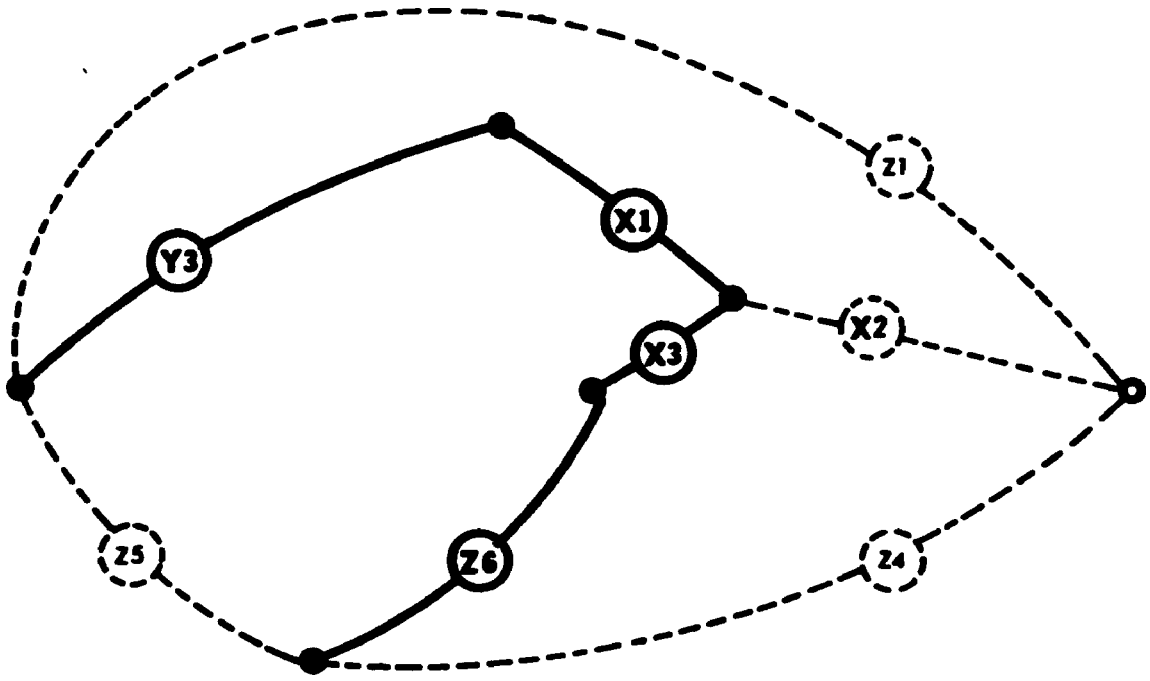


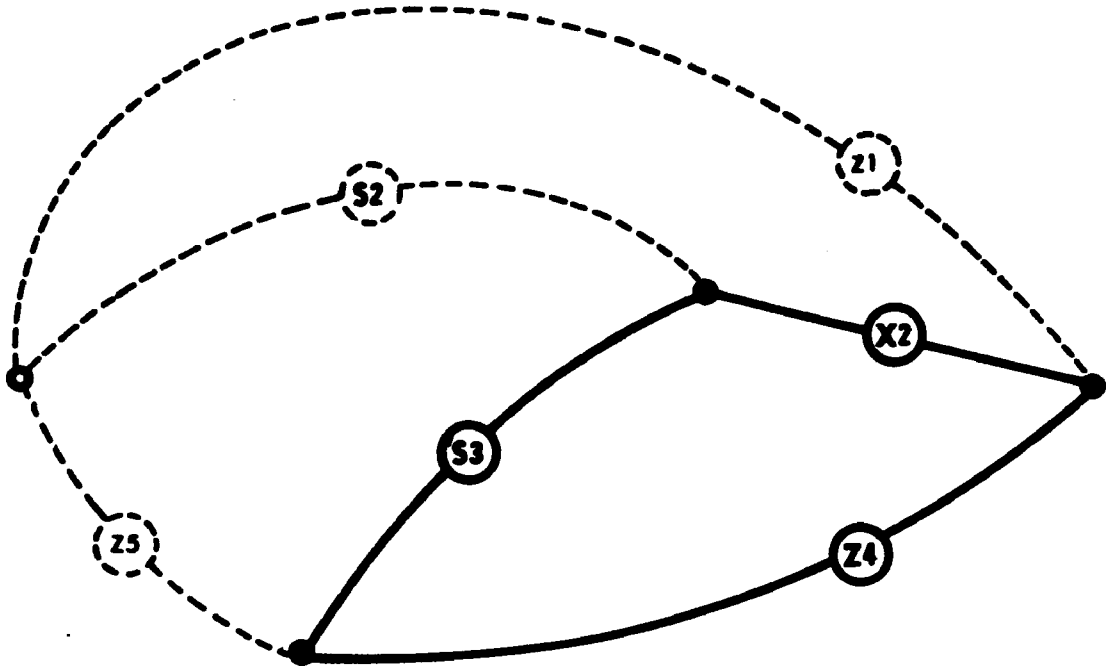
STEP 2. Series (Y1,Z3) is equivalent to (S1)



STEP 3. Another delta(Z2,Y2,S1) is transformed into a wye(X1,X2,X3)

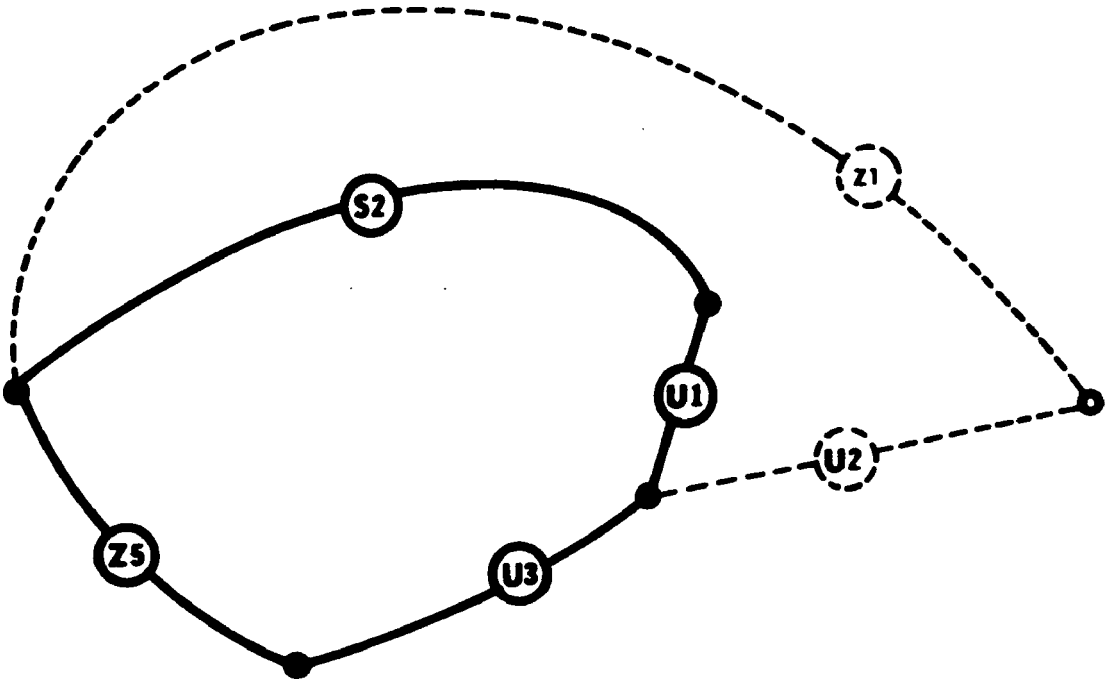
STEP 4. Series(X1,Y3) is replaced by (S2); series(X3,Z6) by (S3)

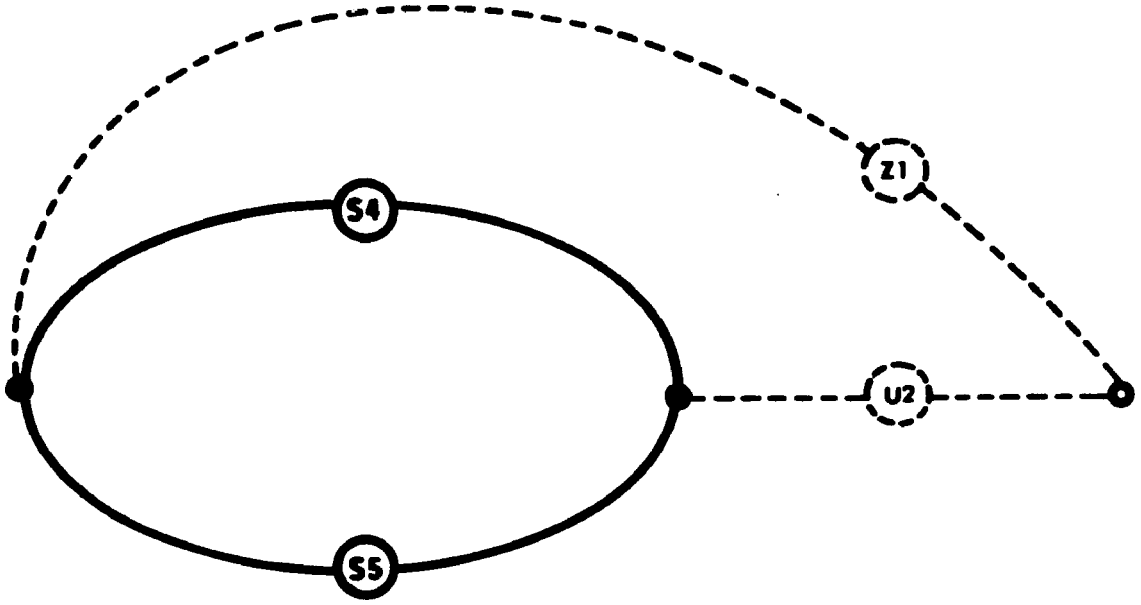




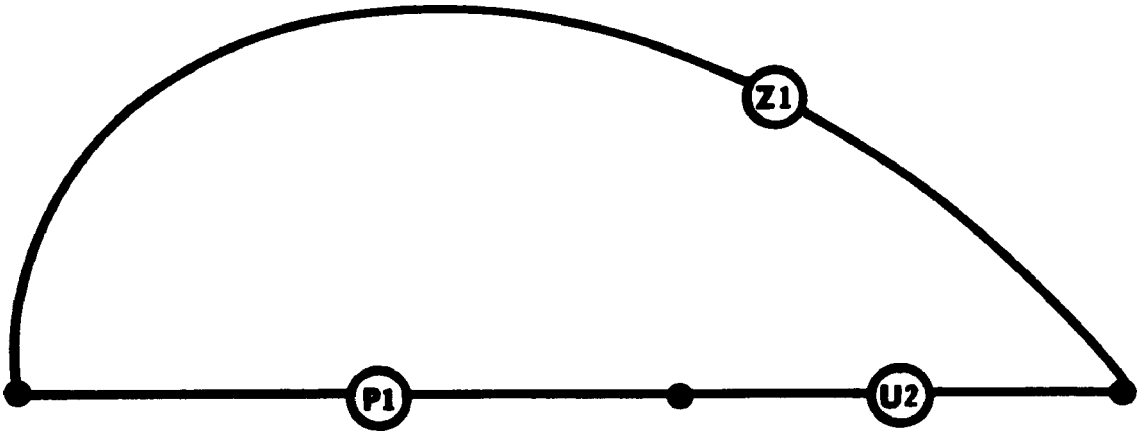
STEP 5. The new delta(Z4,S3,X2) is replaced by a wye(U1,U2,U3)

STEP 6. Now series(U1,S2) and (U3,Z5) are replaced by (S4) and (S5), respectively.





STEP 7. Now, branches (S4,S5) in parallel are equivalent to (P1)



STEP 8. Series(P1,U2) give the last intermediate impedance, which is in parallel with(Z1).



C.4 CONCLUSIONS

It is clear that the advantage of this method is felt when the network is large, in which case the algebraic reduction of the impedance expression becomes very complicated. Small networks that could be reduced algebraically, usually result in relatively simple expressions of Z(w). However this computerized technique can apply to both small and large networks, in which, no more than 3 branches have a common node. Finally, it should be noted that in those cases (multi-branch nodes), additional reduction subroutines may be written; however, mechanical systems seldom result in such complications.